

CHARLES UNIVERSITY IN PRAGUE

Faculty of Science
Department of Organic Chemistry



Mgr. Jindřich Nejedlý

THE SYNTHESIS OF π -ELECTRON SYSTEMS SUITABLE
FOR TRANSFER AND RETENTION OF CHARGES

SYNTÉZA π -ELEKTRONOVÝCH SYSTÉMŮ VHODNÝCH
PRO PŘENOS A RETENCI NÁBOJE

Doctoral Thesis

Supervisor: RNDr. Ivo Starý, CSc.
Consultant: RNDr. Jaroslav Vacek, Ph.D.

Prague, 2020

Acknowledgement

First of all I would like to thank to my supervisor Dr. Ivo Starý, who carefully and kindly guided me through my PhD studies. I am also grateful to Dr. Irena G. Stará for her advice and professional help. I would like to thank to all current and former members of our group for their help and the pleasant environment during my PhD studies, especially, Dr. Jiří Rybáček, Dr. Michal Šámal. I am very grateful to Dr. Jaroslav Vacek for introducing me to computational chemistry and for his useful help in this field as well as for his advice, guidance and assistance in the “break junction project”. My deep thanks also belong to late Dr. Jana Vacek-Chocholoušová for her help with the development of the break junction device, Dr. Ladislav Sieger for his help with the development of electronic measuring units, Prof. Josef Zicha for his advice on break junction device design and engineering, Dr. Ivana Císařová for X-ray diffraction analyses, Dr. Miloš Buděšínský for measurement and interpretation of NMR spectra and Ing. Pavel Fiedler and Dr. Lucie Bednářová for measurement and interpretation of IR and CD spectra and also all members of the mass spectrometry research-service group at the IOCB and all members of the IOCB development center.

I would like to thank the Czech Science Foundation (Reg. No. 14-29667S) and the Institute of Organic Chemistry and Biochemistry ASCR (RVO: 61388963) for founding this project.

Declaration

The Thesis was accomplished at the Institute of Organic Chemistry and Biochemistry, v.v.i., Academy of Sciences of the Czech Republic under supervision of Dr. Ivo Starý. “I hereby declare that I have done this Thesis independently while noting all resources used, as well as all co-authors.” Neither this work, nor any of its sections have been used for acquiring another academic degree.

Prague, 24 August 2020

Signature.....

Jindřich Nejedlý

Prohlášení

Tato práce byla vypracována na Ústavu organické chemie a biochemie, v.v.i, Akademie věd České republiky pod vedením RNDr. Iva Starého, CSc.. Prohlašuji, že jsem závěrečnou práci zpracoval samostatně a že jsem uvedl všechny použité informační zdroje a literaturu. Tato práce ani její podstatná část nebyla předložena k získání jiného nebo stejného akademického titulu.

Prague, 24 August 2020

Signature.....

Jindřich Nejedlý

I hereby declare that Mgr. Jindřich Nejedlý contributed significantly to all scientific publications that are part of this doctoral thesis. He performed experiments and took part in their planning; he interpreted results and participated in manuscript writing. His contributions to the individual publications are quantified below.

- (1) Nejedlý, J.; Šámal, M.; Rybáček, J.; Gay Sánchez, I.; Houska, V.; Warzecha, T.; Vacek, J.; Sieger, L.; Buděšínský, M.; Bednárová, L.; Fiedler, P.; Císařová, I.; Starý, I.; Stará, I. G. Synthesis of Racemic, Diastereopure, and Enantiopure Carba- or Oxa[5]-, [6]-, [7]-, and -[19]Helicene (Di)Thiol Derivatives. *J. Org. Chem.* **2020**, *85* (1), 248–276. <https://doi.org/10.1021/acs.joc.9b02965>. - 40%
- (2) Stetsovych, O.; Mutombo, P.; Švec, M.; Šámal, M.; Nejedlý, J.; Císařová, I.; Vázquez, H.; Moro-Lagares, M.; Berger, J.; Vacek, J.; Stará, I. G.; Starý, I.; Jelínek, P. Large Converse Piezoelectric Effect Measured on a Single Molecule on a Metallic Surface. *J. Am. Chem. Soc.* **2018**, *140* (3), 940–946. <https://doi.org/10.1021/jacs.7b08729>. - 20%
- (3) Nejedlý, J.; Šámal, M.; Rybáček, J.; Tobrmanová, M.; Szydło, F.; Coudret, C.; Neumeier, M.; Vacek, J.; Vacek-Chocholoušová, J.; Buděšínský, M.; Šámal, D.; Bednárová, L.; Sieger, L.; Stará, I. G.; Starý, I. Synthesis of Long Oxahelicenes by Polycyclization in a Flow Reactor. *Angew. Chem. Int. Ed.* **2017**, *56* (21), 5839–5843. <https://doi.org/10.1002/anie.201700341>. - 50%
- (4) Gay Sánchez, I.; Šámal, M.; Nejedlý, J.; Karras, M.; Klívar, J.; Rybáček, J.; Buděšínský, M.; Bednárová, L.; Seidlerová, B.; Stará, I. G.; Starý, I. Oxahelicene NHC Ligands in the Asymmetric Synthesis of Nonracemic Helicenes. *Chem. Commun.* **2017**, *53* (31), 4370–4373. <https://doi.org/10.1039/C7CC00781G>. - 10%

Prague, 24 August 2020

Signature.....

RNDr. Ivo Starý, CSc.

Souhrn

Cílem mé disertační práce bylo vyvinout obecnou syntetickou metodologii pro přípravu dlouhých helicenů, která by zároveň umožnila funkcionalizaci těchto molekul vedoucí ke zvýšení jejich rozpustnosti či zavedení vhodné kotvící skupiny s vysokou afinitou ke kovovým povrchům, především ke zlatu.

Jako klíčový krok v syntéze dlouhých helicenů byla pro tvorbu helikálního skeletu vybrána [2+2+2] cyklotrimerizace katalyzována komplexy přechodných kovů, která je vysoce regioselektivní, efektivní z hlediska atomové ekonomie a tolerantní k široké škále funkčních skupin. Pro syntézu výchozích oligoynů byl použit modulární přístup umožňující vysokou strukturální rozmanitost. Jednotlivé aromatické stavební bloky odvozené od resorcinolu byly pospojovány za použití Sonogashirovy reakce, přičemž poskytly sérii polyynů pro klíčovou cyklizační reakci. Tyto prekursory obsahovaly až dvanáct trojných vazeb s vhodným uspořádáním pro [2+2+2] cyklotrimerizaci, která umožnila konstruovat tři nové šestičlenné kruhy z každé trojice sousedních trojných vazeb. Touto metodologií byla připravena série dlouhých helicenů obsahujících až 19 kondenzovaných kruhů. Čtyřnásobná [2+2+2] cykloizomerizace vedoucí k přípravě oxa[19]helicenu byla provedena ve vysokotlakém průtokovém reaktoru při 250 °C v přítomnosti CpCo(CO)₂. Kolekce připravených molekul obsahuje racemické i opticky čisté heliceny nesoucí sírné nebo dusíkaté kotvící skupiny.

Sírné kotvící skupiny byly zavedeny pomocí nukleofilní aromatické substituce za použití příslušných výchozích chlorderivátů helicenů. Díky nízké reaktivitě arylchloridů za podmínek cross-couplingových reakcí bylo možné použít komerčně dostupné výchozí stavební bloky obsahující atom chloru, který bylo možné nahradit požadovanou sulfanylovou kotvící skupinou za vyšší teploty (200 – 270 °C) na konci syntetické cesty. Tímto postupem byla připravena série [5]-, [6]-, [7]- a [19]helicenů resp. jejich oxaderivátů nesoucích sírné kotvící skupiny v různých polohách.

Souběžně se syntézou byl navržen a zkonstruován „break junction“ přístroj pro měření monomolekulární vodivosti nově připravených molekul v STM i MCBJ módu. Za použití tohoto přístroje byly změřeny vodivosti vybraných nově připravených helicenů se sírnými/dusíkatými kotvícími skupinami. Všechny heliceny měly relativně vysokou vodivost v řádu 10⁻³ G/G₀.

Summary

The aim of my Thesis was to develop a general synthetic methodology for the preparation of long helicenes equipped with suitable functional groups that control their solubility or serve as anchoring groups for attachment to metallic surfaces, especially gold.

The well-established transition metal catalyzed [2+2+2] cyclotrimerization of triynes was selected as the key scaffold-forming transformation in the synthesis of long helicenes because of its high regioselectivity, atom efficiency, functional group tolerance and general robustness. A modular approach was used for the preparation of the starting oligoynes, thus enabling a high level of their structural diversity. Individual resorcinol-based aromatic building blocks were interconnected by Sonogashira cross-coupling reactions, providing complex cyclization precursors encompassing up to twelve alkyne units pre-arranged for the multiple [2+2+2] cycloisomerization to produce three six-membered rings from each set of three neighboring alkyne units. Thus, a small series of long helicenes with up to 19 rings constituting the helical scaffold was synthesized. The quadruple cyclization leading to the longest oxahelicene prepared to date was performed in a high-temperature-high-pressure flow reactor at 250 °C in the presence of $\text{CpCo}(\text{CO})_2$. The set of compounds includes racemic as well as optically pure helicenes functionalized by sulfur or nitrogen anchoring groups.

Sulfur anchoring groups were conveniently introduced into the helicene molecules by nucleophilic aromatic substitution employing the corresponding chloro helicenes. Due to its low reactivity in palladium catalyzed cross-coupling reactions, the chlorine substituent was advantageously carried through the synthesis to be eventually replaced by a sulfanyl group at high temperature (200 – 270 °C). A series of such helicenes with one or two sulfanyl or thioacetate groups attached at different positions was prepared using this approach including carba- and oxa- [5]-, [6]-, [7]- and [19]helicenes.

In parallel to the synthesis, a state-of-the-art break junction (BJ) instrument was designed and constructed in order to study single-molecule conductance of the newly prepared compounds in the STM as well as mechanically controllable BJ modes. Three new helicene molecules with sulfur-based anchor groups and the pyridooxa[9]helicene derivative were investigated, showing conductance in the order of 10^{-3} G/G_0 .

Table of Contents

1	Introduction: Current State of Art	1
1.1	Helicene	1
1.1.1	Definition and Characteristics	1
1.1.2	Application	2
1.1.3	Synthesis	3
1.1.3.1	Photoinduced Cyclodehydrogenation	3
1.1.3.2	[2+2+2] Cycloisomerization	6
1.1.3.3	Other Methodologies	11
1.1.3.4	Nonracemic Helicenes and Methods of their Preparation	13
1.1.3.5	Heterohelicenes	17
1.2	Conductivity at the Nanoscale	19
1.2.1	Break Junction Techniques	19
1.2.1.1	General Principles	20
1.2.1.2	Mechanically Controllable Break Junction	25
1.2.1.3	Scanning Tunneling Microscopy-Based Break Junction	26
1.2.1.4	Materials Used in the Break Junction Techniques	27
1.2.2	Conductance of Organic Molecules	29
1.2.2.1	Electron Transport in Helicene Molecules	35
2	Objectives	36
3	Results and Discussion	39
3.1	The Synthesis of Long Helicenes	39
3.1.1	The Synthesis of Racemic Oxa[n]helicenes	39
3.1.2	The Synthesis of Optically Pure Oxa[19]helicene	47
3.2	The Synthesis of Helicenes with Anchoring Groups	51
3.2.1	The Synthesis of Pyridooxa[9]helicene (-)-(M,R,R)-87	51
3.2.2	The Synthesis of Sulfanylated Helicenes	52
3.2.2.1	The Optimization of Sulfanylation of Chloroaromatics	54
3.2.2.2	The Synthesis of Sulfanylated Carba[n]helicenes	55
3.2.2.3	The Synthesis of Sulfanylated Oxa[n]helicenes	62

3.3	Break Junction Experiments	71
3.3.1	Break Junction Device Development	71
3.3.2	Mechanically Controllable Break Junction (MCBJ)	73
3.3.3	Scanning Tunneling Microscopy-Based Break Junction (STM-BJ)	75
3.3.4	Computer Control and Data Analysis	75
3.4	Single-Molecule Conductance Measurement	77
3.4.1	Evaluation of Standards	77
3.4.2	Single-Molecule Conductance of Helicene Derivatives	79
4	Conclusion	90
5	Experimental Section	94
5.1	Methods	94
5.2	Synthesis	96
5.3	Break Junction	151
6	Abbreviations	155
7	Literature	158
8	Appendix A: 3D structures of helicenes	172

1 Introduction: Current State of Art

Helical shape of an object is not as rare a feature as it might seem, it is a very common phenomenon in the nature. It is possible to find it from the largest entities such as galaxies, across tornados, snails and pea sprigs, down to the notoriously known supramolecular structures of DNA and to helicenes at the molecular level.

1.1 Helicene

1.1.1 Definition and Characteristics

A strict definition of helicenes is that they are *ortho*-condensed polycyclic aromatic compounds,¹ in which benzene rings are angularly annulated to give helically-shaped molecules. This definition may be extended to cover also other (hetero)aromatics such as thiophene or pyridine, smaller and larger rings, partially saturated rings, *etc.* Names of helicenes are constructed from the word helicene used as the radix and a Latin prefix signifying the number of fused rings. A number in square brackets might be used instead of the prefix (*e.g.* [6]helicene is an equivalent of hexahelicene). An example of atom numbering of a helicene is shown in the **Figure 1**.

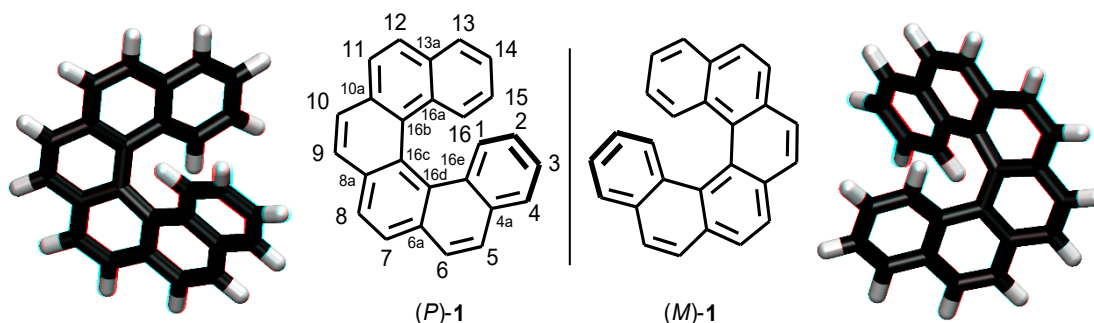


Figure 1: Hexahelicene, (*P*)-1 and (*M*)-1 enantiomers

Helicity is a type of chirality, which does not result from the presence of a chiral center, *e.g.* an asymmetrically substituted atom or a chiral axis caused by a hindered rotation around a single (double) bond, but from a steric repulsion between distant parts of the molecule, which forces it to adopt a helical shape. Depending on the handedness of the helicene, they are conventionally labeled either as ***P***, if the helix winds away from the observer in a clockwise sense, or ***M***, if the direction is counter-clockwise (**Figure 1**).

Their helical shape makes us think of helicenes as molecular springs. This concept of spring-like behavior was supported by X-ray analysis and manifested by

calculations.^{2,3} It is possible to stretch the helix by at least 1.4 Å per turn⁴ without any bond rupture. The pitch of the helicene derivatives studied by Tanaka and co-workers changed depending on the type of solvent used for crystallization. Formation of clathrates with planar aromatic guest molecules was also described.

1.1.2 Application

The significant feature of helicenes is their chiral helical shape, which projects into their intriguing physical properties. One of those is an enormously high optical activity. Due to their conjugated π - electron system, helicenes are expected to behave as molecular conductors with a discrete and adjustable band gap and therefore they might be useful in molecular or organic electronics.⁵ Furthermore, the combination of their helical shape and conductive properties makes them suitable for investigation of spin polarization as well as magneto-chiral anisotropic effect.⁶ Their flexibility, low thermal conductivity and good electrical conductivity suggest helicenes as promising candidates exhibiting the thermo-power and piezoelectric effect.²

Optically pure helicene derivatives have also found applications in enantioselective organocatalysis⁷ (the first report on this topic comes from 1987)⁸, or as chiral ligands in transition metal complexes. For example, enantioselective Pd-catalyzed allylic substitution,⁹ Suzuki-Miyaura coupling,¹⁰ or catalytic hydrogenation have already been studied.^{11,12}

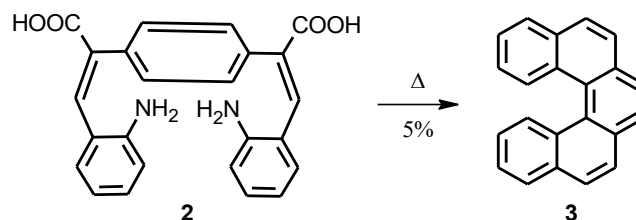
Other perspective applications of helicenes include chiral sensing of amines, alcohols, or phenols based on fluorescence quenching,¹³ or development of materials for circularly polarized light-emitting diodes taking advantage of their high fluorescence in the combination with an enormously high CD response.¹⁴ Furthermore, it is possible to use helicenes for enantioselective sensing.¹⁵

Very recently, helicene-based molecules applied in dye-sensitized solar cells were reported.¹⁶ They contained a push-pull system and were used in either molecular or polymeric form.¹⁷

Helicenes also found applications in materials science due to their second-order non-linear optical properties induced by supramolecular structure folding,¹⁸ or as electric field-responsive liquid crystals.¹⁹

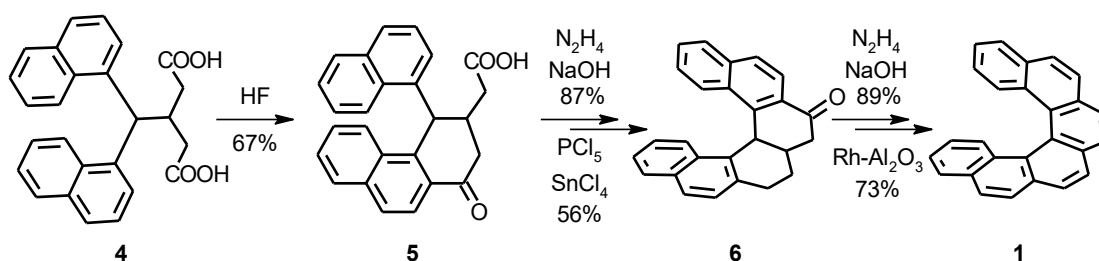
1.1.3 Synthesis

Synthesis of helicenes and helicene-like molecules is a challenging task, therefore it is natural that many different approaches have been developed since the first synthetic report on pentahelicene **3** in 1918 by R. Weitzenböck and A. Klingler²⁰ (**Scheme 1**). This Chapter briefly describes the synthetic methods leading to the longest reported helicenes.



Scheme 1: The first preparation of [5]helicene **3** under thermal conditions

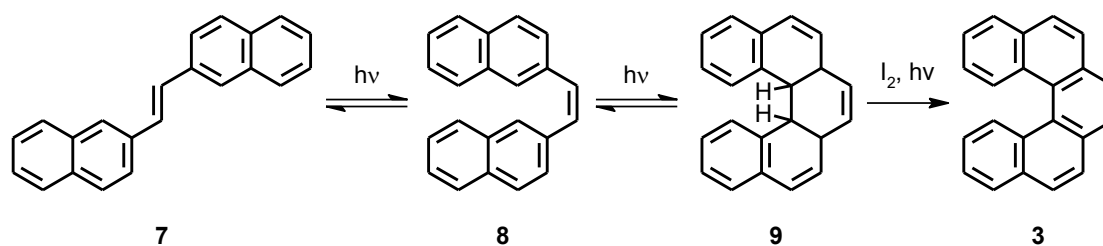
It took almost forty years before hexahelicene was prepared by M. S. Newman and D. Lednicer in 1955 (**Scheme 2**).²¹ It was published the following year and the synthesis consisted of ten steps.²² The two central rings of the [6]helicene **1** were built sequentially, one after the other. The first ring is closed by anhydrous hydrogen fluoride to provide the intermediate **5**. The ketoacid **5** is then reduced and cyclized *via* acyl chloride to yield **6**. The ketone **6** is then further reduced and dehydrated to give the hexahelicene **1**.



Scheme 2: Sequential synthesis of [6]helicene **1**

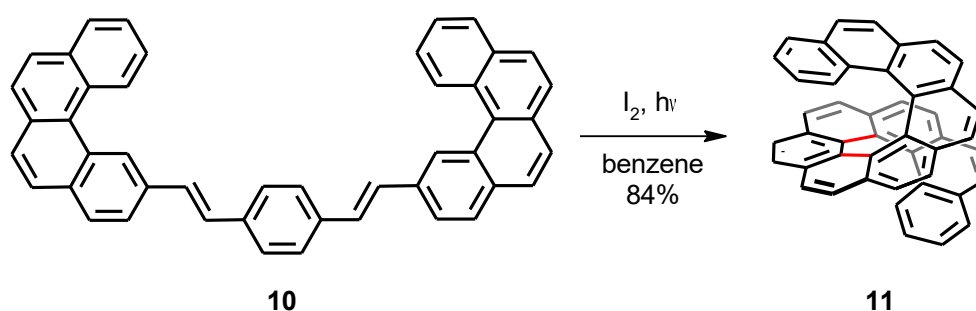
1.1.3.1 Photoinduced Cyclodehydrogenation

A decade later, in 1967, photocyclodehydrogenation (PCDH) was applied for the first time in the synthesis of [7]helicene.²³ This methodology used irradiation by a mercury lamp at ~450 nm in the presence of molecular iodine. The mechanism of PCDH was studied in detail at various stilbene derivatives including the naphthalene analogues and described in 1974 (**Scheme 3**).²⁴



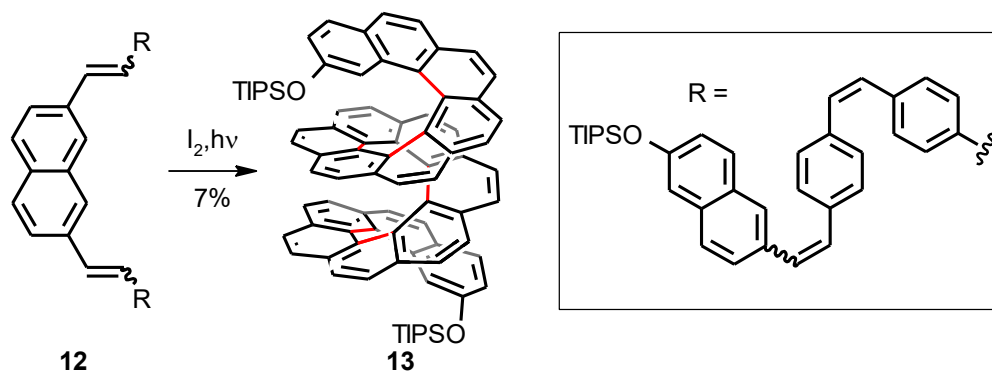
Scheme 3: Mechanism of PCDH shown on the synthesis of [5]helicene **3**²⁴

Even though only the *Z* isomer of the starting stilbene derivative gives rise to the desired helicene product, a mixture of *E/Z* isomers can also be used in the process due to their smooth isomerization under the photochemical reaction conditions. R. H. Martin and co-workers successfully used this synthetic method for the preparation of a homologous series of carbahelicenes, the longest representative was nonahelicene.²⁵ Later on, in 1975, even longer homologs, [11]helicene **11** (Scheme 4) to [14]helicene, were prepared using the same approach.²⁶



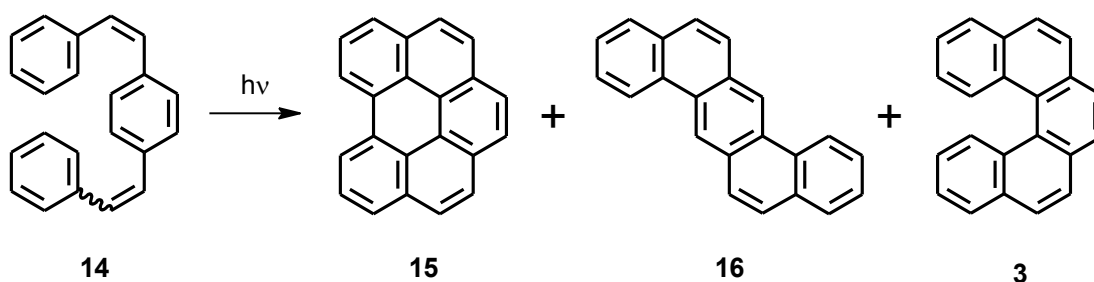
Scheme 4: [11]Helicene **11** prepared *via* photocyclodehydrogenation²⁶

Finally, in 2015, Makoto Fujita *et al.* applied sextuple PCDH reaction to prepare [16]helicene **13** derivative bearing two silylated hydroxy groups (Scheme 5), which could eventually be cleaved off to produce the parent hydrocarbon.²⁷



Scheme 5: Synthesis of [16]helicene **13** using PCDH²⁷

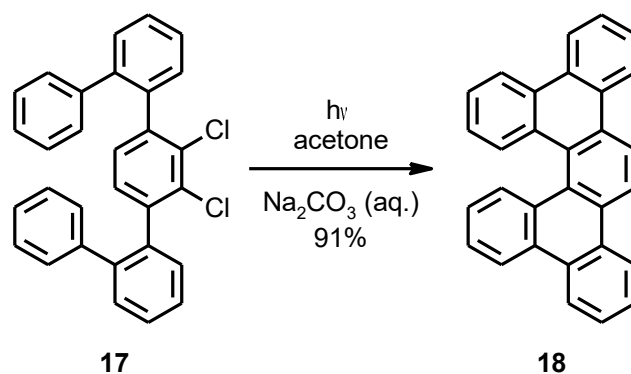
Careful design of the PCDH precursor is essential for good yields and regioselectivity in the synthesis of longer helicenes. In the case of [16]helicene **13**, only the precursor with the structure [2]+[1]+[1]+[2]+[1]+[1]+[2], where “[n]” is the number of *ortho*-fused benzene rings and “+” signifies the vinylene linkers, was found to give a decent yield of the desired product. Other sequences of stilbene units were vulnerable to form the side products with the motives of **15** and **16** (Scheme 6).²⁸



Scheme 6: Typical by-products of dehydrocyclization of precursor **14**

Even though PDCH reaction proved to be a powerful method for synthesis of a wide range of helicenes, it suffers from two main drawbacks. The first is a rather poor regioselectivity, which results in the formation of the dibenzoanthracene-type side product **16** beside the desired [5]helicene **3**. Moreover, some helicene products are susceptible to further oxidation under the reaction conditions, leading for example to benzoperylene **15** (Scheme 6).²⁸ A detailed study of the reaction conditions showed the possibility of suppressing overoxidation by adding a copper complex.²⁹ The second major disadvantage is the difficulty of controlling absolute stereochemistry. Attempts at application of either single- or dual-wavelength circularly polarized light for asymmetric induction so far failed to provide any decent enantiomeric excess of 0.8%.³⁰

A special type of the photochemical approach is the photochemical cyclodehydrochlorination (CDHC),³¹ which is an alternative to the Scholl reaction. Judging by the lack of side products, this reaction is expected to proceed *via* electrocyclization, resulting in good regioselectivity. Contrary to that, bromo and iodo compounds undergo the same reaction *via* a radical mechanism, generating all possible side products. The CDHC reaction was tested in the synthesis of various aromatic compounds such as triphenylene or dibenzo[5]helicene **18** (Scheme 7). Recently, the same methodology was used for the synthesis of helically coiled graphene nanoribbons,³² which are expected to behave as semiconductors, being similar to the graphene but with a well-defined band gap.

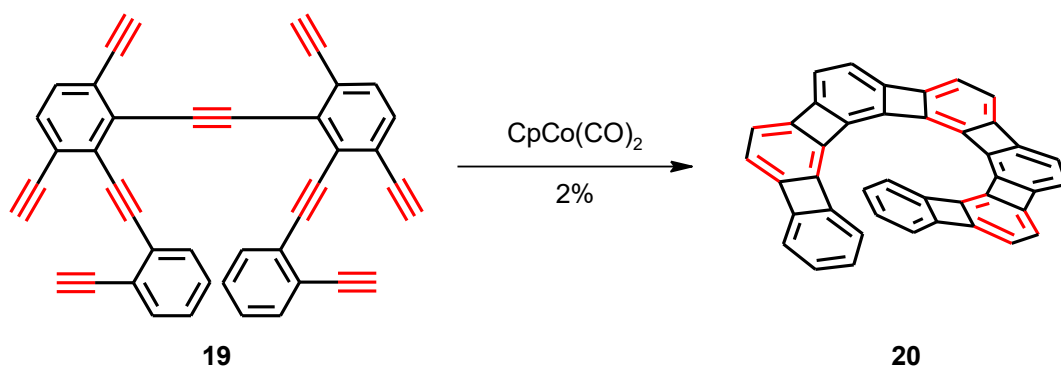


Scheme 7: Photochemical CDHC in the synthesis of dibenzo[5]helicene **18**³¹

1.1.3.2 [2+2+2] Cycloisomerization

Intramolecular [2+2+2] cyclotrimerization of alkynes is another type of reaction frequently used for the preparation of helicenes and helicene-like molecules.

Intermolecular trimerization of various acetylenes to form benzene derivatives was first observed by W. Reppe in 1948.³³ In 1986, K. P. C. Vollhardt reported a novel approach to the synthesis of angularly condensed polyaromatics with alternating aromatic benzene cores and antiaromatic butadiene rings using cobalt catalysis.³⁴ In principle, this methodology has a potential to be used for the synthesis of longer [n]heliophenes (where *n* is number of benzene rings in the structure). However, the yield of the cyclization step is quite low. Despite this drawback, [9]heliophene, containing altogether seventeen rings in the helix, was successfully prepared. The synthesis of the [7]heliophene **20** is shown in Scheme 8.³⁵



Scheme 8: [7]Heliphene **20** prepared *via* multiple [2+2+2] cycloisomerization³⁵

Experimental³⁶ as well as theoretical³⁷ studies suggest a mechanism shown in **Scheme 9**. After dissociation of labile ligands (carbon monoxide), two triple bonds are coordinated to cobalt to form the complex **21**. Unless trapped in a counter-productive cyclodimerization to the cyclobutadiene complex **28**, the catalytic cycle delivers the metallacyclopentadiene complex **22** with an available coordination site, which is then taken by the third acetylene unit to create the complex **23**. The η^4 -bound arene complex **26** is proposed to be formed *via* the bridged metallanorbbornadiene complex **24** or metallacycloheptatriene complex **25**. The structure of the proposed intermediate **26** is supported by the existence of similar η^4 -complex (**Figure 2**).³⁶ The catalytic cycle is completed by the release of the aromatic product **27** through the ligand exchange with two new alkynes.

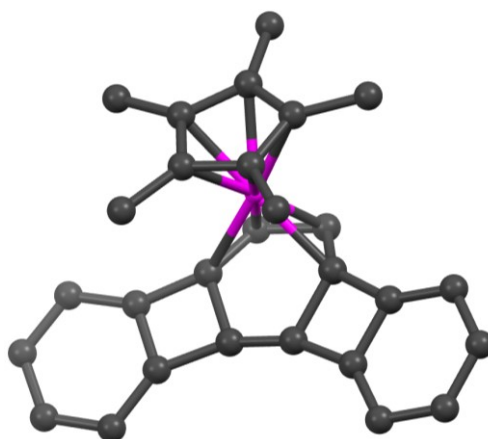
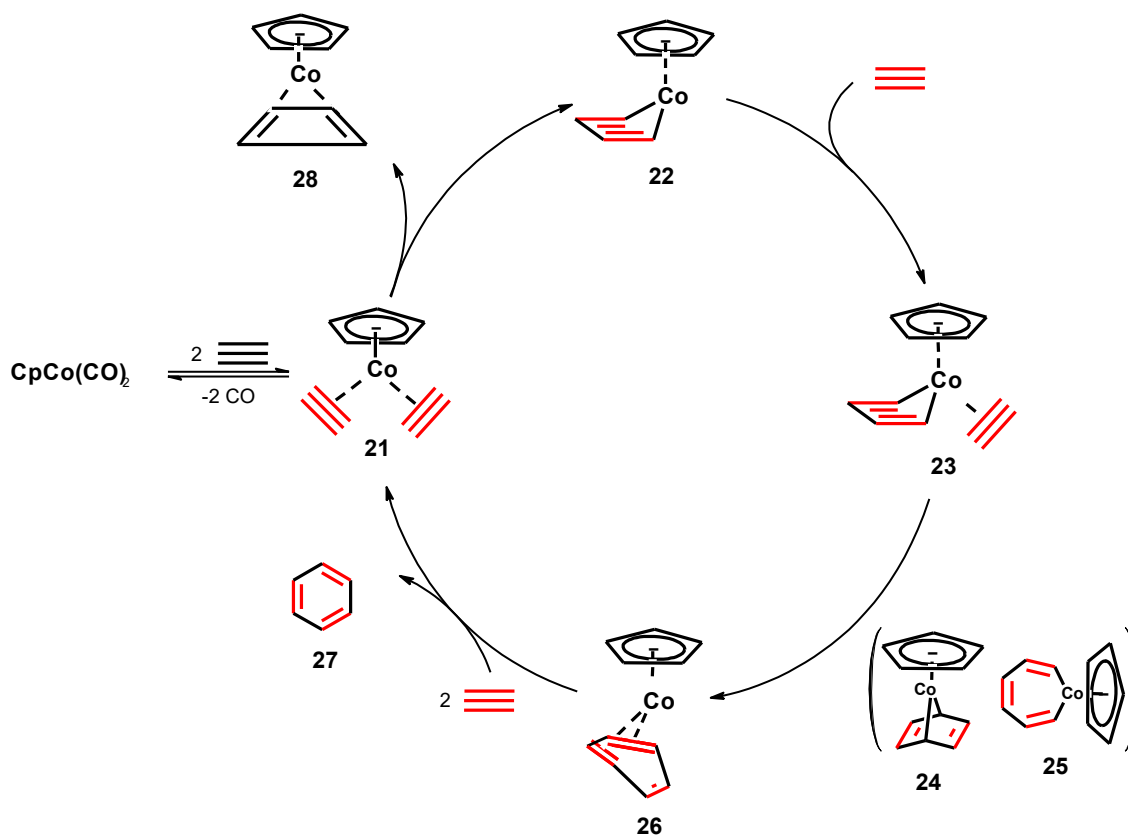
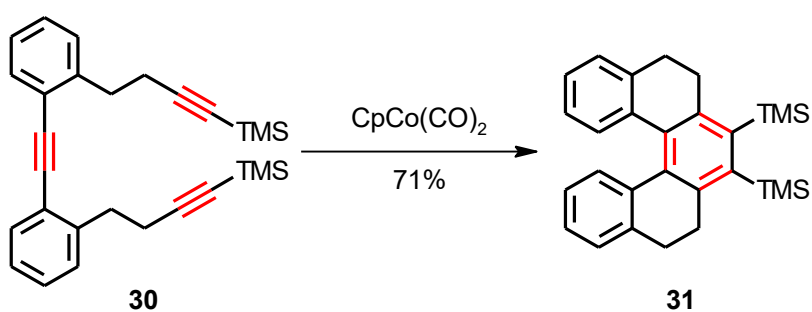


Figure 2: X-ray structure of Co(I) η^4 -complex [3]heliphene³⁶ (hydrogen atoms were omitted for clarity)



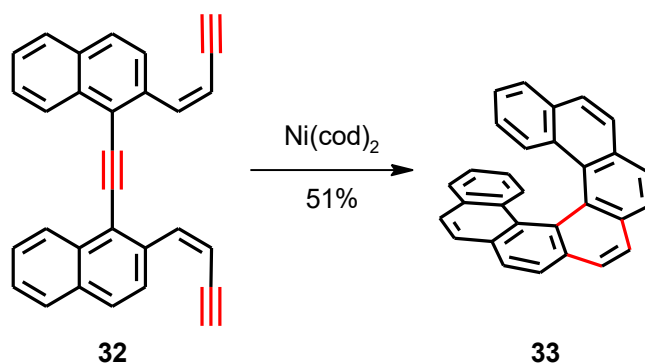
Scheme 9: Catalytic cycle of alkyne [2+2+2] cyclotrimerization

A novel concept of the synthesis of *ortho*-fused helicenes by means of intramolecular [2+2+2] cyclotrimerization of triynes was first published by I. Starý *et al.* (**Scheme 10**).³⁸



Scheme 10: Synthesis of tetrahydro[5]helicene **31**³⁸

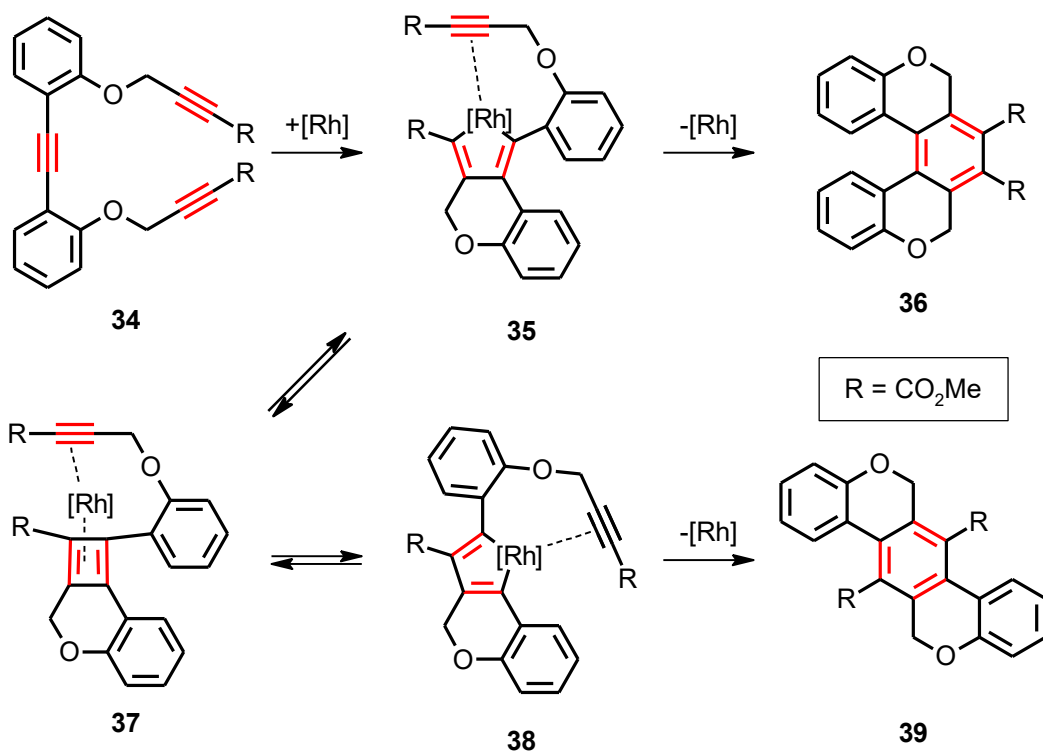
This approach was then extensively developed and a plethora of variously substituted [5]- to [7]helicenes **33** (**Scheme 11**) and helicene-like compounds have been successfully synthesized using transition metal catalysts based mainly on cobalt(I) or nickel(0).³⁹



Scheme 11: Synthesis of [7]helicene **33** by [2+2+2] cyclotrimerization of *cis,cis*-dienediene **32** mediated by a nickel(0) complex³⁹

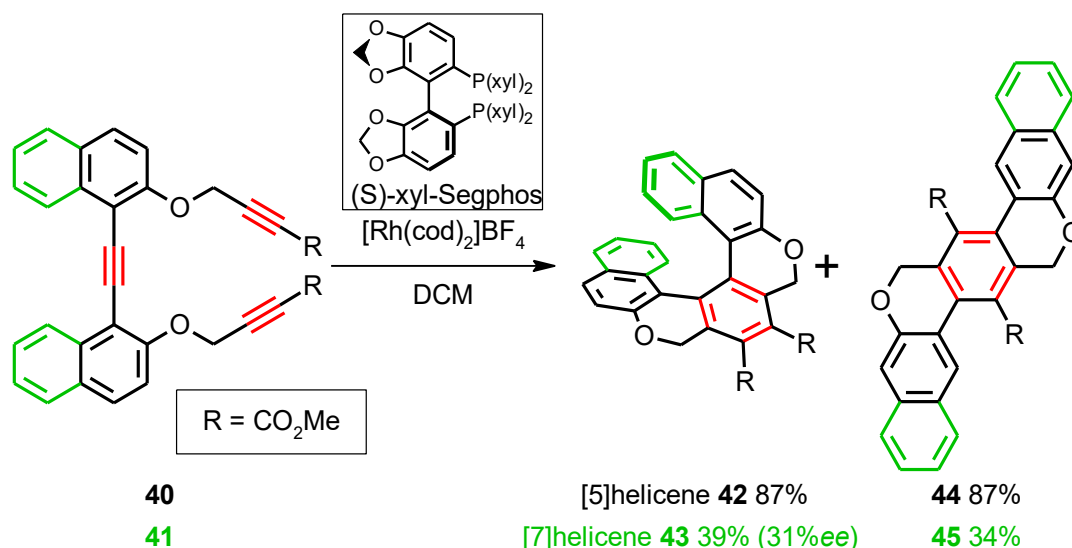
The reason why the formation of the aromatic core is so efficient is that during the cyclotrimerization step approximately 140 kcal·mol⁻¹ are released. This significant energetic gain is mostly the result of aromatization.

It is worth mentioning that rhodium(I) complexes are also frequently used as catalysts for the [2+2+2] cyclotrimerization and they provide very high turnover numbers. However, there is one drawback. Rhodium catalyzed cyclotrimerization, systematically investigated by Tanaka *et al.*,⁴⁰ has an additional reaction channel, the so called [2+1+2+1] cycloisomerization, which results in regioisomeric products with an anthracene-like structural motif. The main reaction pathway and the plausible side reaction channel are shown in **Scheme 12**. While the main reaction pathway leads to the desired helical product **36**, the side channel provides its regioisomer **39**. The mechanism of the competitive reaction involves the isomerization of the metallacyclopentadiene intermediate **35** to **38**, which proceeds *via* the butadiene complex **37**. The regioisomeric product **39** is then formed during the cyclization step.



Scheme 12: Mechanism of [2+2+2] vs. [2+1+2+1] cyclotrimerization of triynes under rhodium catalysis⁴⁰

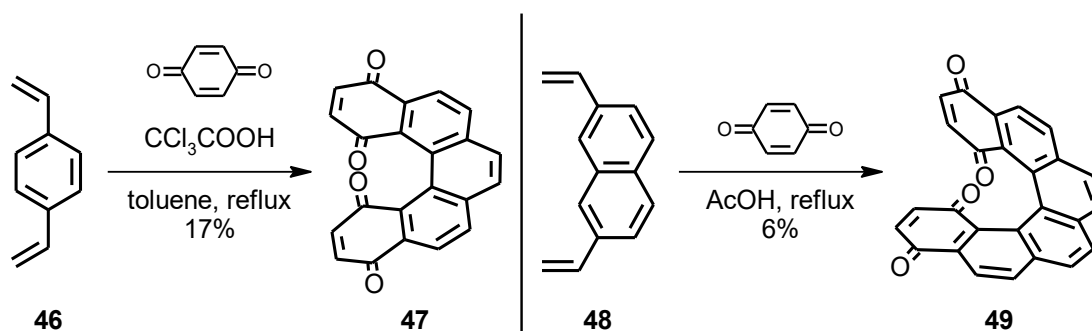
Despite of the presence of a side reaction channel, rhodium(I) catalyzed cyclotrimerization of alkynes was successfully used in the preparation of many helicenes. **Scheme 13** shows the compositions of the reaction mixtures when attempting the synthesis of [5]- and [7]helicene derivatives **42** and **43**, respectively.⁴¹ A similar approach was used to synthesize extended homologues, up to [11]helicene **60** (as mentioned later in **Scheme 20**).



Scheme 13: Rhodium(I) catalyzed [2+2+2] cyclotrimerization⁴¹

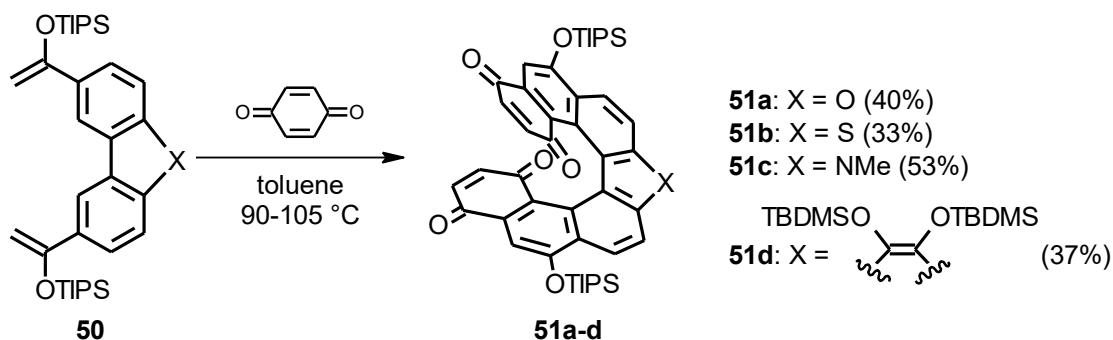
1.1.3.3 Other Methodologies

Diels-Alder reaction is another powerful synthetic tool, rewarded by the Nobel Prize, which found its use in the preparation of helicenes. It was first published by Liu and Katz in 1990 for the [5]helicene bis(quinone) **47** (Scheme 14).⁴² Two years later, the same approach was used in the preparation of the homologous [6]helicene bis(quinone) **49**⁴³ but, in both cases, the yields were rather low, 17% for [5]helicene **47**⁴² and 6% for [6]helicene **49**⁴³, respectively.



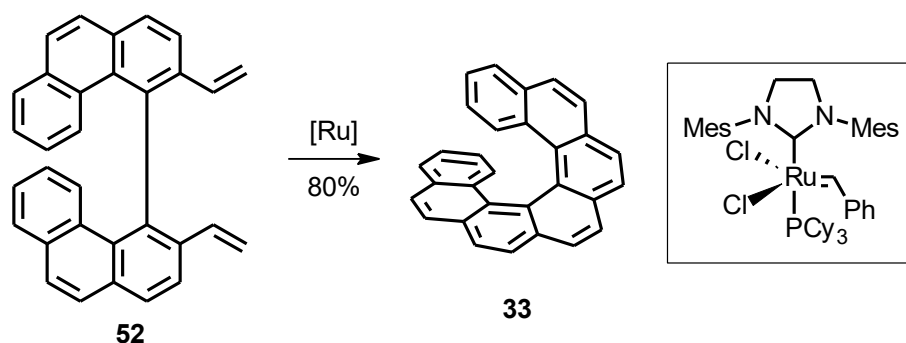
Scheme 14: Diels-Alder reaction applied to the synthesis of [5]helicene bis(quinone) **47**⁴² and [6]helicene bis(quinone) **49**⁴³

On the other hand, good efficiency of this methodology was proven by the multigram-scale synthesis of (hetero)[7]helicene⁴⁴ **51** and its derivatives (Scheme 15).⁴⁵



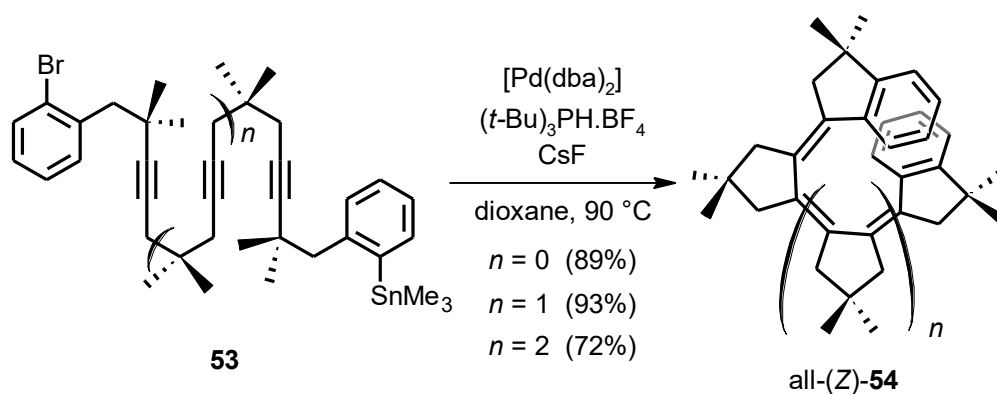
Scheme 15: Diels-Alder reaction applied to the synthesis of the [7]helicene-bis(quinone) derivatives **51**^{44,45}

In 2006, Collins and co-workers first used the ring-closing metathesis of olefins catalyzed by ruthenium complexes (Grubbs catalysts) in the synthesis of a series of [5]- to [7]helicenes, such as **33**, and their derivatives in good yields (**Scheme 16**).⁴⁶ However, this approach seems to be less suitable for the preparation of longer helicenes, because only one ring at a time is formed by the cyclization process and no reports on the synthesis of higher homologues by olefin metathesis have appeared in the literature since.



Scheme 16: Ring-closing metathesis in the synthesis of [7]helicene **33**⁴⁶

A very innovative approach with a novel point of view was demonstrated by Werz and co-workers in 2014.⁴⁷ They truncated the helicene scaffold down to a simple all-(*Z*)-configured polyene **54**. In this design, the helical shape as well as the π -conjugation is preserved. The helical scaffold is constructed in a cascade of carbopalladation reactions (**Scheme 17**). Up to five five-membered rings are formed in this domino sequence, which force the all-(*Z*)-polyene to fold into a coil. The longest truncated helicene prepared from tetrayne **53** ($n = 2$) is an equivalent of [11]helicene **54**.



Scheme 17: Truncated [11]helicene **54** prepared by carbopalladation of oligoyne⁴⁷

1.1.3.4 Nonracemic Helicenes and Methods of their Preparation

Racemization barrier, which is reflected by the configuration stability of the respective helicenes, is shown for the [5]-,⁴⁸ [6]-,²² [7]-,⁴⁹ [8]-⁴⁹ and [9]helicene⁴⁹ in **Figure 3**. It is clearly visible that the height of the barrier does not grow proportionally to the length of the helicene over the whole range, but rather levels off at approximately 45 kcal·mol⁻¹. Consequently, any helicene similar to or longer than [6]helicene **1** is conformationally stable at room temperature, whereas [5]helicene **3** racemizes readily at 25 °C.

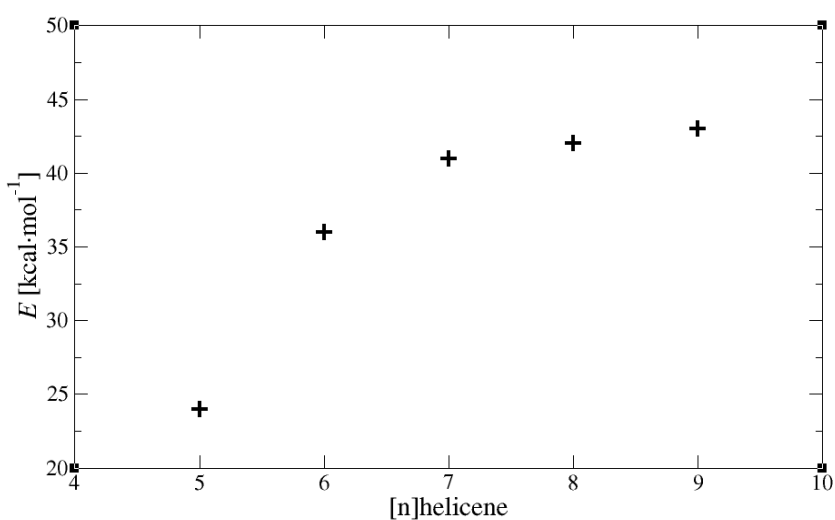
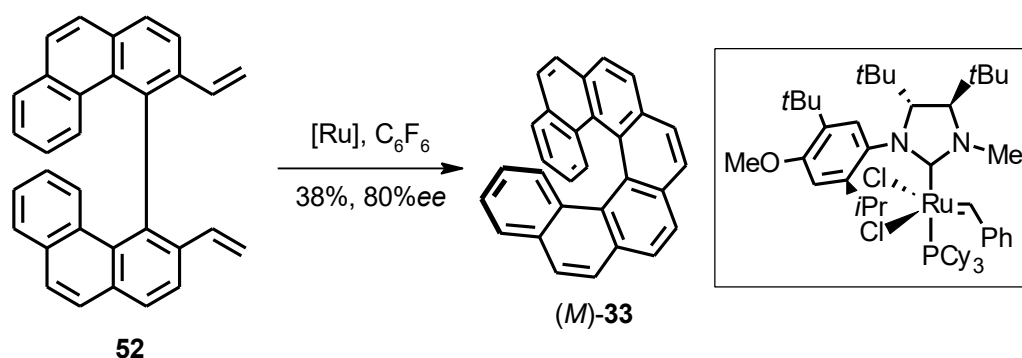


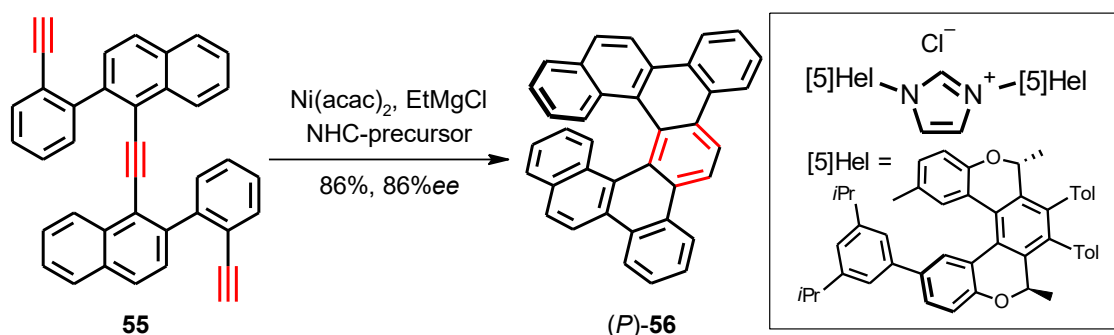
Figure 3: Racemization barriers of [n]helicenes (for $n = 5 - 9$)

Resolution of racemic helicenes by derivatization or co-crystallization with chiral auxiliaries or by chromatography on a chiral stationary phase still remains the most versatile approach to optically pure helicenes.⁵⁰ Nevertheless, several enantio- or diastereoselective synthetic methods have been developed over the recent years. The use of a chiral transition metal catalyst in the key cyclization step seems to be a promising concept, as the chirality of the catalyst can be directly transferred into the helicity of the final product. An illustrative example was reported in 2008: kinetic resolution of the racemic axially chiral **52**, which was subjected to ring-closing olefin metathesis, led to the enantioenriched (*M*)-[7]helicene **33** (Scheme 18).⁵¹



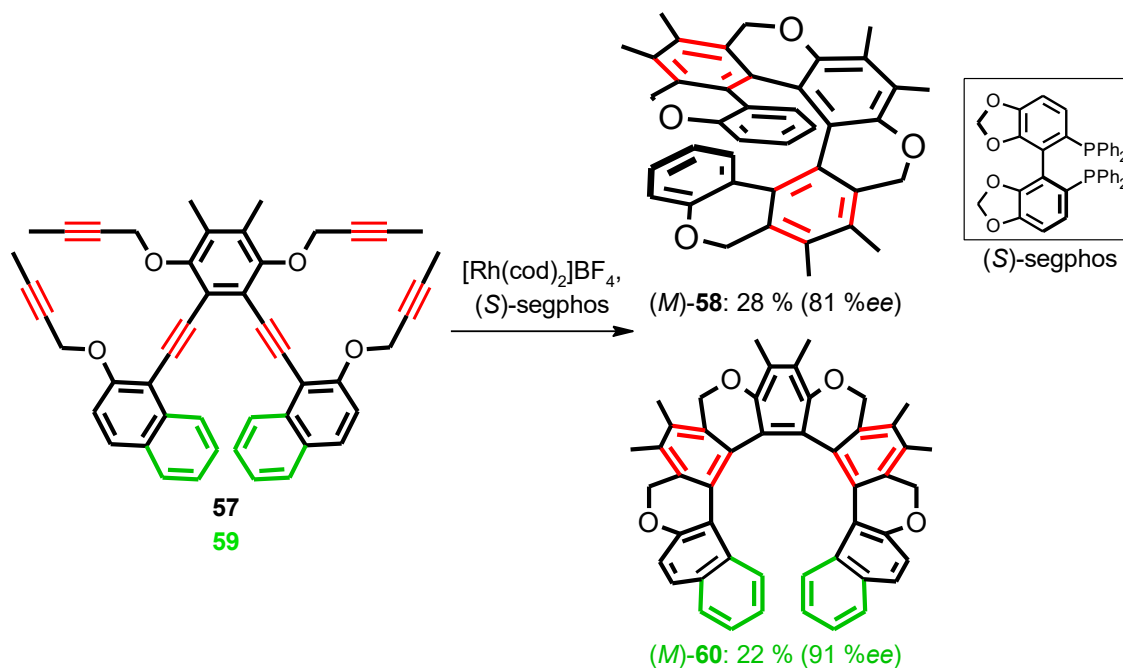
Scheme 18: Enantioselective ring-closing olefin metathesis in the synthesis of the enantioenriched [7]helicene **33**⁵¹

Recently, optically pure helicene-based NHC ligands⁵² as well as commercially available axially chiral phosphines such as QUINAP⁵³ were shown to be effective in controlling helicity of dibenzohelicenes produced by the nickel(0) catalyzed [2+2+2] cyclotrimerization of respective triynes, reaching up to 86%ee (Scheme 19).



Scheme 19: Enantioselective [2+2+2] cyclotrimerization of triyne **55** using helically chiral NHC ligands

Another example of a successful enantioselective synthesis based on [2+2+2] cyclotrimerization describes the use of an axially chiral phosphine ligand attached to cationic rhodium, as reported by Tanaka and co-workers (**Scheme 20**).⁵⁴ The level of stereoinduction was excellent, 91%*ee* in the case of [11]helicene (*M*)-**60**, albeit with moderate preparative yield of 22%.



Scheme 20: The use of the chiral rhodium-based catalyst in enantioselective [2+2+2] cyclotrimerization of hexaynes **57** and **59** to oxahelicenes **58** and **60** respectively

All of the above examples of enantioselective catalysis indicate a very limited substrate scope and incomplete transfer of chirality to obtain enantiopure helicenes. Contrary to that, the well-established method of diastereoselective [2+2+2] cyclotrimerization of centrally chiral triynes predictably provides diastereomerically and enantiomerically pure helicenes over a wide range of substrates.^{55,56} This general method, its principles were firstly demonstrated by Starý *et al.* on synthesis of helicene-like compounds in 2005,⁵⁷ is based on the thermodynamic preference of one of the diastereomers caused by steric repulsion (1,3-allylic type strain) between methyl and tolyl groups attached to the newly formed central benzene ring (**Figure 4**).

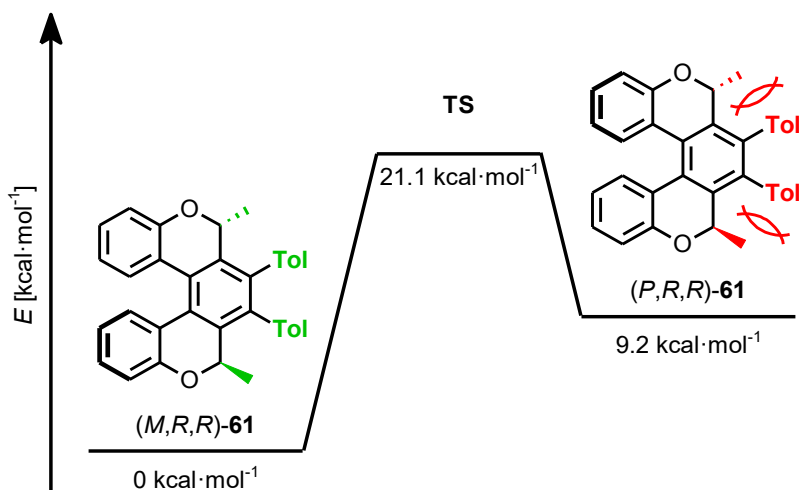
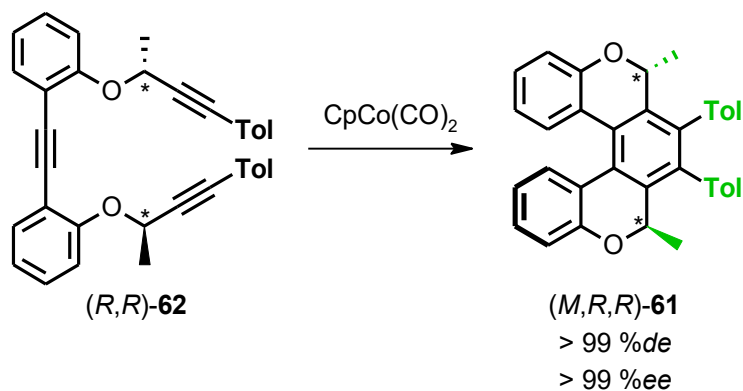


Figure 4: Energy profile of interconversion of (*M,R,R*) and (*P,R,R*) diastereoisomers of the oxa[5]helicene derivative **61** (Gaussian 09, B3LYP/cc-pVTZ)⁵⁵

Regardless of the barrier to epimerization, the stereochemical outcome of the reaction is always governed only by the energy difference between the two diastereomers. This allows the synthesis of the optically pure [5]helicene derivative (*M,R,R*)-**61**, in which the (*P*) helix is energetically disfavored. Thus, the absolute configuration on the carbon stereocenter(s) controls the resulting helicity (**Scheme 21**).



Scheme 21: Diastereo- and enantioselective [2+2+2] cyclotrimerization of the optically pure triyne (*R,R*)-**62** to the entio- and diastereomerically pure oxa[5]helicene (*M,R,R*)-**61**⁵⁵

1.1.3.5 Heterohelicenes

Helicenes containing heteroatoms in their backbone, such as nitrogen, sulfur, phosphorus, or the aforementioned oxygen, are generally called heterohelicenes. Phosphahelicenes^{58,59} were synthesized for use as chiral catalysts or ligands. However, only a few examples are known, as opposed to helicenes bearing phosphine groups, such as phosphahelicene (*P*)-**64** having the phosphorus atom incorporated in the helical scaffold of [7]helicene (**Figure 5**).

Azabora[6]helicene **63** and its higher homologues (up to azabora[10]helicene) were prepared using photooxidation as the helix-forming step.⁶⁰ All these compounds showed moderate to intense luminescence of nonpolarized as well as the circularly polarized light as the result of the boron atom incorporated in the helix being coordinatively bonded to the pyridyl nitrogen atom. The quantum yield depends on the number of boron atoms and the number of rings in the helix.

Very recently, a new class of silicon-containing helicenes was also synthesized employing rhodium catalysis.⁶¹ Another synthetic approach is based on a cascade carboboration reaction that results in closing the rings one by one during the single-step procedure.⁶² Surprisingly, no fluorescence was detected at silahelicenes such as **65**.

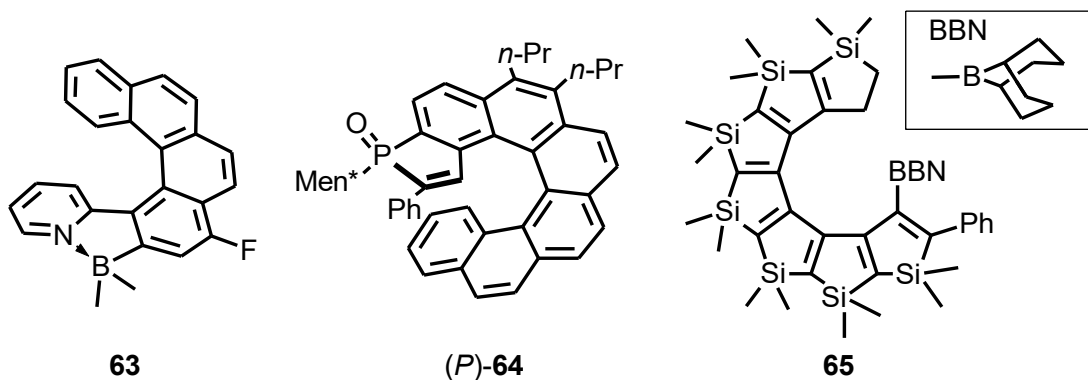


Figure 5: Azabora[6]helicene **63**,⁶⁰ phosphahelicene **64**⁵⁸ and silahelicene **65**⁶²

Azahelicenes are much more common compared to phosphahelicenes. The nitrogen atom(s) are usually part of pyrrole⁶³ or pyridine rings⁵³ that are integral part of the helicene scaffold (**Figure 6**). These compounds are mostly used as chiral catalysts or in on-surface/materials science. Especially the pyridine rings coordinate well to d-metals and are thus frequently used as anchoring groups. Synthetically, azahelicenes are prepared by chemical oxidation, photooxidation (**66**)⁶³ and also

[2+2+2] cyclotrimerization of nitrogen-containing heterocyclic triynes (**67**)⁵³ or diynenitriles, where the pyridine ring is constructed during the cyclization step (**68**).⁶⁴

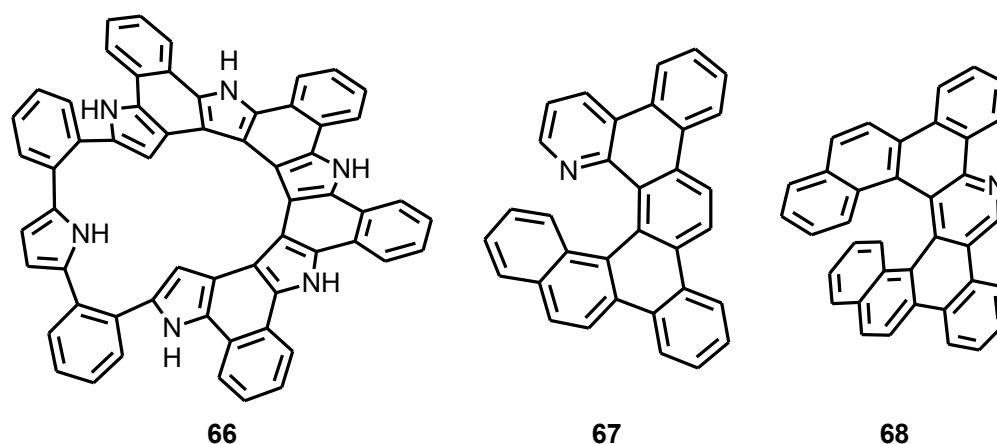
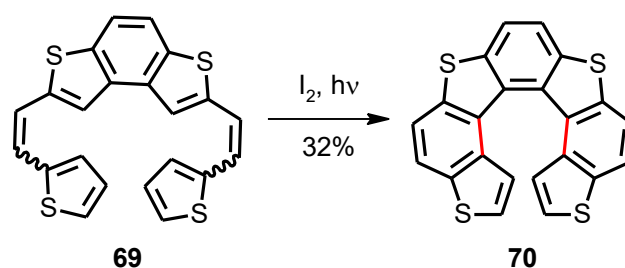


Figure 6: Representative azahelicenes

Thiahelicenes contain at least one thiophene ring in their helical backbone. The synthesis of thiahelicenes is commonly based on photocyclodehydrogenation of thienylethenes such as **69** to deliver the respective helical product such as the [7]helicene analog **70** shown in **Scheme 22**.⁶⁵

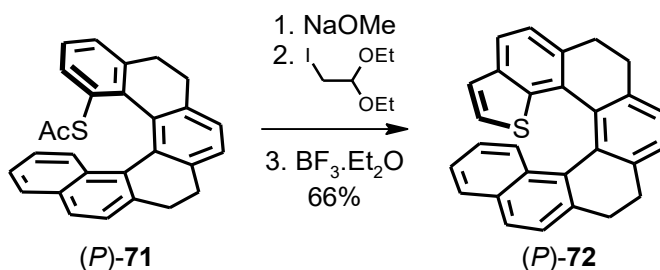


Scheme 22: Synthesis of tetrathia[7]helicene **70** by photocyclodehydrogenation of the respective heterocyclic diene **69**⁶⁵

This approach was firstly described in the late 60's.⁶⁶ Since then, the methodology was developed to afford up to [15]thiahelicenes.⁶⁵ However, the low yields of the cyclization step remain a serious disadvantage of this method, decreasing rapidly with increasing number of helix rings down to 8% for [15]thiahelicene.

Recently, an alternative synthetic pathway was described, in which the thiophene ring is constructed after the helix formation (**Scheme 23**).⁶⁷ The scaffold of (*P*)-**71** is prepared by nickel catalyzed [2+2+2] cyclotrimerization of the respective triyne⁶⁸ and the

thiophene ring is annulated in the last step, thus elongating the thiahelicene helix and delivering the product (*P*)-72.



Scheme 23: Annulation of the thiophene ring in the synthesis of thiahelicene (*P*)-72⁶⁷

1.2 Conductivity at the Nanoscale

The idea of molecular electronics and engineering arose in the 1950's and was published by A. von Hippel in 1956.⁶⁹ He proposed that the only way to satiate the “hunger” for new electronic materials is not to scale down the size of macroscopic electronic components but to design their properties and features directly at the level of molecules. The motivation for using the molecules in the “bottom-up” approach towards nanoscale electronics roots from easy modifiability of their structure. Also, molecules can be prepared as pure, uniform and well-defined species according to a relatively simple and reproducible procedures. The behavior of nanoscale electronics was predicted by Aviram and Ratner in 1974⁷⁰ and the theory is being continuously developed so that it can cover the newly discovered phenomena. But the experimental studies were enabled first with the rapid development of microelectronics, especially transistors⁷¹ and computers in the 80's. Several methods were designed and developed to study objects at the nanoscopic, molecular and even atomic level, for example scanning electron microscopy (SEM),⁷² atomic force microscopy (AFM),⁷³ scanning tunneling microscopy (STM)⁷⁴ and the break junction (BJ) technique.⁷⁵ The first report on the conductance of a single molecule was published in 1997 for 1,4-benzene dithiol (BDT) using the mechanically controllable break junction (MCBJ) technique.⁷⁶ Since then, many molecules were studied with respect to their single-molecule electrical properties.⁷⁷

1.2.1 Break Junction Techniques

This Thesis focuses on the BJ techniques used in the study of the single-molecule conductance. These techniques are described in more detail in this Chapter.

Several types of break junction experiments have been developed over the past decades. These techniques are designed to form nanoscale contacts and, especially, to study properties of single molecules.

Apart from a few scarcely used techniques such as the electromigration technique^{78,79} or electrochemical^{80,81} break junction, the majority of nanoscale conductance measurements has been performed by employing either a scanning tunneling microscopy-based break junction (STM-BJ) or mechanically-controllable break junction (MCBJ) techniques. Both of these are discussed in more detail in the following text. Even though the physical principle is the same in both types of experiments, there are significant differences in the device design: While the nanoscale contacts in the STM-BJ are asymmetric and the molecular junction is oriented vertically, in the MCBJ the contacts are symmetrical and the junction is horizontal. In both of these methods, piezo actuators are used to break and close the junctions to achieve sub-Å resolution.

1.2.1.1 General Principles

The conductance of the gold nanowire decreases proportionally to the cross-sectional area of the conductor as the junction stretches and the wire gets thinner. The diffusive conductance in bulk conductors is affected by atomic defects in the material and thermal dislocations of atoms in the crystal lattice. This behavior of bulk conductor can be described using classical continuum models, namely by Ohm's law (**Formula 1**),⁸² where A is the conductor's cross-section area, L is the length of the conductor and σ is the specific conductivity of the material.

$$G = \frac{\sigma A}{L} = \frac{I}{V} \quad (\text{Formula 1})$$

The conductance G is also defined as the quotient of the current I to the applied voltage V and it is constant in bulk conductors of the fixed geometry.

On the other hand, when the conductor width is reduced to the atomic scale, the electrode is not continuous at infinitesimal volume of the matter but is created by integer number of atoms. Due to the atomic structure of a conductor, continuum models fail and are no longer applicable. The discontinuity results in discrete conductance values, so called "conductance quantization". Therefore, step-wise conductance traces are observed with typical conductance values corresponding to $n \times G_0$ ($n = 1, 2, 3 \dots$). There is only a certain number of atoms in the cross-section of the contact and their individual

contributions to the total conductance value are roughly additive. The “conductance quantization” correlates also with the ballistic transport of the charge carriers (electrons), which can travel through the junction only at discrete energy levels, so-called transmission channels.⁸³ Furthermore, as the contact gets sharper more electrons can scatter back and the range of k-vectors that can participate in transmission (electron/hole transport through the junction is called transmission) gets narrower. The number of accessible transmission channels in a nanowire determines its total conductance, which is thus quantized in increments of G_0 . The G_0 (von Klitzing constant) has the value of $7.748091 \cdot 10^{-5}$ S, which corresponds to resistance of 12.9 k Ω . Mathematically, the total conductance is described by Landauer formula (**Formula 2**),⁸⁴ which sums up all transmission probabilities T_s of the transport channels at the energy equal to the potential μ . e is the elementary charge of the electron and h is the Planck constant.

$$G = G_0 \sum_n T_s(\mu) = \frac{2e^2}{h} \sum_n T_s(\mu) \quad (\text{Formula 2})$$

The theory was experimentally proven a few decades later by studying atomic contacts between metallic nanoelectrodes.⁸⁵

The above described conductance regime is typical for atomically sharp metallic contacts. It is called ballistic transport and it is elastic as the electron tunnels *via* available atomic orbitals without interaction and energy change.

The situation differs in the non-contact regime once the electrodes are separated. In general, several types of conduction mechanism come into play in the non-contact regime such as direct tunneling (**Formula 3**), thermionic emission, hopping conduction (**Formula 4**) or Fowler-Nordheim tunneling (field electron emission).⁸⁶ The two tunneling mechanisms, which determine the conductance of a system mostly at ambient temperature and voltage close to zero volts are described by **Formula 3** and **Formula 4** where tunneling current density J dependence on bias voltage V , temperature T , effective electron mass m^* , elementary charge e , insulator thickness d , Schottky barrier height (work function) Φ , Boltzman constant k_B , band activation energy of electrons ΔE , h reduced Planck constant

$$\text{Direct tunneling} \quad J \sim V e^{\left(\frac{-2d\sqrt{2m^*e\Phi}}{h}\right)} \quad (\text{Formula 3})$$

$$\text{Hopping conduction} \quad J \sim V e^{\left(\frac{-\Delta E/k_B T}{d}\right)} \quad (\text{Formula 4})$$

Even more interesting junctions can be formed when a nonlinear semiconducting element such as a molecule is placed between the metallic electrodes. This is called molecular junction and can be studied using techniques described later. Here, several features come into play: (i) Range of molecular orbitals, (ii) HOMO/LUMO gap and alignment of the Fermi levels, (iii) a localization/delocalization of the molecular orbitals, (iv) anchoring groups and their coupling to electrodes, (v) contact geometry *etc.* Also, the range of conducting regimes is extended, namely with possible inelastic tunneling, where the electron can exchange energy with the molecule, and hopping mechanisms.

All previously mentioned conduction mechanisms operate in electron transport processes at nanoscale and single-molecule level at the same time. In addition to the direct tunneling, the hopping mechanism usually plays the most important role in molecules. This type of conduction mechanism relies on their ability to move the charge through localized states. A so called multiple trapping takes place in larger molecules, which is defined as a series of jumps between several localized states, leading inevitably to lower conductance of these molecules. All these events, including fluctuation of the coupling between the metallic electrodes and the molecule's anchoring groups, attribute to the broadening of conductance peaks in the measurement.⁸⁷

Formula 5⁷⁷ describes the influence of the contact with the electrode on the total conductance of the metal-molecule-metal junction. This simplified form is valid only for the case of symmetrical contacts (a symmetrical molecule is attached between the metallic electrodes made of the same metal). Here Γ is the effective coupling between the anchoring group and the electrode, and Δ is the difference between Fermi energies of the molecule and the metal.

$$G = \frac{2e^2}{h} \frac{4\Gamma}{\Delta^2 + 4\Gamma^2} = G_0 \frac{4\Gamma}{\Delta^2 + 4\Gamma^2} \quad \text{(Formula 5)}$$

The molecular conductance can be calculated using more sophisticated transport theories, such as non-equilibrium Green's function approach (NEGF)^{88,89} with density functional theory (DFT) method, or using semi-empirical methods such as Slater-Koster tight-binding model.

The basic principle of an experimental conductivity measurement at nanoscale is quite simple (**Figure 7**). A metallic conductor is stretched by the external force and thinned till it breaks thus resulting in two separated atomically sharp electrodes. During the process of linear electrode separation the distance-dependent (resp. time-dependent)

current is recorded at a constant voltage. Time-dependent current provides the so called “breaking curves” (**Figure 7**). Alternative expressions which are used for the time dependent current are “breaking traces”, “conductance curves”, or “conductance traces”.

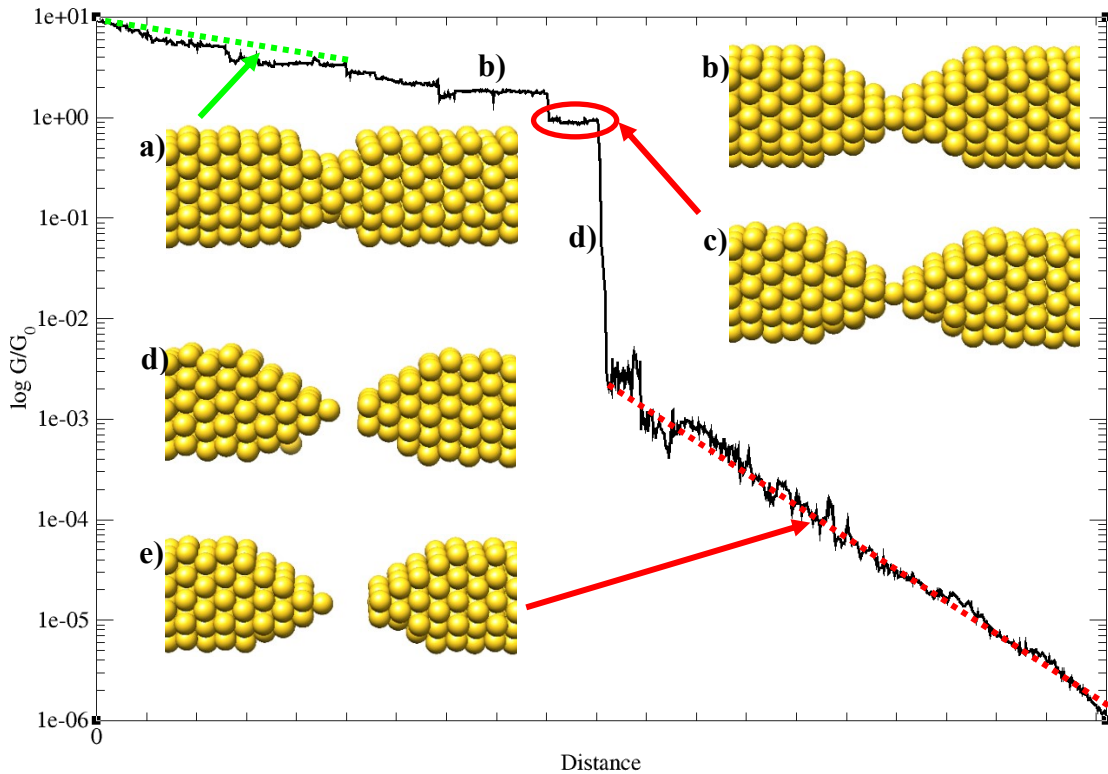


Figure 7: Typical breaking curve of a gold wire (black line) with corresponding electrode geometries; (a) bulk electrode (continuous conductivity; green dotted line); (b) 2-atom contact with conductance $2 G/G_0$; (c) 1-atom contact with conductance $1 G/G_0$ (red ellipse); (d) snap-back (a moment of interruption); (e) direct tunneling, exponential conductance decay (red dotted line)

Events at atomic level are typically chaotic, unpredictable and cannot be controlled by the BJ experiment, especially at room temperature, which necessitates statistical processing of the acquired data.⁹⁰ The breaking-curves data (**Figure 7**) are accumulated over a certain period of time, because a single conductance trace has a very limited interpretation value. The linear electrode separation simplifies the statistical processing, because all acquired values have the same statistical weight. Then the data are statistically processed into the form of conductance histograms (**Figure 8**).⁹¹

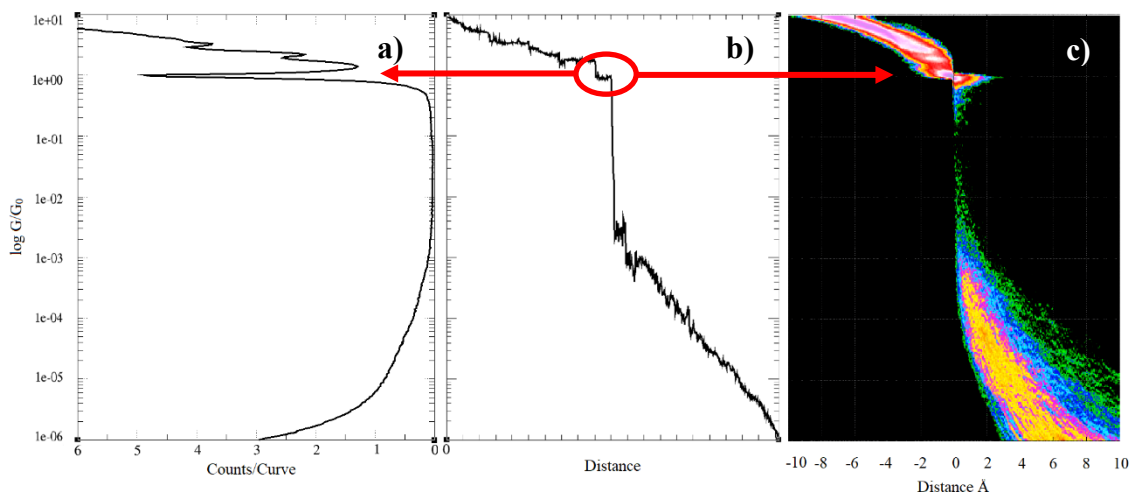


Figure 8: (a) A typical logarithmic conductance histogram of gold (constructed from ~ 12000 curves); (b) a single conductance curve; (c) 2D histogram (constructed from ~ 12000 curves)

Values in histograms are usually normalized to the number of curves. Two types of histogram are typically used for data representation: (i) linear (with linear scale on current axis); (ii) logarithmic (with logarithmic scale on current axis). The linear histogram is only useful for a range of up to one decade, whereas the logarithmic one easily covers several orders of magnitude. Stability and preference of an individual conductive conformation (density of state at the given conductance) is represented by the number of counts at the corresponding conductance level (histogram bin matching to the conductance interval).⁹² In other words, the peak in the spectrum corresponds to accumulations of certain conductance values during the measurement. Single gold atom bridge conductance is highlighted in red oval (**Figure 8b**). The corresponding peaks in logarithmic histogram (**Figure 8a**) and 2D histogram (**Figure 8c**) are pointed with the red arrow. A 2D histogram (**Figure 8c**) can be constructed by correlating conductance traces with the separation distance of the electrodes, providing additional information about the effective length of the molecule trapped in the junction.^{91,93}

When a molecule is attached between the metallic electrodes, the conductance of the system does not decrease exponentially with the increasing electrode separation (**Figure 9**). This event results in an appearance of (i) plateaus in the conductance traces (**Figure 9b**); (ii) peak in the logarithmic histogram (**Figure 9a**) and (iii) peak in the 2D histogram (**Figure 9c**). Broadening of the conductance peak in the histogram correlates

to various junction configuration (*e.g.* molecule binding angle, internal molecule rigidity, molecule length *etc.*).^{90,94}

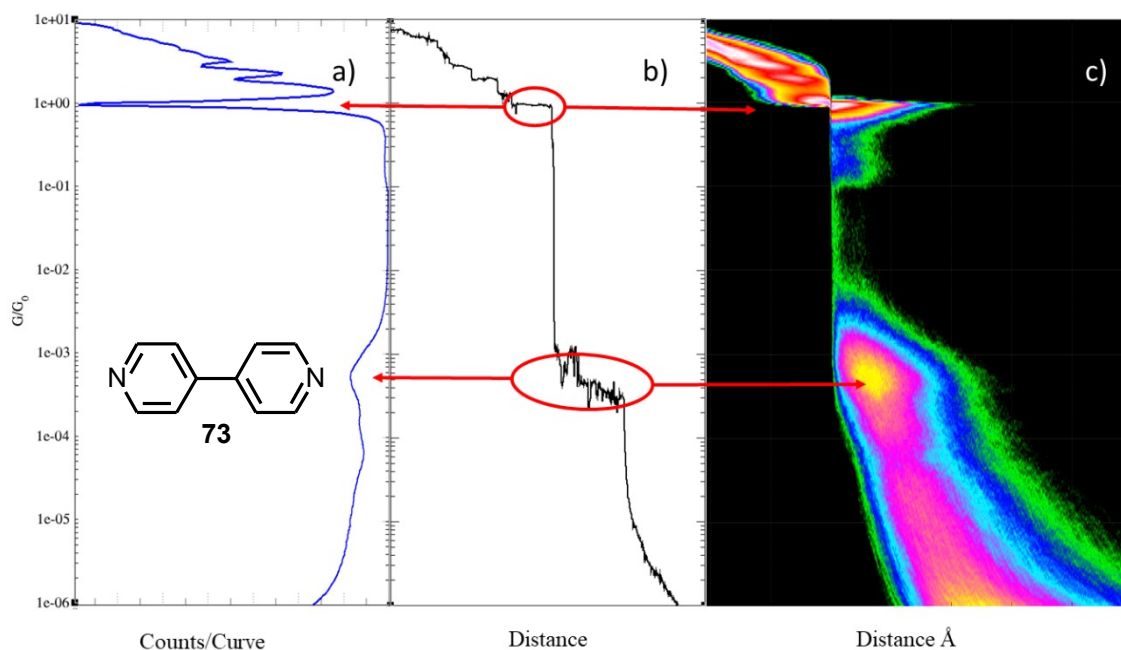


Figure 9: (a) A typical logarithmic conductance histogram of 4,4'-bipyridine **73** (constructed from ~32000 curves); (b) a single conductance curve; (c) 2D histogram (constructed from ~32000 curves)

1.2.1.2 Mechanically Controllable Break Junction

The term of “mechanically controllable break junction” (MCBJ) was first introduced in 1992⁹⁵ for an extension of the previously used break junction technique⁷⁵. A simplified scheme is shown in **Figure 10**.

A gold lead with a free-standing under-etched constriction d (bridge or junction) in its middle is placed on an electrically insulated flexible substrate with thickness t . The insulator layer (grey in **Figure 10**) is usually made of a polyimide film (Kapton) due to its high resistivity of $\sim 10^{16} \Omega \cdot \text{cm}$, chemical, mechanical, and thermal stability, and also good adhesion to various materials. For the flexible substrate, which must survive thousands of bending cycles, elastic materials such as phosphorus bronze or spring steel are used.⁹⁰ A pushing rod presses from the bottom against the gold bridge while the sides of the substrate are held in position by two counter blocks. The junction is stretched until it breaks with electrodes separation s (**Figure 10b**). Ideally, this results in two atomically

sharp electrodes, which can be brought back into contact by relaxing the substrate (retraction of the pushing rod; **Figure 10a**).

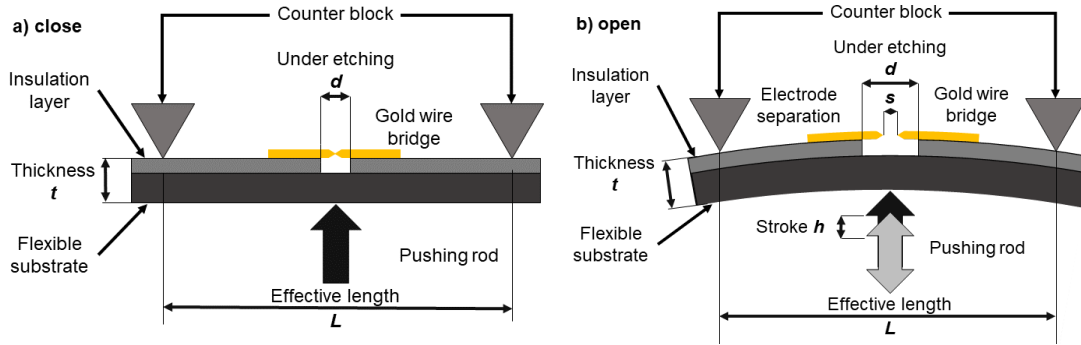


Figure 10: Schematic drawing of a mechanically controllable break junction experiment: (a) closed bridge; (b) open bridge

The distance between separated electrodes s can be adjusted with a sub-Å accuracy by moving the pushing rod. The precision depends on the value of the attenuation factor r (**Formula 6**), which is an expression of the gearing property given by the specific geometry of the particular substrate (chip). Electrode separation s is proportional to the stroke h , the under-etched length of the bridge d and the chip total thickness t divided by the second power of chip effective length L (**Formula 6**).⁹⁶ Typical values of r are usually in the order of 10^{-5} .

$$\Delta s = r \Delta h = \left(\frac{6dt}{L^2} \right) \Delta h \quad (\text{Formula 6})$$

Main advantages of the MCBJ technique are: (i) high mechanical stability of the contact formed, (ii) short distance and fixed geometry of the electrodes together with a large attenuation factor enabling adjustments of the gap (s) with sub-Ångström resolution.

1.2.1.3 Scanning Tunneling Microscopy-Based Break Junction

In the STM-BJ^{97,98} experiment, the electrode system is asymmetric, one of the electrodes is a horizontally oriented flat metallic surface, whereas a very sharp tip, approaching the surface in a perpendicular direction, serves as the other electrode (**Figure 11**). The instrument is very similar to a scanning tunneling microscope⁹⁹ and thus, in principle, also allows nanoscopic imaging of the surface of the planar electrode. The most significant difference in the experimental setup between MCBJ and STM-BJ is

the direct connection of the metallic (usually gold) tip to the piezo actuator in the STM instrument. Due to the absence of any gearing effect, a much higher precision of the actuator motion control is required.

In the imaging mode of the STM technique, a non-contact current is usually measured. When compared with the MCBJ, the conductance may be lower by up to several orders of magnitude. However, in the contact regime the results do not differ significantly.

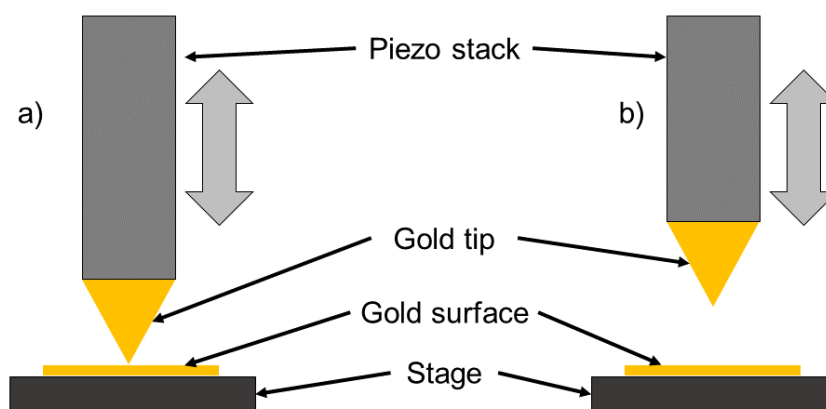


Figure 11: Schematic drawing of a STM-BJ experiment: (a) closed junction; (b) open junction

The main advantage of this technique is the possibility of STM imaging directly before the single-molecule conductance experiment, simpler setup, faster data acquisition and lower contamination, especially in the case of an UHV apparatus.

1.2.1.4 Materials Used in the Break Junction Techniques

Various materials are used as electrodes in single-molecule conductance measurements such as highly oriented pyrolytic graphite (HOPG),^{100,101} semiconductors (e.g. GaAs),^{102,103} and especially metals, which are generally preferred in both of the break junction techniques introduced above, with gold being the ultimate material of choice.^{76,97,104}

Under ambient conditions, gold is advantageously used for its ductility and inertness towards oxidation by oxygen in the air. In comparison, both of the other noble metals, silver and copper, readily form oxides. These oxides form a semi-conductive layer, which strongly interferes with the conductance measurements.¹⁰⁵

When breaking the junction, all three of the noble metals from the group 11 prefer to form one-atom contacts with one accessible transmission channel. As explained above, the stability of the contact corresponds to the bin-counts in the respective histogram (**Figure 12**). As shown in experiments performed at 4.2 K in UHV, the three linear histograms for copper, silver and gold display a high level of similarity, which is caused by the comparable electronic properties of atoms with electron configuration $d^{10}s^1$.¹⁰⁶

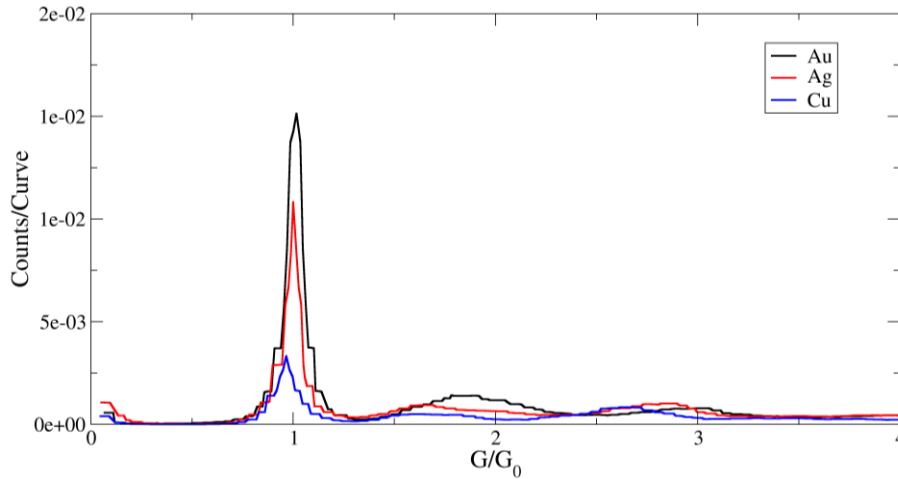


Figure 12: Linear conductance histograms of pure $d^{10}s^1$ metals¹⁰⁶ (group 11 of the periodic table)

This simplified view based only on the number of valence electrons correlates well with the observations on other d-group metals, which have two electrons in their valence shell such as nickel¹⁰⁷ or platinum¹⁰⁸. Their electron configuration is d^8s^2 (**Figure 13**).

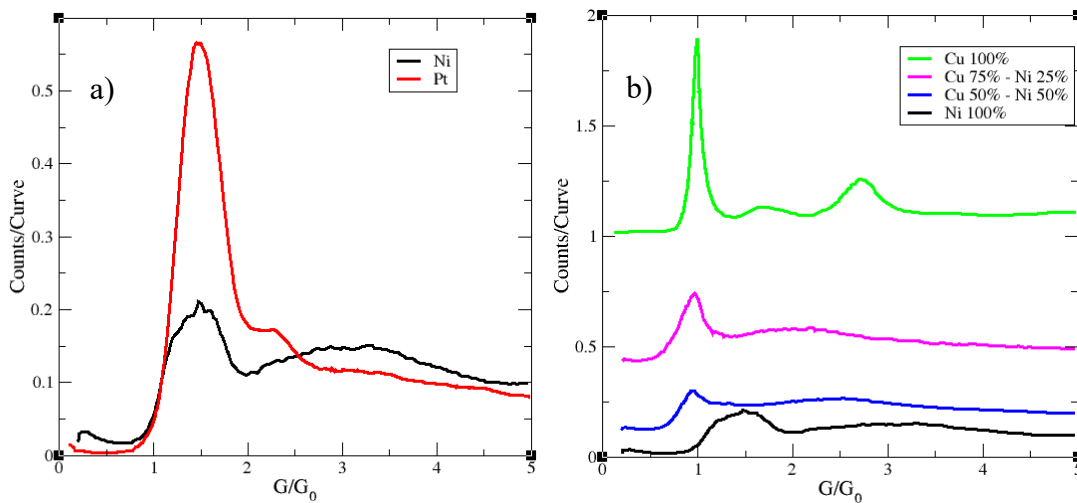


Figure 13: Comparison of conductance histograms of elements in the group 10: (a) nickel¹⁰⁷ and platinum¹⁰⁸; (b) alloy of nickel and copper¹⁰⁷

Purity of the material used as electrodes also plays a very important role in the metal-metal bridge formation because contaminants can strongly influence the contact structure, thus causing the broadening or even vanishing of peaks in the conductance histograms as a result of too many contact states (**Figure 13b**).¹⁰⁷

1.2.2 Conductance of Organic Molecules

Molecules to be investigated at the molecular level using the break junction techniques need to be equipped with anchoring groups, which are suitable to bind the molecule to the bulk material of the electrode. An anchoring group is a part of the molecule, which has a high affinity to the electrode surface.

A number of different anchoring groups have been investigated in the last few decades in order to elucidate their on-surface behavior and conductance properties.^{77,109–111} The most frequently studied ones are thiols,¹¹² despite the complexity of their bonding motifs. It was shown that many redox events take place on the gold surface and the thiols spontaneously disproportionate to form, for example, disulfides.¹¹³ Various modes of thiophenol bonding to the gold surface are shown in **Figure 14**.

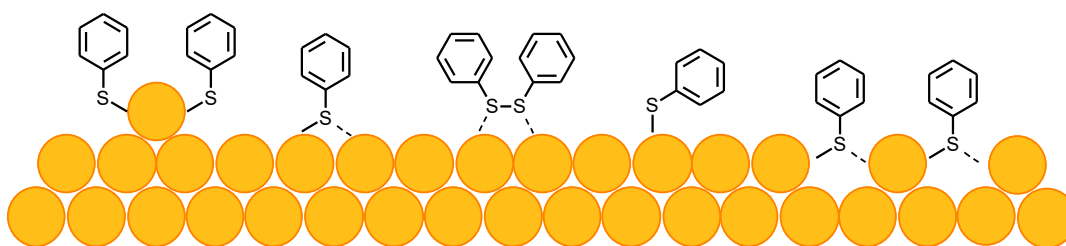


Figure 14: Thiol-gold binding motifs¹¹³

Quantitatively, an anchoring group can be characterized by the bond strength, which can vary from coordination to covalent bonding or even ionic bonding. The bond strengths between gold and several common anchoring groups are summarized in **Table 1**.

Anchoring group	Bond rupture force (nN) ¹¹⁴	Bond dissociation energy (kJ/mol) ¹¹⁵
R-S-Au	1.5	253.6 ± 14.6
Pyridine-Au	0.8	
R-P(Ph) ₂ -Au	0.8 (R = CH ₂)	
R-CN-Au	0.64 (R = Ph)	
R-SH-Au (S coord)	0.6 (R = Alkyl)	60-80
R-SH-Au (SH coord)	0.5 (R = Ph)	~60
R-NH ₂ -Au ¹¹⁶	0.48 (R = Ph)	76 (NH ₃)
R-NO ₂ -Au	0.32 (R = Ph)	
Au-C ₆ H ₆		8.4
Au-Au (chain)	1.5	235

Table 1: Bond strengths between anchoring groups and gold^{114,115}

Another important property is the stability of the anchoring group towards chemical degradability through hydrolysis, oxidation, or protonation. A few specific examples of such transformations are shown in **Table 2**. Importantly, all of these transformations change the binding strength as well as geometry and consequently also the overall conductance properties of the molecular junction. Thiolates are easily oxidized by air to disulfides (**Entry 1**), phosphines to phosphine oxides (**Entry 3**) and N-heterocyclic carbenes to imidazoli(di)ones or they can dimerize (**Entry 4**). Thioacetates can slowly hydrolyze to thiols (**Entry 2**) and amines (or nitrogen heterocycles) may be protonated (**Entry 5-7**).

Entry	Process
(1) ¹¹⁷	$2 \text{R-S}^- \xrightarrow{\text{O}_2} \text{R-S-S-R}$
(2)	$\text{R-S-C(=O)CH}_3 \xrightarrow{\text{H}_2\text{O}} \text{R-SH}$
(3)	$\text{R-P(CH}_3)_3 \xrightarrow{\text{O}_2} \text{R-P(=O)(CH}_3)_3$
(4) ^{118,119}	
(5)	$\text{R-NH}_2 \xrightarrow{\text{H}^+} \text{R-NH}_3^+$
(6) ¹²⁰	
(7) ¹²¹	$\text{R-pyridine} \xrightarrow{\text{H}^+} \text{R-pyridinium}^+$

Table 2: Chemical processes affecting properties of anchoring groups

Unfortunately, the sulfanyl moiety as the widely studied strong anchoring group suffers from a serious disadvantage, which is oxidability (**Entry 1**). Dithiol molecules polymerize and coordinate to the gold surface in the similar fashion as original monomers. The resulting mixture of the analyte and byproducts of oxidation is poorly reproducible and much more difficult to be interpreted. Moreover, benzenedithiol as the simplest representative of aromatic dithiols, forms chain-like oligomers with incorporated gold atoms and clusters, due to the comparable Au-S and Au-Au bond strength.¹¹⁷

Very recently, carbenes, namely N-heterocyclic carbenes (NHC)¹²² have become hot candidates for on-surface studies due to their bond strength and directionality. However, carbenes are incompatible with ambient conditions as they are unstable in air, moisture sensitive and tend to dimerize.¹²³ Therefore NHCs can only be used with the UHV techniques. Metal atoms can also be used as anchoring groups, organotin derivatives being a good example.¹²⁴ In this case, transmetalation reaction takes place to form an Au-C bond. The pyrazole ring shows a very strong double-bonding interaction with metals, employing both of its nitrogen atoms.¹²⁰ Moreover, a significant enhancement of conductance was observed at deprotonated pyrazoles. The carboxylic

group^{125,126} is yet another example of a bidentate anchoring group, although it is much weaker than the pyrazole one. Phosphines are generally excellent ligands for many metals, so it is not surprising that phosphorus containing substituents work as good anchoring groups as well.^{109,127,128}

The conductance of the wire-like organic molecules itself is mainly influenced by the degree of conjugation¹²⁹ and its total effective length^{130,131}. An additional function can be introduced into the molecule by inserting various fragments with interesting nonlinear electronic behavior such as redox active tetrathiafulvalenes^{132,133} (**74**), ferrocenes¹²⁶ (**75**), metal complexes¹³⁴ (**76**) (endowing molecules with magnetic properties), donor-acceptor (D-A) systems^{77,135} (**77**) (introducing the push-pull effect), or electronically nonsymmetrical alkane segments (**78**)¹³⁶ (working as molecular rectifiers) (**Figure 15**).

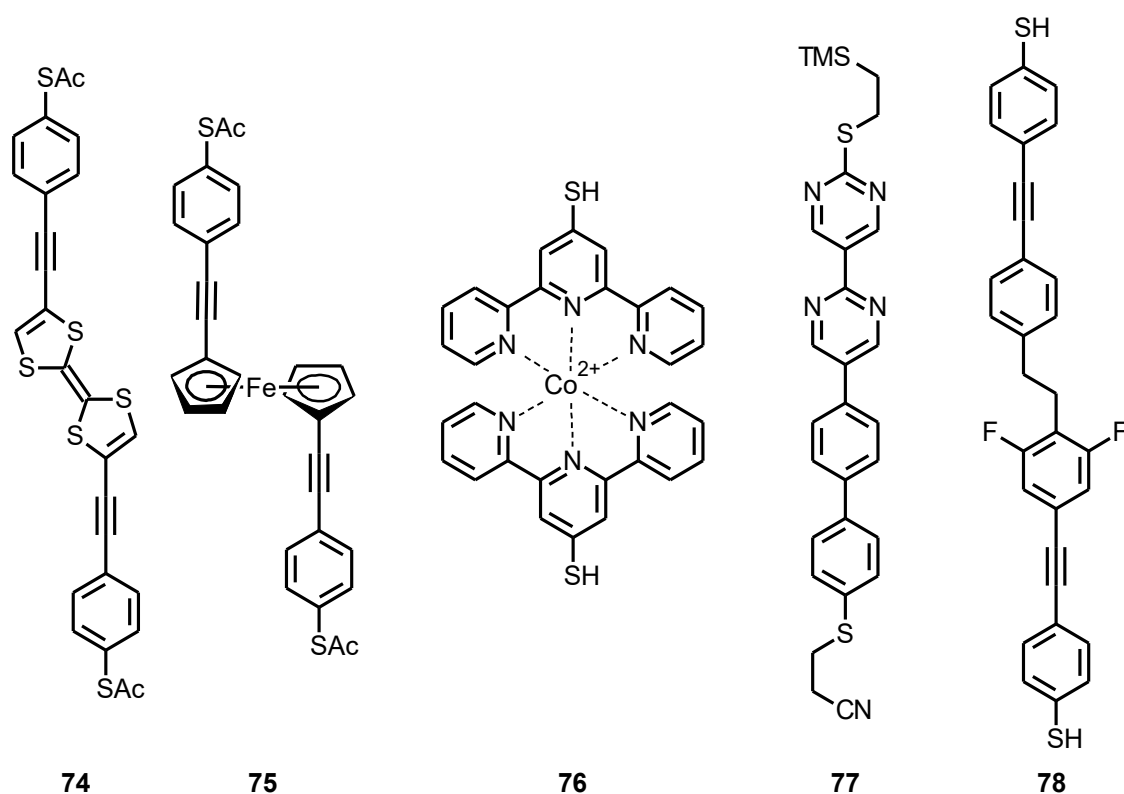


Figure 15: The redox active TTF derivative **74**¹³³ and ferrocene derivative **75**,¹²⁶ cobalt(II) complex¹³⁴ **76** utilized in the spin-dependent transport, D-A system **77**,¹³⁵ or molecular rectifier **78**¹³⁶

So far, not many systematic studies on the single-molecule conductance behavior of different molecular classes have been published.¹¹¹ The dependence of conductance on the effective length of a molecule was nicely described by the Venkataraman's group,

who studied a series of alkanes, silanes and siloxanes by the break junction techniques.¹³¹ The drop of conductance experimentally obtained within particular sets of molecules was approximately 0.78 G_0 per Å for alkanes, 0.36 G_0 per Å for silanes and 1.86 G_0 per Å for siloxanes (**Figure 16**). This finding somewhat correlates with the difference in macroscopic behavior of silicon (semiconductor) and silicon dioxide (dielectric).

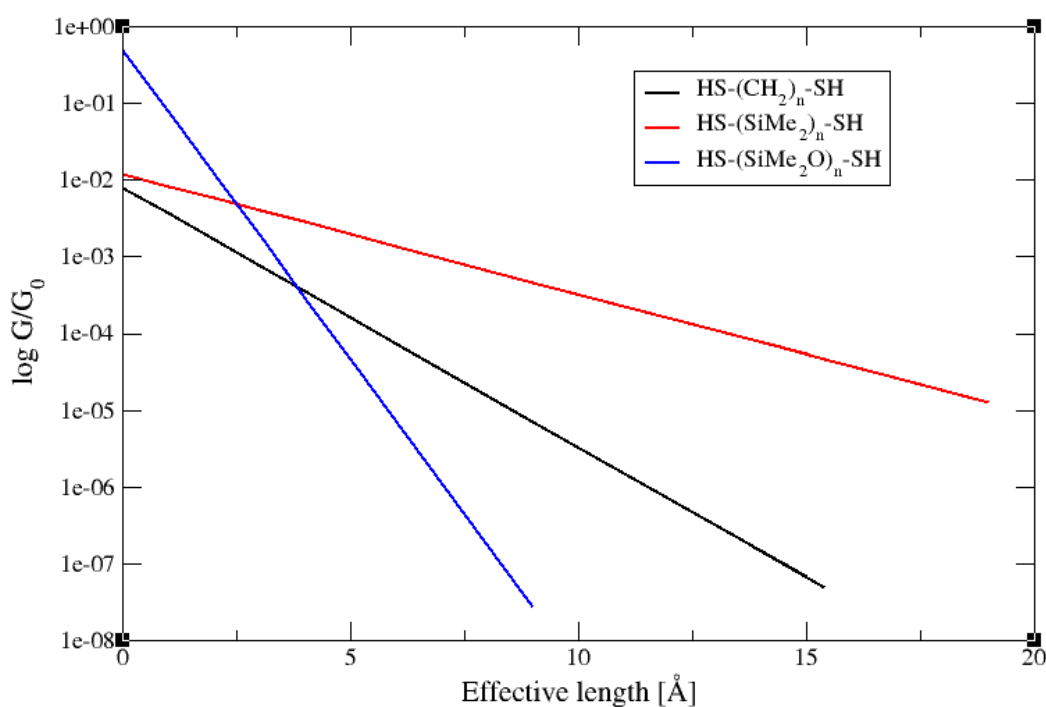


Figure 16: Length-dependent conductance of various organic molecules¹³¹

Not only *p*-benzenedithiol but also other congeners were experimentally as well as computationally studied to show the influence of the molecular structure on the respective single-molecule conductance.^{137,138} The effect of conjugation was shown by Venkataraman and co-workers on a set of *para*- and *meta*-substituted stilbenes (**Table 3**).¹³⁹ In this study, conductance of **79** was found to be about an order of magnitude higher ($1.2 \cdot 10^{-3} G_0$) than that of **80** ($2.9 \cdot 10^{-4} G_0$), which was attributed to the effect of constructive quantum interference in the case of the *para*-substituted benzene ring versus destructive quantum interference in the case of the *meta*-substituted benzene ring.

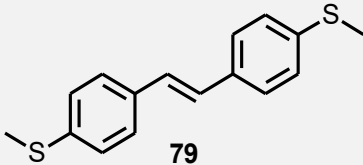
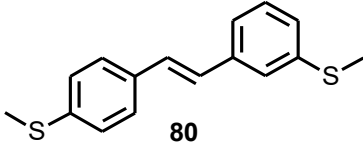
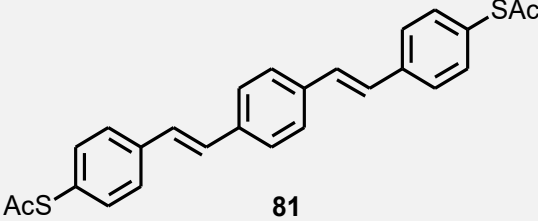
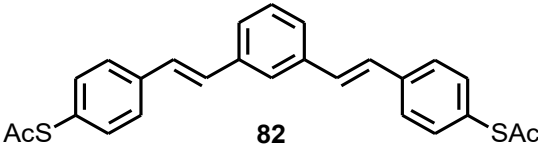
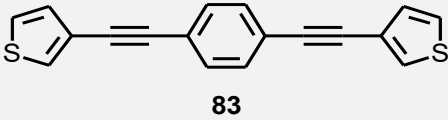
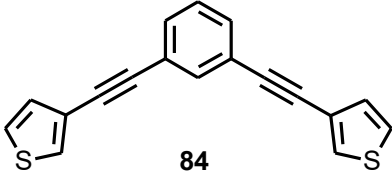
Structure	Conductance	Ref.
 <p>79</p>	$1.2 \cdot 10^{-3} G_0$	[139]
 <p>80</p>	$2.9 \cdot 10^{-4} G_0$	[139]
 <p>81</p>	$1.1 \cdot 10^{-4} G_0$	[140]
 <p>82</p>	$1.5 \times 10^{-5} G_0$	[140]
 <p>83</p>	$7.43 \cdot 10^{-4} G_0$	[141]
 <p>84</p>	$3.03 \cdot 10^{-4} G_0$	[141]

Table 3: Molecules used to study quantum interference^{139–141}

Independently, van der Zant's group published a similar result with different stilbene compounds **81** and **82**.¹⁴⁰ The *meta*-substitution pattern was present in the central benzene ring rather than on the periphery, yet the conductance drop is again an order of magnitude. Similar behavior was observed also for the bis(thienylethynyl)benzene derivatives **83** and **84**.¹⁴¹

1.2.2.1 Electron Transport in Helicene Molecules

Helicenes present an intriguing class of molecules with nonlinear response to external force^{2,142} and high variability in conductance depending on their structure¹⁴³.

In helicenes, two types of electron transport may occur depending on the degree of conjugation and inter-loop distances. The large aromatic system of π -electrons should allow transport of electrons along the helical scaffold, as visualized by the red arrow in **Figure 17**. Such a behavior might result in physical effects of high interest to physicists such as spin filtration^{6,144} described by R. Naaman as the “CISS effect”,¹⁴⁵ electric magneto-chiral anisotropy⁶ or current-induced rotation.¹⁴⁶ The phenomenon of spin-dependent electron scattering was recently observed in helicene monolayers on copper, silver and gold surfaces in the group of K. H. Ernst.¹⁴⁷ Enrichment of one of the spin orientations was observed on surfaces covered with enantiopure helicenes with either *P* or *M* helicity, whereas no spin preference was detected in an experiment on a surface without molecules.

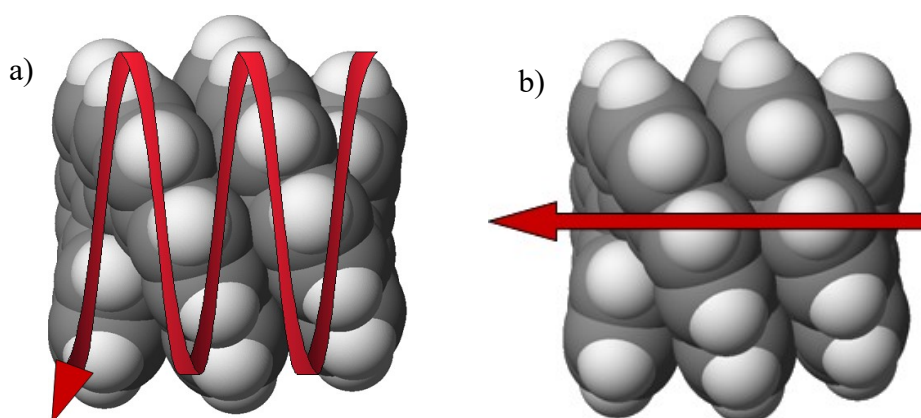


Figure 17: Charge transport in a helicene molecule: (a) along the helix vs. (b) through-space

The other possible mode of charge transport in a helicene molecule is across the loops through π - π stacked benzene rings (**Figure 17b**). In a relaxed geometry, this type of conductance is significantly suppressed according to calculations. However, according to *in silico* experiments, the non-equilibrium conductance is expected to be significantly modulated by either compression (higher conductance) or stretching (lower conductance) of the helicene molecule along its helical axis by an external force.^{2,142} This compressibility might also find applications in materials science as single-molecule piezoelectrics or electrets.²

2 Objectives

The first goal of my Thesis was to develop a synthetic methodology for the preparation of long oxa[n]helicenes based on [2+2+2] cyclotrimerization of alkyne precursors.

Figure 18 presents oxa[19]helicenes **85** and **86**, which were selected as synthetic targets. Ideally, the synthetic methodology should allow the preparation of the final products in their diastereo- and enantiomerically pure form and, moreover, it should be compatible with functional groups, which would eventually serve as anchoring groups with high affinity to the gold surface. Such helical molecules should enable charge transport studies using gold electrodes.

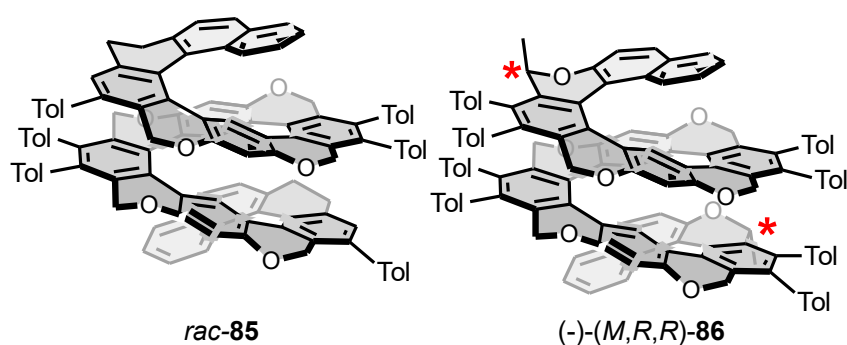


Figure 18: Synthetic targets: racemic oxa[19]helicenes **85** and diastereo- and enantiopure oxa[19]helicenes **86**

Oxa[19]helicene **85** in **Figure 18** with nineteen six-membered rings fused into a single helix represents a challenging synthetic target. It may be accessible by performing an unprecedented intramolecular four-fold [2+2+2] cyclotrimerization of an aptly designed dodecayne. Finally, the racemic product would have to be resolved into enantiomers in an extra step. Thus, as an ultimate goal, two stereogenic centers would be introduced into the target oxa[19]helicene scaffold **86** to control its helicity by 1,3-allylic type strain.

The second goal of my Thesis was to develop a synthetic methodology for the preparation of helicenes equipped with suitable anchoring groups to study single-molecule electrical conductance.

The newly synthesized helicenes need to be decorated with suitable anchoring groups to facilitate a defined contact of the helicene molecule with gold electrodes. To this end, the thiol anchoring group is proposed for its superior Au-S bond strength and the pyridine unit for its good chemical stability and directionality in the bonding to metal.

First, a small series of short fully aromatic carbo[n]helicene dithiols (**Figure 19**) would be synthesized either from dichlorohelicenes by employing nucleophilic aromatic substitution with sulfur nucleophiles or from helicenediols by Miyazaki–Newman–Kwart rearrangement of the respective bis-(thiocarbamates). Such structurally simple helicenes with only a few degrees of freedom and two well-defined contacts should serve the purpose of model compounds for fundamental investigation of charge-transfer behaviors of helicenes at molecular level.

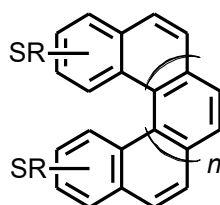


Figure 19: Sulfanyl derivatives of carbo[n]helicenes

Figure 20 presents diastereo- and enantiopure pyrido/sulfanyl oxa[n]helicene derivatives **87** and **88**, which were selected as more challenging synthetic targets for conductance measurements. The former, pyridooxa[9]helicenes **87** (**Figure 20**) should be directly accessible by the multiple [2+2+2] cycloisomerization reaction of an oligoalkyne precursor bearing pyridine moieties.

In the latter case, straightforward synthetic functionalization of chloroderivatives should be merged with modular strategy for synthesis of long helicenes to provide the long helicene **88** bearing two sulfanyl anchoring groups (**Figure 20**).

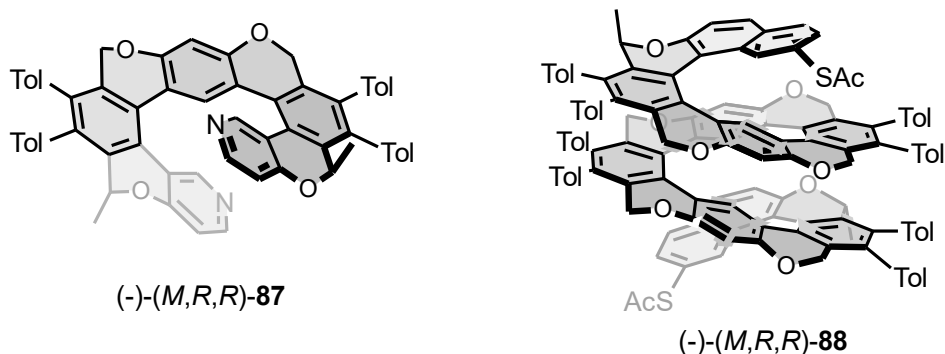


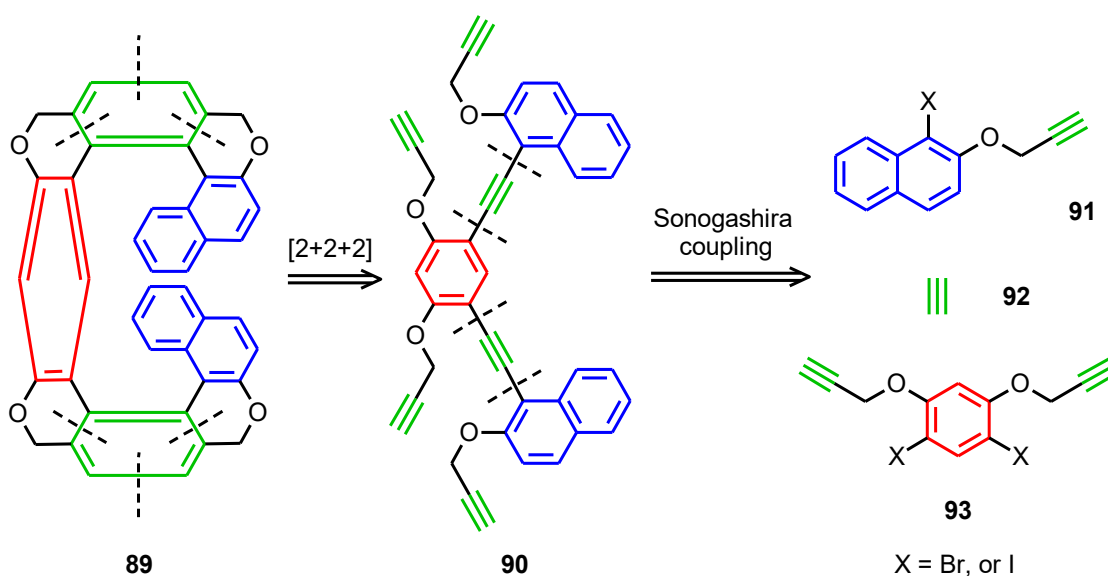
Figure 20: Synthetic targets: diastereo- and enantiopure pyridooxa[9]helicene **87** and sulfanyl oxa[19]helicene **88**

The third goal of my Thesis is to study single-molecule electrical conductance of the prepared helicenes by employing the break junction techniques. Since there is no commercially available and inexpensive instrument for the MCBJ or STM-BJ experiments, it should be designed, custom-made and partially assembled from commercially available parts (piezo actuators, amplifiers or source-meter units). Accordingly, the attention should be paid to the development of the respective instrument(s), measurement methodology and study of single-molecule electrical conductance, massive data processing, and interpretation of results with the support of quantum chemical calculations.

3 Results and Discussion

3.1 The Synthesis of Long Helicenes

A retrosynthetic analysis of oxahelicene **89** with 11 hexacyclic rings fused into a helix is shown in **Scheme 24**. Its design is based on a two-fold [2+2+2] cyclotrimerization reaction of hexayne **90** as the key step, being inspired by an earlier successful synthesis of its shorter analogue (oxa[9]helicene).¹⁴⁸ The two internal triple bonds in hexayne **90** are installed onto the central resorcinol-based building block **93** by means of a Sonogashira coupling reaction with a suitable alkynes **91** and **92**. The substitution pattern of the resorcinol derivative **93** does not allow “all-ortho” annulation of rings in the final helicene product, yet the overall molecular shape remains nicely helically chiral and the synthesis is greatly simplified when compared to those of the 1,2,3,4-tetrasubstituted benzene building blocks.

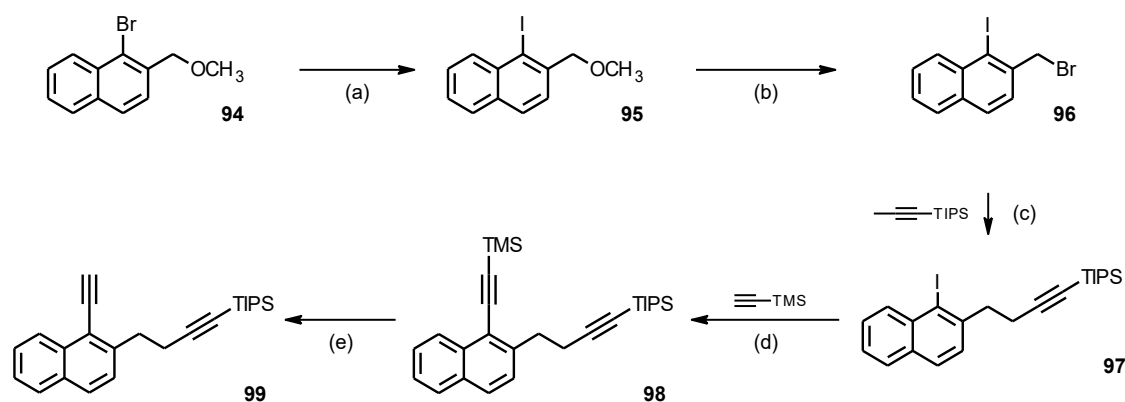


Scheme 24: Retrosynthetic analysis of [11] helicene **89**

3.1.1 The Synthesis of Racemic Oxa[n]helicenes

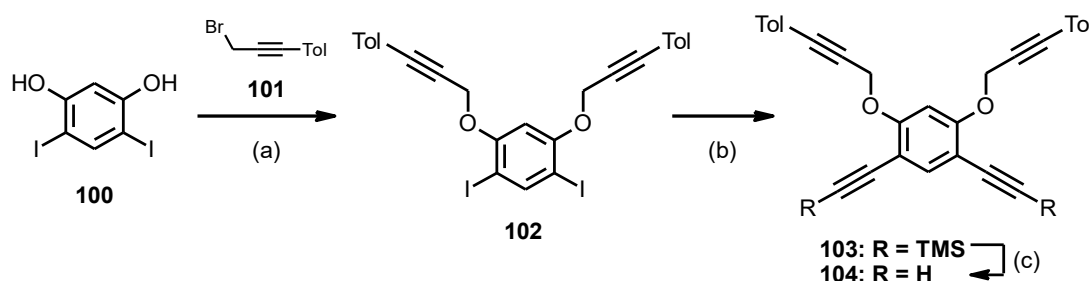
The known naphthalene diyne **99**¹⁴⁹ (**Scheme 25**) is a common building block for the synthesis of racemic oxa[19]helicene **85** (**Scheme 32**), oxa[11]helicenes **107** and **109** (**Scheme 28** and **29**). It, diyne **99**, was prepared from the commercially available bromoderivative **94** through a five-step synthetic sequence including lithium-halogen exchange, substitution and Sonogashira coupling in 68% overall yield (**Scheme 25**). Notably, the bulky triisopropylsilyl protecting group efficiently shields the triple bond

against unwanted carbopalladation reaction during the Sonogashira coupling but has to be removed prior to cyclotrimerization. The previously published procedures¹⁴⁹ were slightly modified in order to simplify a multi-gram synthesis of this material.



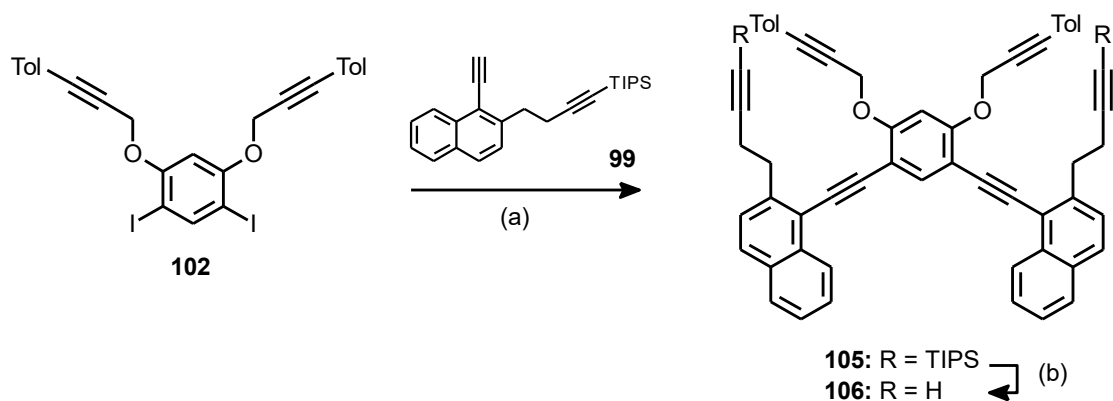
Scheme 25: (a) *n*-BuLi (1.5 equiv.), THF, -78 °C, then I₂, THF, -78 °C, 87%, 15 min; (b) HBr (15.0 equiv.), THF, 0 °C, 1 h, 95%; (c) TIPS-propyne (1.56 equiv.), *n*-BuLi (1.55 equiv.), THF, -78 °C, 2.5 h, 96%; (d) TMSA (1.5 equiv.), Pd(PPh₃)₄ (2 mol%), CuI (4 mol%), DIPA, rt, overnight, 89%; (e) K₂CO₃ (2.0 equiv.), MeOH – diethylether (3:1), rt, 3h 96%.

The common resorcinol building block **102** was prepared from 4,6-diiodoresorcinol **100**¹⁵⁰ and the bromoderivative **101**¹⁵¹ via nucleophilic substitution (**Scheme 26**). This building block **102** bears two iodo groups, which are highly reactive in subsequent cross-coupling reactions. Indeed, tetrayne **103** was prepared from diiodide **102** using a Sonogashira coupling with TMSA followed by deprotection in high overall yield. Such a high reactivity of **102** was promising with respect to the synthesis of long helicenes, *vide infra*.



Scheme 26: (a) **101** (2.1 equiv.), K₂CO₃ (6 equiv.), DMF, rt, 20 h, 70%; (b) TMSA (3.0 equiv.), Pd(PPh₃)₄ (5 mol%), CuI (10 mol%), DIPA-toluene (1:2), rt, 16 h, 93%; (c) NaOMe (2.4 equiv.), MeOH:THF (1:1), rt, 45 min, 95%.

The key precursor of the oxa[11]helicene derivative **107** (Scheme 28), hexayne **106**, was prepared by a twofold Sonogashira coupling of diiodide **102** with an excess of diyne **99** followed by the removal of the bulky triisopropylsilyl protecting groups of **105** using tetrabutylammonium fluoride (Scheme 27).



Scheme 27: (a) **99** (2.1 equiv.), Pd(PPh₃)₄ (10 mol%), CuI (20 mol%), DIPA-toluene (1:3), rt, 16 h, 77%; (b) TBAF·3H₂O (2.4 equiv.), THF, rt, 1 h, 82%.

Being by far the most versatile complex to mediate the intramolecular [2+2+2] cycloisomerization of alkynes, CpCo(CO)₂ was used as a catalyst in the transformation of hexayne **106** into helicene **107** (Scheme 28). Also, it is an affordable and easy-to-handle liquid, which only slowly decomposes under ambient conditions

In addition to the relatively common microwave reactor, a high-temperature-high-pressure flow reactor (Figure 21) was recently introduced to our laboratory toolshed, allowing reactions to be performed at up to 350 °C and 150 bar. The experiment in flow reactor has several advantages: (i) excellent heat exchange; small volume of the reaction mixture is heated and then cooled down again very fast, thus suppressing any overreaction; (ii) very accurate control over short reaction times given by the ratio of the reactor volume to the flow rate; (iii) volatile solvents can be used at high temperatures, which simplifies the work-up; (iv) simplicity of the scale up; the reaction scale is determined simply by the duration of the experiment.

Since the flow reactor was already proven to be useful in some challenging [2+2+2] cyclotrimerizations¹⁵², it became the method of choice also for the envisioned multiple variants.

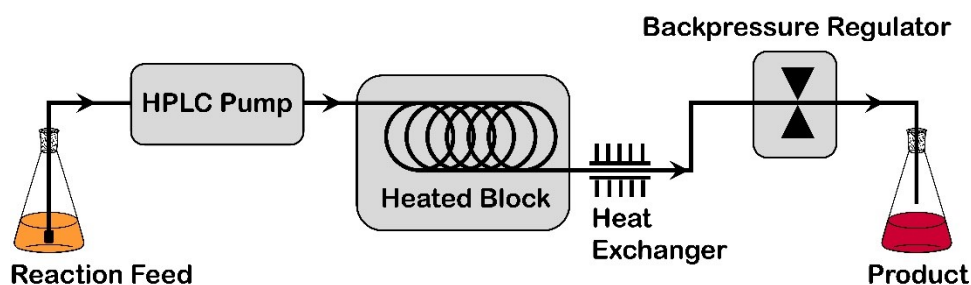
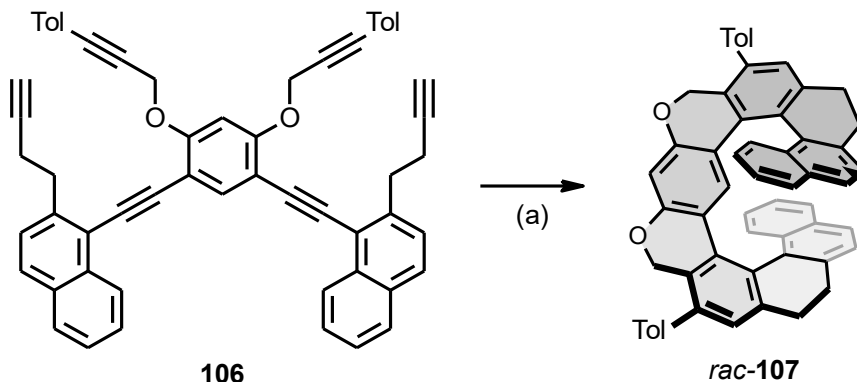


Figure 21: High-temperature-high-pressure flow-reactor schematics

The racemic oxa[11]helicene derivative *rac-107* was obtained under the above conditions as a single product. In such reactions, a high amount of catalyst is usually used (20-50 mol% per one [2+2+2] cycloisomerization) as the cobalt complex decomposes quickly at high temperatures. However, further increase of the catalyst loading did not improve the yield of the reaction. Notably, Ni(0)-based catalysts generated *in situ* from Ni(cod)₂ and a respective phosphine (PPh₃ or PCy₃) provided the same product, which was accompanied by some impurities of a polymeric nature. They probably originated from intermolecular reactions favored by the preferential reactivity of Ni(0) complexes with terminal alkynes.



Scheme 28: (a) CpCo(CO)₂ (0.5 equiv.), THF, flow reactor, 250 °C, 16 min, 50%.

Chirality of the product was confirmed by the separation of enantiomers on an analytical-scale chiral stationary phase high performance liquid chromatography (CSP-HPLC) column (Chiralpak IB) using UV (254 nm) and polarimetric detectors. The chromatogram is shown in **Figure 22**.

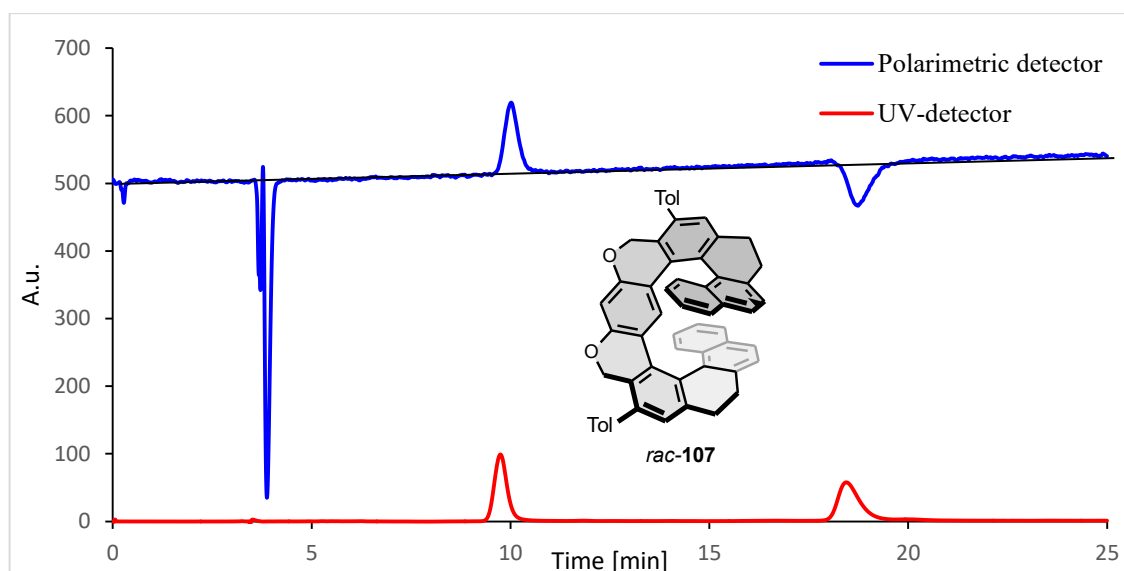


Figure 22: CSP-HPLC analysis of oxa[11]helicene *rac-107* (Chiralpak IB *n*-heptane:MTBE 90:10, with 0.5% *i*PrOH)

The final proof of the chirality of the structure *rac-107* provided the single-crystal analysis (**Figure 23**). The very dense crystal packing of racemic mixture is caused by intercalation of *P* and *M* helicenes, which creates interdigitating heterochiral pairs. These pairs are stabilized by π - π and π -H interactions.

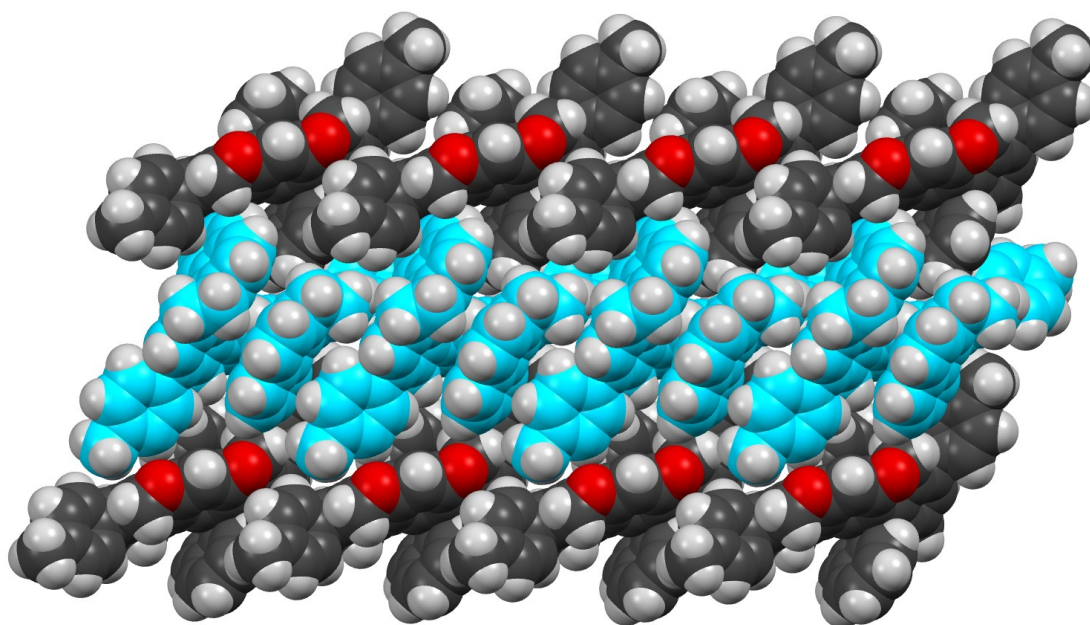
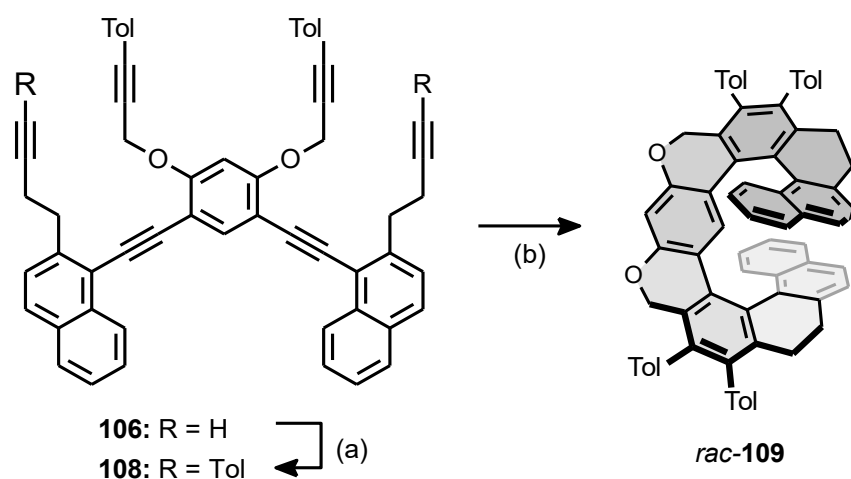


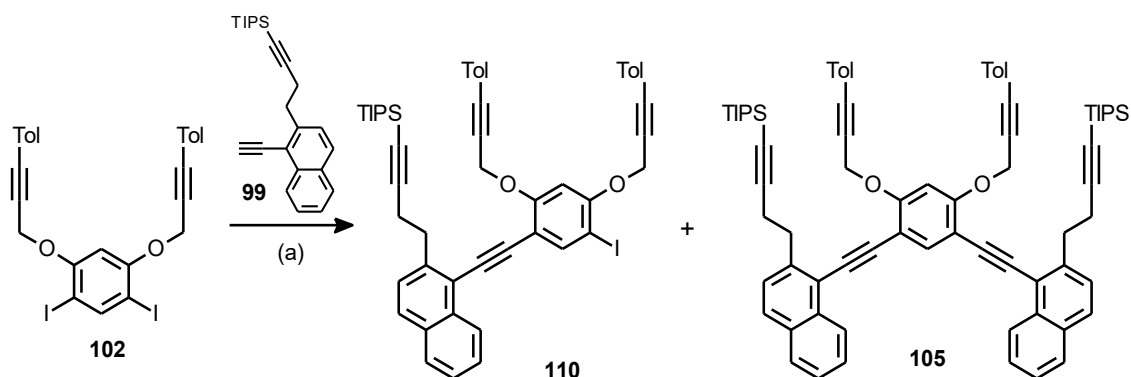
Figure 23: Crystal packing of *rac*-oxa[11] helicene **107**: *P* (cyan); *M* (grey)

Additional *p*-tolyl groups were introduced *via* Sonogashira coupling into the molecule **106** to improve the stability of the hexayne **108** and solubility of the final oxa[11]helicene **109** (**Scheme 29**). In fact, while oxa[11]helicene **107** was poorly soluble (less than 1 mg/mL of acetone), the multiply *p*-tolylated derivative **109** was more soluble (more than 10 mg/mL of acetone). In contrast, no improvement in cycloisomerization yield was observed.



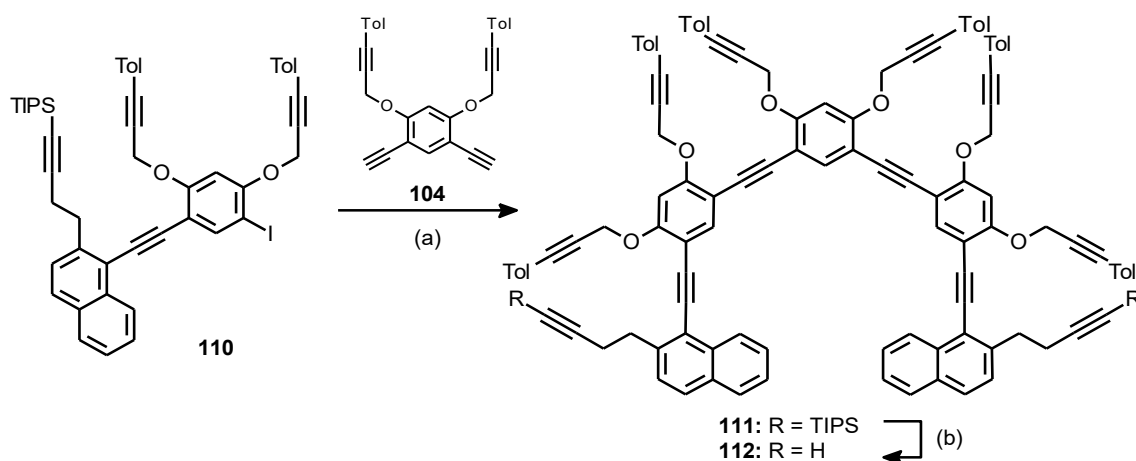
Scheme 29: (a) 4-iodotoluene (6.0 equiv.), Pd(PPh₃)₄ (10 mol%), CuI (20 mol%), DIPAtoluene (1:5), rt, 16 h, 89%; (b) CpCo(CO)₂ (1.0 equiv.), THF, flow reactor, 250 °C, 16 min, 48%.

The key step in the synthesis of higher oligoynes such as **111** (**Scheme 31**) was the desymmetrization of diiodo compound **102** (**Scheme 30**) by Sonogashira coupling with diyne **99**. Using a 2:1 stoichiometry, the desired iododerivative **110** could be obtained in up to 40% yield, in addition to the unavoidable symmetrical byproduct **105**. It was found that the speed of addition of diyne **99** to the reaction mixture had only negligible effect on the reaction outcome. A sequence of two chromatographic separations, first on silica gel and then on C-18 reversed phase silica gel, were needed to isolate both products in a pure form (recovering also the starting material).



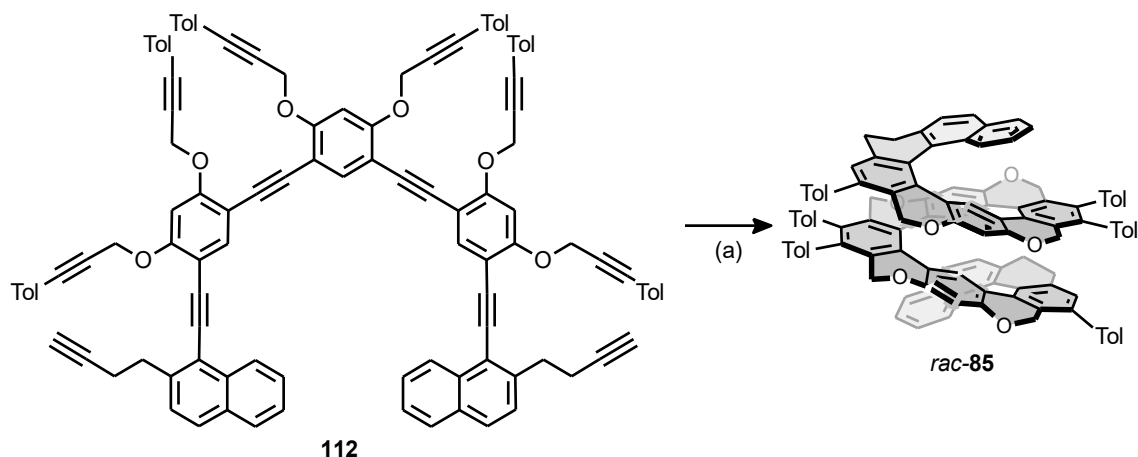
Scheme 30: (a) **99** (0.5 equiv.), Pd(PPh₃)₄ (10 mol%), CuI (20 mol%), DIPA-toluene (5:3), rt, 16 h, 41% for **110**, 40% for **105**.

The iodotetraeyne **110** was then used for the construction of the quadruple cyclotrimerization precursor, dodecayne **112**. The reaction conditions for the twofold Sonogashira coupling of **110** with diyne **104** (**Scheme 31**) were chosen based on previous experience with a similar class of compounds. In particular, the oxidative dimerization of **104** leading to polymeric byproducts was suppressed by its slow addition *via* cannula. Although the removal of the TIPS protecting groups from **111** provided a single product according to the TLC analysis, it was prone to decomposition during work up. Thus, the crude polycyclization precursor **112** was purified only by filtration through a short pad of silica gel using distilled solvents to remove tetrabutylammonium salts from it. The resulting solution was concentrated under the flow of nitrogen and directly used in the cyclization step.



Scheme 31: (a) **104** (0.5 equiv.), Pd(PPh₃)₄ (10 mol%), CuI (20 mol%), DIPA-toluene (2:1), rt, 16 h, 59%; (b) TBAF·3H₂O (4.8 equiv.), THF, rt, 40 min, used without purification.

Using the same reactions conditions, which were successfully applied in the synthesis of oxa[11]helicene derivative *rac-109* (Scheme 29), the [19]helicene derivative *rac-85* was prepared in good yield 56% (Scheme 32). The unreacted starting material, dodecayne **112**, was detected by TLC-analysis when the catalyst amount was decreased below 50 mol% per cyclotrimerization, *i.e.* 2.0 equivalents for the quadruple reaction.



Scheme 32: (a) $\text{CpCo}(\text{CO})_2$ (2.0 equiv.), THF, flow reactor, 250 °C, 16 min, 56% after 2 steps (from **111**).

Also in this case, the (*P*)- and (*M*)-enantiomers could be easily resolved using an analytical HPLC column with chiral stationary phase (Chiralpak IB) as demonstrated in Figure 24.

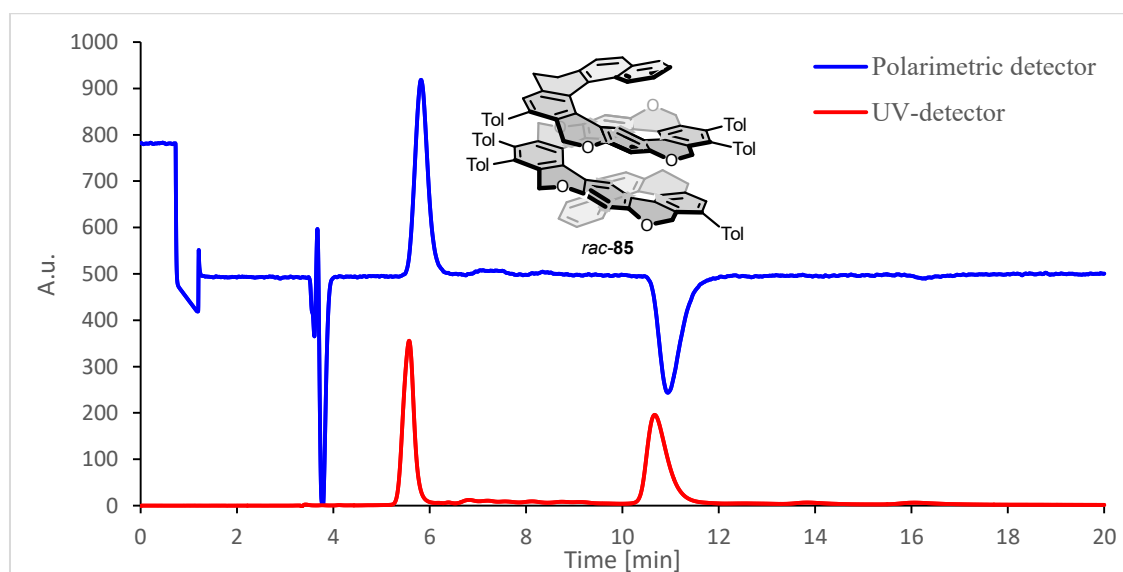
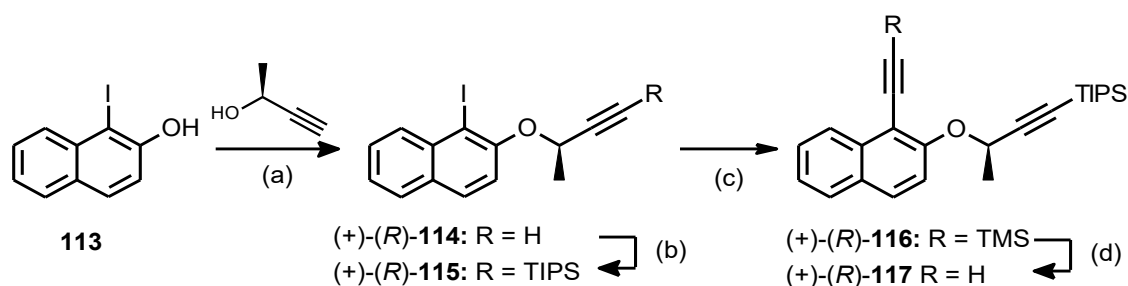


Figure 24: CSP-HPLC analysis of oxa[19]helicene *rac-85* (Chiralpak IB, *n*-heptane:MTBE 90:10, with 0.5% *i*PrOH)

3.1.2 The Synthesis of Optically Pure Oxa[19]helicene

After development of the multiple [2+2+2] cyclootrimerization of oligoynes leading to extremely long helicene-like molecules such as the oxa[19]helicene derivative *rac*-**85** in a racemic form, their stereoselective synthesis was begun. Diastereoselective multiple [2+2+2] cycloisomerization of centrally chiral oligoynes controlled by 1,3-allylic type strain (to favor one of the helices) was thus attempted.

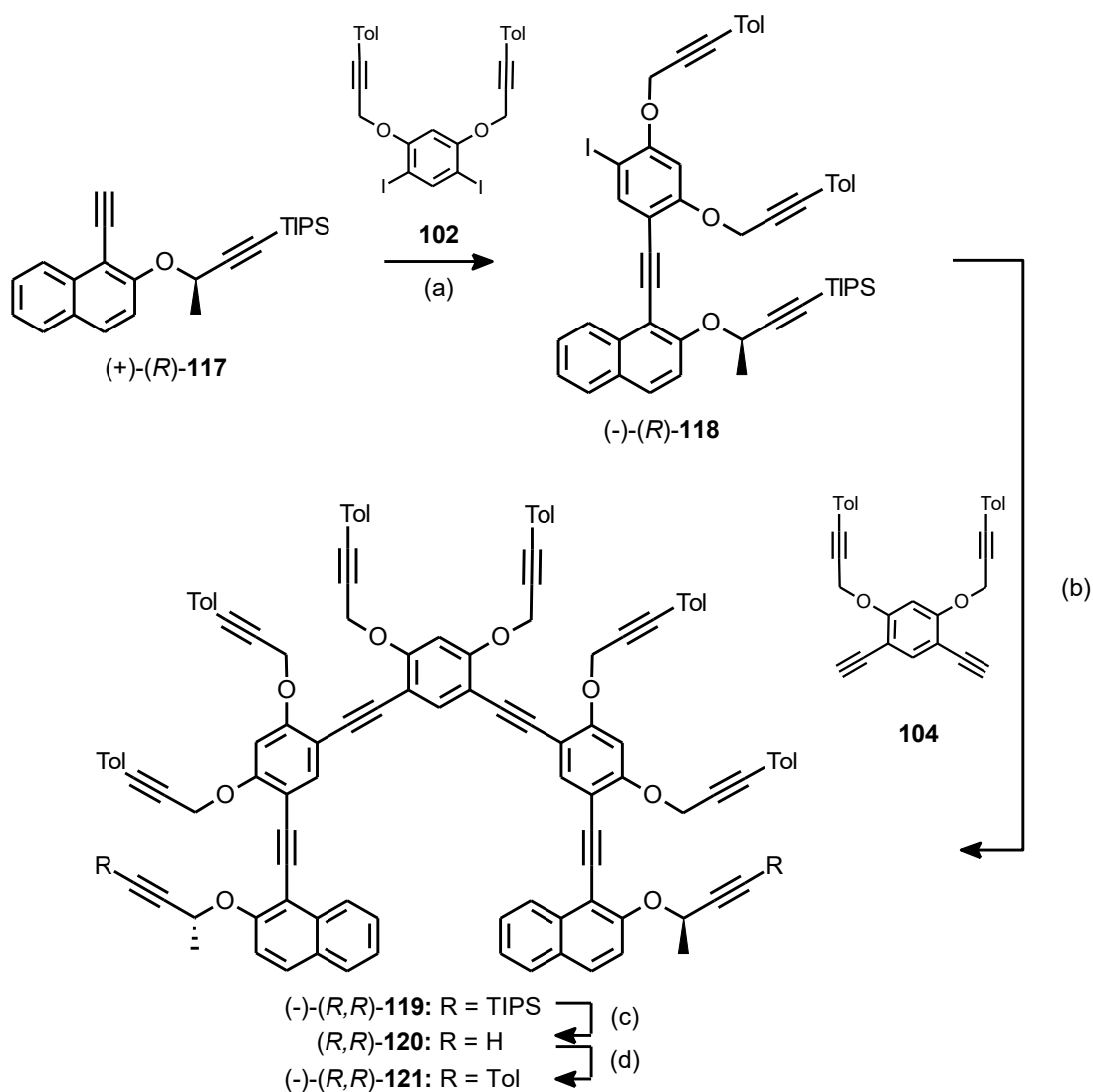
The centrally chiral naphthalene building block **117**, structurally similar to the already successfully utilized building block **99**, was designed in accord with the well-established method for the diastereoselective synthesis of non-racemic helicenes.⁵⁵ Its synthesis started with Mitsunobu reaction of the commercially available iodonaphthol **113**¹⁵³ and the (*S*)-but-3-yn-2-ol (**Scheme 33**), which is also commercially available in both enantiomeric forms. The orthogonally protected chiral diyne (+)-(*R*)-**116** was then prepared by silylation of (+)-(*R*)-**114** and Sonogashira coupling of (+)-(*R*)-**115** with trimethylsilylacetylene. Finally, a base-mediated cleavage of the more reactive silyl group (TMS) led to the chiral alkyne building block (+)-(*R*)-**117**. Its absolute configuration is related to the starting (*S*)-but-3-yn-2-ol and stereospecificity of the S_N2-type Mitsunobu reaction (proceeding with a complete inversion of configuration). The four-step reaction sequence provided a satisfactory overall yield 66% and could be performed on a gram scale.



Scheme 33: (a) (*S*)-but-3-yn-2-ol (1.1 equiv.), PPh₃ (1.2 equiv.), DIAD (1.2 equiv.), benzene, rt, 16 h, 86%; (b) LDA (1.2 equiv.), THF, -78 °C, 1 h, then TIPSCl (1.5 equiv.), -78 °C, 1 h, 98%; (c) TMSA (1.5 equiv.), Pd(PPh₃)₄ (2 mol%), CuI (4 mol%), DIPA, rt, 16 h, 86%; (d) K₂CO₃ (1.5 equiv.), MeOH, rt, 1 h, 91%.

The synthesis of the centrally chiral dodecayne (-)-(*R,R*)-**121** (**Scheme 34**) was performed analogously to the synthesis of the racemic oligoyne **108** (**Scheme 29**) and **112**

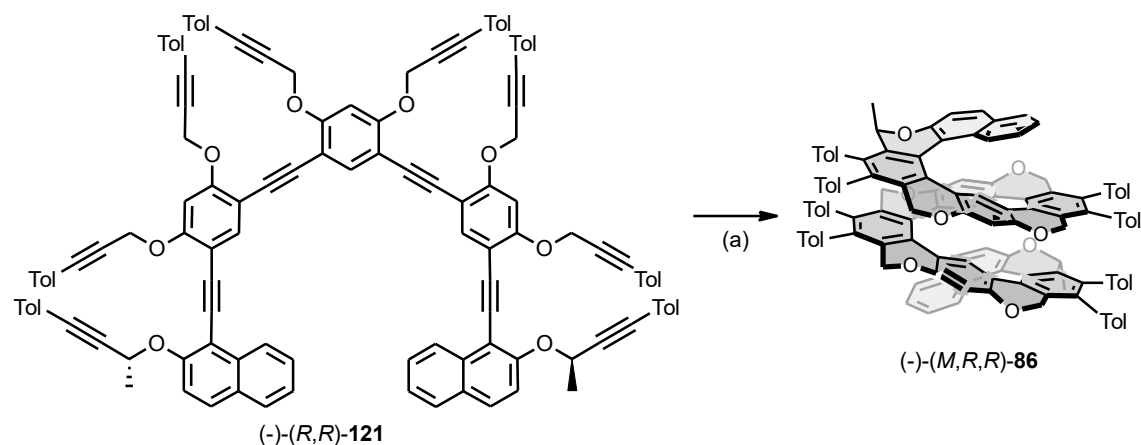
(Scheme 31). The Sonogashira reaction of the chiral diyne (+)-(*R*)-**117** with an excess of diiodide **102** provided only the product of mono-coupling (-)-(*R*)-**118** in moderate yield. The product of a twofold coupling was not even observed. On the other hand, the counterproductive oxidative dimerization of alkyne (+)-(*R*)-**117** could not be avoided. Isolation of the product (-)-(*R*)-**118** by flash column chromatography on silica gel was found feasible in contrast to the achiral tetrayne **110** (**Schema 30**). The iodo derivative (-)-(*R*)-**118** was then subjected to the Sonogashira reaction with tetrayne **104** to afford (-)-(*R,R*)-**119** in good yield. After its desilylation, which led to (*R,R*)-**120**, terminal alkyne units were immediately *p*-tolylated utilizing another twofold Sonogashira coupling to obtain the optically pure dodecayne (-)-(*R,R*)-**121**.



Scheme 34: (a) **102** (2.0 equiv.), Pd(PPh₃)₄ (10 mol%), CuI (20 mol%), DIPA-toluene (1:1), rt, 16 h, 53%; (b) **104** (0.5 equiv.), Pd(PPh₃)₄ (10 mol%), CuI (20 mol%), DIPA-toluene (1:2), rt, 16 h, 60%; (c) TBAF·3H₂O (3.0 equiv.), THF, rt, 40 min, used without purification; (d) 4-iodotoluene (4.0 equiv.), Pd(PPh₃)₄ (10 mol%), CuI (20 mol%), DIPA-toluene (1:2), rt, 16 h, 77% (after 2 steps).

The final multiple cyclization of oligoynes (-)-(R,R)-**121** was performed again in the flow reactor at 250 °C (**Scheme 35**), creating twelve new C-C bonds and twelve new rings. In this case, the energy difference between the two possible diastereoisomers (P,R,R)- and (M,R,R)-**86** is approximately 9.6 kcal/mol (calculated by DFT (B3LYP/cc-pVDZ/GD3)) in favor of (-)-(M,R,R)-**86**, which was formed as an exclusive product. The high reaction temperature is thus essential for the formation of

enantiomerically and diastereomerically pure product by post-cyclization thermodynamic equilibration.



Scheme 35: (a) $\text{CpCo}(\text{CO})_2$ (2.0 equiv.), THF, flow reactor, 250 °C, 16 min, 20%.

The CD spectrum of the oxa[19]helicene (-)-(M,R,R)-86 (red) is shown in **Figure 25**, being overlaid with the spectrum of its shorter analogue, oxa[7]helicene (-)-(M,R,R)-122 (blue).⁵⁵

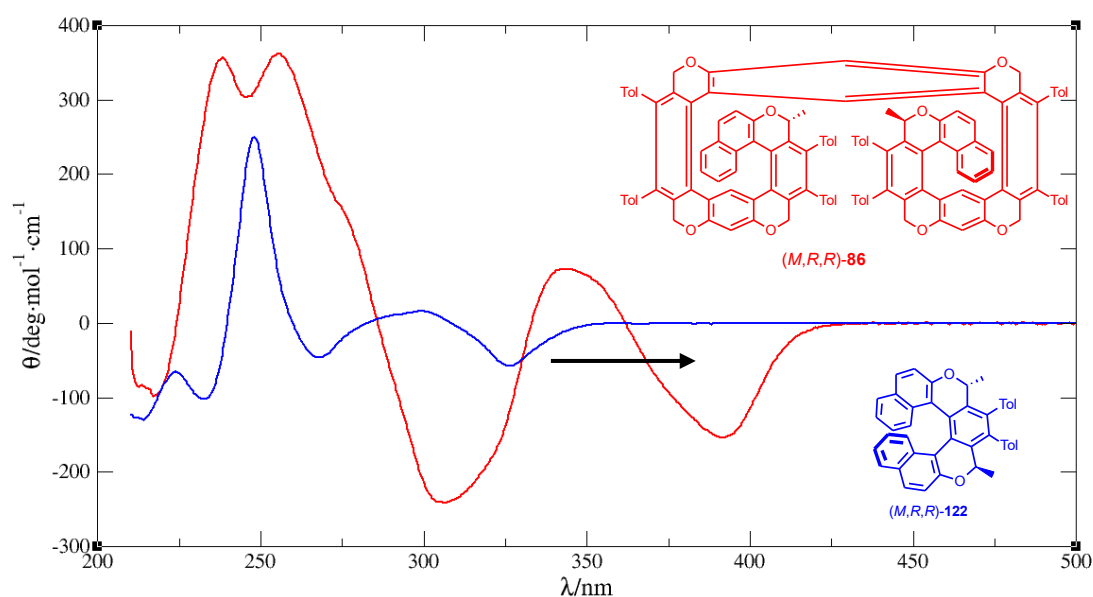


Figure 25: The CD-spectrum of oxa[7]helicene (-)-(M,R,R)-122 (blue), and oxa[19]helicene (-)-(M,R,R)-86 (red)

The two spectra exhibit similar features: the longest-wavelength negative peak indicates *M*-helicity according to the general rule of thumb in helicene chemistry. The red shift

(indicated by a black arrow in **Figure 25**) results from the extended π -electron system of oxa[19]helicene (-)-(M,R,R)-**86**.

An additional evidence of the helical folding comes from the ROESY NMR spectroscopy, where a cross-peak indicating a trough-space interaction between the hydrogen atom attached to the chiral center and the axially oriented hydrogen atom on a spatially close loop was found (**Figure 26a**). Proximity of the two atoms is depicted in green color in the 3D model (optimized structure DFT (B3LYP/cc-pVDZ/GD3) of oxa[19]helicene (-)-(M,R,R)-**86** (**Figure 26b**) along with their distance (\AA).

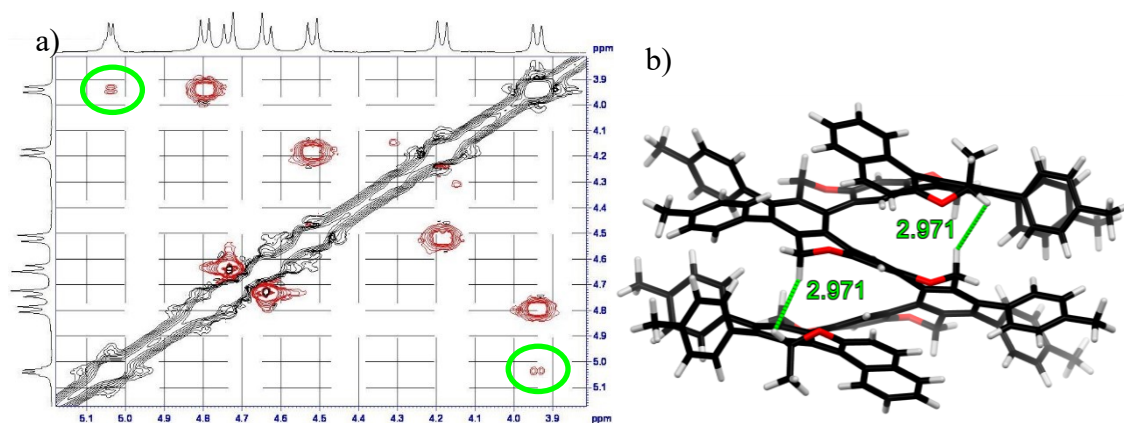


Figure 26: (a) ROESY NMR spectrum; (b) trough-space interaction in oxa[19]helicene (-)-(M,R,R)-**86** (optimized structure DFT (B3LYP/cc-pVDZ/GD3))

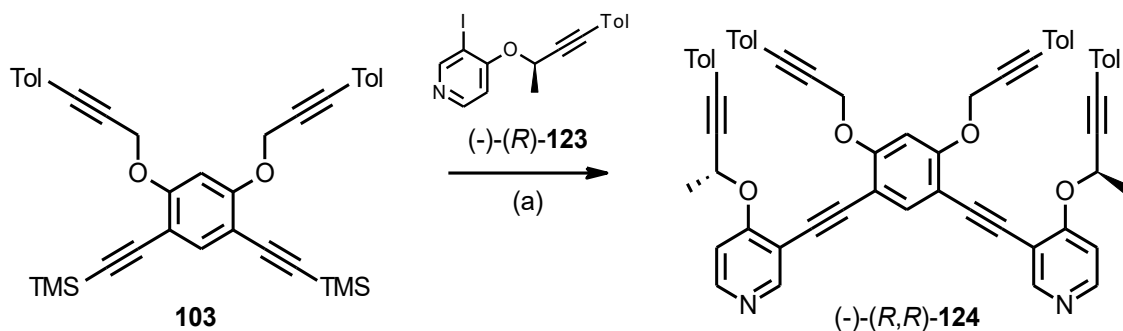
3.2 The Synthesis of Helicenes with Anchoring Groups

The measurement of single-molecule conductance in break junction experiments requires molecules decorated with anchoring groups that enable effective binding to the electrode surface (Chapter 1.2.2). Thus, the synthesis of helicene derivatives comprising pyridine subunits or sulfanyl groups had to be developed.

3.2.1 The Synthesis of Pyridooxa[9]helicene

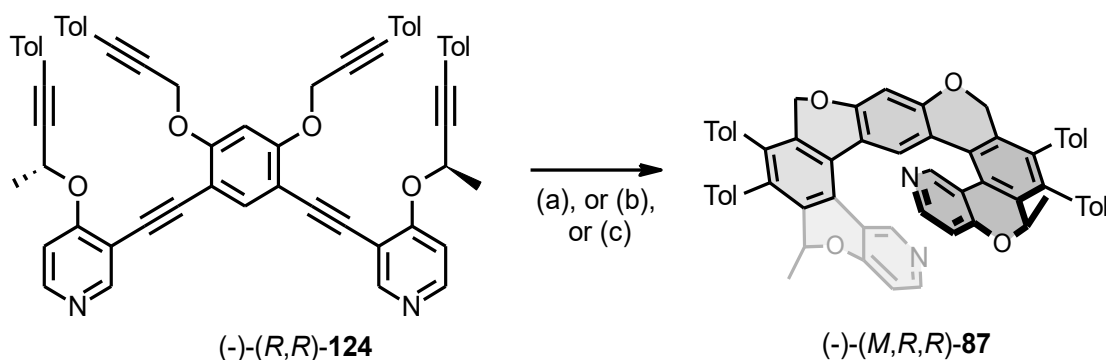
The synthesis of diastereo- and enantiopure pyridooxa[9]helicene (-)-(M,R,R)-**87** relies on the synthetic methodology developed for the unfunctionalized oxa[n]helicenes, *vide supra*. In this case, the use of a properly substituted pyridine building block allowed the installation of pyridine subunits in the helical scaffold.

The readily available iododerivative (-)-(R)-**123** was coupled with a terminal diyne generated *in situ* by desilylation of tetrayne **103** under the Sonogashira reaction conditions (**Scheme 36**). This one-pot procedure afforded hexayne (-)-(R,R)-**124** in good yield 84%.



Scheme 36: (a) TBAF·3H₂O (2.4 equiv.), toluene, rt, 32 min, then (-)-(R)-123 (2.4 equiv.), Pd(PPh₃)₂Cl₂ (5 mol%), CuI (10 mol%), DIPA-toluene (1:3), rt, 1.5 h, 84%.

The highest yield (54%) of the cyclization of hexayne (-)-(R,R)-124 was achieved by employing a flow reactor and CpCo(CO)₂ as catalyst (**Scheme 37**). Carrying out the reaction in a microwave reactor in the presence of CpCo(CO)(*fum*) or at room temperature in the presence of Ni(cod)₂ and PPh₃ led to lower yield 42% or 43%, respectively. As expected, a single diastereomer of enantiopure (-)-(M,R,R)-87 was obtained as the result of thermodynamic equilibration.



Scheme 37: (a) CpCo(CO)(*fum*) (1 equiv.), THF, microwave reactor, 170 °C, 10 min, 42%; (b) Ni(cod)₂ (0.5 equiv.), PPh₃ (1 equiv.), rt, 16h, 43%; (c) CpCo(CO)₂ (1 equiv.), THF, flow reactor, 250 °C, 8 min, 54%.

3.2.2 The Synthesis of Sulfanylated Helicenes

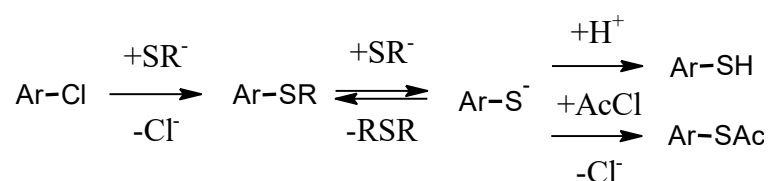
The frequently used sulfanyl moiety as an anchoring group provides significantly stronger binding to gold electrodes than any nitrogen-based functionality. It was installed in the helicene molecule at a late stage of the synthesis to prevent its interference with the Pd-catalyzed coupling reactions¹⁵⁴ used for the construction of helicene scaffolds.

The previously reported reactions of bromo-¹⁵⁵ or iodoaryls¹⁵⁶ as the starting materials afforded the corresponding acetylsulfanyl derivatives. These reactions were photoinduced to follow the radical-nucleophilic aromatic substitution mechanism $S_{RN}1$.¹⁵⁷ The formation of dehalogenated side products (from 6% up to 40%, depending on the substrate)¹⁵⁵ was also observed as the reverse radical disproportionation might take place at high temperatures as well.¹⁵⁸

On the other hand, chlorosubstituted helicenes are expected to be suitable precursors of the corresponding sulfanylated helicenes because chlorine atom is known to be compatible with helicene-forming processes¹⁵⁹ and they can be replaced by sulfur groups *via* a robust nucleophilic substitution reaction.

Installation of a chlorine substituent onto the chosen helicene scaffold should not be a difficult task as it was already shown^{159,160} to be compatible with [2+2+2] cycloisomerization reaction. Indeed, several such derivatives were available in the laboratory as intermediates in other research projects.

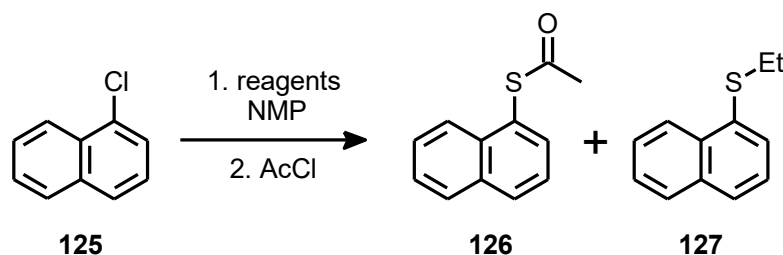
From the synthetic methods commonly used for the introduction of sulfur-based anchoring groups to aromatic systems such as the Miyazaki–Newman–Kwart (MNK) rearrangement of thiocarbamates^{67,149} or the Pd-catalyzed transmetalation reactions¹⁶¹ with tin, indium sulfides or Pd-catalyzed thiolate introduction,¹⁶² nucleophilic aromatic substitution of aromatic chlorides with thiolates was chosen as a simple and robust alternative. This reaction was widely studied by J. Shaw,¹⁶³ who demonstrated the superiority of N-methyl-2-pyrrolidone (NMP) as solvent over the lower-boiling N,N-dimethylformamide (DMF) or highly toxic and expensive hexamethylphosphoramide (HMPA). This approach described by Shaw¹⁶³ (**Scheme 38**) combines the substitution of chlorine atom in the first step with thioether cleavage in the second. The reaction can be quenched either by an acid to give a free thiol or with acetyl chloride to directly protect the sensitive thiol as a thioester.



Scheme 38: Aromatic substitution with *in situ* thioether cleavage

3.2.2.1 The Optimization of Sulfanylation of Chloroaromatics

For optimization purposes, before embarking on the synthesis of desired chlorohelicenes, the commercially available 1-chloronaphthalene **125** as a model compound was subjected to the sulfanylation reaction under various conditions (**Table 4**). The reaction was found to work best when the thiolate was freshly prepared from the corresponding thiol by treatment with a base, with sodium metal being much more effective than sodium hydride.



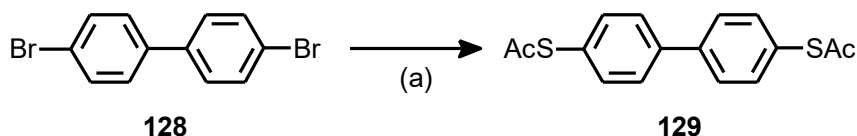
Entry	Reagents (equiv.)	time	T [°C]	126	127
1	<i>t</i> -BuSH + Na (20)	2 h	270	99	-
2	EtSH + NaH (5)	2 h	250	59	41
3	EtSH + Na (10)	2 h	250	99	-
4	DMDS + Na (5)	1 h	200	99	-

Table 4: The optimization of sulfanylation of chloronaphthalene by the S_NAr process (yields (%) of **126** and **127** were estimated by GC-MS)

To push the reaction equilibrium forward, ethanethiol instead of *t*-butanethiol was used so the boiling point of the resulting thioether was reasonably decreased from 150 °C for *t*-butyl to 90 °C for diethylthioether. In addition the steric hindering, which slowing down the second reaction in the **Scheme 38**, was suppressed by using primary thiolates. Using primary thiols instead of tertiary ones also changes the reaction mechanism from S_N1 to S_N2, in which the reaction rate is influenced by the reagent concentration, thus giving another option of its influencing. In the case of the most reactive methyl thiolate, dimethyldisulfide (DMDS) was used as its precursor¹⁶⁴ (**Entry 4**) because it is much easier to handle than gaseous highly toxic methanethiol (it is approximately thousand times more effective in inhibition of mitochondrial electron transfer in comparison to ethanethiol)¹⁶⁵. In addition to its advantageously low steric demands, methyl thiolate-mediated thioether cleavage (2nd step in **Scheme 38**) produces dimethyl thioether as

a byproduct, which is efficiently removed from the reaction mixture thanks to its low boiling point (37 °C), thus shifting the equilibrium towards the final thiol product.

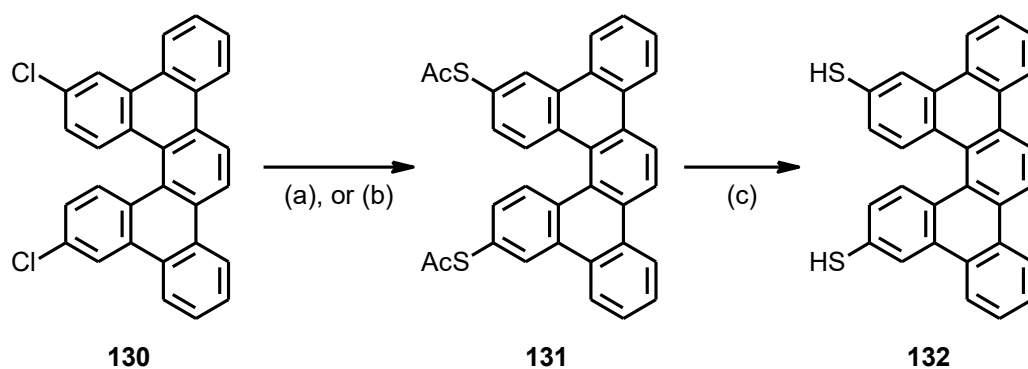
Another model substrate, 4,4'-dibromobiphenyl **128**, was chosen as a slightly more challenging electron rich organic dibromide (**Scheme 39**). Nevertheless, the reaction provided excellent yield of the resulting bis(4,4'-S-acetyl)biphenyl dithiol **129**^{166,167} when the conditions from **Entry 3** in **Table 4** were applied.



Scheme 39: EtSH (24.0 equiv.), Na (20.0 equiv.), NMP, 250 °C, 2 h, then AcCl (30.0 equiv.), rt, 2 h, 92%.

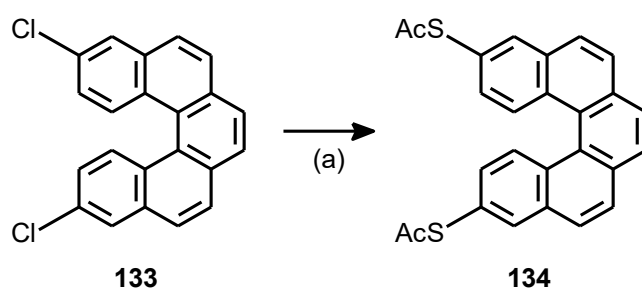
3.2.2.2 The Synthesis of Sulfanylated Carba[n]helicenes

First, dichlorodibenzo[5]helicene **130**¹⁶⁸ was transformed into its bis(acetylsulfanyl) derivative **131** in high yield by treatment with sodium ethanethiolate in NMP at 250 °C followed by *in situ* acetylation with acetyl chloride (**Scheme 40**). DMDS could be also used as the source of thiolate with very similar result. The bis(acetylsulfanyl) derivative **131** allowed conventional purification without the risk of oxidation. The acetyl protecting groups could be easily removed by treatment with a methanolic solution of cesium hydroxide to provide the free thiol **132**. Alternatively, methanolic solution of tetra(*n*-butyl)ammonium hydroxide was found to be a useful reagent for deacetylation, especially for *in situ* cleavage during the conductance measurements.¹⁶⁷



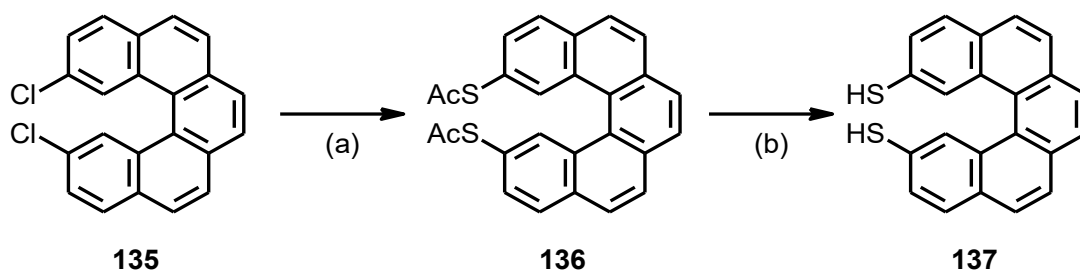
Scheme 40: (a) EtSH (24.0 equiv.), Na (20.0 equiv.), NMP, 250 °C, 2 h, then AcCl (30.0 equiv.), rt, 2 h, 94%; (b) DMDS (31.0 equiv.), Na (50.0 equiv.), NMP, 200 °C, 4 h, then AcCl (70.0 equiv.), rt, 2 h, 93%; (c) CsOH (8.0 equiv.), MeOH-MTBE (3:100), rt, 5 min, then HCl (20.0 equiv.), rt, 10 min, 71%.

The structurally similar dichloro[5]helicene **133**¹⁵⁹ provided the respective bis(acetylsulfanyl) derivative **134** also in good yield (**Scheme 41**). This example demonstrates that structural changes in the aromatic system have a negligible effect on its S_NAr -type reactivity.



Scheme 41: (a) DMDS (31.0 equiv.), Na (50.0 equiv.), NMP, 200 °C, 4 h, then AcCl (75.0 equiv.), rt, 2 h, 86%.

On the other hand, the position of chlorine atoms affects the S_NAr -type reactivity of the respective helicene systems as sulfanylation of dichloro[5]helicene **135**¹⁶⁹ delivered **136** in a slightly decreased yield (**Scheme 42**).



Scheme 42: (a) DMDS (31.0 equiv.), Na (50.0 equiv.), NMP, 200 °C, 4 h, then AcCl (75.0 equiv.), rt, 2 h, 77%; (b) NaOH (40.0 equiv.), CH₃OH-THF (2:1), rt, 3 h, then citric acid (50.0 equiv.), rt, 10 min, 62%.

A racemic single crystal of [5]helicene **136** was grown from a DCM-cyclohexane mixture. X-ray analysis revealed two symmetry-independent geometries nestled in the asymmetric unit of the P2₁/c space group (**Figure 27**). The two forms slightly differ in the values of the torsion angle defining the helical shape of the molecule, namely 29.43° and 29.71°.

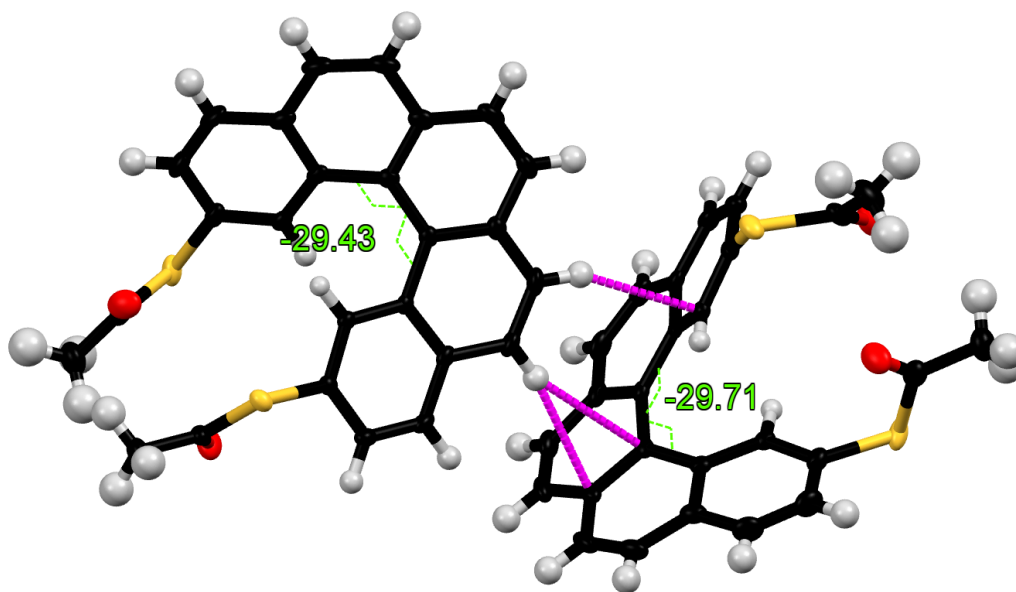
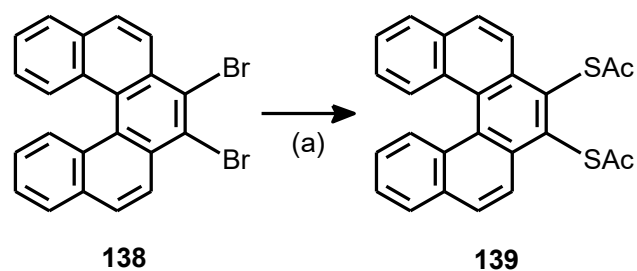


Figure 27: X-ray structure of the bis(acetylsulfanyl)[5]helicene derivative **136**; a CH- π interaction between the two asymmetric units (magenta dashed line)

7,8-Dibromo[5]helicene **138**¹⁶² also reacted smoothly with sodium methanethiolate in NMP at 200 °C affording the bis(acetylsulfanyl)[5]helicene derivative **139** in good overall yield (**Scheme 43**).



Scheme 43: (a) DMDS (31.0 equiv.), Na (50.0 equiv.), NMP, 200 °C, 4 h, then AcCl (75.0 equiv.), rt, 2 h, 71%.

The single-crystal X-ray analysis of helicene **139** revealed a highly symmetric crystal (space group $C2/c$), in which individual molecules are assembled into closely packed layers (**Figure 28b**). In this case, the torsion angle at the central benzene ring was found to be 29.71° (**Figure 28a**).

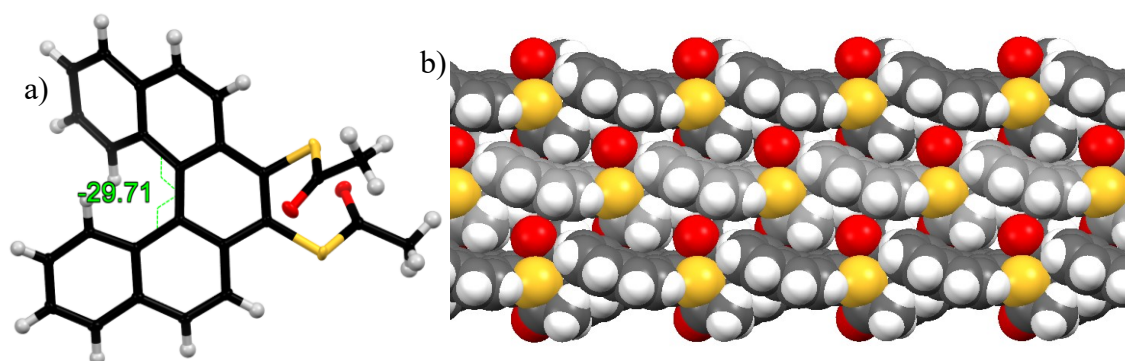
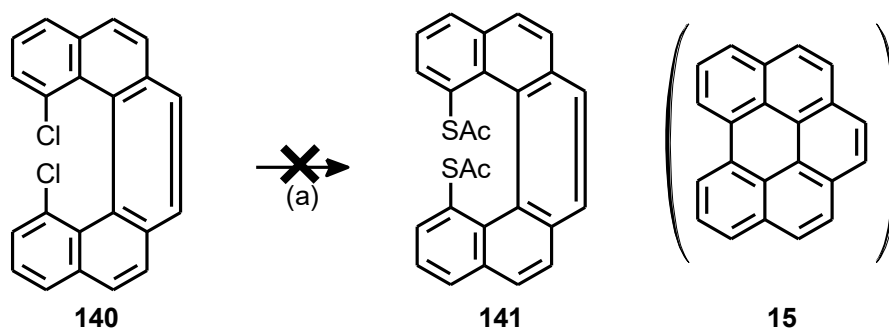


Figure 28: (a) X-ray structure of the bis(acetylsulfanyl)[5]helicene derivative **139**; (b) crystal packing of the bis(acetylsulfanyl)[5]helicene derivative **139**

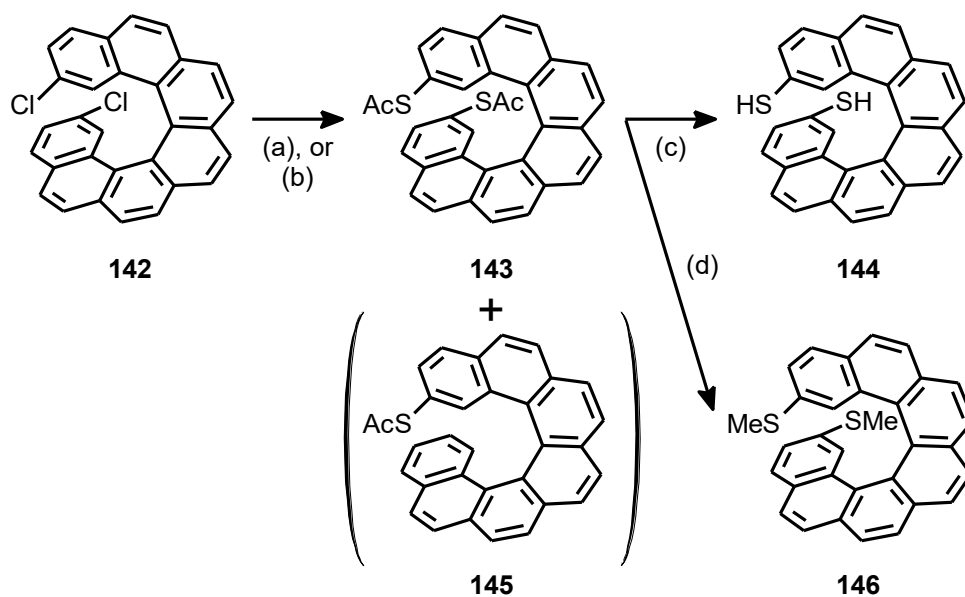
1,14-Dichloro[5]helicene **140**¹⁷⁰ was also subjected to the S_NAr sulfanylation reaction, but only the product of oxidative dehalogenation **15** was isolated (**Scheme 44**). Spontaneous formation of benzoperylene **15** was also observed during heating of **140** in the absence of any reagent.



Scheme 44: DMDS (25.0 equiv.), Na (40.0 equiv.), NMP, 200 °C, 4 h, then AcCl (60.0 equiv.), rt, 2 h, 0% (for **141**); 85% (for **15**).

On the contrary, the sulfanylation reaction performed on the longer dichloro[7]helicene derivatives afforded lower yields of the desired bis(acetylsulfanyl)[7]helicene congeners. Upon treatment with methanethiolate in NMP at 200 °C, the readily available 2,17-dichloro[7]helicene **142**¹⁷¹ provided the respective bis(acetylsulfanyl)[7]helicene derivative **143** in 65% yield (**Scheme 45**). Alternatively, the use of ethanethiolate at 250 °C resulted in faster formation of **143** but partial dehalogenation also took place to deliver the monoacetylsulfanylated [7]helicene **145**. The deprotected dithiol **144** was found to be extremely sensitive to oxidation by air to form insoluble oligomeric disulfides.

The bis(methylsulfanyl)[7]helicene derivative **146** was prepared from the bis(acetylsulfanyl) derivative **143** rather than dichloride **142**¹⁷¹, as it is difficult to control direct methylsulfanylation.



Scheme 45: (a) EtSH (50.0 equiv.), Na (40.0 equiv.), NMP, 270 °C, 2 h, then AcCl (60.0 equiv.), rt, 2 h, 32% (for **143**), 43% (for **145**); (b) DMDS (31.0 equiv.), Na (50.0 equiv.), NMP, 200 °C, 4 h, then AcCl (75.0 equiv.), rt, 2 h, 65% (c) CsOH (8.0 equiv.), THF, rt, 5 min, then citric acid (10.0 equiv.), rt, 10 min, 87%, (d) NaH (8.0 equiv.), MeI (12 equiv.), NMP, rt, 2h, 71%.

Single crystals suitable for X-ray analysis were prepared from both stable derivatives **143** and **146** (**Figure 29**). The distance between overlapping terminal rings is 3.9 Å in the case of **143** and 4.1 Å in the case of **146**. As the intermolecular distances in the crystal packing are quite similar (3.4 Å), the relatively significant difference in the helicene pitch can be most likely attributed to electron density changes on the aromatic rings. These originate from electron-withdrawing character of the acetyl group and electron-donating character of the methyl substituent.

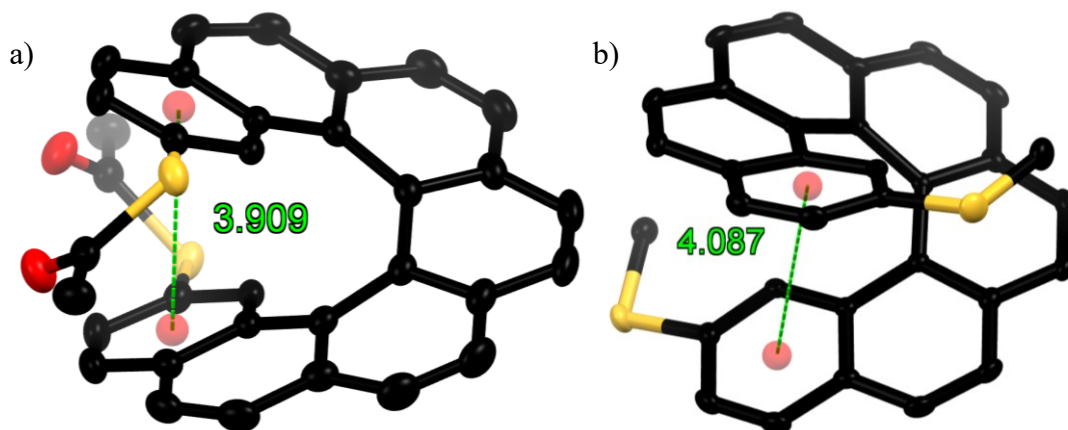
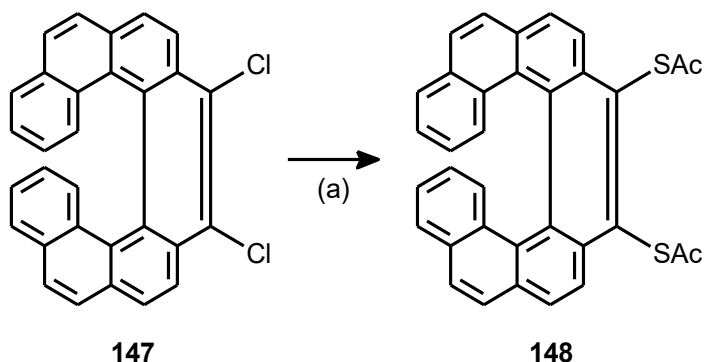


Figure 29: X-ray structures: (a) bis(acetylsulfanyl)[7]helicene derivative **143**; (b) bis(methylsulfanyl)[7]helicene derivative **146**

9,10-Dichlorohelicene **147**¹⁷⁰ was also subjected to the sulfanylation reaction with sodium methanethiolate to provide the bis(acetylsulfanyl)[7]helicene derivative **148** in still reasonable yield (**Scheme 46**).



Scheme 46: (a) DMDS (31.0 equiv.), Na (50.0 equiv.), NMP, 200 °C, 4 h, then AcCl (75.0 equiv.), rt, 2 h, 59%.

Single crystal X-ray analysis of **148** revealed a very close crystal packing with helicene-to-helicene distances as short as 3.6 Å, which is even shorter than the distance between the terminal rings of the same helicene (4.0 Å, **Figure 30**). For comparison, the distance between the two layers in the graphite crystal is 3.3 Å.¹⁷²

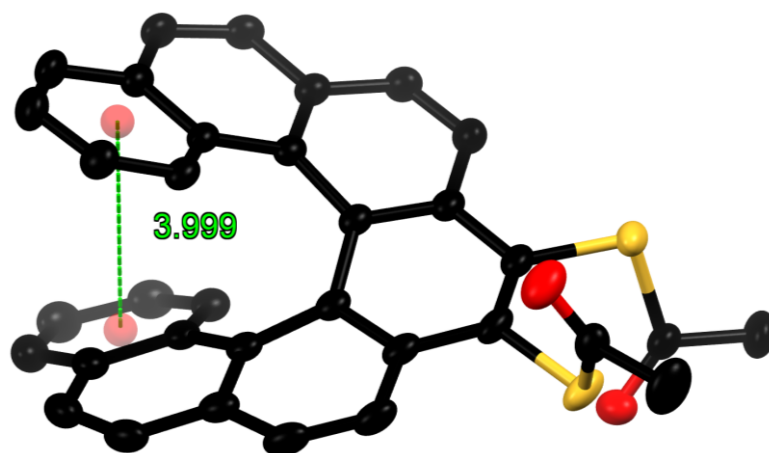
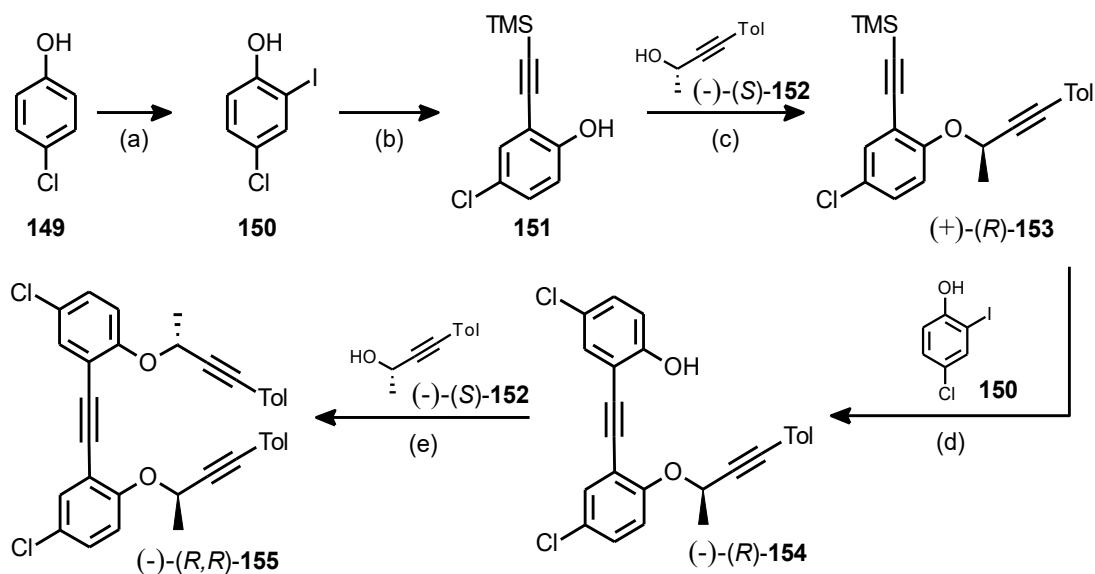


Figure 30: The X-ray structure of the bis(acetylsulfanyl)[7]helicene derivative **148**

3.2.2.3 The Synthesis of Sulfanylated Oxa[n]helicenes

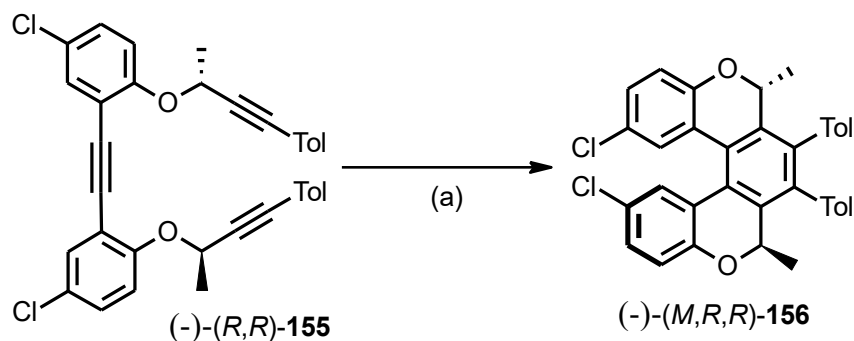
As mentioned in Chapter 2, the aim of this work was to develop the synthesis of long helicenes bearing anchoring groups with high affinity to gold. In the previous chapters, the [2+2+2] cyclotrimerization methodology was shown to be highly robust and versatile to prepare specifically designed racemic as well as optically pure long helicenes. Furthermore, sulfur-based anchoring groups were successfully attached to chlorinated carbahelicenes. The next logical step was to attempt sulfanylation of long oxahelicenes. However, since their electronic nature differs significantly from the fully aromatic helicenes, the dichlorooxa[5]helicene model compound **156** was synthesized first in order to examine the S_NAr -type sulfanylation reaction.

The synthetic sequence leading to the diastereo- and enantiopure oxa[5]helicene dichloride (-)-(*M,R,R*)-**156** is shown in **Scheme 47** and **Scheme 48**. First, the commercially available *p*-chlorophenol **149** was iodinated under basic conditions to provide chloriodophenol **150**.¹⁷³ It was a suitable substrate for the subsequent Sonogashira coupling with (trimethylsilyl)acetylene that furnished the TMS-protected alkyne **151**. Then, a Mitsunobu reaction with the enantiopure butynol (*S*)-**152**¹⁷⁴ was used to prepare the enantiopure diyne (+)-(*R*)-**153**, which was in the following step deprotected and coupled *in situ* with iodide **150** via another Sonogashira reaction to afford diyne (-)-(*R*)-**154**. Finally, the enantiopure triyne (-)-(*R,R*)-**155** was prepared by yet another Mitsunobu reaction with the enantiopure butynol (-)-(*S*)-**152**¹⁷⁴.



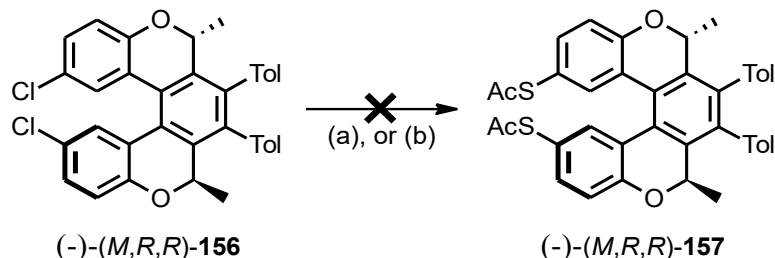
Scheme 47: (a) KI (3 equiv.), I₂ (1 equiv.), NH₃ (aq.), 0 °C, 2 h, 64%; (b) TMSA (1.6 equiv.), Pd(PPh₃)₂Cl₂ (2 mol%), CuI (4 mol%), DIPA (1.2 equiv.), toluene, rt, 3 h, 94%; (c) (*S*)-**152**¹⁷⁴ (1.1 equiv.), PPh₃ (1.1 equiv.), DIAD (1.1 equiv.), benzene, rt, 3 h, 91%; (d) TBAF·3H₂O (1.2 equiv.), THF, rt; then **150** (1.3 equiv.), Pd(PPh₃)₂Cl₂ (2 mol%), CuI (4 mol%), DIPA (1.3 equiv.), toluene, rt, 16 h, 81%; (e) (*S*)-**152**¹⁷⁴ (1.1 equiv.), PPh₃ (1.1 equiv.), DIAD (1.1 equiv.), benzene, rt, 3 h, 75%.

The [2+2+2] cyclotrimerization of the enantiopure triyne (*-*)-(*R,R*)-**155** to the diastereo- and enantiopure dichlorooxa[5]helicene derivative (*-*)-(*M,R,R*)-**156** proceeded smoothly in a microwave reactor (**Scheme 48**), which represents a simpler experimental setup with respect to the use of a flow reactor. The solvent was changed from tetrahydrofuran to chlorobenzene because of its superior ability to absorb microwave irradiation.



Scheme 48: (a) CpCo(CO)₂ (1.0 equiv.), chlorobenzene, microwave reactor, 180 °C, 20 min, 70%.

Unfortunately, sulfanylation of (*M,R,R*)-**156** did not proceed at all under the reaction conditions successfully applied to carbahelicenes (**Scheme 49**). Only partial dehalogenation was observed according to the NMR analysis of the reaction mixture.

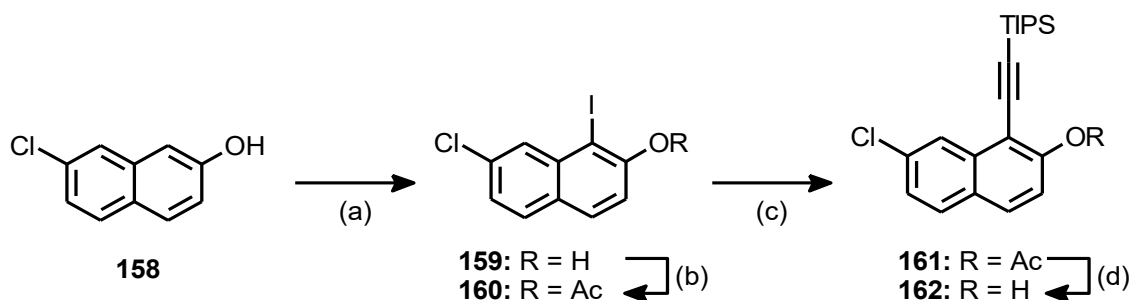


Scheme 49: EtSH (24.0 equiv.), Na (20.0 equiv.), NMP, 250 °C, 2 h, then AcCl (30.0 equiv.), rt, 2 h, 0%; (b) DMDS (31.0 equiv.), Na (50.0 equiv.), NMP, 200 °C, 4 h, then AcCl (70.0 equiv.), rt, 2 h, 0%.

The most probable reason for the low reactivity of (-)-(M,R,R)-**156** is the presence of an alkoxy substituent on the aromatic ring in *para* position with respect to the chlorine atom, which decreases its susceptibility towards nucleophilic attack.

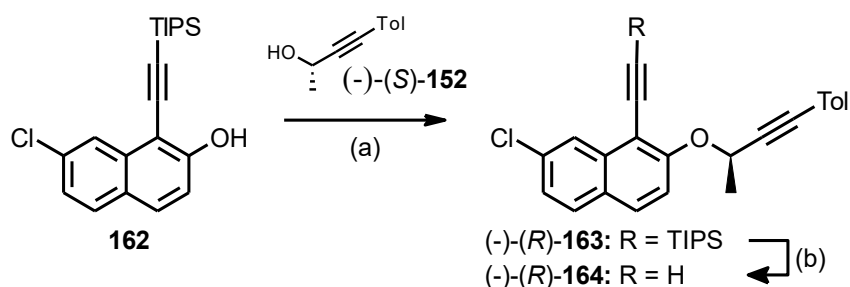
To overcome this obstacle, the naphthalene building block **164**¹⁶⁸ (**Scheme 51**) was selected, in which the undesirable effect of the electron-donating alkoxy substituent is attenuated. Moreover, its use should also provide an oxa[6]helicene analogue.

Regioselective iodination of the commercially available 7-chloronaphthalen-2-ol **158** provided the iodo derivative **159**¹⁶⁸ (**Scheme 50**). The free hydroxy group was acetylated before a Sonogashira coupling with triisopropylsilyl acetylene. It is worth noting that, specifically in this case, the free hydroxy group in a close proximity to the ethynyl moiety tends to add across it to undergo the *endo-5-dig* cyclization leading to a furan derivative under Sonogashira reaction conditions. Consequently, the bulk TIPS protecting group was installed on the triple bond as it survives the basic conditions needed for acetate hydrolysis. In spite of the necessity of additional protection and deprotection steps, high overall yield of naphthylalkyne **162**¹⁶⁸ was obtained.



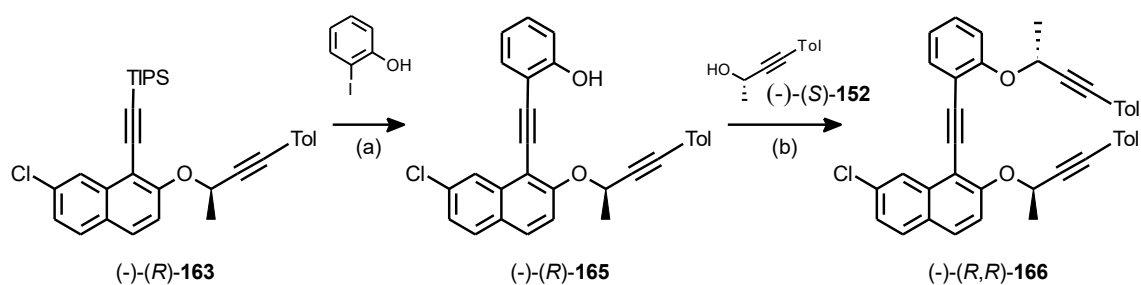
Scheme 50: (a) I₂ (1.0 equiv.), Na₂CO₃ (2.0 equiv.), THF-H₂O (4:1), rt, 4 h, 99%; (b) Et₃N (2.5 equiv.), AcCl (1.5 equiv.), CH₂Cl₂, 0 °C to rt, 5 h, 99%; (c) TIPSA (1.2 equiv.), Pd(PPh₃)₂Cl₂ (2 mol%), CuI (5 mol%), DIPA (1.2 equiv.), toluene, rt, 13 h, 91%; (d) K₂CO₃ (2.0 equiv.), THF-MeOH (1:1), rt, 3 h, 99%.

The chiral alcohol (-)-(*S*)-**152**¹⁷⁴ was then attached to naphthol **162** via Mitsunobu reaction (**Scheme 51**). Unfortunately, the order of the ether formation and Sonogashira coupling cannot be interchanged, although it would shorten the synthesis by eliminating the protection and deprotection steps. The reason is the intramolecular carbopalladation side-reaction that might take place under the Sonogashira reaction conditions.^{175,176}



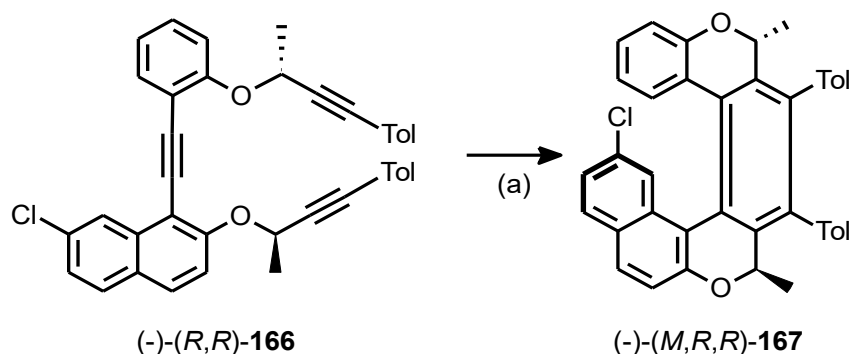
Scheme 51: (a) (-)-(*S*)-**152** (1.1 equiv.), PPh₃ (1.1 equiv.), DIAD (1.1 equiv.), benzene, ice bath to rt, 3 h, 79%; (b) TBAF·3H₂O (3.1 equiv.), THF, rt, 1 h, 99%.

Finally, the enantiopure triyne (-)-(*R,R*)-**166** was prepared by a sequence of Sonogashira reaction with 2-iodophenol and Mitsunobu reaction with the chiral alcohol (-)-(*S*)-**152** (**Scheme 52**).



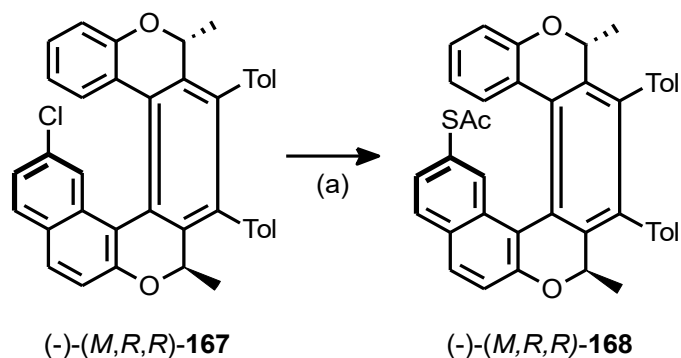
Scheme 52: (a) TBAF·3H₂O (1.2 equiv.), toluene, rt, 30 min, then 2-iodophenol (3.0 equiv.), Pd(PPh₃)₄ (10 mol%), CuI (20 mol%), DIPA (1.1 equiv.), toluene, 45 °C, 16 h, 67%; (b) (-)-(S)-**152** (1.1 equiv.), PPh₃ (1.2 equiv.), DIAD (1.1 equiv.), toluene, ice bath to rt, 3 h, 81%.

Using the reaction conditions successfully applied in the synthesis of the dichlorooxa[5]helicene derivative (-)-(M,R,R)-**156** (Scheme 48), cyclotrimerization of triyne (-)-(R,R)-**166** proceeded in the microwave reactor to give the chlorooxa[6]helicene derivative (-)-(M,R,R)-**167** in good yield (Scheme 53).



Scheme 53: (a) CpCo(CO)₂ (1.0 equiv.), chlorobenzene, microwave reactor, 180 °C, 20 min, 59%.

In contrast to the unsuccessful sulfanylation of the dichlorooxa[5]helicene derivative (-)-(M,R,R)-**156**, the chlorooxa[6]helicene derivative (-)-(M,R,R)-**167** was converted smoothly to the corresponding monoacetylsulfanylated derivative (-)-(M,R,R)-**168** in good yield (Scheme 54). This result confirmed the proper choice of the chloronaphthalene building block (-)-(R)-**164** in the synthesis of optically pure long oxahelicenes bearing sulfur-based anchoring groups.



Scheme 54: (a) DMDS (12.5 equiv.), Na (20.0 equiv.), NMP, 200 °C, 4 h, then AcCl (30.0 equiv.), rt, 2 h, 85%.

Single crystal X-ray analysis (a single crystal grown from a DCM-cyclohexane solution) of (-)-(M,R,R)-168 confirmed its structure (**Figure 31**). The acetyl group is highly disordered with two distinct orientations prevailing in the crystal lattice. In either case the group is oriented perpendicularly to the plane of the adjacent benzene ring, pointing either outwards or inwards with respect to the helix. The two conformers also differ significantly in their helical pitch, where the inward-oriented acetyl group causes the distance between the terminal helicene rings to grow by ~ 0.5 Å. This elongation along the helicene z axis confirms the spring-like behavior of this class of molecules as suggested by calculations.²

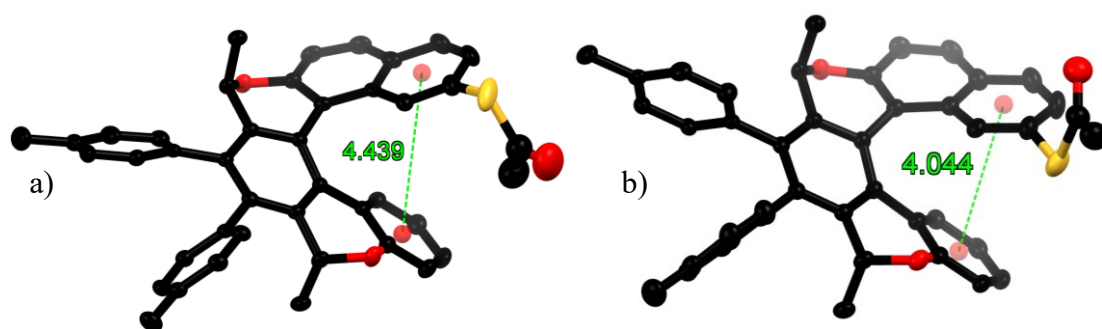
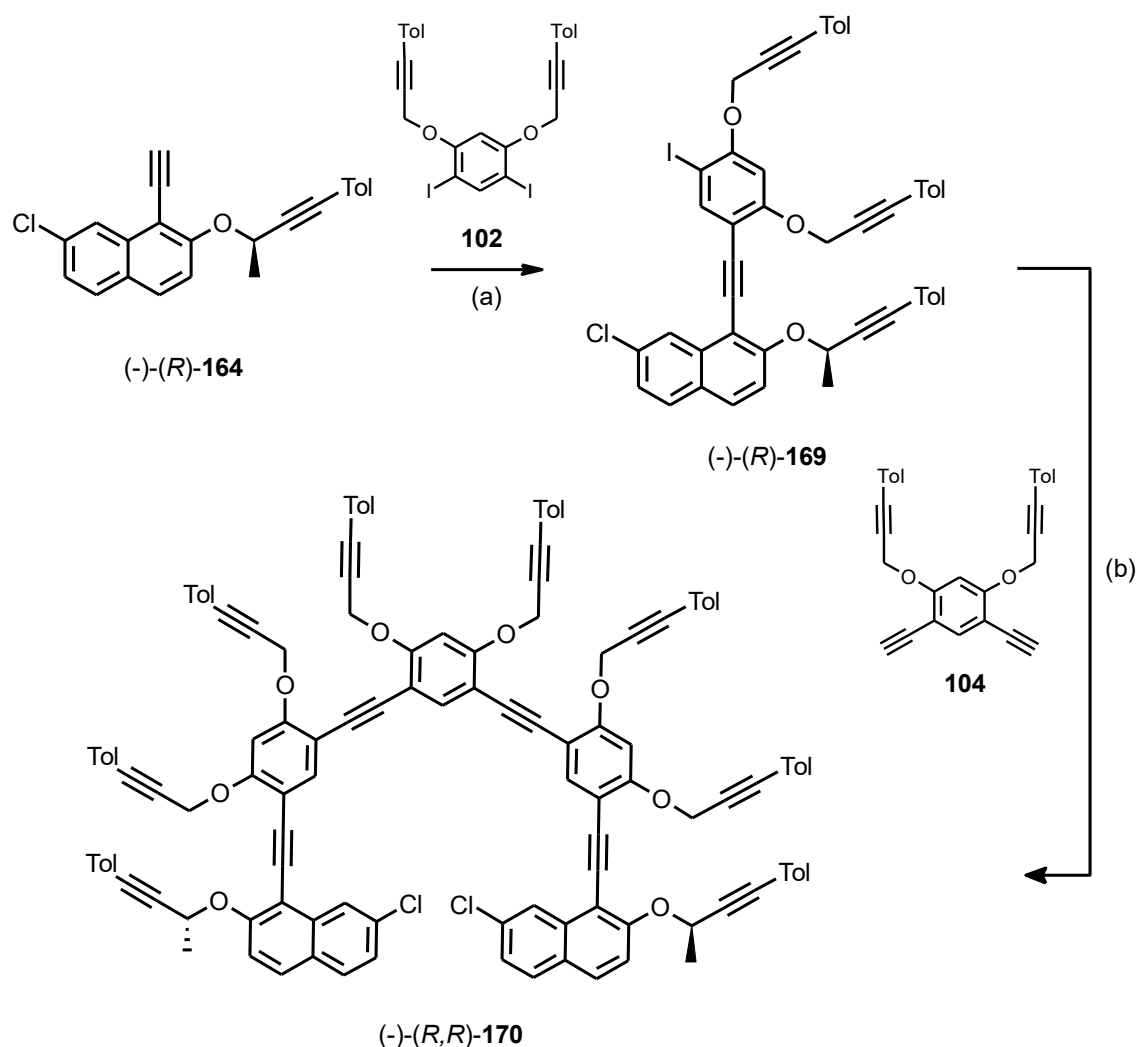


Figure 31: X-ray analysis of the (acetylsulfanyl)oxa[6]helicene derivative (-)-(M,R,R)-168 showing two distinct conformers: with the acetyl group pointing (a) inwards or (b) outwards with respect to the helix

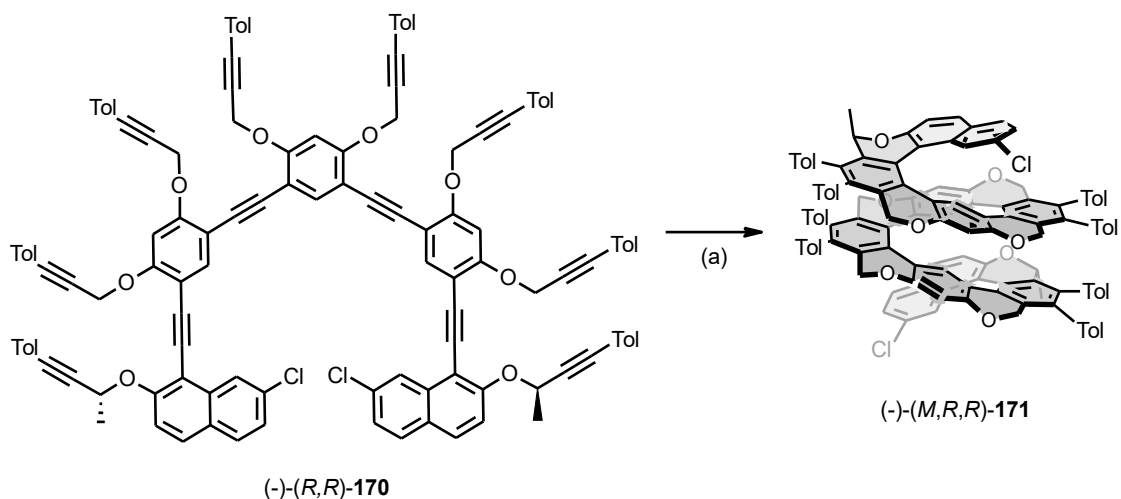
Encouraged by the successful synthesis of oxa[19]helicene (-)-(M,R,R)-86 and usefulness of the chloronaphthalene building block (-)-(R)-164 in the synthesis of the acetylsulfanylated oxa[6]helicene derivative (-)-(M,R,R)-168, the preparation of dodecayne (-)-(R,R)-170 was attempted (**Scheme 55**) *en route* to the diastereo- and

enantiopure oxa[19]helicene dithiol (-)-(*M,R,R*)-**172**. Following the procedures demonstrated earlier, the desymmetrized iodotetrayne (-)-(*R*)-**169** was prepared. Three equivalents of resorcinol building block **102** were used in order to suppress oxidative dimerization of the terminal alkyne (-)-(*R*)-**164**. Then, a two-fold Sonogashira reaction with tetrayne **104** provided the desired compound (-)-(*R,R*)-**170** in high yield. The use of the already tolylated building block (-)-(*R*)-**164** excluded the necessity of a late-stage derivatization, thus simplifying the synthesis and improving the overall yield of the final oligoyne (-)-(*R,R*)-**170**.



Scheme 55: (a) **102** (3.0 equiv.), Pd(PPh₃)₄ (15 mol%), CuI (30 mol%), DIPA-toluene (5:8), rt, 16 h, 84%; (b) **104** (0.45 equiv.), Pd(PPh₃)₄ (9 mol%), CuI (19 mol%), DIPA-toluene (3:4), rt, 16 h, 69%.

Similarly to the oxa[19]helicene **85**, [2+2+2] cyclotrimerization of the chiral dodecayne (-)-(R,R)-**170** proceeded in a flow reactor at 250 °C to deliver the dichlorinated oxa[19]helicene (-)-(M,R,R)-**171** (Scheme 56). In this case, however, the reaction time was reduced by half in order to avoid an unwanted dehalogenation reaction that accompanied the cyclization at such a high reaction temperature.



Scheme 56: (a) CpCo(CO)₂ (2.0 equiv.), THF, flow reactor, 250 °C, 8 min, 20%.

A significant change in the CD spectrum (Figure 32) as well as enhancement of the optical rotation value confirmed the formation of the helical product. According to the helicene-chemistry “rule of thumb”, the negative sign of the longest-wavelength CD band is indicative of *M* helicity of the product (-)-(M,R,R)-**171**.

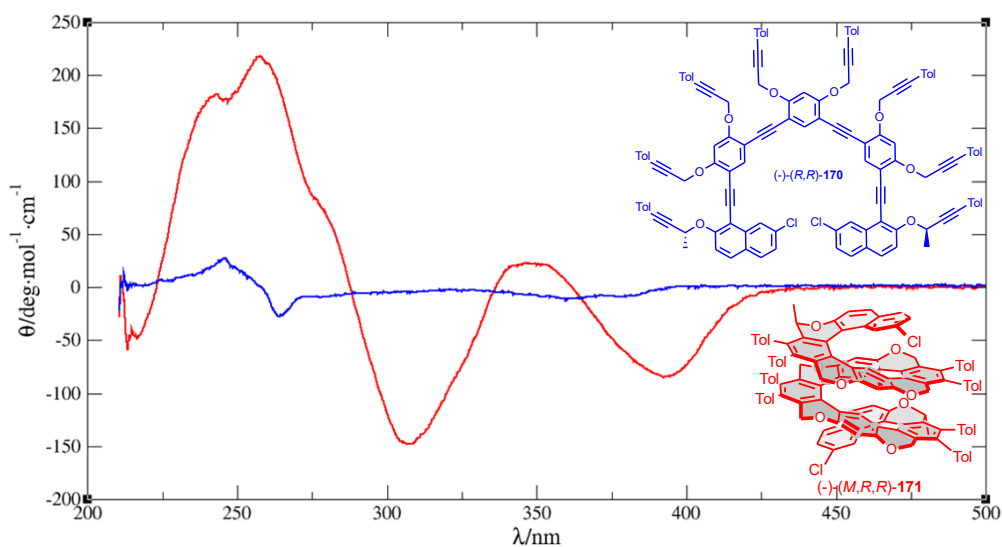


Figure 32: CD spectra of oligoyne (-)-(R,R)-**170** (blue) and dichlorooxa[19]helicene derivative (-)-(M,R,R)-**171** (red)

An unequivocal proof of the structure of the dichlorooxa[19]helicene derivative (-)-(*M,R,R*)-**171** was obtained through the single crystal crystallographic analysis (**Figure 33**), confirming its counterclockwise helicity (*M*) with respect to the known *R*-configuration at the chiral centers.

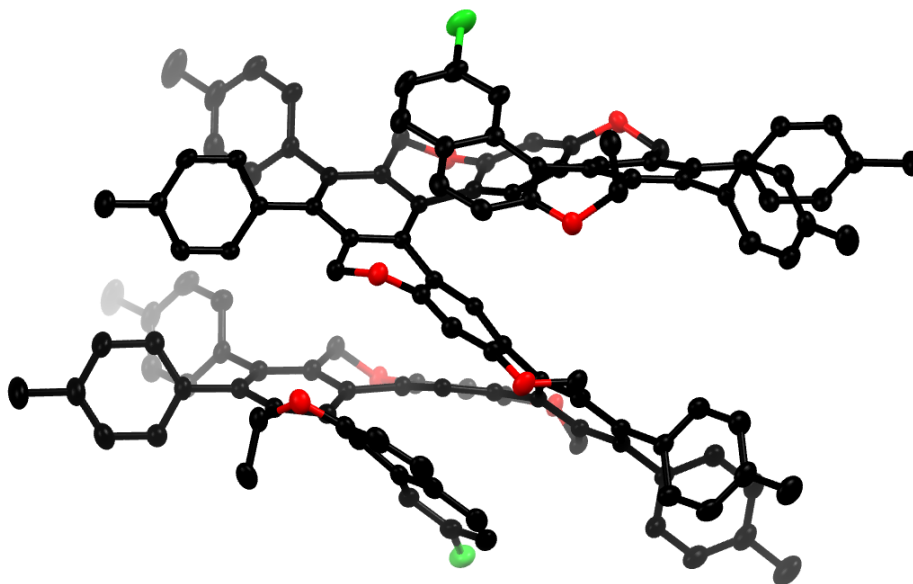
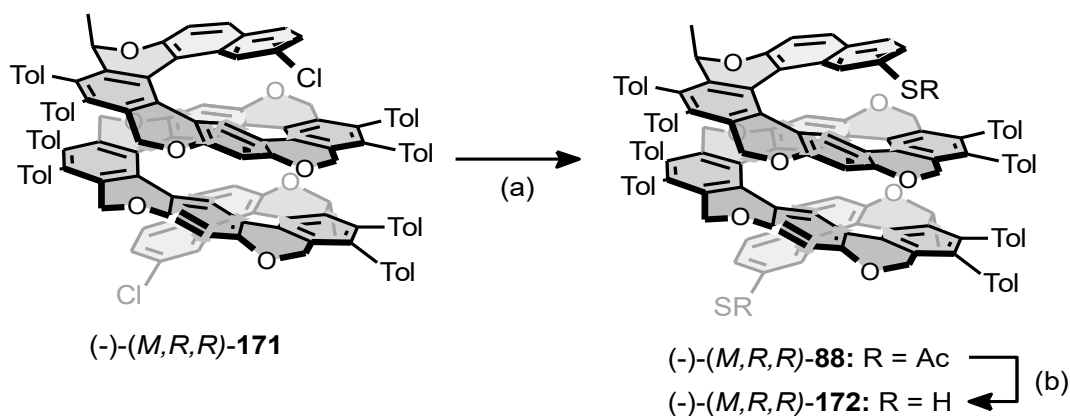


Figure 33: X-ray structure of the dichlorooxa[19]helicene derivative (-)-(*M,R,R*)-**171** (solvent molecules and hydrogen atoms were omitted for clarity)

Finally, bis(acetylsulfanyl)oxa[19]helicene (-)-(*M,R,R*)-**88** was prepared from dichlorooxa[19]helicene (-)-(*M,R,R*)-**171** and sodium methanethiolate being freshly generated from DMDS (**Scheme 57**). The reaction was quenched with acetyl chloride to give overall yield 42%, which is very decent considering the substrate's complexity. The acetyl protecting groups were cleaved by treatment with sodium hydroxide. However, the oxa[19]helicene dithiol (-)-(*M,R,R*)-**172** had to be prepared, isolated and analyzed under strictly oxygen-free conditions due to its extremely high sensitivity towards oxidation in solution. On the other hand, in solid state, this dithiol is quite stable.



Scheme 57: (a) DMDS (31.0 equiv.), Na (50.0 equiv.), NMP, 200 °C, 4 h, then AcCl (75.0 equiv.), rt, 2 h, 42%; (b) NaOH (40.0 equiv.), MeOH-THF (2:1), rt, 3 h, then citric acid (50.0 equiv.), rt, 10 min, 78%.

3.3 Break Junction Experiments

3.3.1 Break Junction Device Development

Even though the break junction (BJ) techniques are irreplaceable for single molecule conductance measurements, we are not aware of any commercially available and inexpensive device for this purpose. Each apparatus is thus a unique, custom-made and self-designed piece of art, which is being continuously improved, developed and extended.

The development of a BJ apparatus is a complex issue, which covers several fields of research activity such as materials science, fine mechanics engineering, electronics, and as such it requires a broad collaboration (Prof. Josef Zicha, Czech Technical University in Prague, Faculty of Mechanical Engineering; Dr. Ladislav Sieger and Prof. Karel Hoffmann, Czech Technical University in Prague, Faculty of Electrical Engineering; BMD a.s.).

In our case, the development of the device was started by the Development Center at IOCB Prague and the state of the device at the beginning of my participation in the project is shown in **Figure 34a**.

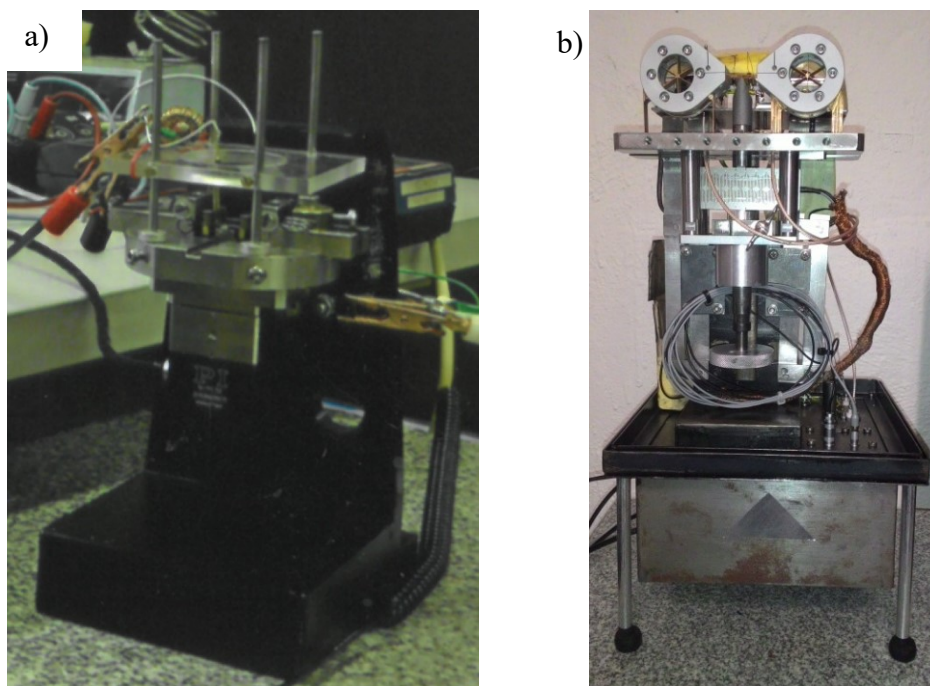


Figure 34: The first prototype of the MCBJ device: a) built by the Development Center of the IOCB Prague, 2012; b) development model of the device in 2016

No molecules could be studied at that time due to the insufficient sampling rate (maximally 5 kSa, kiloSamples per second), low precision (only 3.5 digit of precision at 5 kSa) and accuracy 300 ppm, low actuator force (pushing force 20 N) and stiffness, nonlinearity of actuator motion and ineffective shielding. Many changes have been made since. A development model from the year 2016 is shown for comparison (**Figure 34b**).

Although our STM-BJ device model from 2016 was already able to reproducibly measure single-molecule conductance, we continued in improving the entire apparatus, with the emphasis on electronic parts. These include a logarithmic amplifier and stabilized power sources responsible for improved signal-to-noise ratio as well as high sampling rate and noise suppression. One of the crucial parts of the experiment is the shielding.

Based on the previous knowledge, aluminum alloy was chosen as the shielding material. This alloy has several advantages: (i) it has a very high conductance, which makes it suitable for electric shielding, (ii) it is cheaper than copper, (iii) it has higher chemical stability due to lead additives and (iv) it is much lighter than other materials. This shielding is less effective against magnetic interferences, so further improvements will be needed in the future, for example addition of shielding parts made of Permalloy or other nickel–iron alloys with a very high magnetic permeability.

3.3.2 Mechanically Controllable Break Junction (MCBJ)

Description of the current device: The BJ device contains several essential parts: (i) source of constant voltage for the measurement, (ii) sample holder, (iii) data acquisition unit, (iv) amplifier, (v) actuator, (vi) controlling unit and (vii) shielding box.

Long-range sample movement (several millimeters) is actuated by a micrometric screw, but only piezo actuators have sufficient accuracy for fine handling and mechanical durability for continual service. The whole measurement is controlled by a computer, which is also used for data storage. A custom-made program was composed and is described in more detail in Chapter 3.3.4.

A schematic representation of the MCBJ setup is depicted in **Figure 35** and the actual design of the current device is shown in **Figure 36a**. It allows an acquisition sampling rate of up to 200 kSa and is able to cover the conductance dynamic range of 8 orders of magnitude with the detection limit of 100 fA. The precise digital multimeter Agilent 3458 has 8.5 digits of precision and extremely high accuracy of 4 ppm. The used enhanced piezo has pushing and blocking force 100 N. A precise, self-locking micrometric screw is used for the rough long-range adjustment of the sample. The used travel range of the micrometric screw is up to tenths of millimeters. The custom-built stabilized source was designed so that it can operate at two ranges 20 – 200 mV and 0.2 – 2 V. The commonly used bias is 100.0 mV.

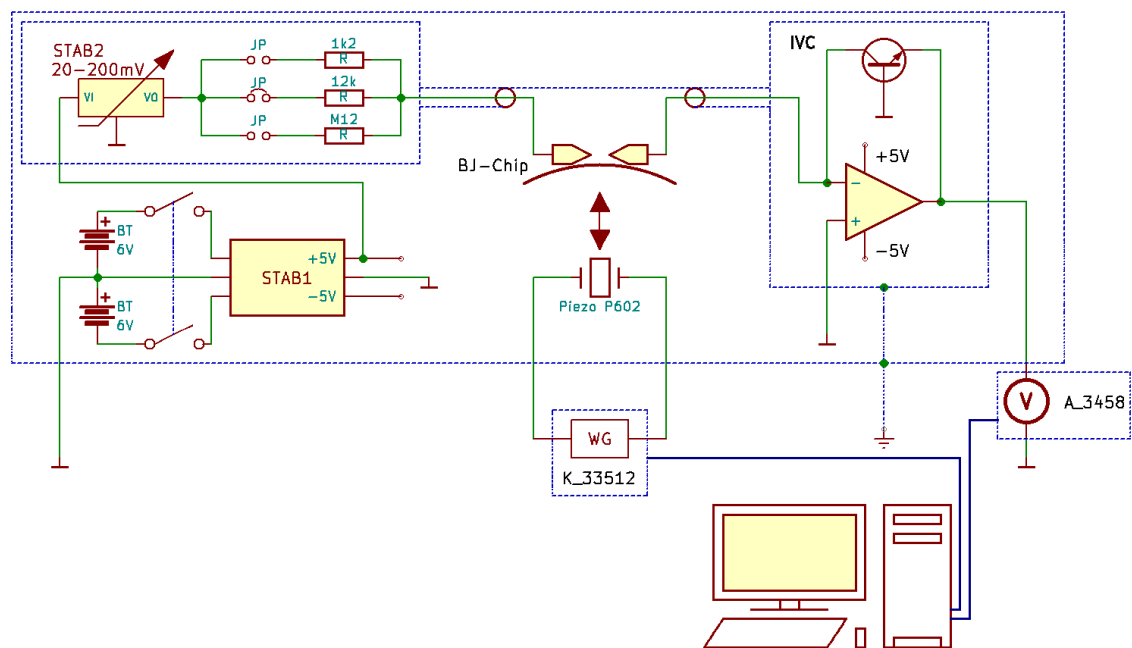


Figure 35: Scheme of the MCBJ measurement circuit

The device is powered by two sets of lead accumulator packs, which allows continuous operation of the device. One battery pack is wired into the electric circuit while the second one is charged. To eliminate any voltage fluctuations, a stabilized source of bias (**STAB1**) is incorporated in the circuit. The stabilized source (**STAB1**, custom-built) has two branches: +5V and -5V to supply (i) another stabilized source (**STAB2**, custom-built), which is used for the actual measurement, and (ii) a custom-made current-to-voltage convertor (**IVC**). The accurate adjustable stabilized source (**STAB2**) suppresses external noise and allows to set the measurement bias with the required precision (tens of μV). The main part of the **IVC** is a logarithmic amplifier, which allows to measure the current in a range of several orders of magnitude. The output voltage is then measured by precise digital multimeter Agilent 3458 (**A_3458**, Keysight Technologies). The adjustment and position corrections of the pushing rod are performed by a piezo actuator (**P602**, Physik Instrumente GmbH & Co. KG), which is controlled by a waveform generator K_33512B (**WG**, Keysight Technologies). The experiment itself takes place on a “**BJ-Chip**”, where the actual gold bridge is located. The whole device is shielded and grounded. Shielding is symbolized by the blue dashed line. Each sensitive component is enclosed inside an individual shielding box as depicted. The data cables are symbolized by thick blue lines in **Figure 35**.

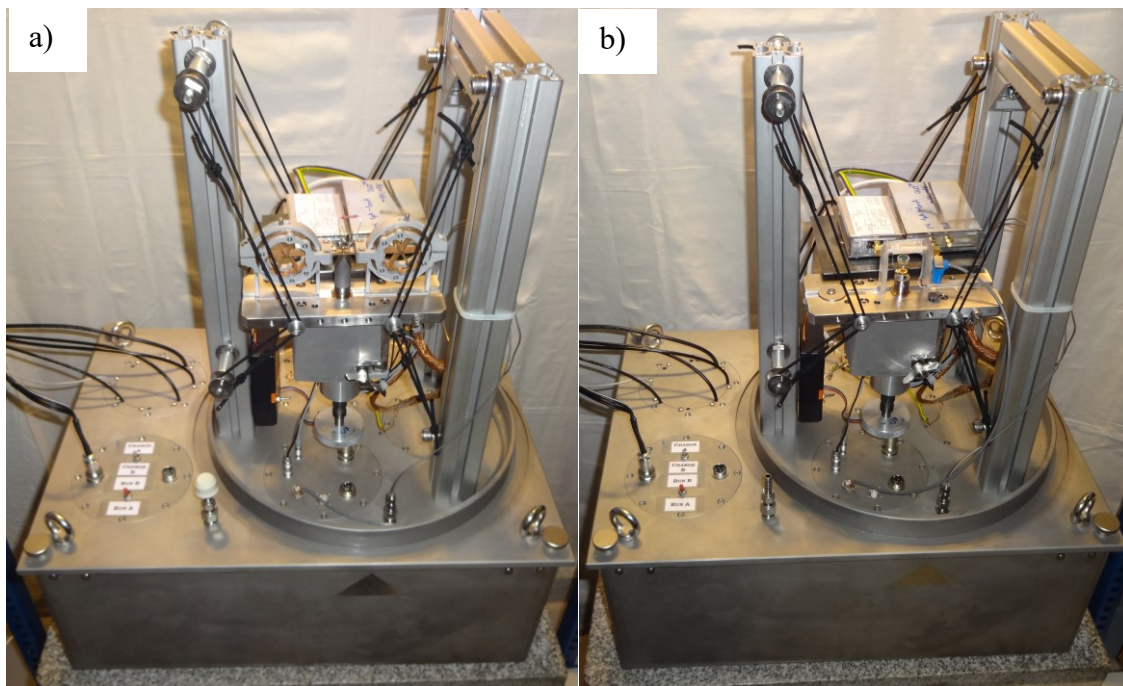


Figure 36: Current state of the device: (a) MCBJ; (b) STM-BJ

3.3.3 Scanning Tunneling Microscopy-Based Break Junction (STM-BJ)

Only a few changes in the MCBJ setup were needed to operate the device in the STM-BJ mode (**Figure 37**). In this configuration, the piezo actuator (**P602**) adjusts the position of the substrate while an additional piezo stack motor (**PZT2**, Mad City Labs GmbH) controlled by another waveform generator (**WG**) performs the tapping motion. The actual design of the current STM-BJ device is shown in **Figure 36b**.

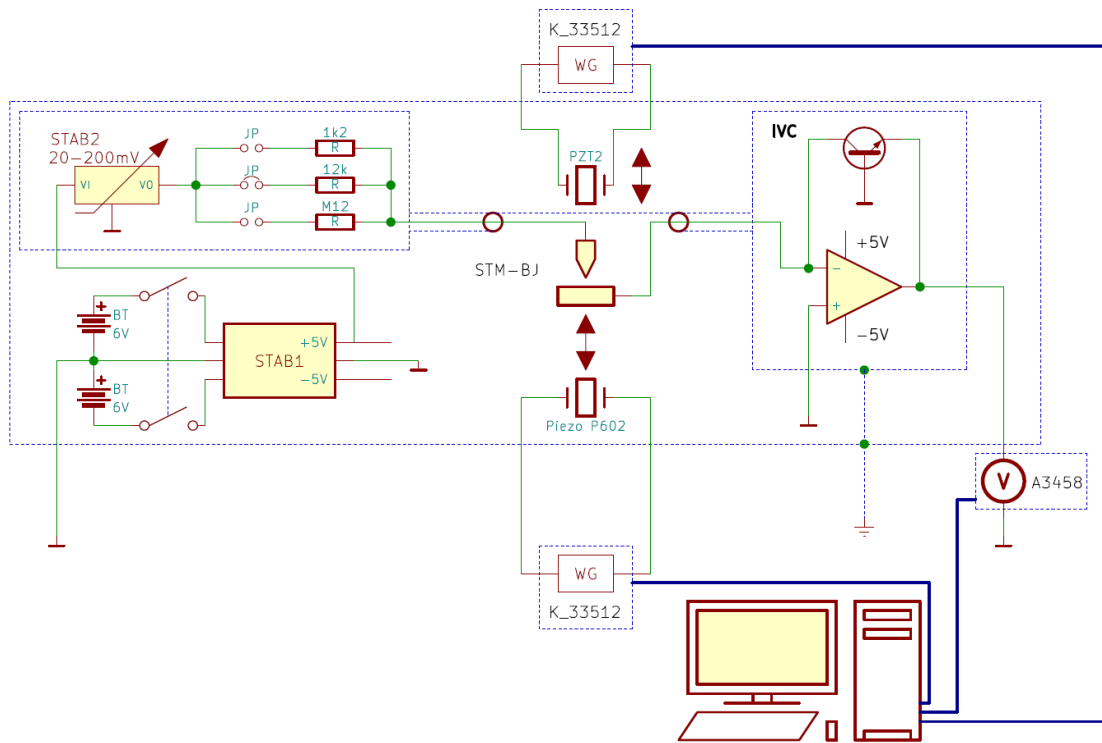


Figure 37: Scheme of the STM-BJ measurement circuit

3.3.4 Computer Control and Data Analysis

The experiment controlling program was created in the LabView¹⁷⁷ environment, its graphical programming language allowing simple incorporation of measurement hardware such as multimeters, actuators, controllers and other devices from various vendors. Its visualization helps to create and understand the logical processes, data analysis algorithms and finally also to optimize the user interface. The actual interface is shown in **Figure 38**. It includes numerous libraries with prepared drivers, which simplify the first steps.

The controlling program has many options and gives the operator full control over the components of the BJ device. Control of the wave generator, piezo actuator and

voltmeter allows the operator to change the frequency and speed of contact breaking, sampling rate as well as sample counts within one data set. It is also possible to use various driving signals for the piezo actuator in order to handle the molecule. This kind of handling can be used for example to investigate molecular switching at certain conductance level. The program can run in a semi-automatic regime, collecting up to hundreds of thousands of curves (gigabytes of data) during the experiment. Finally, the program also provides a preliminary statistical analysis.

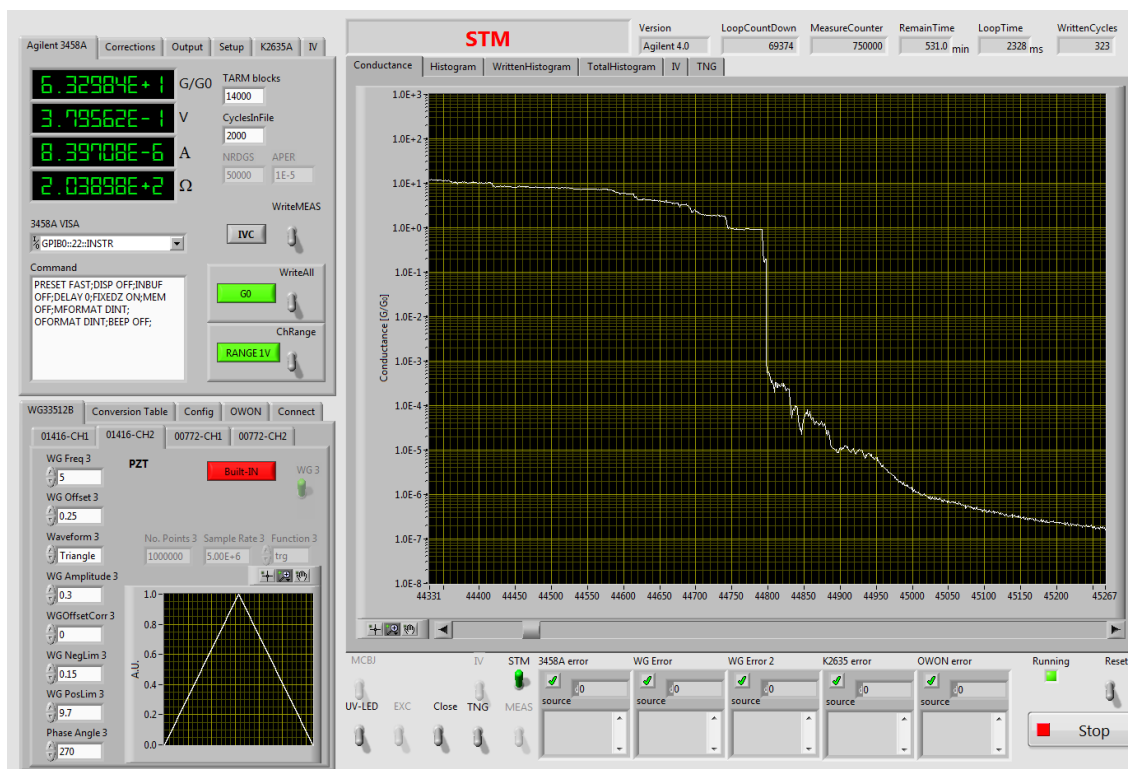


Figure 38: LabView program interface

Data from a small set of curves (usually 5) are immediately saved to a hard drive so that a potential data loss has negligible statistical value.

The complete data set from one BJ experiment (up to tenths of GB), which is usually spread over several files, is then processed with another analyzing program created by Dr. Jaroslav Vacek (Institute of Organic Chemistry and Biochemistry of the Czech Academy of Sciences) using Fortran programming language.¹⁷⁸ This program was specially designed and developed for analysis of extremely large data sets. The program sorts, discards, and selects the breaking curves according to required criteria, *e.g.* breaking curve length, noise level or plateaus appearance, plateaus conductance or plateaus length. Statistical data processing is also performed by the program.

3.4 Single-Molecule Conductance Measurement

Once operational, the BJ device was evaluated by single-molecule conductance measurements of molecules, which were already characterized in this way in the literature.

3.4.1 Evaluation of Standards

To evaluate functionality a reliability of our methodology several experiments had been done. Measurements of standards such as 1,4-bis(methylsulfanyl)benzene (BMSB) **173** or 4,4'-bipyridine (BIPY) **73** bearing typical anchoring groups were performed (**Figure 39**).

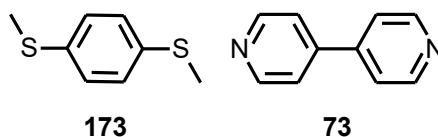


Figure 39: Standard molecules for break junction measurement

The bis(methylsulfanyl) derivative **173**¹⁷⁹ was studied and the resulting histograms are free of artifacts caused by the formation of disulfide bridges. The logarithmic histogram is shown in **Figure 40**. The conductance maximum of $2 \cdot 10^{-2} G/G_0$ is in perfect agreement with the literature.¹⁷⁹

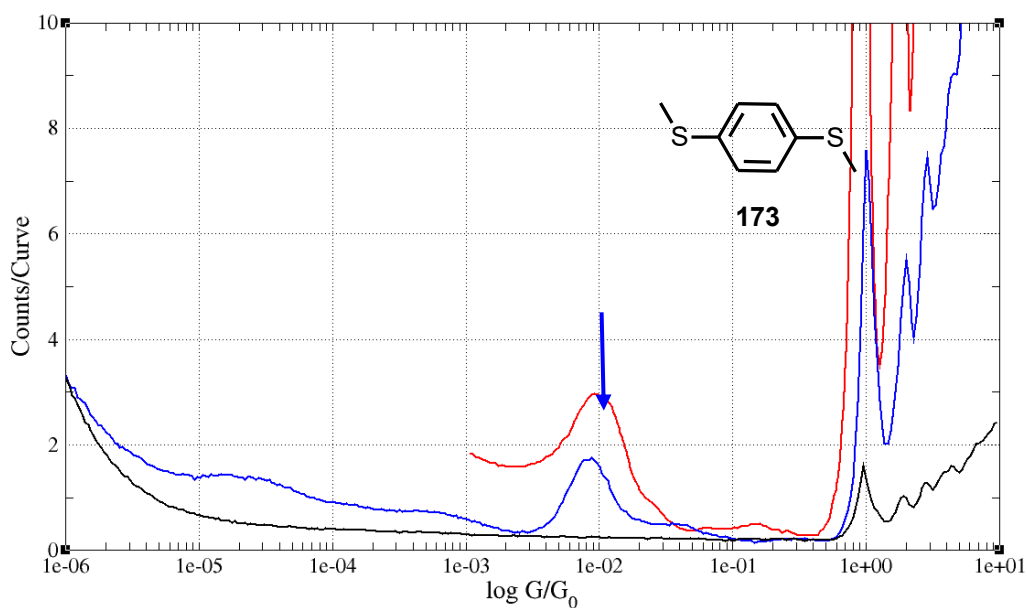


Figure 40: The logarithmic conductance histogram of BMSB **173** (blue), gold (black), previously published data (red)¹⁷⁹

Recently BIPY **73**⁹⁸ became a newly established standard. It was deeply studied by Venkataraman and co-workers^{180,181} to elucidate its conductance and on-surface behavior. This molecule also does not suffer from oxidative degradation and has a typical double peak in the molecule-conductance area. The conductance measured with our device are shown in **Figure 41** and agrees perfectly with the published data.¹⁸¹

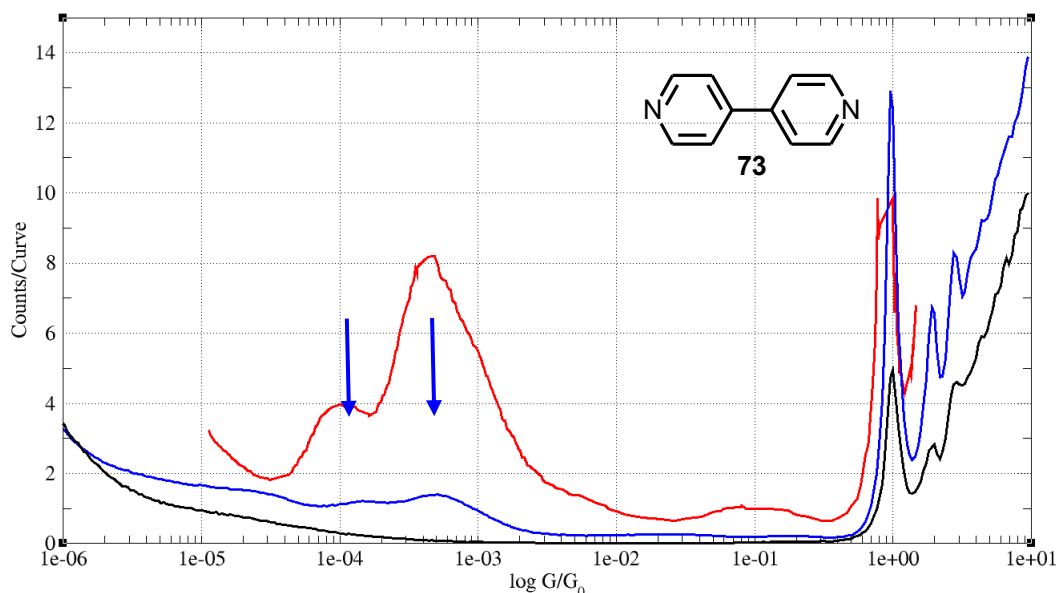


Figure 41: The logarithmic conductance histogram of BIPY **73** (blue), gold (black), previously published data (red)¹⁸¹

On account of this clear agreement between our experiments and literature data it was decided to continue with more complex molecules. A rigid linear molecule had been chosen for these experiments. Rod-like oligo(phenyl acetylenes) bearing two anchoring groups seem to be ideal candidates for this study because of the low number of degrees of freedom. The conductance histograms are thus not complicated by additional influences caused by intramolecular geometrical changes.

The already published dithiol **174**¹⁸² was chosen for this experiment so that the comparison could be easily done. A significant peak appeared after addition of the solution of the dithiol **174**¹⁸², which was in good agreement with the reported conductance of $2.9 \pm 0.5 \cdot 10^{-4} G/G_0$ as shown in the histogram overlay (**Figure 42**).

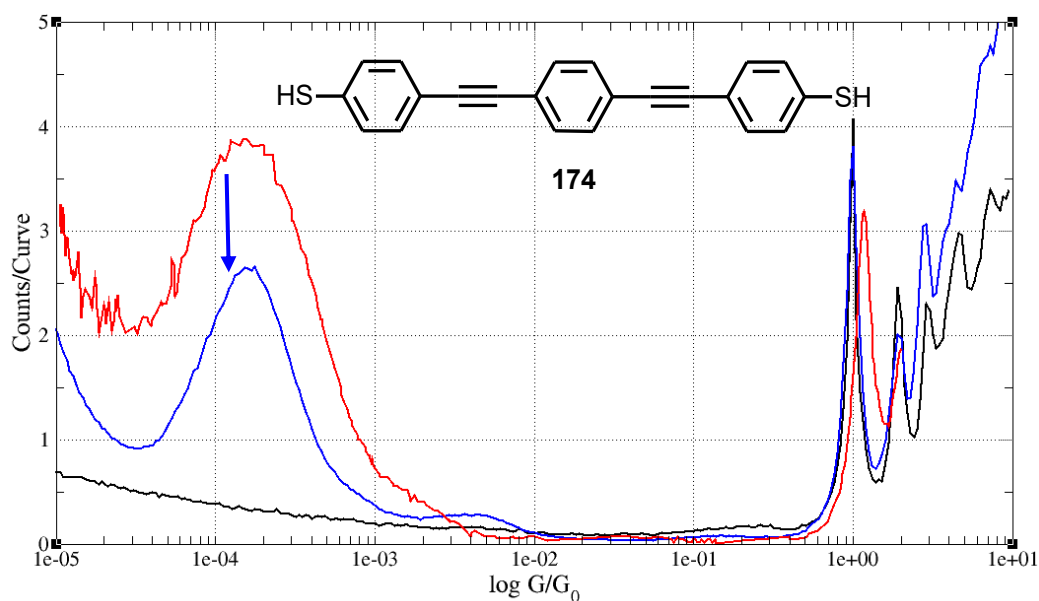


Figure 42: The logarithmic conductance histogram of oligo(phenyl acetylene) **174** (blue) and gold (black), the published conductance histogram (red)¹⁸²

3.4.2 Single-Molecule Conductance of Helicene Derivatives

To the best of our knowledge, no helicene single-molecule break junction measurements have been published prior to our study and the first results published by us.¹⁴⁸

(-)-(M,R,R)-Pyridooxa[9]helicene **87**

The (-)-(M,R,R)-pyridooxa[9]helicene **87** was chosen as a representative of the class of azahelicenes. The choice might be surprising, but there are several reasons for that. Even though it is not fully aromatic helicene, the internal helical π -electron system is present in this molecule. The methyl groups in position 6 and 6' prevent the helicene from the attachment by metallic electrodes through the extended π -electron system, thus opening charge transfer across additional transmission channels through more benzene rings similar to the case of BIPY **73**.^{121,181} The helicene (-)-(M,R,R)-**87** contains two pyridine subunits, which were expected to create sufficiently strong bonds to gold. The blue curve in **Figure 43** shows the conductance peak corresponding to the tunneling regime (MCBJ experiments). This molecule showed surprisingly high conductance with maximum at $8.8 \cdot 10^{-4} G/G_0$. The calculation done by Dr. Jaroslav Vacek (IOCB Prague), using QuantumWise's Atomistix Toolkit (ATK) program^{183,184} and NEGF, provided a slightly higher conductance ($4.5 \cdot 10^{-3} G/G_0$) in comparison with the experiment.

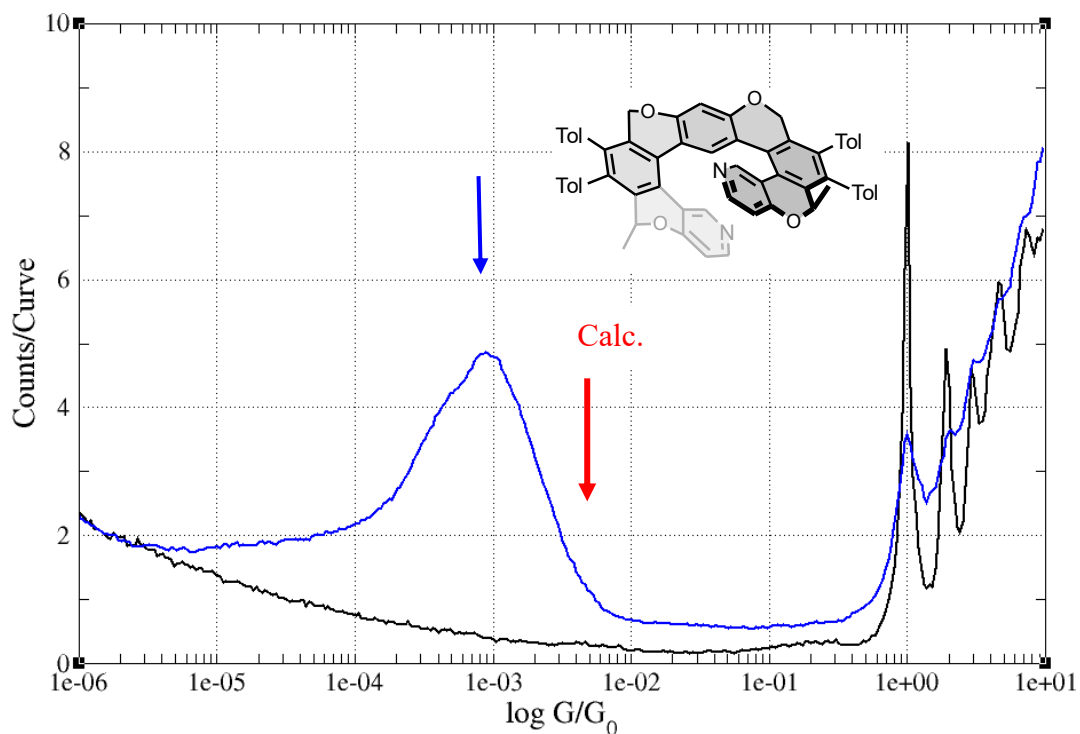


Figure 43: The logarithmic conductance histogram of gold (black) and the (-)-(M,R,R)-pyridooxa[9]helicene **87** (blue) (MCBJ experiments); the red arrow shows the calculated conductance value

The respective two-dimensional histogram (**Figure 44**) showed the length of the molecule (-)-(M,R,R)-**87**, which corresponds well to the calculated distance between nitrogen atoms in the relaxed-state geometry.

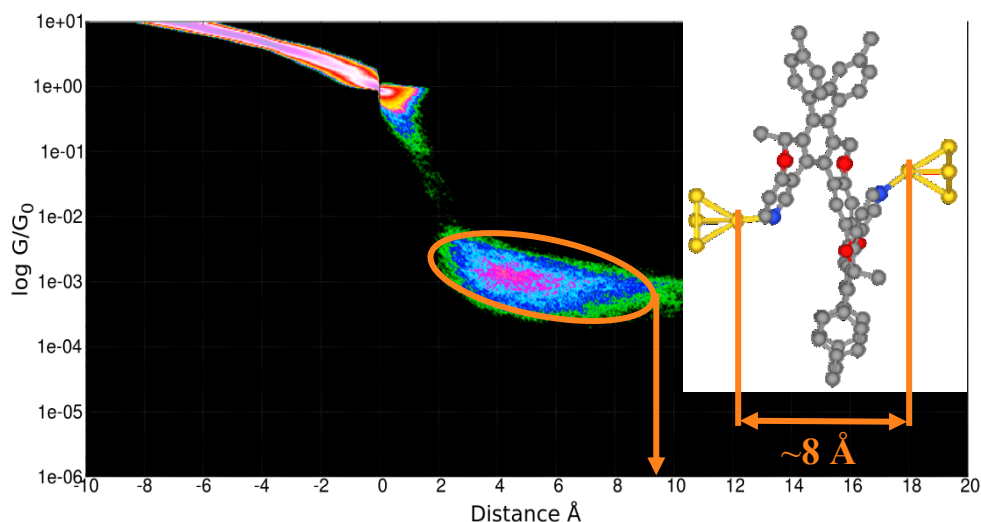


Figure 44: The 2D conductance histogram of (-)-(M,R,R)-**87**, the molecule effective length is marked in orange (MCBJ experiments); inset: the Au-molecule-Au bridge with the calculated distance between the apex gold atoms

Some examples of breaking curves observed during the MCBJ measurements are shown in **Figure 45**.

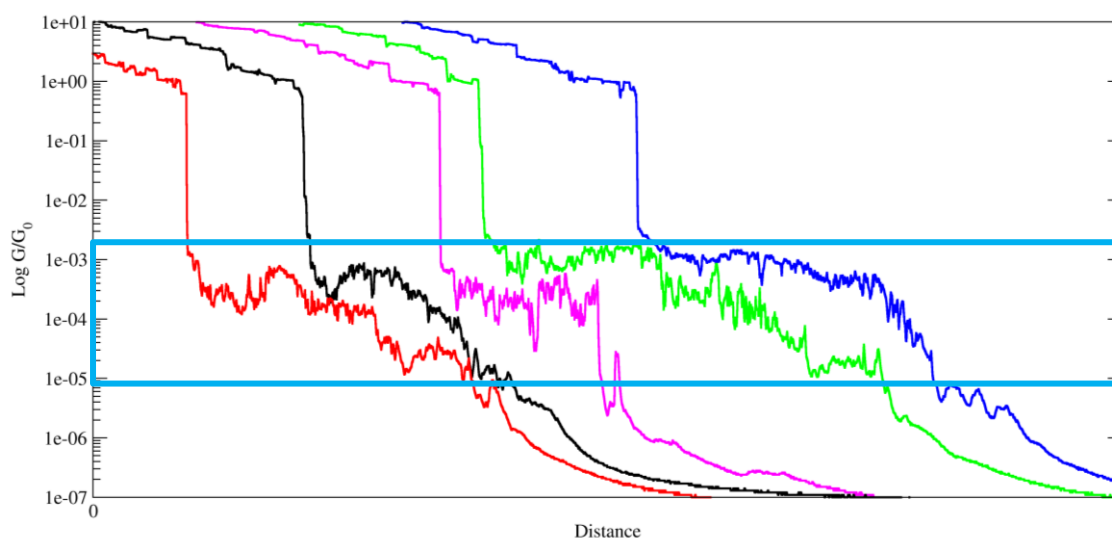


Figure 45: Breaking curves of (-)-(M,R,R)-**87** with conductance plateaus in the blue area (MCBJ experiments)

3,12-Bis(acetylsulfanyl)dibenzo[5]helicene **131**

As far as sulfanylated helicenes are concerned, single-molecule conductance of the bis(acetylsulfanyl)dibenzo[5]helicene derivative **131** was investigated by STM-BJ experiments. This compound contains also the picene subunit, which makes it more rigid

in comparison to simple [5]helicene derivatives. The on-surface behavior of **131** should be more confined because of reduced degrees of freedom. The conductance peak with maximum of $1.1 \cdot 10^{-3} G/G_0$ was obtained from the logarithmic conductance histogram (Figure 46). The calculated conductance value ($8 \cdot 10^{-3} G/G_0$) is slightly higher, but within the same order of magnitude.

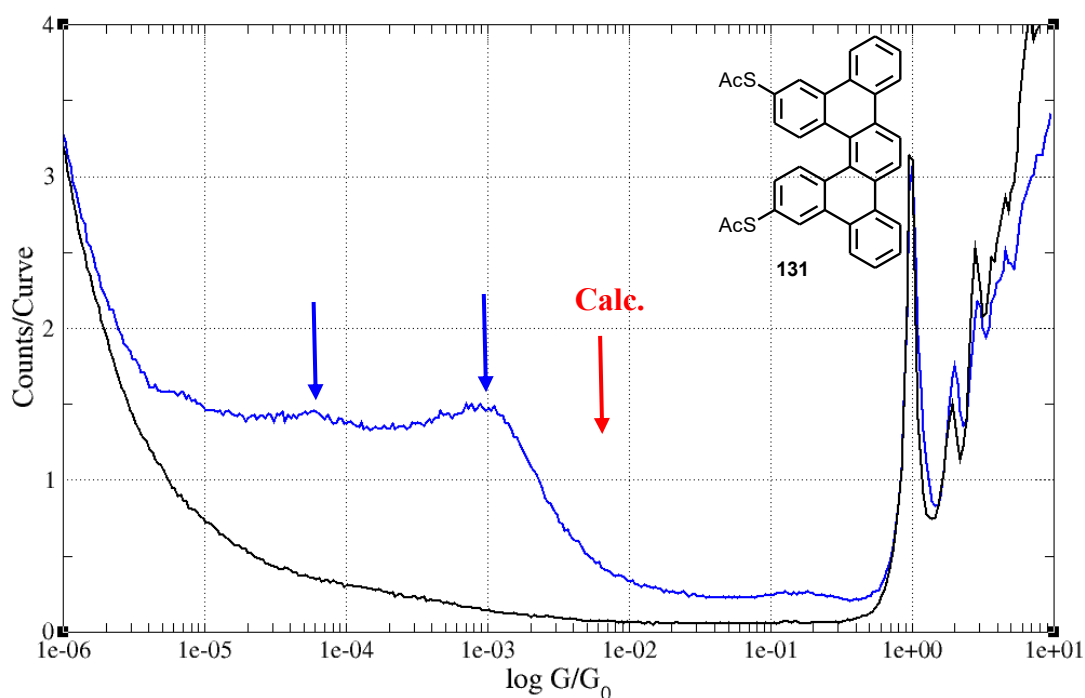


Figure 46: The logarithmic conductance histogram of gold (black) and the bis(acetylsulfanyl)dibenzo[5]helicene **131** (blue)

The minor conductance peak at $6.3 \cdot 10^{-4} G/G_0$ is probably caused by the attachment of the molecule to the electrode through the oxygen atom of the acetylsulfanyl group, similarly to the case of [7]helicene **143** described later. The attachment geometry of the dibenzo[5]helicene **131** (Au-S-molecule-S-Au) is well-defined and recognizable in the 2D conductance histogram (Figure 47). The gap between the electrodes correlates well with the sulfur-sulfur distance in the molecule increased by gold-sulfur bond length of 2.2 \AA .¹⁸⁵

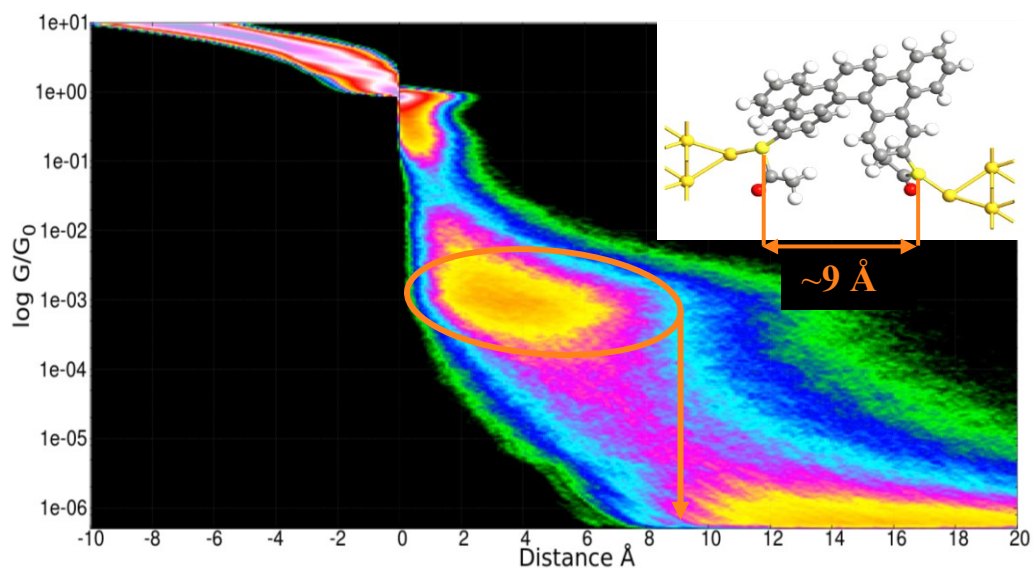


Figure 47: The 2D conductance histogram of [5]helicene **131**, the molecule effective length is marked in orange (STM-BJ experiments); inset: Au-molecule-Au bridge with the calculated distance between the sulfur atoms

The observed breaking curves reveal two preferred geometries: through-sulfur bonding (the higher conductance level) and through-oxygen bonding (the lower conductance level) (**Figure 48**). These conductance states seem to interconvert one into the other that leads to switching the single-molecule conductance value. This effect needs further experimental and computational investigation in order to explore this phenomenon and describe it in more detail.

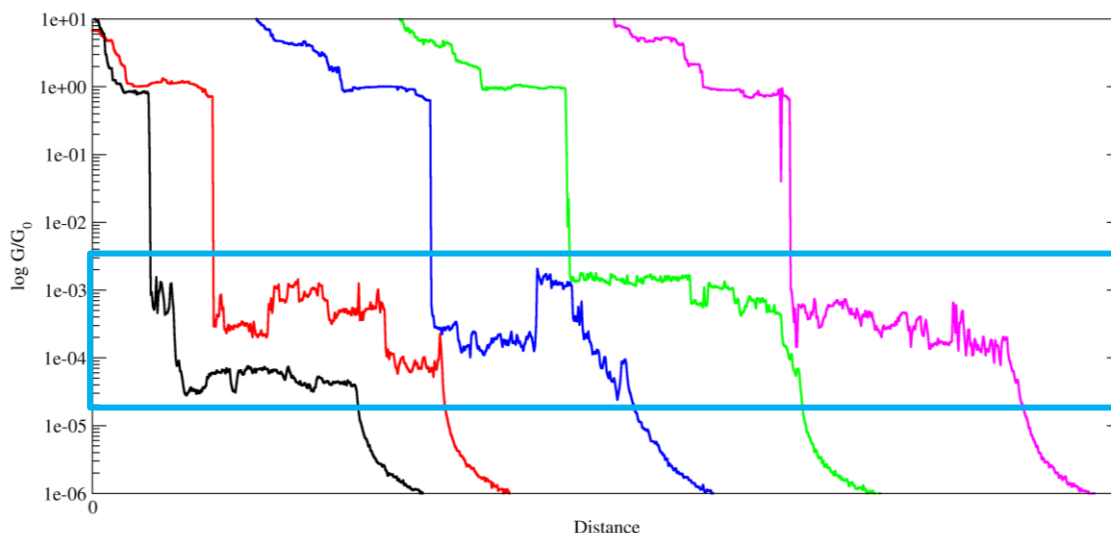


Figure 48: Breaking curves of [5]helicene **131** with conductance plateaus in the blue area indicating the conductance switching (STM-BJ experiments)

2,17-Bis(acetylsulfanyl)[7]helicene **143**

The bis(acetylsulfanyl)[7]helicene **143** is the most deeply studied sulfanylated helicene in this series. Its physical properties were co-investigated in collaboration with other research groups, *vide infra*.

The logarithmic conductance histogram of [7]helicene **143** is depicted in **Figure 49** showing two conductance peaks. The two maxima are indicated by arrows. The higher conductance maximum at approximately 0.01 G/G_0 was assigned to the bonding geometry, where the molecules are attached to the gold electrodes *via* the sulfur atoms of the acetylsulfanyl groups. Additionally, a second bonding geometry, in which attachment to the gold electrodes is facilitated *via* the oxygen atoms of the acetylsulfanyl groups, was proposed. In this case conductance drops down by circa one order of magnitude to the value of $2 \cdot 10^{-3} \text{ G/G}_0$. The calculated conductance value ($1 \cdot 10^{-1} \text{ G/G}_0$) is higher similar to previously mentioned helicenes. This observation is in agreement with the results obtained in the group of Prof. Stefan Müllegger (Johannes Kepler University Linz; unpublished results), where studies on the interaction of this molecule (adsorbed on Au surface) with radiofrequency field are in progress.

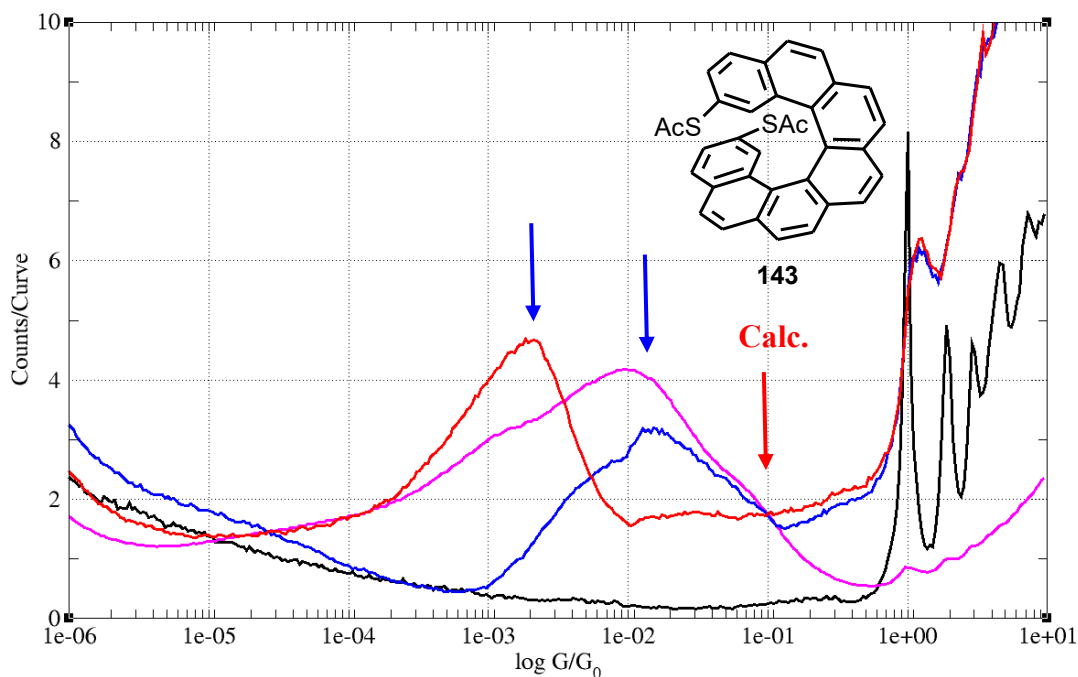


Figure 49: The logarithmic conductance histogram of gold (black), [7]helicene **143** (magenta), through-sulfur bonded [7]helicene **143** (blue; selection), through-oxygen bonded [7]helicene **143** (red, selection) (MCBJ experiments)

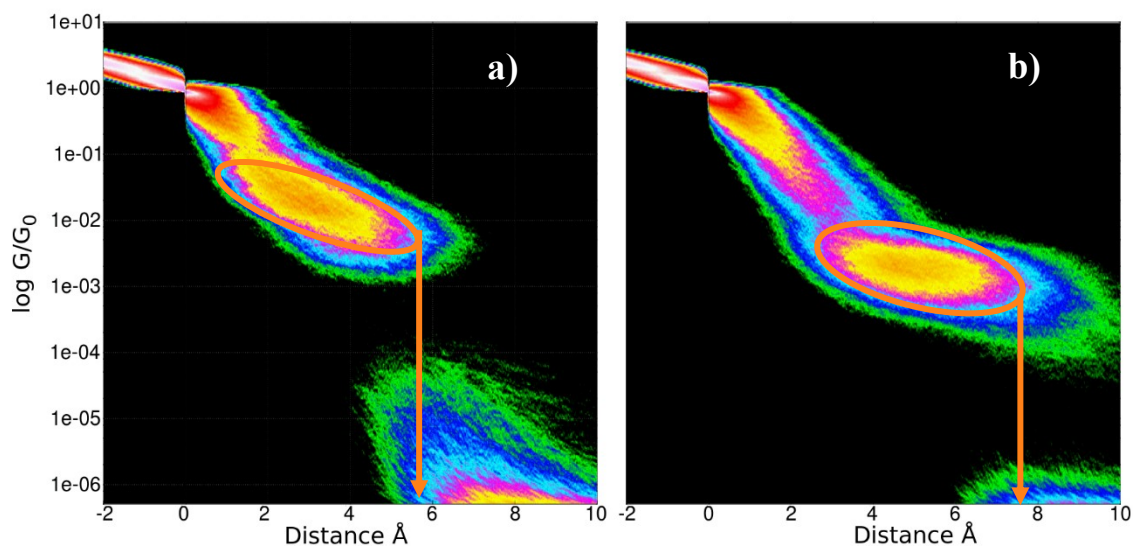


Figure 50: The 2D histograms of [7]helicene **143** (MCBJ experiments) (a) sulfur bonded; (b) oxygen bonded

The distance-dependent conductance is depicted in the 2D-histogram (**Figure 50**), which is in good agreement with the molecule dimensions received from crystallographic

analysis ($\sim 6 \text{ \AA}$ for the sulfur-bonded geometry) or molecular modeling ($\sim 8 \text{ \AA}$ for the oxygen-bonded geometry).

The breaking conductance curves are depicted in **Figure 51**. The black and the green curves show switching between the two bonding states (through-oxygen bonding *versus* through-sulfur bonding). Compared to the other helicenes studied in this Thesis, a significant slope of the plateaus present in the breaking curves of **143** was observed. This is the result of geometry changes during the separation of electrodes. One of the tentative explanations includes mechanical stretching of the flexible helicene molecule. Such a behavior is illustrated by the blue curve in **Figure 51**.

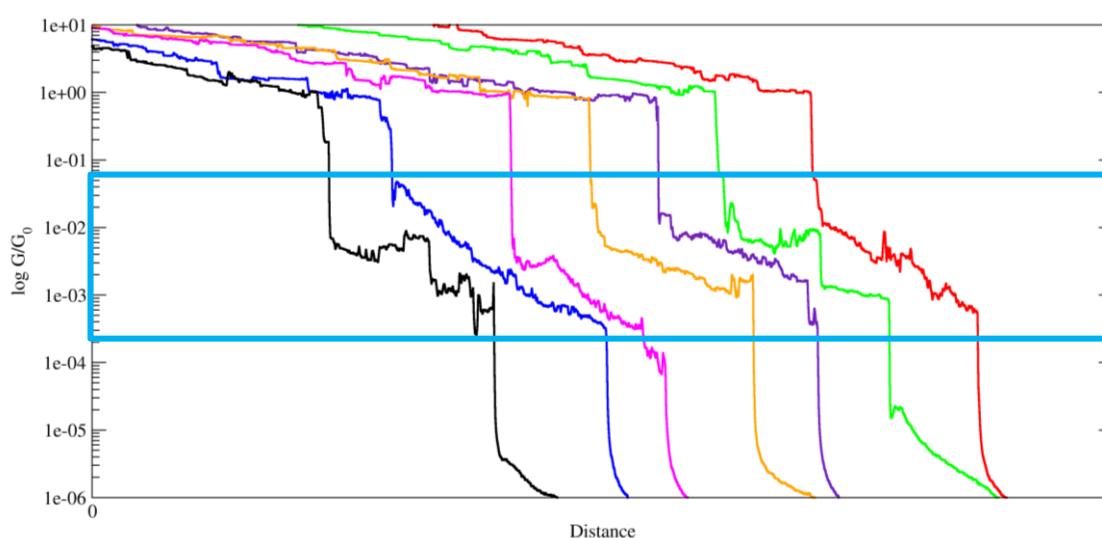


Figure 51: Typical breaking curves of [7]helicene **143** with conductance plateaus in the blue-highlighted area; the blue breaking curve might indicate the mechanical stretching of the spring-like molecule (STM-BJ experiments)

The bis(acetylsulfanyl)[7]helicene derivative **143** was also studied by the high resolution UHV STM technique in the group of doc. Ing. Pavel Jelínek, Ph.D. (Institute of Physics, Czech Academy of Sciences). These studies demonstrated for the first time piezoelectric properties of a single-molecule, helicene **143**, adsorbed on silver surface.¹⁷¹

The UHV STM studies (done by Oleksandr Stetsovych, Ph.D., Institute of Physics, Czech Academy of Sciences) confirmed the two preferred attachment geometries of the acetylsulfanyl group to the Ag(111) surface (**Figure 52**). Two different geometries are clearly visible in the STM image (constant-height scanning mode): the bright and the dark one. The bright one corresponds to the taller molecule conformation as the acetyl group is rotated perpendicular to the surface. On the other hand, the coplanar orientation

of the anchoring group appears dark in the STM image. This observation is further supported by the X-ray analysis of the (acetylsulfanyl)oxa[6]helicene derivative **168** (**Figure 31**), showing similar relaxed conformation of the acetylsulfanyl group in the crystal.

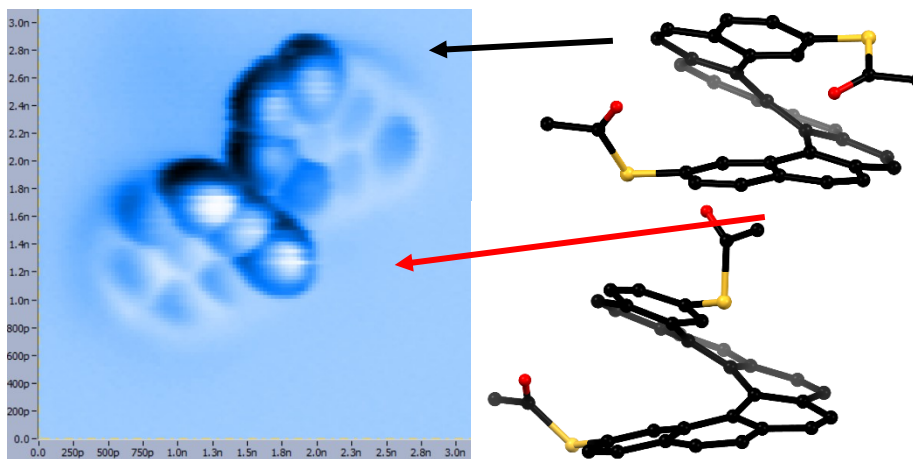


Figure 52: The constant-height STM image of two molecules **143** with the acetylsulfanyl oxygen atom pointing up (red arrow) or pointing down (black arrow)

(-)-(M,R,R)-2,38-Bis(acetylsulfanyl)oxa[19]helicene **88**

Finally, the single-molecule conductance of the (-)-(M,R,R)-bis(acetylsulfanyl)oxa[19]helicene **88** was investigated by STM-BJ experiments. The first set of measurements yielded surprisingly high conductance (**Figure 53**) starting at $4 \cdot 10^{-3} G/G_0$ and crossing more than one order of magnitude with the same molecular length according to the 2D conductance histogram of [19]helicene (-)-(M,R,R)-**88** (**Figure 54**). The conductance curves show also plateaus of the similar length, but these plateaus are statistically distributed over a wide range of conductance (**Figure 55**).

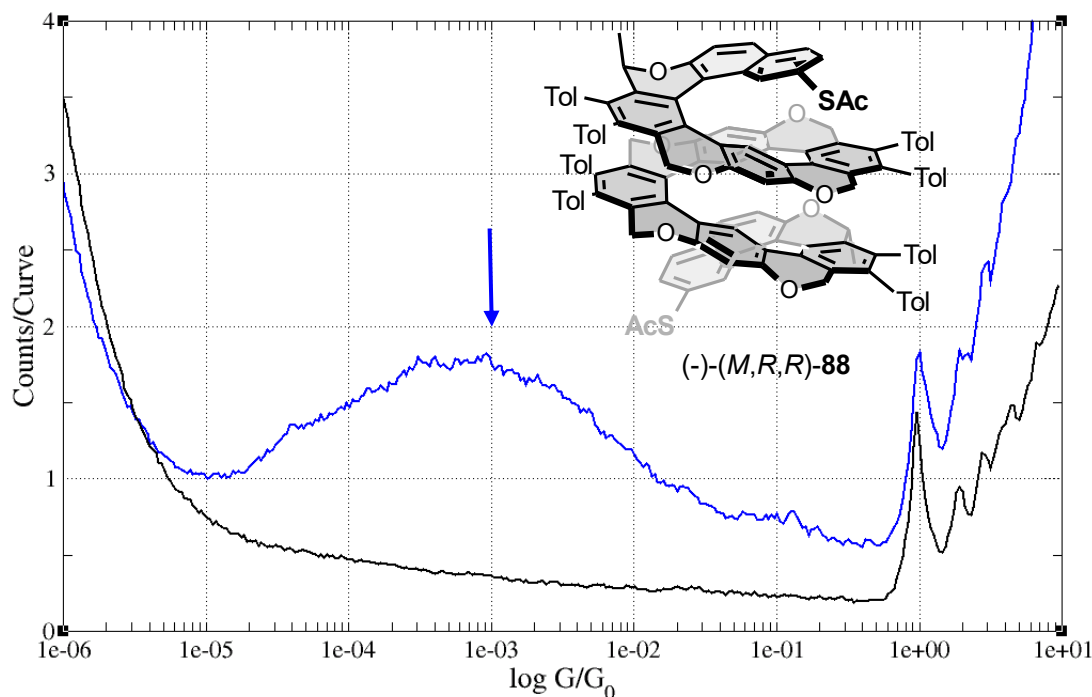


Figure 53: The logarithmic conductance histogram of gold (black) and (-)-(M,R,R)-88 (blue) (STM-BJ experiments)

The unusually broad conductance peak is most likely caused by many attachment configurations occupied by the molecule that is supported also by calculations. Conductance was calculated by employing Quantum ATK. Molecular dynamics was also used for simulation of many different geometries and to investigate the actual breaking process. Calculated conductance values of the molecule (-)-(M,R,R)-88 being attached to gold electrodes and adopting different geometries were in the range of 10^{-4} to 10^{-2} G/G₀.

On the other hand, the conductance plateaus are reasonably defined, which excludes random noise or measurement errors. These preliminary results point to the ability of helicene derivatives to serve as controllable single-molecule conductors. Further development of the break junction devices is desirable to refine the data and to allow studies on other properties such as external force dependent conductance or I-V characteristics.

The present study has already motivated physicists and chemists to conduct collaborative studies on physico-chemical properties of helicene derivatives, which were published shortly before this Thesis manuscript was submitted.^{186,187}

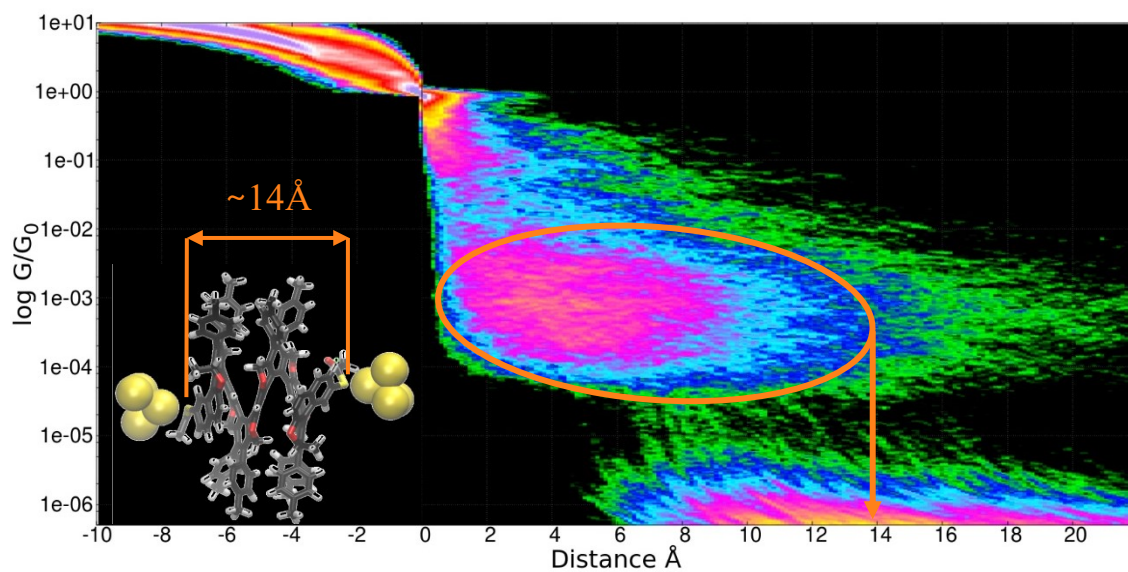


Figure 54: The 2D histogram of (-)-(M,R,R)-88, the molecule effective length is marked in orange (STM-BJ experiments); inset: the Au-molecule-Au bridge with the calculated distance between the sulfur atoms

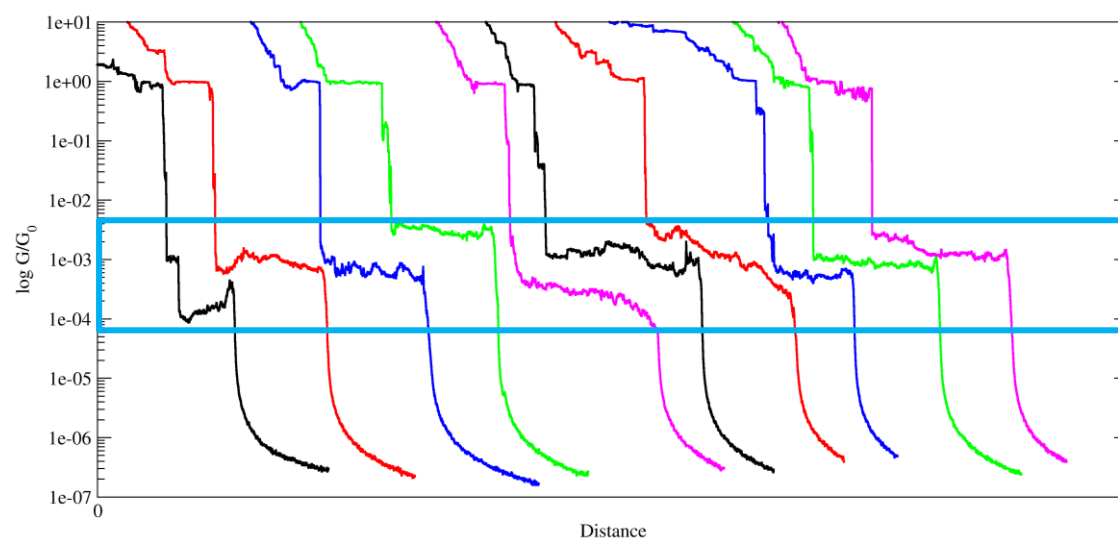


Figure 55: Breaking curves of (-)-(M,R,R)-88 with conductance plateaus (blue area)

4 Conclusion

The multidisciplinary research I pursued at IOCB Prague during my PhD studies contributed to the development of synthetic methodologies for the preparation of extremely long oxa[n]helicenes in a racemic or diastereo- and enantiopure form. In this context, I prepared the longest helicene derivative reported to date. I also demonstrated that these attractive helical molecules can be endowed with useful functional groups such as pyrido units or (acetyl)sulfanyl moieties. Selected helicene derivatives bearing nitrogen or sulfur anchoring groups were employed in physical studies on single-molecule conductance. To this purpose I used mechanically controllable break junction (MCBJ) or scanning tunneling microscopy-based break junction (STM-BJ) techniques employing in-house developed experimental setups. In this context, I measured for the first time single-molecule conductance of selected helicene molecules.

In summary, I have achieved the following most important results:

(1) I have developed a modular synthesis of racemic or diastereo- and enantiopure oxa[11]helicenes and oxa[19]helicenes (**Figure 56**) where alkyne [2+2+2] cycloisomerization is central to their preparation. I demonstrated the advantageous use of a high-pressure-high-temperature flow reactor to pursue the key cyclization. Aptly designed oligoynes precursors were thus transformed into long helicenes in very reasonable yields (20-50%) by the action of $\text{CpCo}(\text{CO})_2$ complex in THF at 250 °C.

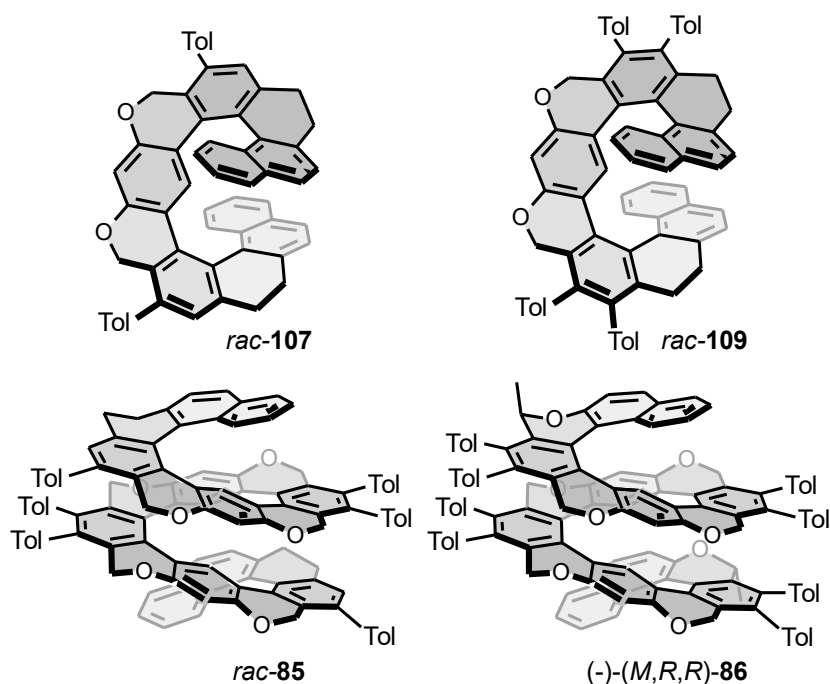


Figure 56: Long oxahelicenes

(2) I have successfully proven and optimized the metal-free approach towards protected helicene (di)thiols, which was based on aromatic nucleophilic substitution. A series of sulfanylated [5]-, [6]-, and [7]helicenes or their oxa analogues were prepared by reacting the respective aryl chlorides with sulfur nucleophiles (**Figure 57**). Selected helicene dithiols were subjected to single-molecule conductance measurements by break-junction techniques.

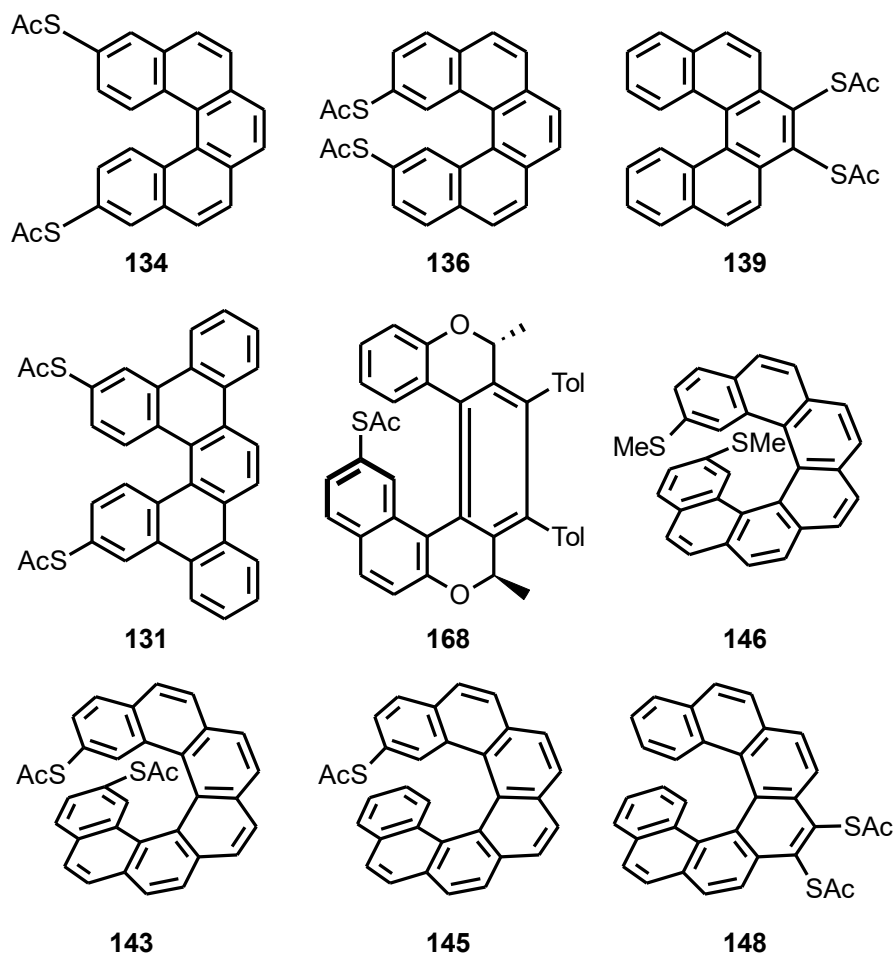


Figure 57: A series of sulfanylated helicene derivatives

Starting from pyridine-based precursors, I have prepared the pyridooxa[9]helicene derivative (-)-(M,R,R)-**87** by employing the same modular synthetic approach used for the synthesis of other long helicenes. Combining two strategies, *i.e.* [2+2+2] cycloisomerization of alkynes and sulfanylation of intermediary chlorohelicenes *via* aromatic nucleophilic substitution of intermediary chlorohelicenes, allowed me to synthesize the longest oxa[19]helicene dithiol derivative (-)-(M,R,R)-**88** reported so far (**Figure 58**).

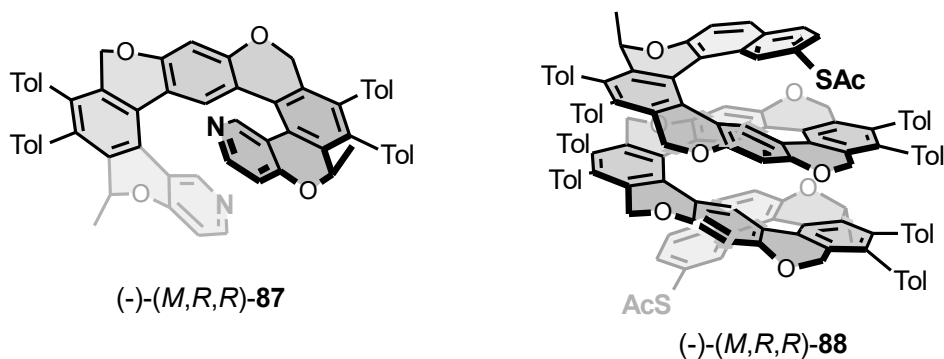


Figure 58: Pyridooxa[9]helicene (-)-(M,R,R)-**87** and oxa[19]helicene dithiol derivative (-)-(M,R,R)-**88**

Molecular structure of diastereo- and enantiopuredichlorooxa[19]helicene (-)-(M,R,R)-**171** was proven by single-crystal X-ray analysis, along with structures of some other helicenes presented in this Thesis.

(3) A new break junction device to measure single-molecule conductance was designed and constructed within a collaborative project. I have contributed significantly to the following parts of the device development: sampling rate optimization, noise level suppression by means of a new shielding design, and LabView control software programming. The apparatus hardware is designed in such a way that it can easily be adjusted for either mechanically controllable break junction measurement or STM-break junction measurement (**Figure 59**).

The control program enables to run the BJ device in semi-automatic regime and collect up to hundreds of thousands of “breaking curves”. The program also allows the operator to control all subsystems of BJ apparatus separately and provides a preliminary statistical analysis.

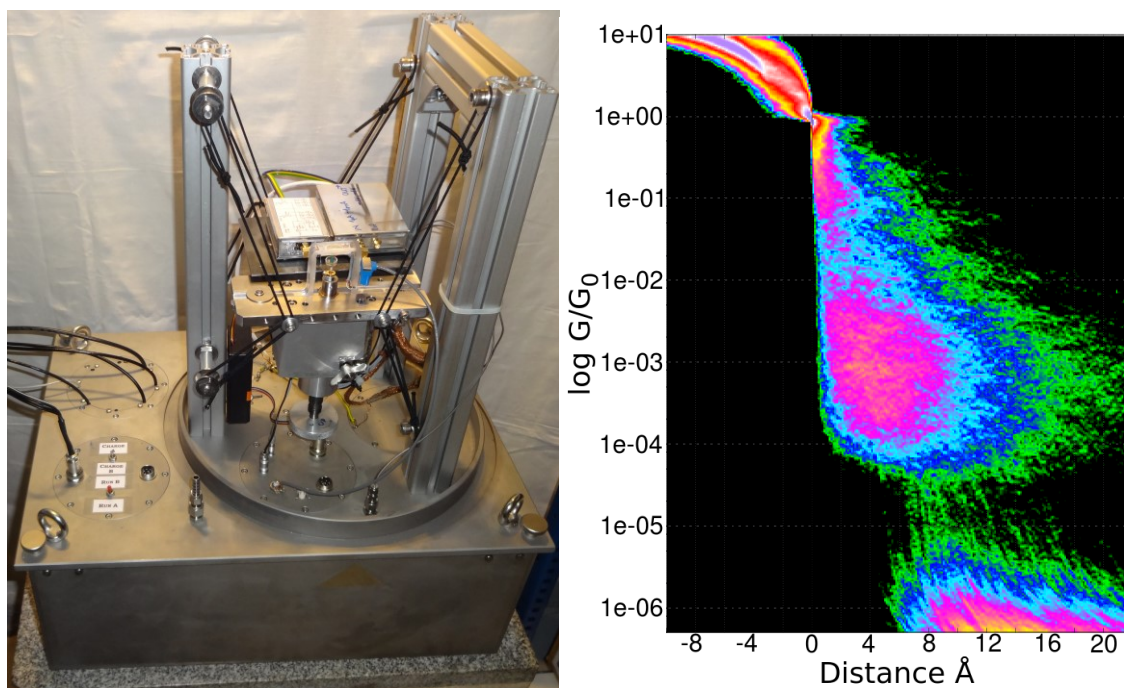


Figure 59: (a) STM-BJ device; (b) 2D-histogram of the single-molecule conductance measurement on the sulfanylated oxa[19]helicene derivative *(M,R,R)*-**88**

By repeating the published measurements of single-molecule conductance of model compounds, I obtained identical results, which proved the full functionality of the constructed break-junction device. Accordingly, I measured single-molecule conductance on [5]-, [7]-, and the longest oxa[19]helicene sulfanyl derivatives **131**, **143** and (-)-*(M,R,R)*-**88**, respectively, along with the conductance of pyridooxa[9]helicene (-)-*(M,R,R)*-**87**. The experimental data showed their single-molecule conductance in the order of $10^{-3} G/G_0$ (e.g. **Figure 59b**).

5 Experimental Section

5.1 Methods

General

Melting points were determined on Mikro-Heiztisch Polytherm A (Hund, Wetzlar) apparatus and are uncorrected.

The NMR spectra were measured on Bruker Advance III HD 400, 500 and 600 instruments, respectively. The ^1H NMR spectra were measured at 400.13 MHz, 499.88 MHz, and 600.13 MHz, the ^{13}C NMR spectra at 100.61 MHz, 125.71 MHz, and 150.90 MHz in CDCl_3 , CD_2Cl_2 or acetone- d_6 as indicated. For referencing of ^1H NMR spectra, the residual solvent signals (δ 7.26 for CHCl_3 , δ 5.32 for CH_2Cl_2 and δ 2.05 for acetone) were used. In the case of ^{13}C spectra, the signals of solvents (δ 77.16 for CDCl_3 , δ 54.00 for CD_2Cl_2 and δ 29.84 for acetone- d_6) were used. The chemical shifts are given in δ -scale, the coupling constants J are given in Hz. For the assignment of both the ^1H and ^{13}C NMR spectra of key compounds, homonuclear 2D-H,H-COSY, 2D-H,H-ROESY, and heteronuclear 2D-H,C-HSQC, and 2D-H,C-HMBC experiments were performed by Dr. Miloš Buděšínský.

The IR spectra were measured in CHCl_3 , CCl_4 or KBr on FT-IR spectrometer Bruker Equinox 55. The CD spectra were acquired on a J-815 CD spectrometer (Jasco Analytical Instruments, Inc.) in THF (10^{-4} M solutions) using 10 mm quartz sample cell.

The EI mass spectra were determined at an ionizing voltage of 70 eV, the m/z values are given along with their relative intensities (%). The low resolution ESI mass spectra were recorded on Q-ToF micro (Waters) and high resolution ESI mass spectra and APCI spectra using the Orbitrap mass analyzer (LTQ Orbitrap XL, Thermo Fisher Scientific). The MALDI-TOF spectra were measured on UltrafleXtremeTM MALDI-TOF/TOF mass spectrometer (Bruker Daltonics, Germany). Optical rotations were measured in CHCl_3 , THF using an Autopol IV instrument (Rudolph Research Analytical).

TLC was performed on Silica gel 60 F₂₅₄-coated aluminium sheets (Merck) and spots were detected by the solution of $\text{Ce}(\text{SO}_4)_2 \cdot 4\text{H}_2\text{O}$ (1%) and $\text{H}_3\text{P}(\text{Mo}_3\text{O}_{10})_4$ (2%) in sulfuric acid (10%). The flash chromatography was performed on Silica gel 60 (0.040-0.063 mm, Merck) or on Biotage[®] KP-C18-HS cartridges using the Isolera One HPFC system (Biotage, Inc.). Biotage Initiator EXP EU (300 W power) was used for reactions carried out in microwave oven.

Flow experiments were performed in a high-temperature & high-pressure continuous flow reactor constructed by connecting an analytical HPLC pump (Knauer) to a stainless-steel capillary (VICI, 10 m, 1.0 mm ID, internal volume 8 mL) embedded in an electrically heated block (Development workshops at the IOCB Prague, temperature range rt to 350 °C) and an automatic backpressure regulator with a pressure limit of 150 bar (ThalesNano Nanotechnology Inc.). Enantiomers separation were done using the HPLC column Chiralpak IB, 250 x 4.6 mm, 5 μm, mobile phase *n*-heptane:MTBE 90:10, with 0.5% isopropyl alcohol and flow rate 1.0 mL/min

N,N-Diisopropylamine (DIPA) and triethylamine were distilled from calcium hydride under nitrogen and degassed by three freeze-pump-thaw cycles before use; DCM was distilled from calcium hydride under nitrogen; tetrahydrofuran (THF), diethyl ether, and methyl *tert*-butyl ether (MTBE) was freshly distilled from sodium/benzophenone under nitrogen; benzene, toluene and mesitylene were distilled from sodium under nitrogen. HPLC-grade N-methyl-2-pyrrolidone (NMP) was distilled under nitrogen (for the nucleophilic substitution reactions). Otherwise, all commercially available solvents, catalysts, and reagent grade materials were used as received. 4-iodotoluene, propargyl alcohol, 4,4'-bipyridine **73**, 1-bromo-2-(methoxymethyl)naphthalene **94**, 1-chloronaphthalene **115**, 4,4'-dibromobiphenyl **128**, *p*-chlorophenol **154**, (-)-(*S*)-but-3-yn-2-ol, 7-chloro-2-naphthol **158**, and 2-iodophenol were purchased. [4-(1-ethynyl-naphthalen-2-yl)but-1-yn-1-yl][tri(propan-2-yl)]silane **99**¹⁴⁹, 4,6-diiodoresorcinol **100**¹⁵⁰, 1-(3-bromoprop-1-yn-1-yl)-4-methylbenzene **101**¹⁵¹, 1-iodonaphthalen-2-ol **113**¹⁵³, (2*S*)-4-(4-methylphenyl)but-3-yn-2-ol **152**¹⁷⁴ and oligo(phenyl acetylene) **174**¹⁸² were synthesized according to the literature procedures. Helicene **130**¹⁶⁸ was prepared by Mgr. Václav Houska. Compounds **123**¹⁴⁸, **133**¹⁷⁰, **135**¹⁶⁸, **138**¹⁷⁰, **140**¹⁷⁰, **142**¹⁷¹, **147**¹⁷⁰ were prepared by Michal Šámal, Ph.D. as a part of other projects. Compounds **159**¹⁶⁸, **160**¹⁶⁸, **161**¹⁶⁸, **162**¹⁶⁸, **163**¹⁶⁸, **164**¹⁶⁸ were prepared by joint effort with Isabel Gay Sánchez.

Crystallographic Analysis

Crystallographic data were collected on Bruker D8 VENTURE Kappa Duo PHOTON 100 by IμS micro-focus sealed tube MoK α radiation ($\lambda = 0.71073 \text{ \AA}$) or CuK α ($\lambda = 1.54178 \text{ \AA}$) at a temperature of 120 K or 150 K. The structures were solved by direct methods (XP)¹⁸⁸ or methods (XT) and refined by full matrix least squares based on F^2 (SHELXL2014 or SHELXL2018).¹⁸⁹ The hydrogen atoms on carbon were fixed into idealized positions (riding model) and assigned temperature factors either

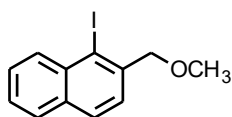
$H_{\text{iso}}(\text{H}) = 1.2 U_{\text{eq}}$ (pivot atom) or $H_{\text{iso}}(\text{H}) = 1.5 U_{\text{eq}}$ (pivot atom) for methyl moiety. The determination of absolute configuration for (-)-(M,R,R)-**171** was based on anomalous scattering; Flack parameter 0.006 (4). All crystallographic measurements were performed by Dr. Ivana Císařová.

General Procedure for Reactions Carried out in a Flow Reactor

To a solution of the oligoyne (1.0 equiv., 5 mg/mL) in distilled THF $\text{CpCo}(\text{CO})_2$ (0.5 – 2.0 equiv.) was added in one portion under argon. The reaction mixture was pumped through the high-temperature high-pressure flow reactor (internal volume 8 mL) at a flow rate of 0.5 or 1.0 mL/min. The pressure of the system was set to 80 bar and the temperature was maintained at 250 °C. The resulting reaction mixture was concentrated *in vacuo*. Purification of the residue by flash chromatography on silica gel afforded desired oxahelicene.

5.2 Synthesis

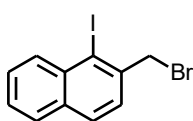
1-Iodo-2-(methoxymethyl)naphthalene **95**¹⁹⁰



To a solution of 1-bromo-(2-methoxymethyl)naphthalene **94** (2.00 g, 7.96 mmol) in distilled THF (40 mL) *n*-BuLi (7.5 mL of a 1.6 M solution in hexanes, 12 mmol, 1.5 equiv.) was dropwise added at -78 °C. Then a solution of iodine (4.01 g, 15.9 mmol, 2.0 equiv.) in distilled THF (20 mL) was added. The reaction mixture was stirred at -78 °C for 15 min and then allowed to warm up to rt. The solvents were removed *in vacuo*. The residue was dissolved in DCM (150 mL) and washed 5% aq. $\text{Na}_2\text{S}_2\text{O}_3$ (50 mL), and dried over anhydrous Na_2SO_4 . The solvent was removed *in vacuo* and the crude product was purified by flash chromatography on silica gel (hexane:DCM, 80:20) to give **95** (2.08 g, 87%).

The spectra were in an agreement with the published ones.¹⁹⁰

2-(Bromomethyl)-1-iodonaphthalene **96**¹⁹⁰

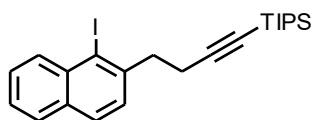


The 1-iodo-2-(methoxymethyl)naphthalene **95** (2.07 mg, 6.94 mmol) was dissolved in distilled THF (10 mL) and cooled down to 0 °C under nitrogen. Then HBr in acetic acid (33%, 18.3 mL, 104 mmol, 15 equiv.)

was added and the reaction mixture was stirred at 0 °C for 1 h. The reaction was quenched with saturated solution of sodium bicarbonate (100 mL) and extracted with DCM (3 × 30 mL). The solvent was removed *in vacuo* and the crude product was flushed with hexane to give bromide **96** (2.28 g, 95%) as an amorphous solid.

The spectra were in an agreement with the published ones.¹⁹⁰

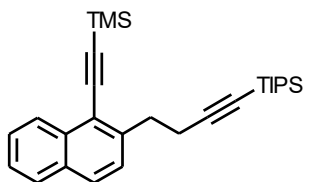
[4-(1-Iodonaphthalen-2-yl)but-1-yn-1-yl][tris(1-methylethyl)silane **97**]¹⁹⁰



n-BuLi (1.6 M solution in hexanes, 9.0 mL, 14 mmol, 1.55 equiv.) was added dropwise to a solution of TIPS-propyne (3.50 mL, 14.4 mmol, 1.56 equiv.) in distilled THF (20 mL) at -78 °C under argon. After stirring at -78 °C for 2.5 h, bromide **96** (3.20 g, 9.22 mmol) in distilled THF (60 mL) was added dropwise. The mixture was stirred at -78 °C for 2.5 h and then allowed to warm up to rt. The solvents were removed *in vacuo* and purified by chromatography on silica gel (hexane:ether, 98:2) to give alkyne **97** (4.13 g, 96%) as an oil.

The spectra were in an agreement with the published ones.¹⁹⁰

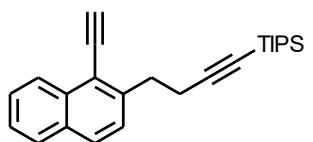
Trimethyl[(2-{4-[tris(1-methylethyl)silyl]but-3-yn-1-yl}naphthalen-1-yl)ethynyl]silane **98**]¹⁹⁰



A Schlenk flask was charged with iodide **97** (3.03 g, 6.55 mmol), Pd(PPh₃)₄ (151 mg, 0.13 mmol, 2 mol%), CuI (50 mg, 0.26 mmol, 4 mol%), and flushed with argon. The degassed DIPA (12 mL) was added and the mixture was stirred at rt for 5 min before TMSA (966 mg, 9.83 mmol, 1.5 equiv.) was added. The reaction mixture was stirred at the rt overnight. The solvents were evaporated under reduced pressure and the residue was purified by flash chromatography on silica gel (hexane) to afford alkyne **98** (2.53g, 89%) as a yellowish oil.

The spectra were in an agreement with the published ones.¹⁹⁰

[4-(1-Ethynynaphthalen-2-yl)but-1-yn-1-yl][tris(1-methylethyl)silane **99**]¹⁹⁰

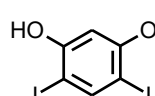


Protected diyne **98** (200 mg, 0.46 mmol) was dissolved in anhydrous methanol (3 mL) and distilled ether (1 mL). K₂CO₃ (128 mg, 0.92 mmol, 2 equiv.) was added to this

solution and the mixture was stirred at rt for 3 h. After this period, the solvents were evaporated under reduced pressure and the residue was purified by flash chromatography on silica gel (hexane) to afford **99** (160 mg, 96%) as an amorphous solid.

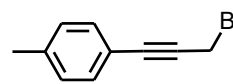
The spectra were in an agreement with the published ones.¹⁹⁰

4,6-Diiodoresorcinol **100**¹⁵⁰

 Iodine monochloride (8.20 g, 50.5 mmol, 2.02 equiv.) was dissolved in distilled diethyl ether (30 mL), cooled down to -7 °C and slowly cannulated to the solution of resorcinol (2.75 g, 25.0 mmol) in distilled diethyl ether (25 mL) at -7 °C. Then the reaction mixture was allowed to heat up to room temperature and stirred for 1 h. Reaction mixture was quenched with Na₂SO₃ solution (2.0 g in 20 mL of water) and extracted with diethyl ether (4 × 25 mL). The collected organic layers were evaporated *in vacuo* to afford the product **100** as a pinkish powder (8.50 g, 94%).

The spectra were in an agreement with the published ones.¹⁵⁰

1-(3-Bromoprop-1-yn-1-yl)-4-methylbenzene **101**¹⁵¹

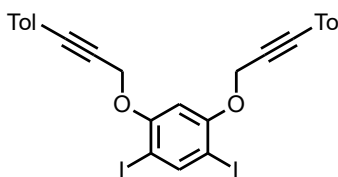
 A Schlenk flask was charged with 4-iodotoluene (20.0 g, 91.7 mmol), Pd(PPh₃)₄ (530 mg, 0.5 mmol, 0.5 mol%), CuI (175 mg, 0.9 mmol, 1 mol%), flushed with argon and a mixture of degassed solvents of DIPA-toluene (280 mL, 1:2) was added. The mixture was stirred at rt for 5 min before propargyl alcohol (5.40 g, 96.3 mmol, 1.05 equiv.) was added and the mixture was vigorously stirred at rt overnight. The solvents were evaporated under reduced pressure and the residue was washed with hexane (300 mL). The hexane solution was evaporated *in vacuo* to afford 3-(4-methylphenyl)prop-2-yn-1-ol **101a** (13.3 g, 99%) as an off-white oil.

The spectra were in an agreement with the published ones.¹⁵¹

The alcohol **101a** (13.4 g, 91.2 mmol) was dissolved in distilled MTBE (92 mL), anhydrous pyridine (2.8 mL 34.2 mmol, 0.38 equiv.) was added and cooled down to -7 °C, PBr₃ (4.3 mL, 45.6 mmol, 0.5 equiv.) was dissolved in MTBE (46 mL), cooled down to -7 °C and slowly added to the solution of the alcohol **101a**. The mixture was vigorously stirred at rt for 2 h. Then the reaction mixture was filtered through small pad of silica, flush with DCM (150 mL). The solvents were evaporated *in vacuo* and the residue was purified by flash chromatography on silica gel (hexane:DCM, 70:30) to afford the bromoderivative **101** (13.6 g, 71%) as a pale orange oil.

The spectra were in an agreement with the published ones.¹⁵¹

1,5-Diiodo-2,4-bis[[3-(4-methylphenyl)prop-2-yn-1-yl]oxy]benzene **102**



A flask was charged with diiodoresorcinol **100** (1.66 g, 4.59 mmol), anhydrous potassium carbonate (4.20 g, 28.0 mmol, 6.0 equiv.) and dissolved in anhydrous DMF (100 mL). Then a solution of 1-(3-bromoprop-1-yn-1-yl)-4-methylbenzene **101**¹⁵¹ (2.02 g, 9.63 mmol, 2.1 equiv.) in anhydrous DMF (20 mL) was added and the reaction mixture was stirred at rt overnight. After filtration through a pad of Celite the solvents were evaporated under reduced pressure and the residue was purified by flash chromatography on silica gel (hexane: diethyl ether, 95:5) to afford alkyne **102** (2.01 g, 70%) as a white solid.

M.p.: 117.0 - 118.0 °C (hexane-EtOAc).

¹H NMR (400 MHz, CDCl₃): 2.33 (s, 6H), 4.97 (s, 4H), 7.04 (s, 1H), 7.07 (d, *J* = 8.0, 4H), 7.29 (d, *J* = 8.0, 4H), 8.10 (s, 1H).

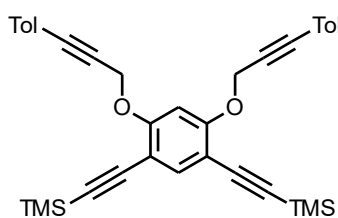
¹³C NMR (101 MHz, CDCl₃): 21.48, 58.42, 77.55, 82.17, 88.54, 100.66, 118.78, 129.07, 131.71, 139.10, 147.14, 158.00.

IR (CHCl₃): 3084 w, 3053 w, 3034 w, 2244 w, 2232 w, 2217 w, 1608 w, 1570 m, 1562 m, 1510 vs, 1456 s, 1407 w, 1394 s, 1269 vs, 1250 s, 1220 m, 1182 s, 1135 vw, 1118 w, 1023 s, 1013 s, 947 w, 883 w, 818 vs, 708 w, 646 w, 600 w, 445 w cm⁻¹.

EI MS: 618 (M⁺, 1), 491 (18), 129 (100), 57 (10).

HR EI MS: calculated for C₂₆H₂₀O₂I₂ 617.9553, found 617.9558.

[(4,6-Bis[[3-(4-methylphenyl)prop-2-yn-1-yl]oxy]benzene-1,3-diyl)diethyne-2,1-diyl]bis(tri-methylsilane) **103**



A Schlenk flask was charged with diiodide **102** (1.13 g, 1.83 mmol), Pd(PPh₃)₄ (115 mg, 0.10 mmol, 5 mol%), CuI (38 mg, 0.20 mmol, 10 mol%), flushed with argon and a mixture of degassed solvents of DIPA-toluene (30 mL, 1:2) was added. The mixture was stirred at rt for 5 min before TMSA (539 mg, 0.780 mL, 5.48 mmol, 3.0 equiv.) was added and the mixture was stirred at rt overnight. The solvents were evaporated under reduced pressure and the residue was

purified by flash chromatography on silica gel (hexane:ethyl acetate, 98:2) to afford protected tetrayne **103** (952 mg, 93%) as a yellowish solid.

M.p.: 94.5 - 96.0 °C (hexane-EtOAc).

¹H NMR (400 MHz, CD₂Cl₂): 0.25 (d, *J* = 0.6, 18H), 2.33 (s, 6H), 5.03 (s, 4H), 6.91 (s, 1H), 7.09 (d, *J* = 8.2, 4H), 7.29 (d, *J* = 8.2, 4H), 7.51 (s, 1H).

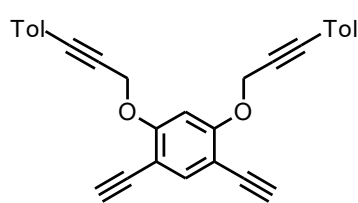
¹³C NMR (101 MHz, CD₂Cl₂): 0.23, 21.77, 58.37, 82.88, 88.68, 98.36, 100.04, 100.49, 106.88, 119.33, 129.64, 132.16, 139.55, 139.83, 160.39.

IR(CHCl₃): 3052 vw, 3033 w, 2924 m, 2900 w, 2870 w, 2239 w, 2212 w, 2150 s, 1603 m, 1596 m, 1565 w, 1510 s, 1494 s, 1454 m, 1408 s, 1371 m, 1361 m, 1298 s, 1251 s, 1198 s, 1181 m, 1120 m, 1023 s, 1015 s, 1006 s, 904 m, 869 vs, 845 vs, 818 s, 707 w, 700 w, 641 m, 528 m cm⁻¹.

ESI MS: 559 ([M+H]⁺), 581 ([M+Na]⁺) .

HR ESI MS: calculated for C₃₆H₃₈O₂Si₂Na 581.2303, found 581.2303.

1,5-Diethynyl-2,4-bis{[3-(4-methylphenyl)prop-2-yn-1-yl]oxy}benzene **104**



The protected tetrayne **103** (135 mg, 0.240 mmol) was dissolved in anhydrous methanol (5 mL) and freshly distilled THF (5 mL). NaOMe (1.45 M in methanol, 400 μL, 0.59 mmol, 2.4 equiv.) was added to this solution and the reaction mixture was stirred at rt for 45 min. After this period, the solvents were evaporated under reduced pressure and the residue was purified by flash chromatography on silica gel (hexane:ethyl acetate, 9:1) to afford the deprotected tetrayne **104** (95 mg, 95%) as a pale yellow solid.

M.p.: 141.0 - 142.0 °C (hexane-EtOAc).

¹H NMR (400 MHz, CD₂Cl₂): 2.33 (s, 6H), 3.27 (s, 2H), 5.04 (s, 4H), 6.95 (s, 1H), 7.09 (d, *J* = 8.1, 4H), 7.29 (d, *J* = 8.1, 4H), 7.56 (s, 1H).

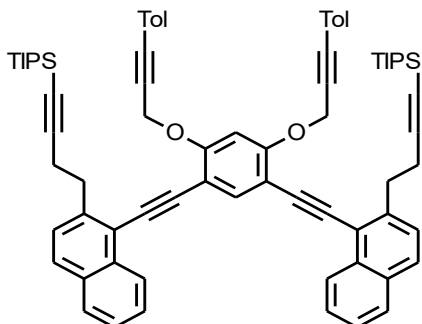
¹³C NMR (101 MHz, CD₂Cl₂): 21.76, 58.29, 79.14, 81.10, 82.66, 88.76, 99.40, 105.59, 119.22, 129.66, 132.21, 139.64, 139.94, 160.93.

IR (CHCl₃): 3304 s, 3052 w, 2958 w, 2925 m, 2858 w, 2237 w, 2212 w, 2108 w, 1605 s, 1600 s, 1566 m, 1501 vs, 1495 vs, 1454 m, 1409 s, 1372 m, 1359 m, 1289 vs, 1191 s, 1181 m, 1119 w, 1100 s, 1022 s, 1015 s, 1009 s, 905 m, 818 vs, 708 w, 661 w, 607 m, 528 m cm⁻¹.

APCI MS: 415 ([M+H]⁺).

HR APCI MS: calculated for C₃₀H₂₃O₂ 415.1693, found 415.1691.

[(4,6-Bis{[3-(4-methylphenyl)prop-2-yn-1-yl]oxy}benzene-1,3-diyl)bis(ethyne-2,1-diynaphthalene-1,2-diylbut-1-yne-4,1-diyl)]bis[tri(propan-2-yl)silane] **105**



A Schlenk flask was charged with diiodide **102** (686 mg, 1.11 mmol), Pd(PPh₃)₄ (128 mg, 0.11 mmol, 10 mol%), CuI (42 mg, 0.22 mmol, 20 mol%) and flushed with argon. Degassed DIPA (5 mL) and degassed toluene (5 mL) was added. Then a solution of alkyne **99**¹⁹⁰ (839 mg, 2.33 mmol, 2.1 equiv.) in degassed toluene (10 mL) was slowly added at rt

within 1 h. The reaction mixture then was stirred at the same temperature overnight. The solvents were evaporated under reduced pressure and the residue was purified by flash chromatography on silica gel (DCM:cyclohexane, 30:70) to afford hexayne **105** (928 mg, 77%) as a yellow amorphous solid.

¹H NMR (400 MHz, CDCl₃): 1.02 (m, 42H), 2.35 (s, 6H), 2.84 (t, *J* = 7.2, 4H), 3.39 (t, *J* = 7.2, 4H), 5.18 (s, 4H), 7.08-7.12 (m, 4H), 7.15 (s, 1H), 7.35 (d, *J* = 8.1, 4H), 7.47 (ddd, *J* = 8.1, 6.8, 1.2, 2H), 7.51 (d, *J* = 8.4, 2H), 7.58 (ddd, *J* = 8.3, 6.8, 1.3, 2H), 7.75 (d, *J* = 8.3, 2H), 7.80-7.84 (m, 2H), 7.85 (s, 1H), 8.61 (dd, *J* = 8.4, 1.1, 2H).

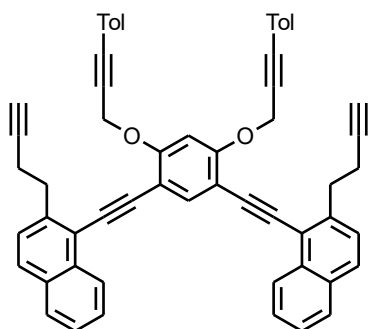
¹³C NMR(101 MHz, CDCl₃): 11.32, 18.63, 21.11, 21.54, 34.78, 58.09, 81.06, 82.58, 88.40, 89.78, 94.10, 99.26, 107.16, 108.59, 118.98, 119.70, 125.66, 126.51, 126.76, 127.78, 127.93, 129.12, 131.73, 131.78, 132.00, 133.56, 136.48, 139.03, 141.48, 159.76.

IR (CHCl₃): 3084 vw, 3057 w, 2959 s, 2944 vs, 2926 s, 2892 m, 2865 vs, 2236 w, 2207 vw, 2169 m, 1620 vw, 1604 m, 1590 w, 1565 w, 1510 s, 1497 s, 1463 m, 1452 m, 1429 vw, 1417 w, 1383 w, 1368 m, 1308 m, 1267 m, 1241 m, 1178 m, 1147 w, 1122 w, 1073 w, 1053 m, 1023 s, 1015 s, 997 m, 961 w, 899 w, 884 m, 868 w, 818 vs, 708 vw, 678 m, 659 m, 626 w, 617 w, 529 w, 441 w, 416 vw cm⁻¹.

ESI MS: 1105 ([M+Na]⁺).

HR ESI MS: calculated for C₇₆H₈₂O₂Si₂Na 1105.57456, found 1105.57393.

1,1'-[(4,6-Bis{[3-(4-methylphenyl)prop-2-yn-1-yl]oxy}benzene-1,3-diyl)diethyne-2,1-diyl]-bis[2-(but-3-yn-1-yl)naphthalene] 106



The protected hexayne **105** (40 mg, 0.037 mmol) was dissolved in distilled THF (2 mL). To this solution, a solution of TBAF·3H₂O (28 mg, 0.089 mmol, 2.4 equiv.) in THF (2 mL) was added and the mixture was stirred at rt for 1 h. After this period, the reaction mixture was filtered over a short pad of silica (THF). The solvent was evaporated under reduced pressure and the residue was subjected to flash chromatography on silica gel (hexane:ethyl acetate, 100:0 → 90:10) to afford **106** (23 mg, 82%) as an amorphous solid.

¹H NMR (500 MHz, CDCl₃): 2.04 (t, *J* = 2.6 Hz, 2H), 2.35 (s, 6H), 2.76 (ddd, *J* = 8.0, 7.4, 2.7 Hz, 4H), 3.39 (t, *J* = 7.7 Hz, 4H), 5.18 (s, 4H), 7.08 – 7.11 (m, 4H), 7.15 (s, 1H), 7.33 – 7.36 (m, 4H), 7.45 (d, *J* = 8.4 Hz, 2H), 7.47 (ddd, *J* = 8.3, 6.8, 1.3 Hz, 2H), 7.57 (ddd, *J* = 8.3, 6.8, 1.3 Hz, 2H), 7.78 (d, *J* = 8.1 Hz, 2H), 7.81 – 7.86 (m, 2H), 7.90 (s, 1H), 8.59 – 8.64 (m, 2H).

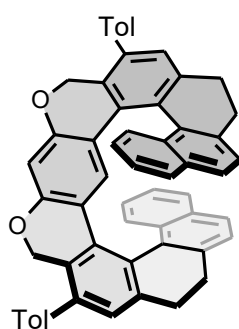
¹³C NMR (126 MHz, CDCl₃): 19.81, 21.65, 34.75, 58.17, 69.06, 82.70, 84.46, 88.52, 89.69, 94.48, 99.25, 107.12, 119.07, 119.96, 125.94, 126.60, 127.02, 127.55, 128.11, 128.21, 129.25, 131.90, 132.12, 133.60, 136.91, 139.18, 141.28, 159.93.

IR (CHCl₃): 3308 m, 3083 vw, 3057 w, 3035 vw, 2961 w, 2929 m, 2867 w, 2236 w, 2208 w, 2117 w, 1620 vw, 1604 m, 1591 w, 1565 m, 1510 vs, 1497 s, 1453 m, 1431 w, 1417 m, 1384 w, 1371 m, 1362 m, 1310 m, 1267 s, 1241 s, 1178 s, 1148 w, 1122 m, 1052 m, 1023 s, 1015 s, 961 w, 898 w, 868 w, 819 vs, 708 vw, 638 m, 544 vw, 529 w, 441 w, 418 vw cm⁻¹.

APCI MS: 771 ([M + H]⁺).

HR APCI MS: calculated for C₅₈H₄₃O₂ 771.32478, found 771.32576.

rac-10,16-Ditolyl(oxa[11]helicene) **107**



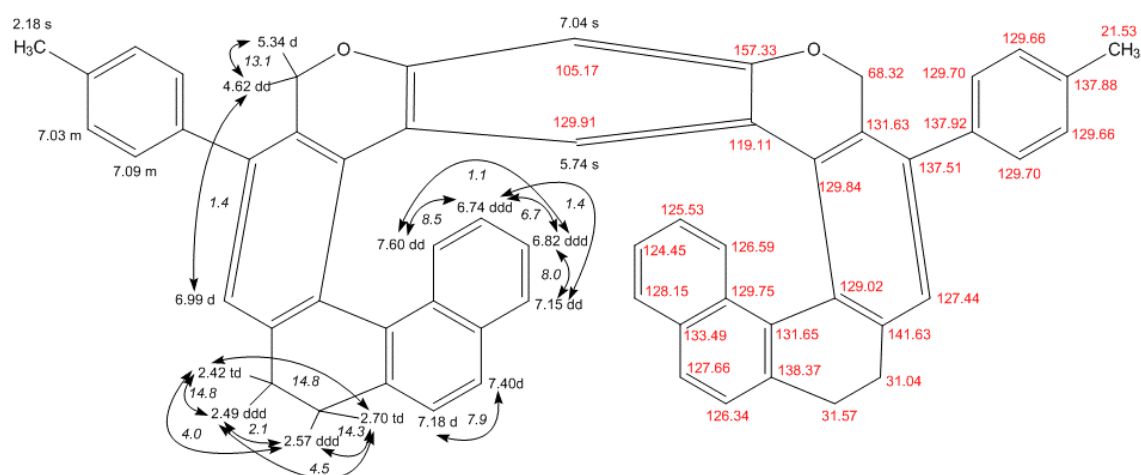
Oxa[11]helicene *rac*-**107** was prepared according to the **General procedure for reaction in a flow reactor** from hexayne **106** (50 mg, 0.065 mmol) and CpCo(CO)₂ (12 mg, 9 μL, 0.07 mmol, 1.0 equiv.) in THF (10 mL) at a flow rate of 0.5 mL/min (residence time of 16 min). The purification by a flash chromatography on silica gel (hexane-ethyl acetate 4:1) gave *rac*-**107** (25 mg, 50%) as a white solid.

M.p.: >350 °C (DCM-acetonitrile).

UV/Vis (CHCl₃): λ_{max} (log ε) = 262 (4.47), 282 sh (4.28), 334 (4.16) nm.

¹H NMR (600 MHz, C₆D₆): 2.18 (s, 6H), 2.42 (td, *J* = 14.8, 14.8, 4.0, 2H), 2.49 (ddd, *J* = 14.8, 4.5, 2.1, 2H), 2.57 (ddd, *J* = 14.3, 4.0, 2.1, 2H), 2.70 (ddd, *J* = 14.8, 14.3, 4.5, 2H), 4.62 (dd, *J* = 13.1, 1.4, 2H), 5.34 (d, *J* = 13.1, 2H), 5.74 (s, 1H), 6.74 (ddd, *J* = 8.5, 6.7, 1.4, 2H), 6.82 (ddd, *J* = 8.0, 6.7, 1.4, 2H), 6.99 (d, *J* = 1.4, 2H), 7.03 (m, 4H), 7.04 (s, 1H), 7.09 (m, 4H), 7.15 (dd, *J* = 8.0, 1.4, 2H), 7.18 (d, *J* = 7.9, 2H), 7.40 (d, *J* = 7.9, 2H), 7.60 (dd, *J* = 8.5, 1.1, 2H).

¹³C NMR (151 MHz, C₆D₆): 21.53, 31.04, 31.57, 68.32, 105.17, 119.11, 124.45, 125.53, 126.34, 126.59, 127.44, 127.66, 128.15, 129.02, 129.66 (2C), 129.70 (2C), 129.75, 129.84, 129.91, 131.63, 131.65, 133.49, 137.51, 137.88, 137.92, 138.37, 141.63, 157.33.

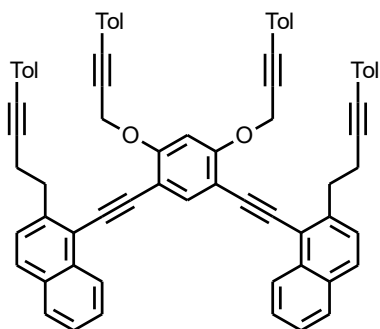


IR (CHCl₃): 3051 w, 2961 m, 2942 m, 2840 w, 1620 m, 1598 w, 1573 w, 1547 vw, 1515 m, 1496 m, 1462 w sh, 1412 w, 1379 m, 1300 w, 1262 s, 1147 m, 1125 m, 1022 s, 883 w, 864 w, 819 vs, 811 vs, 705 vw, 690 w, 537 vw, 431 vw cm⁻¹.

APCI MS: 771.3 ([M+H]⁺).

HR APCI MS: calculated for C₅₈H₄₃O₂ 771.3258, found 771.3257.

1,1'-[(4,6-Bis{3-(4-methylphenyl)prop-2-yn-1-yl}oxy}benzene-1,3-diyl)diethyne-2,1-diyl]bis{2-[4-(4-methylphenyl)but-3-yn-1-yl]naphthalene} 108



The hexayne **106** (130 mg, 0.169 mmol) was dissolved in degassed toluene (13 mL) under argon and dropwise added to a mixture of 4-iodotoluene (221 mg, 1.01 mmol, 6.0 equiv.), Pd(PPh₃)₄ (20 mg, 0.1 mmol, 10 mol%), CuI (7 mg, 0.034 mmol, 20 mol%) in degassed mixture of toluene (3 mL) and DIPA (3 mL) at rt within 3 h. The reaction mixture was stirred at the

same temperature overnight. The solvents were evaporated under reduced pressure and the residue was purified by flash chromatography on silica gel (cyclohexane:DCM, 60:40) to afford the product **108** (143 mg, 89%) as a yellowish amorphous solid.

¹H NMR (400 MHz, CD₂Cl₂): 2.27 (s, 6H), 2.34 (s, 6H), 2.97 (t, *J* = 7.4 Hz, 4H), 3.45 (t, *J* = 7.4 Hz, 4H), 5.22 (s, 4H), 7.01 – 7.05 (m, 4H), 7.09 – 7.12 (m, 4H), 7.14 (s, 1H), 7.26 – 7.30 (m, 4H), 7.32 – 7.36 (m, 4H), 7.49 (ddd, *J* = 8.1, 6.8, 1.3 Hz, 2H), 7.54 (d, *J* = 8.4 Hz, 2H), 7.58 (ddd, *J* = 8.3, 6.8, 1.4 Hz, 2H), 7.81 – 7.84 (m, 2H), 7.85 – 7.89 (m, 2H), 7.96 (s, 1H), 8.60 – 8.64 (m, 2H).

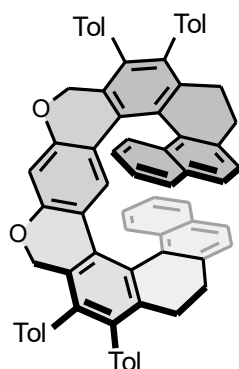
¹³C NMR (101 MHz, CD₂Cl₂): 21.19, 21.62, 21.78, 35.34, 58.58, 81.80, 83.13, 88.74, 89.64, 90.15, 94.79, 99.52, 107.41, 119.41, 120.20, 121.38, 126.35, 126.81, 127.48, 128.21, 128.55, 129.48, 129.67, 131.86, 132.28, 132.57, 133.97, 137.15, 138.20, 139.84, 142.21, 160.43.

IR (CHCl₃): 3081 vw, 3056 w, 3033 w, 2957 w, 2925 m, 2864 w, 2236 w, 2208 w, 1604 m, 1565 m, 1510 vs, 1497 m, 1452 m, 1431 w, 1417 m, 1371w, 1363 w, 1345 w, 1311 m, 1265 m, 1240 m, 1178 m, 1147 w, 1122 m, 1106 w, 1052 m, 1022 s, 1015 m, 961 w, 898 w, 868 w, 818 s, 709vw, 694 vw, 647 vw, 567w, 557 w, 543 w, 529 m, 491 w, 442 w cm⁻¹.

APCI MS: 951 (M⁺).

HR APCI MS: calculated for C₇₂H₅₅O₂ 951.41966, found 951.41977.

rac-9,10,16,17-Tetratolyloxa[11]helicene **109**



Oxa[11]helicene *rac*-**109** was prepared according to the **General procedure for reaction in a flow reactor** from hexayne **108** (50 mg, 0.053 mmol) and $\text{CpCo}(\text{CO})_2$ (10 mg, 7 μL , 0.053 mmol, 1.0 equiv.) in THF (8 mL) at a flow rate of 0.5 mL/min (residence time of 16 min). The purification by a flash chromatography on silica gel (cyclohexane:DCM, 40:60) gave *rac*-**109** (24 mg, 48%) as a white solid.

M.p.: >350 °C (DCM - cyclohexane).

UV/Vis (THF): λ_{max} (log ϵ) = 269 (4.48), 293 sh (4.68), 330 (4.43) nm.

$^1\text{H NMR}$ (400 MHz, CD_2Cl_2): 2.12 – 2.23 (m, 2H), 2.29 (s, 6H), 2.31 (s, 6H), 2.38 – 2.49 (m, 4H), 2.55 – 2.63 (m, 2H), 4.34 (dd, $J = 13.5, 1.3$ Hz, 2H), 4.64 (d, $J = 13.5$ Hz, 2H), 6.44 (s, 1H), 6.73 (dd, $J = 7.8, 1.9$ Hz, 2H), 6.79 (dt, $J = 7.8, 1.2$ Hz, 2H), 6.87 (ddd, $J = 8.3, 6.7, 1.4$ Hz, 2H), 6.92 – 6.95 (m, 2H), 6.97 (bd, $J = 7.9$ Hz, 2H), 7.03 – 7.11 (m, 9H), 7.13 – 7.16 (m, 2H), 7.23 (bd, $J = 8.6$ Hz, 2H), 7.29 (d, $J = 8.1$ Hz, 2H), 7.45 – 7.48 (m, 2H), 7.55 (d, $J = 8.2$ Hz, 2H).

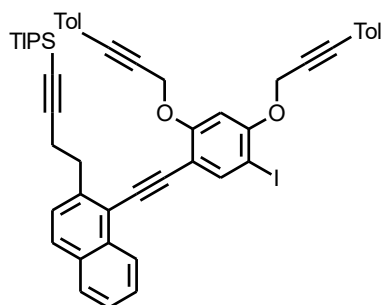
$^{13}\text{C NMR}$ (101 MHz, CD_2Cl_2): 21.44, 21.46, 29.15, 31.29, 68.44, 104.36, 118.85, 124.32, 125.23, 126.00, 126.26, 127.66, 127.85, 128.12, 128.58, 128.74, 128.77, 129.04, 129.08, 129.19, 129.33, 130.42, 130.70, 130.78, 131.40, 131.47, 131.56, 133.10, 136.38, 136.50 (2C), 136.79, 137.92, 138.34, 138.82, 140.49, 156.52.

IR (CHCl_3): 3050 w, 2941 m, 2924 m, 2897 w, 2868 w, 2841 w, 1617 m, 1584 w, 1573 w, 1518 m, 1489 m, 1459 w, 1433 m, 1422 w, 1392 w, 1381 w, 1371 w, 1347 vw, 1333 vw, 1292 m, 1263 w, 1251 w, 1183 m, 1150s, 1134 w, 1111 w, 1081 w, 1068 w, 1048 w, 1030 w, 1022 m, 1002 m, 978 w, 958 w, 921 w, 878 w, 864 w, 844 m, 822 m, 815 s, 701 w, 661 w, 626 w, 601 m, 593 w, 573 w, 556 w, 529 m, 515 w, 503 m, 485 w, 481 w, 474 w, 464 w cm^{-1} .

APCI MS: 951 (M^+).

HR APCI MS: calculated for $\text{C}_{72}\text{H}_{55}\text{O}_2$ 951.41966, found 951.41970.

(4-{1-[(5-Iodo-2,4-bis{[3-(4-methylphenyl)prop-2-yn-1-yl]oxy}phenyl)ethynyl]naphthalen-2-yl}but-1-yn-1-yl)[tri(propan-2-yl)silane 110



A Schlenk flask was charged with diiodide **102** (703 mg, 1.14 mmol), Pd(PPh₃)₄ (132 mg, 0.114 mmol, 10 mol%), CuI (44 mg, 0.23 mmol, 20 mol%) and flushed with argon. Degassed DIPA (10 mL) was added. Then a solution of diyne **99**¹⁹⁰ (205 mg, 0.570 mmol, 0.5 equiv.) in toluene (6 mL) was slowly added at rt within 1 h. The reaction mixture then was stirred at the same temperature overnight. The solvents were evaporated under reduced pressure and the residue was purified by flash chromatography first on silica gel (hexane-ethyl acetate 98:2 to 80:20) and then on reversed-phase C-18 silica gel (methanol-ethyl acetate, 100:0 →50:50) to afford hexayne **105** (123 mg, 40% of total conversion to this product) as a yellow amorphous solid and tetrayne **110** (198 mg, 41%) as a yellowish amorphous solid.

¹H NMR (400 MHz, CDCl₃): 0.98-1.04 (m, 21H), 2.33 (s, 6H), 2.78 (t, *J* = 7.3, 2H), 3.33 (t, *J* = 7.3, 2H), 5.04 (s, 2H), 5.10 (s, 2H), 7.04 – 7.12 (m, 5H), 7.28 – 7.34 (m, 4H), 7.44 (ddd, *J* = 8.1, 6.8, 1.2, 1H), 7.46 (d, *J* = 8.4, 1H), 7.53 (ddd, *J* = 8.3, 6.8, 1.3, 1H), 7.73 (bd, *J* = 8.4, 1H), 7.80 (bd, *J* = 8.1, 1H), 7.98 (s, 1H), 8.54 (bd, *J* = 8.4, 1H).

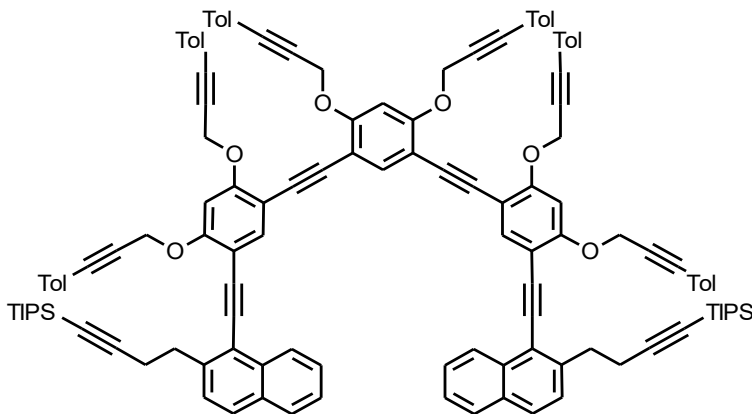
¹³C NMR (101 MHz, CDCl₃): 11.29, 18.61, 21.06, 21.49 (2C), 34.78, 58.12, 58.34, 75.82, 81.01, 82.19, 82.52, 88.31, 88.56, 90.24, 93.46, 99.83, 108.45, 109.25, 118.79, 118.91, 119.52, 125.65, 126.36, 126.77, 127.63, 127.90, 128.00, 129.08, 129.09, 131.72 (2C), 131.93, 133.44, 139.00, 139.09, 141.39, 142.15, 157.66, 160.00.

IR (CHCl₃): 3082 vw, 3057 w, 3034 vw, 2959 s, 2944 s, 2925 s, 2891 m, 2866 s, 2244 w, 2231 w, 2216 w, sh, 2169 m, 1622 vw, sh, 1608 w, sh, 1591 m, 1566 w, 1555 w, 1510 s, 1494 s, 1484 m, sh, 1463 m, 1454 m, 1431 vw, 1402 m, 1385 vw, sh, 1366 m, 1300 m, 1267 s, 1242 m, 1180 s, 1155 m, 1119 vw, 1076 w, sh, 1058 m, 1042 m, 1023 s, 1015 s, 996 m, sh, 962 w, 884 m, 867 w, sh, 818 vs, 709 vw, 679 m, 660 m, 626 w, 616 w, 529 w, 443 w, 416 vw cm⁻¹.

EI MS: 850 (M⁺, 14), 724 (10), 681 (8), 642 (13), 596 (4), 553 (4), 516 (11), 450 (4), 402 (3), 388 (3), 293 (39), 276 (4), 254 (40), 213 (10), 185 (20), 167 (23), 128 (100), 97 (9), 59 (7).

HR EI MS: calculated for C₅₁H₅₁O₂ISi 850.2703, found 850.2698.

{(4,6-Bis{[3-(4-methylphenyl)prop-2-yn-1-yl]oxy}benzene-1,3-diyl)bis[ethyne-2,1-diyl(4,6-bis{[3-(4-methylphenyl)prop-2-yn-1-yl]oxy}benzene-3,1-diyl)ethyne-2,1-diyl)naphthalene-1,2-diylbut-1-yne-4,1-diyl}bis[tri(propan-2-yl)silane] **111**

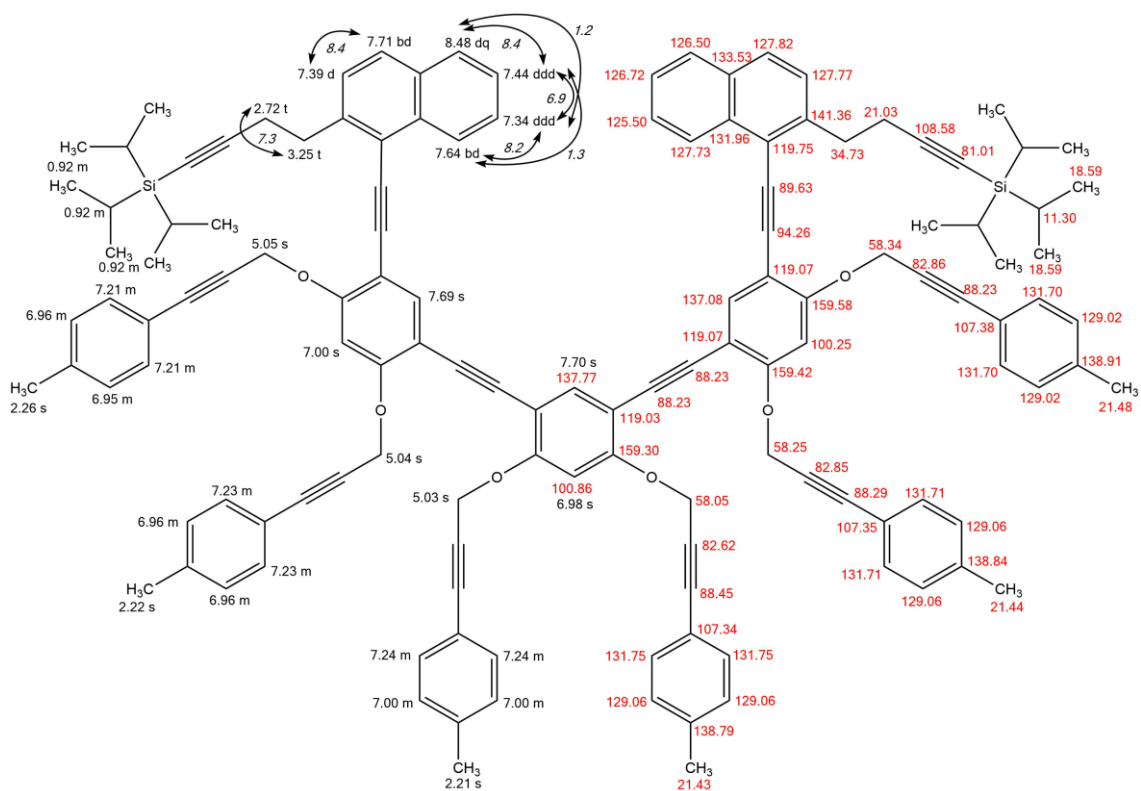


A Schlenk flask was charged with iodide **110** (265 mg, 0.31 mmol, 1.0 equiv.), Pd(PPh₃)₄ (36 mg, 0.031 mmol, 10 mol%), CuI (12 mg, 0.063 mmol, 20 mol%) and flushed with argon. Degassed DIPA (7 mL) was

added. Then a solution of tetrayne **104** (64 mg, 0.16 mmol, 0.5 equiv.) in a degassed mixture of DIPA-toluene (14 mL, 1:1) was slowly added at rt within 1.5 h. The reaction mixture was stirred at the same temperature overnight. The solvents were evaporated under reduced pressure and the residue was purified by flash chromatography on silica gel (hexane:ethyl acetate, 80:20) to afford dodecayne **111** (170 mg, 59%) as a yellowish amorphous solid.

¹H NMR (600 MHz, CDCl₃): 0.92 (m, 42H), 2.21 (s, 6H), 2.22 (s, 6H), 2.26 (s, 6H), 2.72 (t, *J* = 7.3, 4H), 3.25 (t, *J* = 7.3, 4H), 5.03 (s, 4H), 5.04 (s, 4H), 5.05 (s, 4H), 6.95 (m, 2H), 6.96 (m, 6H), 6.98 (s, 1H), 7.00 (m, 4H), 7.00 (s, 2H), 7.21 (m, 4H), 7.23 (m, 4H), 7.24 (m, 4H), 7.34 (ddd, *J* = 8.2, 6.9, 1.2, 2H), 7.39 (d, *J* = 8.4, 2H), 7.44 (ddd, *J* = 8.4, 6.9, 1.3, 2H), 7.64 (dd, *J* = 8.2, 1.3, 2H), 7.69 (s, 2H), 7.70 (s, 1H), 7.71 (bd, *J* = 8.4, 2H), 8.48 (dd, *J* = 8.4, 1.2, 2H).

¹³C NMR (151 MHz, CDCl₃): 11.30, 18.59, 21.03, 21.43, 21.44, 21.48, 34.73, 58.05, 58.25, 58.34, 81.01, 82.62, 82.85, 82.86, 88.23 (3C), 88.29, 88.45, 89.63, 94.26, 100.25, 100.86, 107.34, 107.35, 107.38, 108.58, 119.03, 119.07 (2C), 119.75, 125.50, 126.50, 126.72, 127.73, 127.77, 127.82, 129.02, 129.06 (2C), 131.70, 131.71, 131.75, 131.96, 133.53, 137.08, 137.77, 138.79, 138.84, 138.91, 141.36, 159.30, 159.42, 159.58.

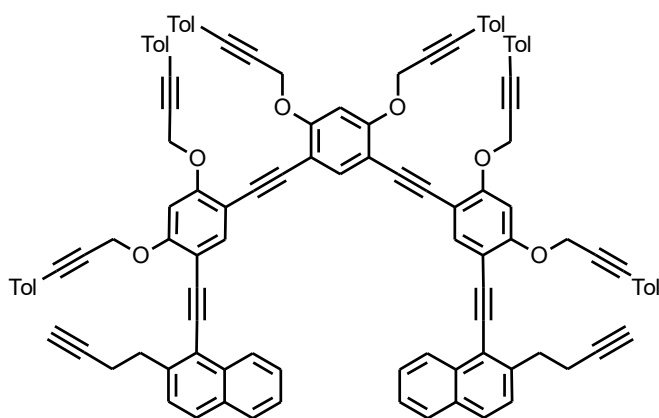


IR (CHCl₃): 3056 w, 2958 m, 2943 m, 2925 m, 2865 m, 2237 w, 2212 vw, 2169 w, 1607 m, 1591 w, 1564 w, 1510 vs, 1501 s, 1461 m, 1454 m, 1408 w, 1387 vw, 1373 m, 1235 m, 1178 m, 1119 vw, 1023 s, 1016 s, 997 m, 884 w, 818 s, 708 vw, 678 w, 661 w cm⁻¹.

APCI MS: 1859 (M⁺).

HR APCI MS: calculated for C₁₃₂H₁₂₂O₆Si₂ 1858.87799, found 1858.87476.

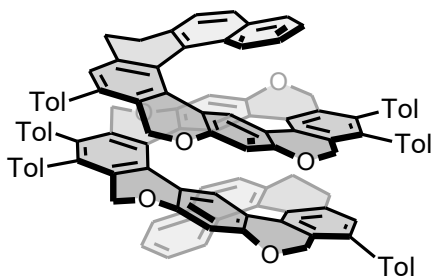
1,1'-{(4,6-Bis{[3-(4-methylphenyl)prop-2-yn-1-yl]oxy}benzene-1,3-diyl)bis[ethyne-2,1-diyl-(4,6-bis{[3-(4-methylphenyl)prop-2-yn-1-yl]oxy}benzene-3,1-diyl)ethyne-2,1-diyl]}bis[2-(but-3-yn-1-yl)naphthalene] 112



A Schlenk flask was charged with the protected dodecayne **111** (74 mg, 0.040 mmol) and distilled THF (10 mL) under argon. Then a solution of TBAF·3H₂O (1 M in THF, 200 μl, 0.19 mmol, 4.8 equiv.) was added. The reaction mixture was stirred at rt for 40 min,

then filtered through a short pad of silica gel (THF) and the resulting solution of the deprotected dodecayne **112** was used in the next cyclisation step without purification.

rac-Oxa[19]helicene **85**



Oxa[19]helicene *rac*-**85** was prepared according to the **General procedure for reaction in a flow reactor** from the crude dodecayne **112** (63 mg, 0.04 mmol in 20 mL THF) and CpCo(CO)₂ (15 mg, 0.083 mmol, 2.0 equiv.) at a flow rate of 0.5 mL/min (residence time of 16 min). The purification by a flash chromatography on silica gel (hexane:ethyl acetate, 4:1) gave *rac*-**85** (35 mg, 56%, after 2 steps from **111**) as a pale yellow solid.

M.p.: >350 °C (acetone-acetonitrile).

UV/Vis (CHCl₃): λ_{\max} (log ϵ) = 274 (4.94), 319 (4.58) nm.

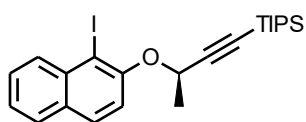
¹H NMR (600 MHz, CDCl₃): 2.24 (s, 6H), 2.30 (s, 6H), 2.43 (s, 6H), 2.65 – 2.80 (m, 8H), 3.90 (d, J = 13.2, 2H), 4.16 (d, J = 13.8, 2H), 4.465 (d, J = 13.8, 2H), 4.475 (d, J = 13.2, 2H), 4.75 (d, J = 13.2, 2H), 5.10 (d, J = 13.2, 2H), 5.675 (s, 1H), 6.39 (s, 4H), 6.40 (m, 2H), 6.46 (m, 2H), 6.65 (m, 2H), 6.70 (s, 2H), 6.71 (m, 2H), 6.745 (dd, J = 8.5, 6.5, 2H), 6.79 (m, 2H), 6.865 (m, 2H), 6.89 (m, 2H), 6.915 (dd, J = 8.5, 6.5, 2H), 7.08 (m, 2H), 7.17 (bd, J = 8.5, 2H), 7.18 (s, 1H), 7.19 (m, 8H), 7.19 (bd, J = 8.5, 2H), 7.23 (d, J = 8.2, 2H), 7.39 (d, J = 8.2, 2H).

¹³C NMR (151 MHz, CDCl₃): 21.17, 21.20, 21.22, 30.22, 30.41, 67.61, 68.07, 68.29, 103.49, 104.46, 115.99, 117.20, 117.69, 123.19, 124.04, 124.60, 125.02, 125.45, 125.96, 126.26, 126.92, 127.55, 127.66, 127.91, 128.10, 128.46, 128.58, 128.70, 128.87, 128.91, 128.96, 129.00 (2C), 129.13 (2C), 129.57, 129.62, 129.97, 130.21, 130.44, 132.50, 132.91, 133.57, 134.74, 135.00, 135.02, 135.09, 135.12, 136.09, 136.12, 136.63, 136.68, 137.03, 137.83, 140.80, 155.91, 155.96, 157.86.

EI MS: 322 (M^+ , 35), 270 (100), 241 (20), 195(20), 165 (10), 142 (15), 114 (25), 88 (5).

HR EI MS: calculated for $C_{14}H_{11}IO$ 321.9855, found 321.9857.

(+)-{(3*R*)-3-[(1-Iodonaphthalen-2-yl)oxy]but-1-yn-1-yl}[tri(propan-2-yl)silane 115



To a solution of freshly prepared LDA from distilled DIPA (433 mg, 4.28 mmol, 1.25 equiv.) and *n*-BuLi (1.6 M in hexane, 2.6 mL, 4.1 mmol, 1.2 equiv.) in THF (5 mL) was added dropwise to a solution of alkyne (+)-(*R*)-**114** (1.10 g, 3.43 mmol) in degassed THF (10 mL) at -78 °C. The reaction mixture was stirred at the same temperature for 1 h. After this period, TIPS chloride (1.10 mL, 5.14 mmol, 1.5 equiv.) was added and the reaction mixture was stirred at -78 °C for 1 h. The solvents were evaporated under reduced pressure and the residue was purified by flash chromatography on silica gel (hexane) to afford the silylated alkyne (+)-(*R*)-**115** (1.61 g, 98%) as a yellowish oil.

Optical rotation: $[\alpha]_D^{20} +9^\circ$ (c 0.259, THF).

¹H NMR (400 MHz, $CDCl_3$): 0.99 (s, 21H), 1.83 (d, $J = 6.6$, 3H), 5.04 (q, $J = 6.6$, 1H), 7.40 (ddd, $J = 7.9$, 6.8, 1.0, 1H), 7.48 (d, $J = 8.9$, 1H), 7.54 (ddd, $J = 8.4$, 6.8, 1.3, 1H), 7.74 (d, $J = 8.2$, 1H), 7.77 (d, $J = 8.9$, 1H), 8.16 (d, $J = 8.5$, 1H).

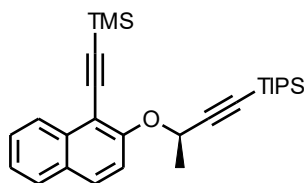
¹³C NMR (101 MHz, $CDCl_3$): 11.19, 18.61, 22.89, 67.52, 88.04, 91.13, 106.37, 117.56, 124.81, 127.92, 128.22, 129.81, 130.67, 131.75, 135.72, 155.63.

IR ($CHCl_3$): 3061 w, 2959 vs, 2944 vs, 2866 vs, 2169 w, 1622 s, 1594 s, 1556 m, 1501 s, 1461 vs, 1427 m, 1384 m, 1367 m, 1347 m, 1323 s, 1261 vs, 1240 vs, 1150 m, 1090 s, 1075 m, 1050 s, 1029 s, 997 vs, 948 s, 883 s, 862 m, 803 s, 679 vs, 519 m, 412 $m\text{ cm}^{-1}$.

EI MS: 478 (M^+ , 10), 383 (3), 351 (4), 309 (3), 269 (100), 223 (2), 190 (2), 165 (2), 125 (4), 111 (3), 96 (2), 83 (2), 59 (2).

HR EI MS: calculated for $C_{23}H_{31}IOSi$ 478.1189, found 478.1190.

(+)-Trimethyl{[2-((2R)-4-[tri(propan-2-yl)silyl]but-3-yn-2-yl)oxy)naphthalen-1-yl]ethynyl}-silane 116



A Schlenk flask was charged with iodide (+)-(R)-**115** (1.58 g, 3.24 mmol), Pd(PPh₃)₄ (76 mg, 0.066 mmol, 2 mol%), CuI (25 mg, 0.13 mmol, 4 mol%) and flushed with argon. Degassed DIPA (5 mL) was added and the mixture was stirred at rt for 5 min before TMSA (487 mg, 4.95 mmol, 1.5 equiv.) was added. The reaction mixture was stirred at the rt overnight. The solvent was evaporated under reduced pressure and the residue was purified by flash chromatography on silica gel (hexane:diethyl ether, 95:5) to afford the protected diyne (+)-(R)-**116** (1.27 g, 86%) as a yellowish oil.

Optical rotation: [α]²⁰_D +55° (c 0.335, THF).

¹H NMR (400 MHz, CDCl₃): 0.39 (s, 9H), 1.05 (m, 21H), 1.81 (d, *J* = 6.6, 3H), 5.18 (q, *J* = 6.5, 1H), 7.43 (ddd, *J* = 8.1, 6.8, 1.2, 1H), 7.50 (d, *J* = 9.0, 1H), 7.57 (ddd, *J* = 8.3, 6.8, 1.3, 1H), 7.76 – 7.82 (m, 2H), 8.32 (dd, *J* = 8.4, 1.1, 1H).

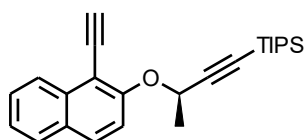
¹³C NMR (101 MHz, CDCl₃): 0.33, 11.22, 18.63, 22.79, 67.44, 87.47, 99.46, 104.45, 106.85, 109.64, 118.67, 124.77, 125.70, 127.17, 128.11, 129.52, 129.75, 134.64, 158.41.

IR (CHCl₃): 3061 w, 2960 s, 2945 s, 2893 m, 2866 s, 2146 w, 2107 w, 2067 vw, 1621 w, 1589 m, 1544 w, 1522 w, 1509 m, 1505 w, 1464 m, 1433 w, 1408 vw, 1380 w, 1373 w, 1323 m, 1251 s, 1148 w, 1087 m, 1075 m, 1037 m, 993 m, 879 s, 846 vs, 699 w, 680 m, 644 m cm⁻¹.

EI MS: 448 (M⁺, 25), 405 (5), 375 (2), 363 (2), 291 (4), 240 (100), 225 (45), 209 (4), 165 (4), 125 (3), 115 (2), 111 (2), 83 (2), 73 (9), 59 (4).

HR EI MS: calculated for C₂₈H₄₀OSi₂ 448.2618, found 448.2620.

(+)-[(3R)-4-(1-Ethynyl-naphthalen-2-yl)-3-methylbut-1-yn-1-yl][tri(propan-2-yl)silane 117



The protected diyne (+)-(R)-**116** (100 mg, 0.22 mmol) was dissolved in methanol (5 mL). To this solution, potassium carbonate (46 mg, 0.33 mmol, 1.5 equiv.) was added and the mixture was stirred at rt for 1 h. After this period, the reaction was quenched with a saturated ammonium chloride solution (10 mL), extracted with ethyl acetate (2 × 10 mL) and the combined organic layers were dried over anhydrous

MgSO₄. The solvents were evaporated under reduced pressure and the residue was purified by flash chromatography on silica gel (hexane:DCM, 10:1) to afford the protected diyne (+)-(R)-**117** (77 mg, 91%) as a yellowish oil.

Optical rotation: $[\alpha]_D^{20} +57^\circ$ (c 0.426, CHCl₃).

¹H NMR (400 MHz, CDCl₃): 1.00 (m, 21H), 1.80 (d, *J* = 6.6, 3H), 5.12 (q, *J* = 6.6, 1H), 7.41 (ddd, *J* = 8.1, 6.8, 1.2, 1H), 7.51 (d, *J* = 9.1, 1H), 7.55 (ddd, *J* = 8.4, 6.9, 1.3, 1H), 7.77 – 7.82 (m, 2H), 8.30 (dd, *J* = 8.5, 1.0, 1H).

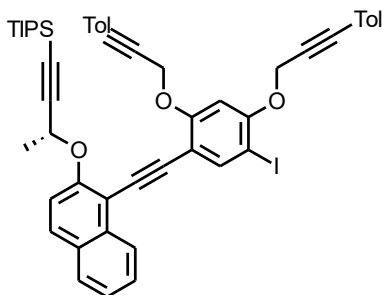
¹³C NMR (101 MHz, CDCl₃): 11.20, 18.61, 22.77, 67.03, 78.25, 86.65, 87.81, 106.58, 107.78, 117.52, 124.72, 125.50, 127.34, 128.15, 129.25, 130.06, 134.85, 158.56.

IR (CHCl₃): 3307 s, 3063 w, 2945 vs, 2959 s, 2866 vs, 2168 w, 2101 w, 1622 m, 1590 s, 1510 m, 1506 m, 1465 s, 1434 w, 1383 w, 1374 m, 1323 m, 1270 s, 1250 vs, 1232 m, 1148 m, 1089 s, 1045 m, 1036 m, 997 m, 883 s, 867 vw, 808 m, 679 s, 650 m, 607 m, 562 w, 437 w cm⁻¹.

ESI MS: 377 ([M+H]⁺), 399 ([M+Na]⁺).

HR ESI MS: calculated for C₂₅H₃₃OSi 377.2295, found 377.2297.

(-)-[(3R)-3-({1-[(5-Iodo-2,4-bis{3-(4-methylphenyl)prop-2-yn-1-yl}oxy}phenyl)ethynyl]-naphthalen-2-yl}oxy)but-1-yn-1-yl][tri(propan-2-yl)silane
118



A Schlenk flask was charged with diiodide **102** (883 mg, 1.43 mmol, 2.0 equiv.), Pd(PPh₃)₄ (83 mg, 0.072 mmol, 10 mol%), CuI (27 mg, 0.14 mmol, 20 mol%), flushed with argon before the degassed DIPA (10 mL) was added. Diyne (+)-(R)-**117** (269 mg, 0.715 mmol) was dissolved in degassed toluene (10 mL) under argon and added

dropwise to a reaction mixture at rt within 3 h. The reaction mixture was stirred at the same temperature overnight. The solvents were evaporated under reduced pressure and the residue was purified by flash chromatography on silica gel (hexane:ethyl acetate, 96:4) to afford iodide (-)-(R)-**118** (328 mg, 53%) as a yellowish amorphous solid.

Optical rotation: $[\alpha]_D^{20} -24^\circ$ (c 0.213, THF).

¹H NMR (400 MHz, CDCl₃): 1.01 (d, *J* = 1.0, 21H), 1.85 (d, *J* = 6.6, 3H), 2.34 (s, 6H), 5.04 (s, 2H), 5.13 (s, 2H), 5.22 (q, *J* = 6.5, 1H), 7.03 – 7.13 (m, 5H), 7.31 (t, *J* = 7.8,

4H), 7.38 (ddd, $J = 8.1, 6.8, 1.2$, 1H), 7.48 – 7.61 (m, 2H), 7.73 – 7.82 (m, 2H), 8.01 (s, 1H), 8.49 (dd, $J = 8.4, 1.1$, 1H).

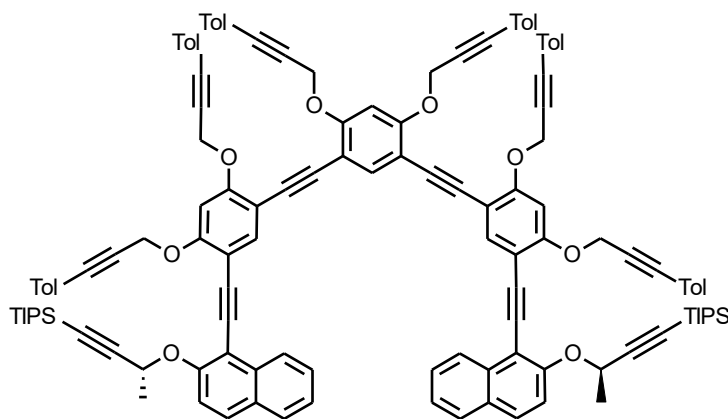
^{13}C NMR (101 MHz, CDCl_3): 11.12, 18.54, 21.54 (2C), 22.80, 58.28, 58.39, 67.22, 76.09, 82.29, 82.71, 87.49, 88.28, 88.50, 88.54, 93.76, 100.45, 106.78, 109.61, 109.71, 118.30, 118.86, 119.01, 124.60, 125.86, 127.11, 127.93, 129.09, 129.11, 129.33, 129.43, 131.76, 131.77, 134.38, 138.98, 139.08, 142.50, 157.23, 157.54, 159.84.

IR (CHCl_3): 3059 w, 2959 s, 2944 s, 2925 m, 2866 s, 2244 w, 2231 w, 2218 w, 2169 w, 1620 w, 1609 vw, 1589 s, 1571 w, 1555 w, 1510 vs, 1495 s, 1485 m, 1463 s, 1454 m, 1403 m, 1383 vw, 1371 m, 1254 s, 1178 m, 1120 w, 1023 s, 1015 s, 996 m, 884 m, 818 s, 709 w, 679 m cm^{-1} .

APCI MS: 867 ($[\text{M}+\text{H}]^+$).

HR APCI MS: calculated for $\text{C}_{51}\text{H}_{52}\text{IO}_3\text{Si}$ 867.27208, found 867.27249.

(-)-{(4,6-Bis{[3-(4-methylphenyl)prop-2-yn-1-yl]oxy}benzene-1,3-diyl)bis[ethyne-2,1-diyl-(4,6-bis{[3-(4-methylphenyl)prop-2-yn-1-yl]oxy}benzene-3,1-diyl)ethyne-2,1-diyl]naphtha-lene-1,2-diyloxy(3*R*)but-1-yne-3,1-diyl}bis[tri(propan-2-yl)silane]
119



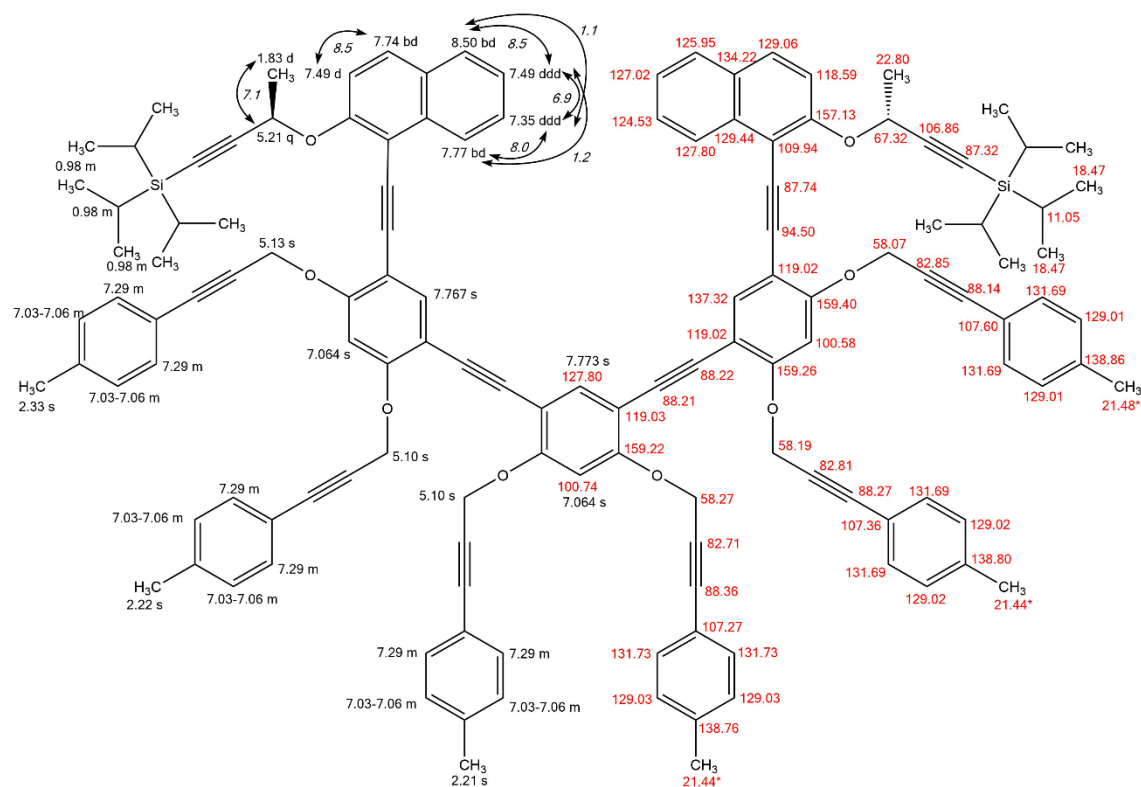
A Schlenk flask was charged with iodide (-)-(*R*)-**118** (790 mg, 0.911 mmol, 1.0 equiv.), $\text{Pd}(\text{PPh}_3)_4$ (105 mg, 0.091 mmol, 10 mol%), CuI (35.0 mg, 0.183 mmol, 20 mol%) and flushed with argon.

A degassed mixture of DIPA-toluene (20 mL, 3:1) was added. Then a solution of tetrayne **104** (208 mg, 0.502 mmol, 0.5 equiv.) in toluene (25 mL) was slowly added at rt within 1.5 h. The reaction mixture was stirred at the same temperature overnight. The solvents were evaporated under reduced pressure and the residue was purified by flash chromatography on silica gel (hexane:ethyl acetate, 80:20) to afford dodecayne (-)-(*R,R*)-**119** (516 mg, 60%) as a yellowish amorphous solid.

Optical rotation: $[\alpha]^{20}_{\text{D}} -6^\circ$ (c 0.214, THF).

¹H NMR (500 MHz, CDCl₃): 0.98 (m, 42H), 1.83 (d, *J* = 7.1, 6H), 2.21 (s, 6H), 2.22 (s, 6H), 2.33 (s, 6H), 5.10 (s, 8H), 5.13 (s, 4H), 5.21 (q, *J* = 7.1, 2H), 7.03 - 7.06 (m, 12H), 7.064 (s, 3H), 7.29 (m, 12H), 7.35 (ddd, *J* = 8.0, 6.9, 1.1, 2H), 7.49 (d, *J* = 8.5, 2H), 7.49 (ddd, *J* = 8.5, 6.9, 1.2, 2H), 7.74 (bd, *J* = 8.5, 2H), 7.767 (s, 2H), 7.77 (bd, *J* = 8.0, 1.2, 2H), 7.773 (s, 1H), 8.50 (dd, *J* = 8.5, 1.1, 2H).

¹³C NMR (126 MHz, CDCl₃): 11.05, 18.47, 21.44 (2C), 21.48, 22.80, 58.07, 58.19, 58.27, 67.32, 82.71, 82.81, 82.85, 87.32, 87.74, 88.14, 88.21, 88.22, 88.27, 88.36, 94.50, 100.58, 100.74, 106.86, 107.27, 107.36, 107.60, 109.94, 118.59, 119.02 (2C), 119.03, 124.53, 125.95, 127.02, 127.80 (2C), 129.01 (2C), 129.02 (2C), 129.03(2C), 129.06, 129.44, 131.69 (4C), 131.73 (2C), 134.22, 137.32, 138.76, 138.80, 138.86, 157.13, 159.22, 159.26, 159.40.

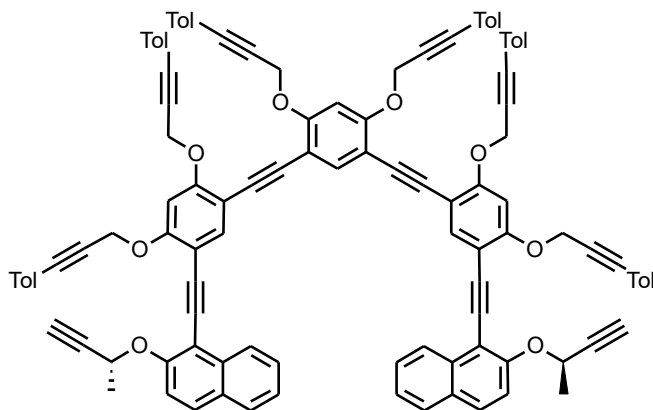


IR (CHCl₃): 3058 w, 2959 m, 2944 m, 2925 m, 2866 s, 2237 w, 2214 w, 2169 vw, 1621 w, 1607 m, 1589 m, 1572 w, 1565 w, 1510 vs, 1501 s, 1462 m, 1454 m, 1408 m, 1388 vw, 1372 m, 1234 s, 1172 m, 1122 m, 1023 s, 1016 s, 998 m, 883 m, 818 s, 708 w, 679 m cm⁻¹.

MALDI MS: 1891 ([M]⁺).

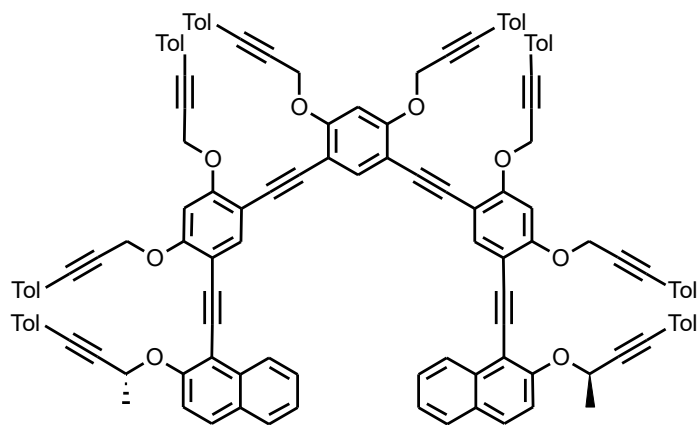
HR MALDI MS: calculated for C₁₃₂H₁₂₂O₈Si₂ 1890.8678, found 1890.8673.

1,1'-{(4,6-Bis{[3-(4-methylphenyl)prop-2-yn-1-yl]oxy}benzene-1,3-diyl)bis[ethyne-2,1-diyl-(4,6-bis{[3-(4-methylphenyl)prop-2-yn-1-yl]oxy}benzene-3,1-diyl)ethyne-2,1-diyl]}bis-{2-[(2*R*)-but-3-yn-2-yloxy]naphthalene} 120



A Schlenk flask was charged with the protected dodecayne (-)-(*R,R*)-**119** (466 mg, 0.246 mmol) and dissolved in distilled THF (4 mL). Under argon atmosphere, a solution of TBAF·3H₂O (1 M in THF, 75 μ L, 0.75 mmol, 3.0 equiv.) was added. The reaction mixture was stirred at rt for 40 min. The solvent was evaporated in a stream of nitrogen and the crude product (*R,R*)-**120** was directly used without further purification.

(-)-1,1'-{(4,6-Bis{[3-(4-methylphenyl)prop-2-yn-1-yl]oxy}benzene-1,3-diyl)bis[ethyne-2,1-diyl-(4,6-bis{[3-(4-methylphenyl)prop-2-yn-1-yl]oxy}benzene-3,1-diyl)ethyne-2,1-diyl]}bis(2-[(2*R*)-4-(4-methylphenyl)but-3-yn-2-yl]oxy)naphthalene} 121

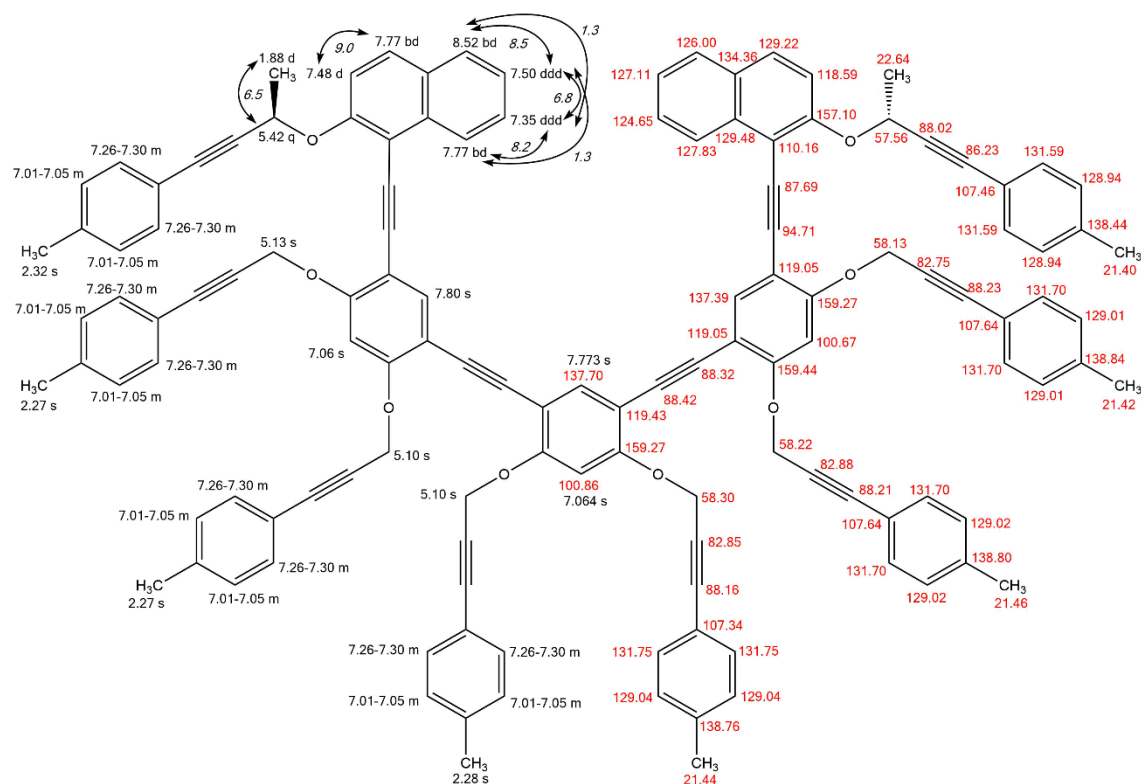


The crude product (*R,R*)-**120** (389 mg, 0.246 mmol) was dissolved in degassed toluene (10 mL) under argon and dropwise added to a mixture of 4-iodotoluene (218 mg, 1.00 mmol, 4.0 equiv.), Pd(PPh₃)₄ (29 mg, 0.025 mmol, 10 mol%), CuI (10 mg, 0.053 mmol, 20 mol%) in degassed DIPA (5 mL) at rt within 3 h. The reaction mixture was stirred at the same temperature overnight. The solvents were evaporated under reduced pressure and the residue was purified by flash chromatography on silica gel (hexane:ethyl acetate, 80:20) to afford dodecayne (-)-(*R,R*)-**121** (333 mg, 77%, after 2 steps) as a yellowish amorphous solid.

Optical rotation: $[\alpha]_D^{20} -45^\circ$ (c 0.220, THF).

¹H NMR (500 MHz, CDCl₃): 1.88 (d, *J* = 6.5, 6H), 2.27 (s, 12H), 2.28 (s, 6H), 2.32 (s, 6H), 5.10 (s, 8H), 5.13 (s, 4H), 5.42 (q, *J* = 6.5, 2H), 7.01 – 7.05 (m, 16H), 7.06 (s, 2H), 7.064 (s, 1H), 7.26 – 7.30 (m, 16H), 7.35 (ddd, *J* = 8.2, 6.8, 1.3, 2H), 7.48 (d, *J* = 9.0, 2H), 7.50 (ddd, *J* = 8.5, 6.8, 1.3, 2H), 7.77 (dd, *J* = 8.2, 1.3, 2H), 7.77 (bd, *J* = 9.0, 2H), 7.773 (s, 1H), 7.80 (s, 2H), 8.52 (dd, *J* = 8.5, 1.3, 2H).

¹³C NMR (126 MHz, CDCl₃): 21.40, 21.42, 21.44, 21.46, 22.64, 57.56, 58.13, 58.22, 58.30, 82.75, 82.85, 82.88, 86.23, 87.69, 88.02, 88.16, 88.21, 88.23, 88.32, 88.42, 94.71, 100.67, 100.86, 107.34, 107.46, 107.64 (2C), 110.16, 118.59, 119.05 (2C), 119.43, 124.65, 126.00, 127.11, 127.83, 128.94 (2C), 129.01 (2C), 129.02 (2C), 129.04 (2C), 129.22, 129.48, 131.59 (2C), 131.70 (4C), 131.75 (2C), 134.36, 137.39, 137.70, 138.44, 138.76, 138.80, 138.84, 157.10, 159.27 (2C), 159.44.

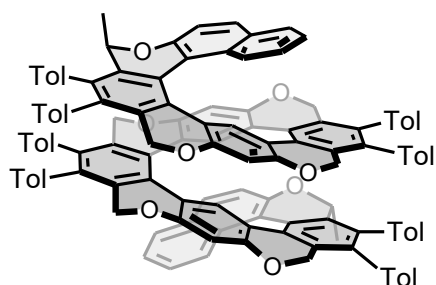


IR (CHCl₃): 3082 w, 3056 w, 2236 w, 2215 w, 1620 w, 1607 m, 1589 w, 1572 w, 1565 w, 1510 s, 1503 m, 1439 w, 1423 w, 1408 w, 1320 m, 1268 m, 1254 m, 1236 m, 1174 m, 1120 w, 1083 m, 1057 w, 1023 m, 1016 m, 867 w, 818 s, 709 w, 542 w, 528 w cm⁻¹.

MALDI MS: 1759 ([M+H]⁺), 1758 (M⁺).

HR MALDI MS: calculated for C₁₂₈H₉₄O₈ 1758.6949, found 1758.6943.

(-)-(M,R,R)-Oxa[19]helicene 86



Oxa[19]helicene (-)-(M,R,R)-**86** was prepared according to the **General procedure for reaction in a flow reactor** from dodecayne (-)-(R,R)-**121** (70 mg, 0.040 mmol) and CpCo(CO)₂ (15 mg, 0.083 mmol, 2.0 equiv.) in THF (14 mL) at a flow rate of 0.5 mL/min (residence time of 16 min). The purification by a flash chromatography on silica gel (hexane:ethyl acetate, 3:2) gave (-)-(M,R,R)-**86** (14 mg, 20%) as a pale yellow solid.

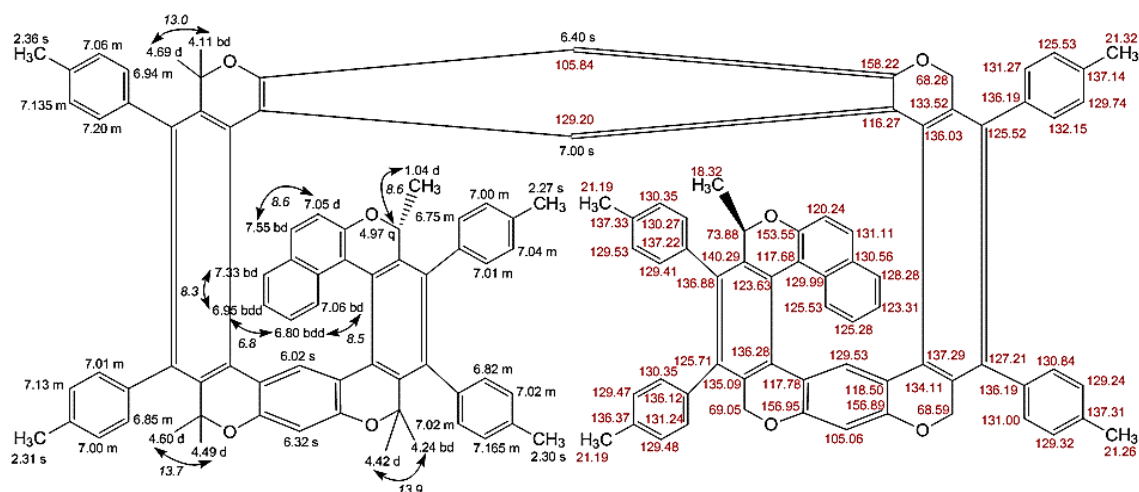
M.p.: >350 °C (acetone-acetonitrile).

Optical rotation: $[\alpha]_D^{20} = -1027^\circ$ (c 0.026, THF).

UV/Vis (THF): λ_{\max} (log ϵ) = 235 (5.02), 264 (4.99), 273 (4.98), 317 (4.61) nm.

¹H NMR (600 MHz, acetone-*d*₆): 1.04 (d, *J* = 8.6, 6H), 2.27 (s, 6H), 2.30 (s, 6H), 2.31 (s, 6H), 2.36 (s, 6H), 4.11 (bd, *J* = 13.0, 2H), 4.24 (bd, *J* = 13.9, 2H), 4.42 (d, *J* = 13.9, 2H), 4.49 (d, *J* = 13.7, 2H), 4.60 (d, *J* = 13.7, 2H), 4.69 (d, *J* = 13.0, 2H), 4.97 (q, *J* = 8.6, 2H), 6.02 (s, 2H), 6.32 (s, 2H), 6.40 (s, 1H), 6.75 (m, 2H), 6.80 (bdd, *J* = 8.5, 6.8, 2H), 6.82 (m, 2H), 6.85 (m, 2H), 6.94 (m, 2H), 6.95 (bdd, *J* = 8.3, 6.8, 2H), 7.00 (m, 4H), 7.00 (s, 1H), 7.01 (m, 4H), 7.02 (m, 4H), 7.04 (m, 2H), 7.05 (d, *J* = 8.6, 2H), 7.06 (m, 2H), 7.06 (bd, *J* = 8.5, 2H), 7.13 (m, 2H), 7.135 (m, 2H), 7.165 (m, 2H), 7.20 (m, 2H), 7.33 (bd, *J* = 8.3, 2H), 7.55 (bd, *J* = 8.6, 2H).

¹³C NMR (151 MHz, acetone-*d*₆): 18.32, 21.19 (2C), 21.26, 21.32, 68.28, 68.59, 69.05, 73.88, 105.06, 105.84, 116.27, 117.68, 117.78, 118.50, 120.24, 123.31, 123.63, 125.28, 125.52, 125.53 (2C), 125.71, 127.21, 128.28, 129.20, 129.24, 129.32, 129.41, 129.47, 129.48, 129.53 (2C), 129.74, 129.99, 130.27, 130.35 (2C), 130.56, 130.84, 131.00, 131.11, 131.24, 131.27, 132.15, 133.52, 134.11, 135.09, 136.03, 136.12, 136.19 (2C), 136.28, 136.37, 136.88, 137.14, 137.22, 137.29, 137.31, 137.33, 140.29, 153.55, 156.89, 156.95, 158.22.

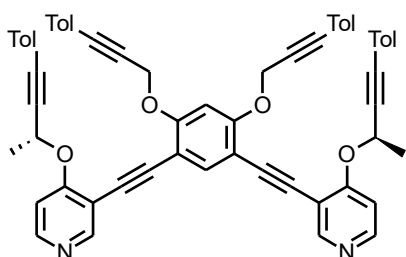


IR (CCl₄): 3049 w, 2956 m, 2924 s, 2854, 1666 m, 1618 m, 1591 m, 1518 m, 1489 m, 1464 m, 1425 s, 1379 m, 1304 w, 1260 m, 1226 m, 1183 m, 1157s, 1109 m, 1087 m, 1022 m, 982 m, 958 w, 943 w, 896 w, 812 m, 788 m, 751 m, 643 w, 605 w, 552 w, 528 m cm⁻¹.

APCI MS: 1760 ([M+H]⁺).

HR APCI MS: calculated for C₁₂₈H₉₅O₈ 1759.70215, found 1759.70217.

(-)-3,3'-[(4,6-Bis{[3-(4-methylphenyl)prop-2-yn-1-yl]oxy}benzene-1,3-diyl)diethyne-2,1-diyl]bis(4-[(1*R*)-1-methyl-3-(4-methylphenyl)prop-2-yn-1-yl]oxy}pyridine) **124**



The Schlenk flask A was charged with iodide (-)-(*R*)-**123**¹⁴⁸ (94 mg, 0.26 mmol, 2.4 equiv.), Pd(PPh₃)₂Cl₂ (4 mg, 0.005 mmol, 5 mol%), CuI (2 mg, 0.01 mmol, 10 mol%), flushed with argon and a degassed mixture of DIPA and toluene (10 mL, 1:1) was added. The Schlenk flask B was charged with **103** (60 mg, 0.107 mmol, 1.0 equiv.) and dissolved in distilled toluene (8 mL). Then TBAF·3H₂O (1 M solution in THF, 260 μL, 2.4 equiv.) was added, the reaction mixture was stirred for 30 min at rt and slowly cannulated into the Schlenk flask A during 1.5 h. The solvents were evaporated under reduced pressure and the residue was purified by flash chromatography on silica gel (DCM:MeOH, 98:2) to afford hexayne (-)-(*R*)-**124** (80 mg, 84%) as a yellowish amorphous solid.

Optical rotation: [α]_D²⁰ -450° (c 0.337, CHCl₃).

¹H NMR (400 MHz, CDCl₃): 1.86 (d, *J* = 6.5, 6H), 2.32 (s, 12H), 5.10 (s, 4H), 5.21 (q, *J* = 6.5, 2H), 7.05 (d, *J* = 7.9, 4H), 7.08 (d, *J* = 7.9, 4H), 7.08 (s, 1H), 7.12 (d, *J* = 5.6, 2H), 7.28 (d, *J* = 8.2, 4H), 7.29 (d, *J* = 8.1, 4H), 7.72 (s, 1H), 8.42 (bs, 2H), 8.65 (bs, 2H).

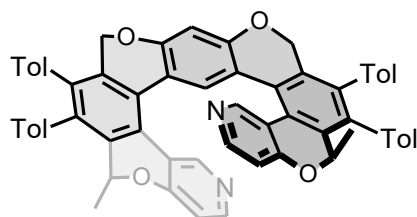
¹³C NMR (101 MHz, CDCl₃): 21.60 (2C), 22.26, 58.26, 65.27, 82.63, 86.06, 86.29, 87.39, 88.52, 91.48, 100.62, 106.92, 108.79, 111.19, 118.91, 119.02, 129.17 (2C), 131.74, 131.81, 138.13, 139.06, 139.10, 150.03, 153.88, 159.80, 163.62.

IR (CHCl₃): 3084 vw, 3051 w, 2960 m, 2925 m, 2870 w, 2238 w, 2217 w, 1605 m, 1581 m, 1563 m, 1510 vs, 1500 s, 1490 s, 1486 s, 1417 m, 1405 m, 1377 m, 1328 s, 1265 s, 1247 s, 1185 m, 1177 m, sh, 1120 m, 1086 s, 1032 s, 1020 m, 1015 m, sh, 965 w, sh, 948 m, 894 w, 818 vs, 708 w cm⁻¹.

ESI MS: 885 ([M+H]⁺).

HR ESI MS: calculated for C₆₂H₄₉N₂O₄ 885.3687, found 885.3691.

(-)-(M,R,R)-Pyridooxa[9]helicene **87**



Method A: Microwave vial was charged with 30 mg of ionic liquid (1-butyl-2,3-dimethylimidazolium tetrafluoroborate) a solution of the (-)-(R,R)-**124** (24 mg, 0.027 mmol) in THF (5 mL) CpCo(CO)(*fum*) (8 mg, 0.03 mmol, 1.0 equiv.) was added in one portion

under argon. The reaction mixture was heated to 170 °C for 10 min in the microwave reactor. The resulting reaction mixture was concentrated *in vacuo*. The purification by a flash chromatography on silica gel (hexane:ethyl acetate, 5:1) gave (-)-(M,R,R)-**87** (10 mg, 42%) as a slightly yellow solid.

Method B: In a glove box a vial was charged with Ni(cod)₂ (5 mg, 0.02 mmol, 0.5 equiv.) and PPh₃ (9 mg, 0.03 mmol, 1.0 equiv.). A second vial was filled with hexayne (-)-(R,R)-**124** (30 mg, 0.034 mmol) and purged with argon. To both vials freshly distilled tetrahydrofuran (2 x 1 ml) was injected through a septum and stirred at room temperature for 2 min. Then a solution of hexayne (-)-(R,R)-**124** was slowly added to a solution of catalyst and the resulting dark solution was stirred at room temperature for 16 h. The resulting reaction mixture was concentrated *in vacuo*. The purification by a flash chromatography on silica gel (hexane:ethyl acetate, 5:1) gave (-)-(M,R,R)-**87** (13 mg, 43%) as a slightly yellow solid.

Method C: Pyridooxa[9]helicene (-)-(M,R,R)-**87** was prepared according to the **General procedure for reaction in a flow reactor** from hexayne (-)-(R,R)-**124** (24 mg, 0.027 mmol) and CpCo(CO)₂ (5 mg, 0.03 mmol, 1.0 equiv.) in THF (5 mL) at a flow rate of 1.0 mL/min (residence time of 8 min). The purification by a flash chromatography on silica gel (hexane:ethyl acetate, 5:1) gave (-)-(M,R,R)-**87** (13 mg, 54%) as a slightly yellow solid.

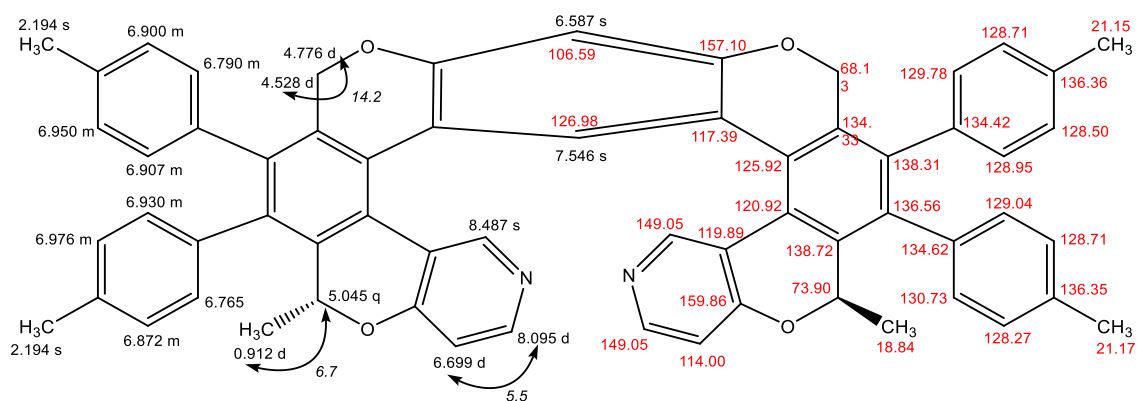
M.p.: 323.0 - 324.0 °C (methanol).

Optical rotation: $[\alpha]_D^{20} = -651^\circ$ (c 0.239, CHCl₃).

UV/Vis (THF): λ_{\max} (log ϵ) = 277 (4.88), 317 (4.30), 366 (3.98) nm.

¹H NMR (600 MHz, CDCl₃): 0.91 (d, $J = 6.7$, 6H), 2.19 (s, 12H), 4.53 (d, $J = 14.2$, 2H), 4.78 (d, $J = 14.2$, 2H), 5.05 (q, $J = 6.7$, 2H), 6.59 (s, 1H), 6.70 (d, $J = 5.5$, 2H), 6.77 (m, 2H), 6.79 (m, 2H), 6.87 (m, 2H), 6.90 (m, 2H), 6.91 (m, 2H), 6.93 (m, 2H), 6.95 (m, 2H), 6.98 (m, 2H), 7.55 (s, 1H), 8.10 (d, $J = 5.5$, 2H), 8.49 (s, 2H).

¹³C NMR (151 MHz, CDCl₃): 18.84, 21.15, 21.17, 68.13, 73.90, 106.59, 114.00, 117.39, 119.89, 120.92, 125.92, 126.98, 128.27, 128.50, 128.71 (2C), 128.95, 129.04, 129.78, 130.73, 134.33, 134.42, 134.62, 136.35, 136.36, 136.56, 138.31, 138.72, 149.05 (2C), 157.10, 159.86.

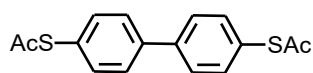


IR (CHCl₃): 3087 vw, 3048 w, 2957 s, 2927 vs, 2855 m, 1617 m, 1593 s, 1579 m, 1564 w, sh, 1549 vw, sh, 1519 m, 1493 m, 1485 s, 1431 m, 1423 s, 1404 vw, 1379 m, 1371 m, 1328 w, 1258 s, 1253 s, 1175 s, 1112 w, 1085 m, sh, 1078 s, 1022 s, 1018 s, 1008 w, sh, 968 m, sh, 900 m, 824 m, 690 vw, 531 w cm⁻¹.

ESI MS: 885 ([M+H]⁺).

HR ESI MS: calculated for C₆₂H₄₉N₂O₄ 885.3687, found 885.3688.

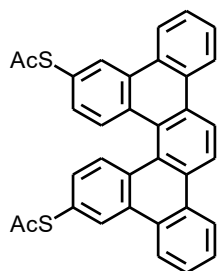
4,4'-bis(thioacetyl)biphenyl **129**¹⁶⁶



A Schlenk flask was charged with sodium ethanethiolate freshly prepared from sodium (690 mg, 30.0 mmol, 20.0 equiv.) and ethanethiol (2.24 g, 2.60 mL, 36.0 mmol, 24.0 equiv.) in freshly distilled NMP (20 mL), and flushed with argon. A degassed suspension of 4,4'-dibromobiphenyl **128** (468 mg, 1.50 mmol) in NMP (5 mL) was added and the reaction mixture was stirred at 250 °C for 2 h. The reaction mixture was cooled down to rt and acetyl chloride (3.53 g, 3.30 mL, 45.0 mmol, 30.0 equiv.) was added. The reaction mixture was stirred at rt for 2 h, poured into ice, and extracted with DCM (3 × 70 mL). The organic layer was washed with brine (3 × 50 mL), the solvents were evaporated under reduced pressure, and the residue was purified by flash chromatography (hexane:ethyl acetate, 80:20) to afford **129** (415 mg, 92%) as a white solid.

The spectra were in an agreement with the published data.¹⁶⁶

rac-3,16-Bis(Thioacetyl)Dibenzo[5]helicene **131**



Method A: A Schlenk flask was charged with sodium ethanethiolate freshly prepared from sodium (230 mg, 10.0 mmol, 20.0 equiv.) and ethanethiol (746 mg, 0.87 mL, 12.0 mmol, 24.0 equiv.) in freshly distilled NMP (10 mL), and flushed with argon. A degassed suspension of *rac*-**130**¹⁶⁸ (224 mg, 0.50 mmol) in NMP (5 mL) was added and the reaction mixture was stirred at 250 °C for 2 h. The reaction mixture was cooled down to rt and acetyl chloride (1.18 g, 1.10 mL, 15 mmol, 30.0 equiv.) was added. The reaction mixture was stirred at rt for 2 h, poured into ice, and extracted with DCM (3 × 50 mL). The organic layer was washed with brine (3 × 30 mL), the solvents were evaporated under reduced pressure, and the residue was purified by flash chromatography (hexane:ethyl acetate, 80:20) to afford *rac*-**131** (249 mg, 94%) as white solid.

Method B: A Schlenk flask was charged with sodium methanethiolate freshly prepared from sodium (289 mg, 12.5 mmol, 50.0 equiv.) and dimethyl disulfide (731 mg, 0.69 mL, 7.8 mmol, 31.0 equiv.) in freshly distilled NMP (10 mL), and flushed with argon. A degassed solution of *rac*-**130**¹⁶⁸ (112 mg, 0.25 mmol) in NMP (10 mL) was added and the reaction mixture was stirred at 200 °C for 4 h. The reaction mixture was cooled down to rt and acetyl chloride (1.74 g, 1.35 mL, 18.8 mmol, 70.0 equiv.) was added. The

reaction mixture was stirred at rt for 2 h, poured into ice, and extracted with DCM (3 × 30 mL). The organic layers were washed with brine (3 × 20 mL), the solvents were evaporated under reduced pressure, and the residue was purified by flash chromatography (hexane:ethyl acetate, 80:20) to afford *rac*-**131** (123 mg, 93%) as a white solid.

M.p.: 281.0–283.0 °C (hexane–ethyl acetate).

UV/Vis (THF): λ_{max} (log ϵ) = 245 (5.05), 260 (5.06), 288 (5.05), 315 (5.05), 357 (4.42) nm.

¹H NMR (400 MHz, CDCl₃): 2.51 (s, 6H), 7.22 (dd, J = 8.6, 1.8, 2H), 7.64 – 7.85 (m, 4H), 8.27 (d, J = 8.6, 2H), 8.56 – 8.70 (m, 8H).

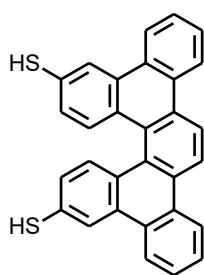
¹³C NMR (101 MHz, CDCl₃): 30.47, 122.49, 123.45, 123.82, 126.69, 127.23, 127.70, 128.11, 129.72, 129.83, 130.14, 130.56, 130.77, 130.98, 131.28, 131.53, 194.09.

IR (CHCl₃): 3104 vw, 3075 w, 3065 w, 2956 w, 2927 m, 2855 w, 1702 s, 1634 vw, 1606 vw, 1599 vw, 1563 vw, 1533 vw, 1492 m, 1473 m, 1443 m, 1416 w, 1392 m, 1354 m, 1301 vw, 1287 w, 1278 vw, 1251 w, 1172 vw, 1158 w, 1126 s, 1120 s, 1105 s, 1054 vw, 1049 vw, 1021 w, 1000 w, 951 m, 882 w, 861 w, 855 w, 828 m, 821 w, 628 m, 618 m, 595 w, 592 w, 535 vw, 523 vw, 497 vw, 457 vw, 430 vw cm⁻¹.

ESI MS: 527 ([M+H]⁺), 549 ([M+Na]⁺).

HR ESI MS: calculated for C₃₄H₂₂O₂NaS₂ 549.0953, found 549.0954.

rac-Dibenzo[5]helicene-3,16-dithiol **132**



A Schlenk flask was charged with *rac*-**131** (20 mg, 0.038 mmol), flushed with argon, and degassed MTBE (10 mL) was added. Then a solution of cesium hydroxide monohydrate (51 mg, 0.30 mmol, 8.0 equiv.) in methanol (300 μ L) was added dropwise at rt. The reaction mixture was stirred for 5 min. Then the reaction mixture was slowly acidified with hydrochloric acid (1M in water, 760 μ L, 20.0 equiv.) during 10 min. The mixture was extracted with MTBE (3 × 10 mL). The organic layers were left to evaporate under flow of argon to afford *rac*-**132** (12 mg, 71%) as a yellow powder.

M.p.: Decomposition ~310 °C (water).

¹H NMR (400 MHz, CDCl₃): 3.68 (s, 2H), 7.08 (dd, J = 8.6, 2.0, 2H), 7.70 – 7.80 (m, 4H), 8.09 (d, J = 8.7, 2H), 8.46 (d, J = 2.0, 2H), 8.58 – 8.66 (m, 8H).

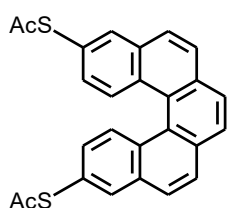
¹³C NMR (101 MHz, CDCl₃): 121.86, 123.31, 123.64, 123.88, 126.81, 127.19, 127.55, 128.01, 128.80, 129.52, 129.86, 129.94, 130.21, 130.78, 131.40.

IR (CHCl₃): 3419 m, 3064 w, 2963 m, 2922 m, 2852 w, 2555 vw, 1944 vw, 1598 m, 1532 vw, 1491 m, 1473 w, 1439 m, 1394 m, 1343 w, 1262 s, 1220 m, 1157 m, 1099 s, 1022 s, 869 w, 851 m, 816 s, 803 s, 744 s, 719 w, 688 w, 625 w, 582 w, 493 w, 461 w, 430 w cm⁻¹.

ESI MS: 441 ([M-H]⁻).

HR ESI MS: calculated for C₃₀H₁₇S₂ 441.0777, found 441.0775.

***rac*-3,12-Bis(thioacetyl)pentahelicene 134**



A Schlenk flask was charged with sodium methanethiolate freshly prepared from sodium (331 mg, 14.4 mmol, 50.0 equiv.) and DMDS (850 mg, 0.80 mL, 8.9 mmol, 31.0 equiv.) in freshly distilled NMP (7 mL), and flushed with argon. A degassed solution of *rac*-**133**¹⁷⁰ (100 mg, 0.29 mmol) in freshly distilled NMP (3 mL) was added and the reaction mixture was stirred at 200 °C for 4 h. The reaction mixture was cooled down to rt and acetyl chloride (1.71 g, 1.55 mL, 21.8 mmol, 75.0 equiv.) was added. The reaction mixture was stirred at rt for 2 h, poured into ice, and extracted with DCM (3 × 25 mL). The organic layers were washed with brine (3 × 30 mL), the solvents were evaporated under reduced pressure, and the residue was purified by flash chromatography (cyclohexane:DCM, 40:60 → 20:80) to afford *rac*-**134** (105 mg, 86%) as a white solid.

M.p.: 205.4 - 206.0 °C (DCM-cyclohexane).

UV/Vis (THF): λ_{max} (log ε) = 244 (5.00), 260 (5.06), 273 (4.83), 315 (4.89), 352 (4.21) nm.

¹H NMR (400 MHz, CDCl₃): 2.49 (s, 6H), 7.28 (dd, *J* = 8.8, 2.0, 2H), 7.89 (s, 2H), 7.91 (s, 4H), 8.06 (d, *J* = 1.9, 2H), 8.50 (d, *J* = 8.8, 2H).

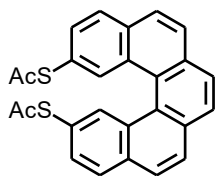
¹³C NMR (101 MHz, CDCl₃): 30.48, 125.87, 126.80, 127.28, 127.54, 127.93, 129.63, 129.72, 130.96, 133.01, 133.11, 134.19, 194.11.

IR (CHCl₃): 3087 vw, 3048 w, 3028 w, 1703 vs, 1616 w, 1594 w, 1553 w, 1504 w, 1481 w, 1469 wm, 1433 m, 1334 vw, 1313 w, 1268 vw, 1260 vw, 1258 vw, 1122 s, 1102 m, 1051 vw, 1035 vw, 1003 vw, 952 m, 945 m, 925 w, 889 m, 851 m, 840 m, 834 m, 826 m, 650 m, 620 w, 589 vw, 570 w, 545 w, 525 vw, 473 vw, 469 vw, 457 vw, 409 vw cm⁻¹.

ESI MS: 449 ($[M+Na]^+$).

HR ESI MS: calculated for $C_{26}H_{18}O_2S_2Na$ 449.064, found 449.0634.

***rac*-2,13-Bis(thioacetyl)pentahelicene 136**



A Schlenk flask was charged with sodium methanethiolate freshly prepared from sodium (331 mg, 14.04 mmol, 50.0 equiv.) and dimethyl disulfide (840 mg, 0.79 mL, 8.9 mmol, 31.0 equiv.) in freshly distilled NMP (13 mL), and flushed with argon. A degassed solution of **135**¹⁶⁸ (100 mg, 0.29 mmol) in NMP (13 mL) was added and the reaction mixture was stirred at 200 °C for 4 h. The reaction mixture was cooled down to rt and acetyl chloride (1.69 g, 1.10 mL, 21.6 mmol, 75.0 equiv.) was added. The reaction mixture was stirred at rt for 2 h, poured into ice, and extracted with DCM (3 × 50 mL). The organic layers were washed with brine (3 × 30 mL), the solvents were evaporated under reduced pressure, and the residue was purified by flash chromatography (hexane:ethyl acetate, 80:20) to afford *rac*-**136** (94 mg, 77%) as a white solid.

M.p.: 193.5 - 194.5 °C (hexane-ethyl acetate).

UV/Vis (THF): λ_{max} ($\log \epsilon$) = 238 (5.31), 260 (5.06), 276 (5.05), 307 (4.89), 315 sh (4.87), 337 sh (4.61) nm.

¹H NMR (400 MHz, $CDCl_3$): 2.36 (s, 6H), 7.54 (dd, $J = 8.3, 1.6$, 2H), 7.87 (s, 2H), 7.89 – 7.95 (m, 4H), 7.99 (d, $J = 8.4$, 2H), 8.59 (d, $J = 1.1$, 2H).

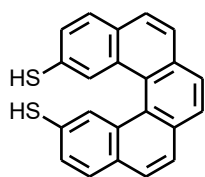
¹³C NMR (101 MHz, $CDCl_3$): 30.29, 124.51, 126.52, 127.48, 127.76, 127.82, 129.04, 130.96, 132.20, 132.74, 132.91, 134.33, 194.50.

IR ($CHCl_3$): 3049 w, 3013 m, 2976 vw, 2298 vw, 1924 vw, 1906 vw, 1797 vw, 1700 s, 1615 vw, 1597, vw, 1563 vw, 1548 vw, 1500 w, 1475 w, 1431 w, 1422 w, 1396 w, 1354 m, 1339 vw, 1298 w, 1261 vw, 1227 m, 1199 vw, 1153 w, 1142 m, 1123 m, 1102 m, 1066 vw, 1003 vw, 947 m, 910 w, 877 vw, 861 w, 851 s, 839 m, 826 w, 811 vw, 719 vw, 685 vw, 664 w, 638 m, 623 s, 607 m, 587 vw, 568 w, 538 m, 502 w, 469 vw 455 vw, 430 vw, 418 vw, 408 vw cm^{-1} .

ESI MS: 427 ($[M+H]^+$), 449 ($[M+Na]^+$).

HR ESI MS: calculated for $C_{26}H_{19}O_2S_2$ 427.0821, found 427.0822.

rac-Pentahelicene-2,13-dithiol **137**



A Schlenk flask was charged with *rac*-**136** (30 mg, 0.07 mmol), flushed with argon, and degassed THF (1.4 mL) was added. Then a solution of sodium hydroxide (112 mg, 2.8 mmol, 40.0 equiv.) in degassed methanol (2.8 mL) was added dropwise at rt. The reaction mixture was stirred for 3 h. Then the reaction mixture was slowly acidified with a solution of citric acid (0.5 M in water, 7.0 mL, 35 mmol, 50 equiv.) and stirred at rt for 10 min. The product was filtered off, washed with water (3 × 10 mL) and was dried under argon to afford *rac*-**137** (15 mg, 62%) as a grey powder.

M.p.: 214.0 – 216.0 °C (water).

¹H NMR (400 MHz, CDCl₃): 3.52 (s, 2H), 7.42 (bd, *J* = 8.1, 2H), 7.80 – 7.85 (m, 8H), 8.47 (bs, 2H).

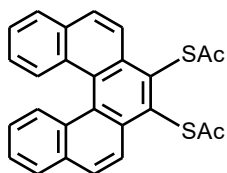
¹³C NMR (101 MHz, CDCl₃): 125.95, 126.28, 127.10, 127.31, 127.76, 128.00, 128.85, 129.00, 130.78, 130.91, 132.94.

IR (CHCl₃): 3049 w, 3010 m, 2928 vw, 2880 vw, 2583 vw, 1898 vw, 1637 w, 1559 m, 1588 w, 1510 vw, 1500 m, 1482 w, 1475 w, 1431 w, 1399 w, 1375 w, 1355 vw, 1336 vw, 1299 w, 1277 vw, 1262 vw, 1199 vw, 1177 vw, 1155 w, 1141 w, 1108 m, 1095 vw, 1086 vw, 1068 vw, 1030 vw, 1013 vw, 987 w, 960 w, 946 w, 917 vw, 860 m, 849 s, 835 w, 822 w, 810 vw, 719 vw, 710 vw, 685 vw, 649 vw, 616 m, 579 vw, 559 vw, 527 s, 501 w, 457 vw, 427 vw, 417 vw cm⁻¹.

APCI MS: 341 ([M-H]⁻).

HR APCI MS: calculated for C₂₂H₁₃S₂ 341.0464, found 341.0459.

rac-7,8-Bis(thioacetyl)pentahelicene **139**



A Schlenk flask was charged with sodium methanethiolate freshly prepared from sodium (270 mg, 11.7 mmol, 50.0 equiv.) and dimethyl disulfide (680 mg, 0.65 mL, 7.3 mmol, 31.0 equiv.) in freshly distilled NMP (6 mL), and flushed with argon. A degassed solution of **138**¹⁷⁰ (100 mg, 0.23 mmol) in freshly distilled NMP (6 mL) was added and the reaction mixture was stirred at 200 °C for 4 h. The reaction mixture was cooled down to rt and acetyl chloride (1.38 g, 1.25 mL, 17.6 mmol, 75.0 equiv.) was added. The reaction mixture was stirred at rt for 2 h, poured into ice, and extracted with DCM (3 × 25 mL). The organic layers were washed with brine (3 × 30 mL), the solvents were

evaporated under reduced pressure, and the residue was purified by flash chromatography (cyclohexane:DCM, 40:60 → 0:100) to afford *rac*-**139** (69 mg, 71%) as a yellow solid.

M.p.: 240.0 - 242.2 °C (DCM-cyclohexane).

UV/Vis (THF): λ_{max} (log ϵ) = 241 (4.98), 260 (5.06), 269 (4.68) sh, 279 (4.77), 304 (4.69), 318 (4.85), 336 sh (4.50), 363 sh (4.05) nm.

¹H NMR (600 MHz, CD₂Cl₂): 2.53 (s, 6H), 7.24 (ddd, J = 8.5, 6.8, 1.5, 2H), 7.54 (ddd, J = 8.1, 6.8, 1.5, 2H), 7.94 (dd, J = 8.1, 1.5, 2H), 7.97 (d, J = 9, 2H), 8.30 (bd, J = 8.5, 2H), 8.45 (bd, J = 9.0, 2H).

¹³C NMR (150.3 MHz, CD₂Cl₂): 30.37, 123.98, 124.94, 127.30, 127.55, 128.47, 129.28, 129.87, 130.50, 132.53, 132.67, 132.82, 193.97.

IR (CHCl₃): 3064 m, 3046 m, 2963 w, 2927 w, 2856 vw, 1704 vs, 1613 vw, 1601 w, 1554 vw, 1514 m, 1504 w, 1468 m, 1433 m, 1354 m, 1341 m, 1325 m, 1306 w, 1269 vw, 1250 w, 1167 m, 1118 s, 1095 s, 1036 m, 1002 w, 950 s, 872 vw, 857 m, 826 m, 814 s, 681 m, 660 m, 653 w, 631 m, 615 s, 603 m, 583 w, 563 vw, 530 m, 514 m, 453 w, 443 w, 411 vw cm⁻¹.

ESI MS: 427 ([M+H]⁺), 449 ([M+Na]⁺).

HR ESI MS: calculated for C₂₆H₁₉O₂S₂ 427.0821, found 427.0820.

rac*-2,17-Bis(thioacetyl)heptahelicene **143** and *rac*-2-(thioacetyl) heptahelicene **145*

Method A: A Schlenk flask was charged with sodium ethanethiolate freshly prepared from sodium (221 mg, 9.60 mmol, 40.0 equiv.) and ethanethiol (730 mg, 0.85 mL, 11.7 mmol, 50.0 equiv.) in freshly distilled NMP (10 mL) and flushed with argon. A degassed suspension of **142**¹⁷¹ (109 mg, 0.240 mmol) in NMP (5 mL) was added and the reaction mixture was stirred at 270 °C for 2 h. The reaction mixture was cooled down to rt and acetyl chloride (1.09 g, 0.99 mL, 14.4 mmol, 60.0 equiv.) was added. The reaction mixture was stirred at rt for 2 h, poured into ice and extracted with DCM (3 × 30 mL). The organic layers were washed with brine (3 × 30 mL), evaporated under reduced pressure, and the residue was purified by flash chromatography (hexane:ethyl acetate, 80:20) to afford **143** (41 mg, 32%) and **145** (47 mg, 43%) as yellow solids.

Method B: A Schlenk flask was charged with sodium methanethiolate freshly prepared from sodium (257 mg, 11.2 mmol, 50.0 equiv.) and dimethyl disulfide (653 mg, 0.620 mL, 6.93 mmol, 31.0 equiv.) in freshly distilled NMP (5 mL) and flushed with argon. A degassed solution of *rac*-**142**¹⁷¹ (100 mg, 0.224 mmol) in freshly distilled NMP

(3 mL) was added and the reaction mixture was stirred at 200 °C for 4 h. The reaction mixture was cooled down to rt and acetyl chloride (1.32 g, 1.20 mL, 16.8 mmol, 75.0 equiv.) was added. The reaction mixture was stirred at rt for 2 h, poured into ice, and extracted with DCM (3 × 20 mL). The organic layers were washed with brine (3 × 20 mL), the solvents were evaporated under reduced pressure, and the residue was purified by flash chromatography (cyclohexane:DCM, 40:60 → 0:100) to afford *rac*-**143** (76 mg, 65%) as a yellow solid.

rac-2,17-Bis(thioacetyl)heptahelicene **143**



M.p.: 216.0 - 218.0 °C (hexane-EtOAc).

UV/Vis (THF): λ_{max} (log ϵ) = 279 (4.82), 311 (4.26), 341 (4.05) nm.

¹H NMR (400 MHz, CDCl₃): 2.19 (s, 6H), 6.96 (dd, J = 8.3, 1.7, 2H), 7.23 – 7.25 (m, 2H), 7.38 (d, J = 8.3, 2H), 7.52 (d, J = 8.5, 2H), 7.83 (d, J = 8.5, 2H), 7.98 (d, J = 8.2, 2H), 8.04 (d, J = 8.6, 2H), 8.05 (s, 2H).

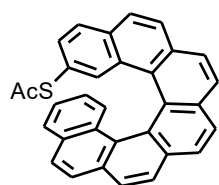
¹³C NMR (101 MHz, CDCl₃): 30.06, 123.71, 124.80, 127.04, 127.29, 127.51, 127.62, 127.67, 127.71, 127.73, 129.43, 130.59, 130.69, 131.49, 132.08, 132.41, 194.56.

IR (CHCl₃): 3055 w, 2961 vw, 2928 vw, 2872 vw, 2856 vw, 1698 s, 1612 vw, 1596 w, 1488 w, 1424 w, 1404 vw, 1393 vw, 1354 m, 1338 vw, 1308 w, 1275 w, 1261 vw, 1246 w, 1130 m, 1119 s, 1097 w, 1002 vw, 971 w, 951 m, 909 w, 892 w, 850 s, 838 s, 830 w, 809 vw, 713 vw, 659 w, 642 w, 623 m, 607 m, 586 w, 550 s, 525 vw, 501 vw cm⁻¹.

ESI MS: 527 ([M+H]⁺), 549 ([M+Na]⁺), 565 ([M+K]⁺).

HR ESI MS: calculated for C₃₄H₂₂O₂NaS₂ 549.0953, found 549.0954.

rac-2-(Thioacetyl)heptahelicene **145**



M.p.: 267.0 - 269.0 °C (hexane-EtOAc).

UV/Vis (THF): λ_{max} (log ϵ) = 275 (4.80), 307 (4.28), 338 (4.04) nm.

¹H NMR (400 MHz, CDCl₃): 2.20 (s, 3H), 6.41 (ddd, J = 8.4, 6.9, 1.4, 1H), 6.92 (ddd, J = 8.0, 6.8, 1.2, 1H), 6.97 (dd, J = 8.3, 1.7, 1H), 7.16 (m, 1H), 7.27 – 7.29 (m, 1H), 7.32 – 7.38 (m, 2H), 7.52 (t, J = 8.1, 2H), 7.78 (d, J = 5.7, 1H), 7.81 (d, J = 5.7, 1H), 7.93 (d, J = 8.2, 1H), 7.98 – 8.06 (m, 5H).

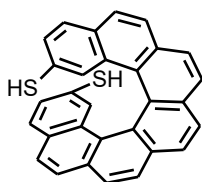
^{13}C NMR (101 MHz, CDCl_3): 30.02, 123.51, 123.77, 124.31, 124.99, 125.05, 125.17, 126.02, 126.83, 126.87, 126.95, 127.11, 127.18, 127.31, 127.45, 127.46, 127.56, 127.71, 127.87, 128.07, 129.20, 129.71, 130.53, 130.55, 131.08, 131.22, 131.81, 132.02, 132.16, 132.27, 194.70.

IR (CHCl_3): 3055 w, 3011 w, 2961 vw, 2929 vw, 2876 vw, 2856 vw, 1700 s, 1608 vw, 1492 w, 1424 w, 1404 vw, 1354 m, 1316 w, 1280 w, 1263 vw, 1247 w, 1191 w, 1128 m, 1117 s, 1035 vw, 1000 vw, 951 m, 909 w, 888 vw, 850 s, 831 s, 712 vw, 664 vw, 653 vw, 640 w, 619 m, 610 m, 587 vw, 567 m, 527 m, 521 w, 504 w, 473 w, 438 vw, 419 vw cm^{-1} .

ESI MS: 453 ($[\text{M}+\text{H}]^+$), 475 ($[\text{M}+\text{Na}]^+$), 491 ($[\text{M}+\text{K}]^+$).

HR ESI MS: calculated for $\text{C}_{32}\text{H}_{20}\text{ONaS}$ 475.1127, found 475.1127.

rac-Heptahelicene-2,17-dithiol **144**



Method A: A Schlenk flask was charged with **143** (20 mg, 0.038 mmol), flushed with argon, and degassed MTBE (10 mL) was added. Then a solution of cesium hydroxide monohydrate (51 mg, 0.30 mmol, 8.0 equiv.) in methanol (300 μL) was added dropwise at rt. The reaction mixture was stirred for 5 min. Then the reaction mixture was slowly acidified with hydrochloric acid (1M in water, 760 μL , 0.76 mmol 20.0 equiv.). The mixture was extracted with MTBE (3×10 mL). The organic layers were left to evaporate under flow of argon to afford **144** (13 mg, 76%) as a yellow powder.

Method B: A Schlenk flask was charged with **143** (15 mg, 0.028 mmol), flushed with argon, and degassed THF (0.6 mL) was added. Then a solution of cesium hydroxide monohydrate (38 mg, 0.23 mmol, 8.0 equiv.) in methanol (230 μL) was added dropwise at rt. The reaction mixture was stirred for 5 min. Then the reaction mixture was slowly acidified with citric acid (0.5 M in water, 570 μL , 10 equiv.). The mixture was diluted with water (20 mL) and the precipitated solid was filtered off on a frit to afford **144** (11 mg, 87%) as a light yellow powder.

M.p.: 274.0 - 276.0 $^{\circ}\text{C}$ (MTBE).

UV/Vis (THF): λ_{max} ($\log \epsilon$) = 273 (4.58), 310 (4.02), 339 (3.89) nm.

^1H NMR (400 MHz, CDCl_3): 2.90 (d, $J = 0.5$, 2H), 6.85 (dd, $J = 8.5$, 1.8, 2H), 7.12 (dd, $J = 1.8$, 0.8, 2H), 7.26 (d, $J = 8.2$, 2H), 7.57 (d, $J = 8.4$, 2H), 7.77 (d, $J = 8.5$, 2H), 7.98 (d, $J = 8.2$, 2H), 8.04 (d, $J = 8.2$, 2H), 8.06 (s, 2H).

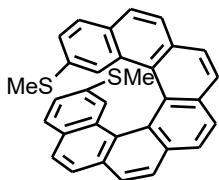
¹³C NMR (101 MHz, CDCl₃): 25.51, 124.88, 125.88, 126.08, 126.78, 127.08, 127.21, 127.29, 127.45, 127.61, 127.63, 129.49, 130.24, 131.61, 132.23.

IR (CHCl₃): 3423 w, 3047 m, 2962 m, 2923 m, 2852m, 2539 w, 1898 vw, 1721 w, 1658 vw, 1593 m, 1506 w, 1490 m, 1462 w, 1421 w, 1403 w, 1393 w, 1360 w, 1336 w, 1307 m, 1261 s, 1191 w, 1098 s, 1021 s, 969 w, 954 w, 899 w, 889 w, 846 s, 833 s, 806 s, 752 w, 711 m, 656 w, 635 vw, 611 w, 584 vw, 530 s, 480 w, 441 vw cm⁻¹.

ESI MS: 441 ([M-H]⁻).

HR ESI MS: calculated for C₃₀H₁₇S₂ 441.0777, found 441.0775.

***rac*-2,17-Bis(methylsulfanyl)-heptahelicene 146**



A Schlenk flask was charged with **143** (80 mg, 0.15 mmol) and NaH (60% suspension in mineral oil, 49 mg, 1.2 mmol, 8.0 equiv.) in freshly distilled NMP (3 mL) was added. The reaction mixture was stirred for 30 min, then methyl iodide (120 μL, 260 mg, 1.8 mmol, 12 equiv.) was added. The reaction mixture was stirred at rt for 2 h, poured into water, and extracted with DCM (3 × 20 mL). The organic layers were washed with brine (3 × 20 mL), the solvents were evaporated under reduced pressure, and the residue was purified by flash chromatography (cyclohexane:DCM, 40:60) to afford *rac*-**146** (51 mg, 71%) as a yellow solid.

M.p.: 262.1 - 264.2 °C (cyclohexane-DCM).

UV/Vis (THF): λ_{max} (log ε) = 228 (4.92), 265 (5.02) sh, 275 (5.08), 338 (4.42) nm.

¹H NMR (400 MHz, CDCl₃): 1.93 (s, 6H), 6.87 (dd, *J* = 8.4, 1.9, 2H), 7.00 (d, *J* = 1.8, 2H), 7.28 (d, *J* = 8.4, 2H), 7.55 (d, *J* = 8.4, 2H), 7.73 (d, *J* = 8.4, 2H), 7.93 (d, *J* = 8.2, 2H), 8.02 (d, *J* = 8.2, 2H), 8.05 (s, 2H).

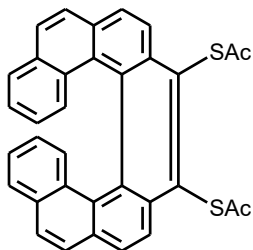
¹³C NMR (101 MHz, CDCl₃): 14.89, 121.30, 124.79, 125.07, 125.19, 126.92, 127.19, 127.31, 127.37, 127.55, 127.59, 129.77, 129.83, 131.63, 132.08, 134.34.

IR (CHCl₃): 3054 w, 3011 w, 2963 vw, 2924 vw, 2856 vw, 2835 wv, 1599 m, 1594 m, 1572 vw, 1515 vw, 1505 vw, 1491 w, 1457 vw, 1439 w, 1424 w, 1403 vw, 1392 vw, 1369 vw, 1359 vw, 1318 w, 1306 vw, 1276 vw, 1263 vw, 1247 w, 1230 vw, 1199 vw, 1191 vw, 1180 vw, 1154 vw, 1141 w, 1125 m, 1095 w, 1075 w, 1036 vw, 963 w, 954 w, 903 vw, 890 vw, 880 w, 848 vs, 837 vs, 827 m, 808 w, 711 vw, 658 w, 634 vw, 629 vw, 613 w, 586 w, 537 s, 481 m, 441 vw cm⁻¹.

APCI MS: 471 ([M+H]⁺).

HR APCI MS: calculated for C₃₂H₂₃S₂ 471.1236, found 471.1227.

***rac*-9,10-Bis(thioacetyl)heptahelicene 148**



A Schlenk flask was charged with sodium methanethiolate freshly prepared from sodium (180 mg, 7.82 mmol, 50.0 equiv.) and dimethyl disulfide (467 mg, 0.440 mL, 4.85 mmol, 31.0 equiv.) in freshly distilled NMP (4 mL), and flushed with argon. A degassed solution of *rac*-**147**¹⁷⁰ (70 mg, 0.16 mmol) in freshly distilled NMP (2.5 mL) was added and the reaction mixture was stirred at 200 °C for 4 h. The reaction mixture was cooled down to rt and acetyl chloride (920 mg, 0.85 mL, 11.7 mmol, 75.0 equiv.) was added. The reaction mixture was stirred at rt for 2 h, poured into ice, and extracted with DCM (3 × 20 mL). The organic layers were washed with brine (3 × 20 mL), the solvents were evaporated under reduced pressure, and the residue was purified by flash chromatography (cyclohexane:DCM, 40:60 → 80:20) to afford *rac*-**148** (49 mg, 59%) as a yellow solid.

M.p.: 216.0 - 217.1 °C (DCM-cyclohexane).

UV/Vis (THF): λ_{max} (log ε) = 233 (5.12), 275 (5.36), 308 (4.96), 335 (4.80) nm.

¹H NMR (600 MHz, CD₂Cl₂): 2.57 (s, 6H), 6.46 (ddd, *J* = 8.6, 6.8, 1.4, 2H), 6.92 (bd, *J* = 1.15, 2H), 6.94 (ddd, *J* = 7.9, 6.8, 1.2, 2H), 7.32 (ddt, *J* = 7.9, 0.7, 0.7 2H), 7.52 (dt, *J* = 8.6, 0.7, 2H), 7.74 (d, *J* = 8.6, 2H), 8.03 (d, *J* = 8.8, 2H), 8.59 (d, *J* = 8.8, 2H).

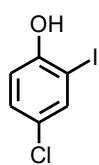
¹³C NMR (150.9 MHz, CD₂Cl₂): 30.84, 124.65, 124.89, 125.42, 125.57, 125.66, 127.10, 127.48, 128.43, 128.93 (2C), 132.05, 129.54, 132.22, 132.66, 132.99, 193.31.

IR (CHCl₃): 2960 vw, 2929 vw, 1707 vs, 1619 vw, 1603 vw, 1590 vw, 1549 vw, 1505 vw, 1495 w, 1455 vw, 1437 vw, 1414 vw, 1388 vw, 1369 vw, 1354 w, 1317 vw, 1290 vw, 1230 w, 1206 vw, 1159 w, 1113 s, 1074 vw, 1037 vw, 995 vw, 951 m, 926 vw, 870 vw, 856 vw, 835 vs, 794 vw, 778 vw, 657 vw, 642 w, 633 m, 629 m, 615 s, 587 vw, 577 vw, 563 vw, 539 w, 523 vw, 510 vw, 489 vw, 473 vw, 439 vw cm⁻¹.

ESI MS: 527 ([M+H]⁺), 549 ([M+Na]⁺).

HR ESI MS: calculated for C₃₄H₂₂O₂NaS₂ 549.0953, found 549.0954.

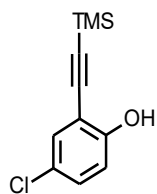
4-Chloro-2-iodophenol **150**



A solution of KI (15.50 g, 93.4 mmol, 3.0 equiv.) and I₂ (7.90 g, 31.1 mmol, 1.0 equiv.) in distilled water (30 mL) was added dropwise into a solution of 4-chlorophenol **149** (4.00 g, 31.1 mmol) in aqueous ammonia (20 mL) precooled to 0 °C. The reaction mixture was stirred at 0 °C for 2 h, then acidified with 1M HCl (15mL) and extracted with ethyl acetate (3 × 50 mL). The combined organic layers were dried over anhydrous Na₂SO₄. The solvent was removed *in vacuo* and the residue was purified by flash chromatography on silica gel (hexane:DCM, 75:25) to afford iodophenol **150** (5.05 g, 64%) as a pale pink solid.

NMR spectra were in agreement with the published ones.¹⁷³

4-Chloro-2-[(trimethylsilyl)ethynyl]phenol **151**



A Schlenk flask was charged with phenol **150** (3.50 g, 13.8 mmol), Pd(PPh₃)₂Cl₂ (193 mg, 0.275 mmol, 2 mol%) and CuI (114 mg, 0.599 mmol, 4 mol%) and purged with argon. The degassed toluene (20 mL) and DIPA (2.30 mL, 16.4 mmol, 1.2 equiv.) were added. Then TMSA (3.00 mL, 21.7 mmol, 1.6 equiv.) in degassed toluene (5 mL) was added dropwise *via* cannula to a reaction mixture and the reaction was stirred at rt for 3 h. The solvent was evaporated *in vacuo* and the residue was flash chromatographed on silica gel (hexane:ethyl acetate, 10:1) to afford phenol **151** (2.90 g, 94%) as an oil.

¹H NMR (400 MHz, CDCl₃): 0.28 (s, 9H), 5.78 (s, 1H), 6.87 (bd, *J* = 8.8, 1H), 7.19 (dd, *J* = 8.8, 2.6, 1H), 7.31 (bd, *J* = 2.6, 1H).

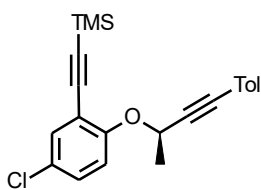
¹³C NMR (101 MHz, CDCl₃): 0.15, 97.50, 103.72, 110.93, 115.86, 124.84, 130.62, 130.88, 155.66.

IR (CHCl₃): 3515 w, 3076 vw, 2963 w, 2901 w, 2156 w, 2146 w, 1568 w, 1480 vs, 1413 w, 1400 vw, 1253 s, 1170 w, 1152 vw, sh, 1111 w, 1085 w, 942 vw, 847 vs, 821 m, 702 w, 645 m, 480 w cm⁻¹.

EI MS: 224 (M⁺, 47), 211 (69), 209 (100), 193 (35), 149 (6), 104 (4), 73 (6).

HR EI MS: calculated for C₁₁H₁₃³⁵ClOSi 224.0424, found 224.0423.

(+)-[(5-Chloro-2-[(1*R*)-1-methyl-3-(4-methylphenyl)prop-2-yn-1-yl]oxy}phenyl)ethynyl](trimethyl)silane **153**



To a solution of phenol **151** (854 mg, 3.80 mmol), PPh₃ (1.10 g, 4.18 mmol, 1.1 equiv.), alcohol (-)-(*S*)-**152**¹⁷⁴ (670 mg, 4.18 mmol, 1.1 equiv.) in distilled benzene (4.5 mL), DIAD (825 μL, 4.18 mmol, 1.1 equiv.) was added dropwise under argon. The reaction mixture was stirred at rt for 3 h, then the solvent was evaporated *in vacuo*. The residue was chromatographed on silica gel (hexane) to afford diyne (+)-(*R*)-**153** (1.28 g, 91%) as a pale yellow oil.

Optical rotation: $[\alpha]_D^{20} +19.5^\circ$ (c 0.410 M, CHCl₃).

¹H NMR (400 MHz, CDCl₃): 0.26 (s, 9H), 1.77 (d, *J* = 6.5, 3H), 2.34 (s, 3H), 5.08 (q, *J* = 6.5, 1H), 7.07 – 7.13 (m, 3H), 7.22 (dd, *J* = 8.8, 2.7, 1H), 7.26 – 7.27 (m, 2H), 7.41 (bd, *J* = 2.7, 1H).

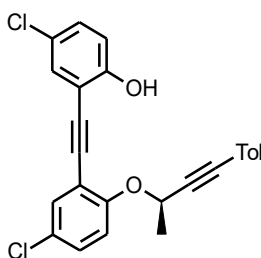
¹³C NMR (101 MHz, CDCl₃): 0.03, 21.62, 22.40, 66.66, 86.69, 87.15, 99.89, 100.35, 115.95, 117.45, 119.30, 126.54, 129.60, 131.71, 133.14, 138.90, 157.63.

IR (CHCl₃): 3083 vw, 3053 vw, 2962 w, 2900 w, 2235 w, 2160 w, 1608 vw, 1591 w, 1567 vw, 1510 m, 1483 s, 1465 m, 1407 vw, 1396 w, 1375 w, 1331 m, 1266 m, sh, 1251 vs, 1237 w, sh, 1120 w, 1113 w, 1095 w, sh, 1084 m, 1035 w, 1020 w, 946 w, 872 m, 846 vs, 819 s, 808 w, 708 vw, 700 vw, 683 vw, 646 w, 483 w cm⁻¹.

ESI MS: 367 ([M+H]⁺).

HR ESI MS: calculated for C₂₂H₂₄O³⁵ClSi 367.1280, found 367.1280.

(-)-4-Chloro-2-[(5-chloro-2-[(1*R*)-1-methyl-3-(4-methylphenyl)prop-2-yn-1-yl]oxy}phenyl)ethynyl]phenol **154**



A Schlenk flask **A** was charged with phenol **150** (330 mg, 1.3 mmol, 1.3 equiv.), Pd(PPh₃)₂Cl₂ (14 mg, 0.02 mmol, 2 mol%), CuI (8 mg, 0.04 mmol, 4 mol%), flushed with argon. Degassed DIPA (132 mg, 185 μL, 1.3 mmol, 1.3 equiv.) was added and dissolved in degassed toluene (5 mL). A Schlenk flask **B** was charged with protected diyne (+)-(*R*)-**153** (367 mg, 1.0 mmol) dissolved in degassed toluene (10 mL) and the degassed solution TBAF·3H₂O (1M in THF, 1.2 mL, 1.2 mmol, 1.2 equiv.) was dropwise added. The resulting solution was stirred for 30 min and then added dropwise into the Schlenk flask **A** at rt within 1.5 h. The reaction mixture was

stirred at the same temperature overnight (16 h). The solvents were evaporated under reduced pressure and the residue was purified by flash chromatography on silica gel (cyclohexane:DCM, 70:30) to afford alcohol (-)-(*R*)-**154** (343 mg, 81%) as a white microcrystalline solid.

M.p.: 155.8 - 156.3 °C (cyclohexane-DCM).

Optical rotation: $[\alpha]_D^{20}$ -195° (c 0.239, THF).

¹H NMR (400 MHz, CDCl₃): 1.85 (d, *J* = 6.6, 3H), 2.33 (s, 3H), 5.15 (q, *J* = 6.6, 1H), 6.55 (s, 1H), 6.93 (d, *J* = 8.8, 1H), 7.08 – 7.12 (m, 2H), 7.17 (d, *J* = 8.8, 1H), 7.21 (d, *J* = 2.6, 1H), 7.25 (dd, *J* = 8.8, 2.4, 1H), 7.27-7.29 (m, 2H), 7.35 (d, *J* = 2.6, 1H), 7.45 (d, *J* = 2.6, 1H).

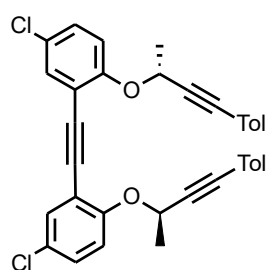
¹³C NMR (101 MHz, CDCl₃): 21.63, 22.41, 65.95, 86.27, 87.28, 88.43, 93.31, 111.03, 113.79, 114.77, 115.98, 118.90, 124.90, 126.28, 129.20, 129.61, 129.98, 130.72, 131.39, 131.79, 139.18, 156.26, 156.61.

IR (CHCl₃): 3457 w, 3083 vw, 3051 vw, 2994 w, 2939 vw, 2871 vw, 2235 w, 2204 vw, 1606 vw, 1592 w, 1567 vw, 1510 m, 1486 s, 1478 vs, 1452 w, 1422 vw, 1400 w, 1378 vw, 1347 w, 1331 m, 1299 vw, 1281 m, 1272 m, 1264 m, 1243 s, 1196 m, 1182 w, 1156 vw, 1131 m, 1121 w, 1107 w, 1090 w, 1084 m, 1035 m, 1020 w, 945 m, 920 m, 881 w, 843 w, 819 m, 807 m, 657 w, 620 vw, 584 vw, 570 w, 543 vw, 519 vw, 478 vw, 462 vw, 439 vw cm⁻¹.

ESI MS: 443 ([M+Na]⁺).

HR ESI MS: calculated for C₂₅H₁₈O₂³⁵Cl₂Na 443.0576, found 443.0576.

(-)-1,1'-Ethyne-1,2-diylbis(5-chloro-2-[(1*R*)-1-methyl-3-(4-methylphenyl)prop-2-yn-1-yl]oxy}benzene) **155**



To a solution of phenol **154** (333 mg, 0.79 mmol), PPh₃ (228 g, 0.87 mmol, 1.1 equiv.), alcohol (-)-(*S*)-**152**¹⁷⁴ (137 mg, 0.87 mmol, 1.1 equiv.) in distilled benzene (10 mL), DIAD (176 mg, 170 μL, 0.87 mmol, 1.1 equiv.) was added dropwise under argon while cooling in an ice bath. The reaction mixture was stirred at rt for 3 h, quenched with MeOH (1 mL) then the solvents were evaporated *in vacuo*. The residue was chromatographed on silica gel (hexane:ethyl acetate, 90:10) to afford diyne (-)-(*R,R*)-**155** (336 mg, 75%) as a white solid.

M.p.: 124.0 - 125.0 °C (hexane-ethyl acetate).

Optical rotation: $[\alpha]_D^{20}$ -327° (c 0.254, THF).

¹H NMR (400 MHz, CDCl₃): 1.82 (d, *J* = 6.5, 6H), 2.33 (s, 6H), 5.15 (q, *J* = 6.5, 2H), 7.06 – 7.11 (m, 4H), 7.14 (d, *J* = 8.8, 2H), 7.25 (dd, *J* = 8.8, 2.6, 2H), 7.27 – 7.29 (m, 4H), 7.47 (d, *J* = 2.6, 2H).

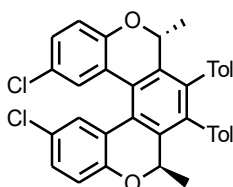
¹³C NMR (101 MHz, CDCl₃): 21.61, 22.57, 66.50, 86.71, 87.12, 89.92, 115.90, 117.06, 119.26, 126.50, 129.16, 129.53, 131.74, 133.01, 138.90, 156.98.

IR (CHCl₃): 3083 vw, 3053 vw, 2994 m, 2939 w, 2924 w, 2892vw, 2869 vw, 2234 w, 2203 vw, 1607 vw, 1594 w, 1568 w, 1510 vs, 1490 vs, 1480 vs, 1461 m, 1410 m, 1375 m, 1338 m, 1331 m, 1280 s, 1259 s, 1237 s, 1181 vw, 1158 vw, 1139 m, 1131 m, 1121 s, 1107 m, 1085 s, 1037 m, 1020 m, 946 m, 931 w, 917 w, 882 m, 841 w, 831 w, 819 vs, 807 m, 709 vw, 682 vw, 657 w, 647 vw, 617 vw, 573 w, 556 w, 541 w, 529 w, 527 w, 506 vw, 497 vw, 470 w, 432 vw, 410 vw cm⁻¹.

ESI MS: 585 ([M+Na]⁺).

HR ESI MS: calculated for C₃₆H₂₈O₂³⁵Cl₂Na 585.1359, found 585.1361.

(-)-(M)-1,1'-Ethyne-1,2-diylbis(5-chloro-2-[(1R)-1-methyl-3-(4-methylphenyl)prop-2-yn-1-yl]oxy}benzene) 156



A microwave vial was charged with a solution of the triyne (-)-(R,R)-**155** (40 mg, 0.071 mmol), dissolved in chlorobenzene (4 mL) and bubbled for 15 min with nitrogen. Then CpCo(CO)₂ (10 μL, mg, 0.071 mmol, 1.0 equiv.) was added in one portion under nitrogen. The reaction mixture was heated to 180 °C for 20 min in a microwave reactor. The resulting reaction mixture was concentrated *in vacuo*. The purification by a flash chromatography on silica gel (cyclohexane:DCM, 70:30) gave (-)-(M,R,R)-**156** (28 mg, 70%) as a yellowish solid.

M.p.: 158.0 - 160.9 °C (cyclohexane-DCM).

Optical rotation: $[\alpha]_D^{20}$ -676° (c 0.337, THF).

UV/Vis (THF): λ_{\max} (log ϵ) = 262 (4.74), 270 (4.81), 307 (4.35), 341 (4.48) nm.

¹H NMR (400 MHz, CDCl₃): 0.95 (d, *J* = 6.7, 6H), 2.26 (s, 6H), 5.25 (q, *J* = 6.6, 2H), 6.65 (dd, *J* = 7.9, 1.6, 2H), 6.87 (d, *J* = 7.9, 2H), 6.96 (d, *J* = 8.6, 2H), 7.06 – 7.13 (m, 4H), 7.17 (dd, *J* = 8.6, 2.5, 2H), 7.41 (d, *J* = 2.5, 2H).

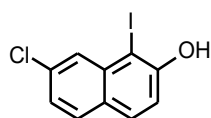
¹³C NMR (101 MHz, CDCl₃): 18.44, 21.33, 73.28, 120.71, 124.35, 124.42, 126.20, 128.64, 128.75, 128.83, 129.03, 129.30, 130.69, 134.56, 136.47, 138.02, 139.29, 152.17.

IR (CHCl₃): 3086 vw, 3050 vw, 2985 m, 2928 w, 2868 vw, 1600 vw, 1579 vw, 1544 vw, 1517 m, 1483 s, 1446 m, 1429 vs, 1356 m, 1336 m, 1328 w, 1316 vw, 1309 vw, 1263 s, 1244 m, 1235 m, 1198 vw, 1183 vw, 1154 m, 1123 w, 1105 m, 1092 m, 1061 s, 1042 vw, 1023 w, 1006 s, 940 vw, 905 w, 899 w, 868 m, 855 m, 839 m, 819 m, 808 w, 704 w, 686 vw, 652 m, 641 m, 631 m, 628 m, 592 vw, 578 vw, 565 w, 534 w, 529 w, 500 w, 469 m, 447 vw, 440 vw, 427 w, 412 vw cm⁻¹.

ESI MS: 585 ([M+Na]⁺).

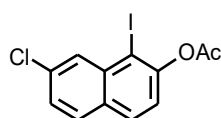
HR ESI MS: calculated for C₃₆H₂₈O₂³⁵ClNa 585.1359, found 585.1361.

7-Chloro-1-iodonaphthalen-2-ol **159**¹⁶⁸



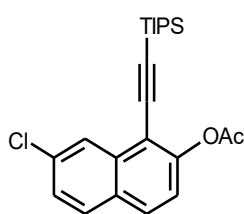
Naphthol **158** (10.1 g, 56.5 mmol), sodium carbonate (12.0 g, 113 mmol, 2.0 equiv.), were dissolved in a mixture of THF (200 mL) and water (50 mL). Then iodine (14.4 g, 56.5 mmol, 1.0 equiv.) was added at once to the solution. The reaction mixture was stirred at rt for 4 h, the reaction was quenched with a saturated solution of NH₄Cl (300 mL) and the saturated Na₂S₂O₃ solution (100 mL). The water phase was extracted with DCM (3 × 250 mL) and the combined organic layers were dried over anhydrous Na₂SO₄. The solvents were removed *in vacuo* and to afford iodonaphthol **159** (17.10 g, 99%) as off-white needles. The spectra were in an agreement with literature.¹⁶⁸

7-Chloro-1-iodonaphthalen-2-yl acetate **160**¹⁶⁸



To a solution of naphthol **159** (17.10 g, 56.2 mmol), triethylamine (20 mL, 140 mmol, 2.5 equiv.) in distilled DCM (225 mL), acetyl chloride (6.0 mL, 84.2 mmol, 1.5 equiv.) was added dropwise at 0 °C under argon. The reaction mixture was stirred at rt for 5 h, the solvent was evaporated *in vacuo* and the residue was purified by flash chromatography on silica gel (hexane:diethyl ether, 2:1) to afford the compound **160** (19.20 g, 99%) as an off-white amorphous solid. The spectra were in an agreement with literature.¹⁶⁸

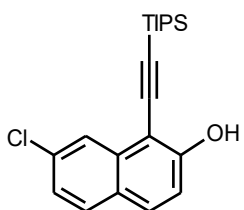
7-Chloro-1-{{tris(1-methylethyl)silyl}ethynyl}naphthalen-2-yl acetate **161**¹⁶⁸



A Schlenk flask was charged with iodide **160** (18.00 g, 52.9 mmol), PdCl₂(PPh₃)₂ (729 mg, 1.04 mmol, 2 mol%), CuI (495 mg, 2.60 mmol, 5 mol%), and purged with argon, and degassed toluene (210 mL) and DIPA (8.74 mL, 62.3 mmol, 1.2 equiv.) were added. Then TIPSA (14.0 mL, 62.3 mmol, 1.2 equiv.) was added dropwise to the reaction mixture and the reaction was stirred at rt for 13 h. The solvent was evaporated *in vacuo* and the residue was flash chromatographed on silica gel (hexane:ethyl acetate, 80:20) to afford **161** (18.90 g, 91%) as an oil, which solidified in the fridge.

The spectra were in an agreement with literature.¹⁶⁸

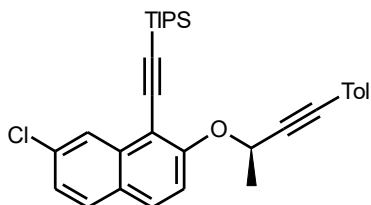
7-Chloro-1-{{tris(1-methylethyl)silyl}ethynyl}naphthalen-2-ol **162**¹⁶⁸



Acetate **161** (16.90 g, 42.2 mmol) was dissolved in THF (170 mL) and MeOH (170 mL), and K₂CO₃ (11.7 g, 84.3 mmol, 2.0 equiv.) was added in one portion. The reaction mixture was stirred at rt for 3 h, then it was quenched with a saturated solution of NH₄Cl (150 mL) and extracted with DCM (3 × 200 mL). The combined organic layers were dried over anhydrous Na₂SO₄. The solvents were evaporated *in vacuo* to afford naphthol **162** (15.00 g, 99%) as an oil, which solidified in the fridge.

The spectra were in an agreement with literature.¹⁶⁸

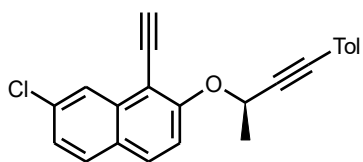
(-)-[(7-Chloro-2-{{(1*R*)-1-methyl-3-(4-methylphenyl)prop-2-yn-1-yl}oxy}naphthalen-1-yl)-ethynyl][tris(1-methylethyl)silane **163**¹⁶⁸



To a solution of naphthol **162** (16.5 g, 46.0 mmol), (-)-(*S*)-**152**¹⁷⁴ (8.10 g, 50.6 mmol, 1.1 equiv.), PPh₃ (13.2 g, 50.6 mmol, 1.1 equiv.) in toluene (140 mL), DIAD (10.0 mL, 50.6 mmol, 1.1 equiv.) was added dropwise under argon while cooling in an ice bath. The reaction mixture was let to heat up to rt and stirred for 3 h. The reaction was quenched with methanol 10 mL, the solvents were evaporated *in vacuo*, and the residue was purified by flash chromatography on silica gel (hexane:ethyl acetate, 35:1) to afford the protected diyne (-)-(*R*)-**163** (18.2 g, 79%) as a white amorphous solid.

The spectra were in an agreement with literature.¹⁶⁸

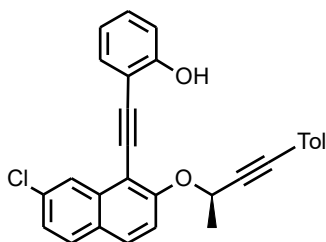
(-)-7-Chloro-1-ethynyl-2-{[(1*R*)-1-methyl-3-(4-methylphenyl)prop-2-yn-1-yl]oxy}naphthalene 164¹⁶⁸



To a solution of the protected diyne (-)-(*R*)-**163** (7.00 g, 14.0 mmol) in a mixture of THF (56 mL) and methanol (6 mL), a solution of TBAF·3H₂O (13.7 g, 43.3 mmol, 3.1 equiv.) in THF (44 mL) was added. The reaction mixture was stirred at rt for 1 h. The solvent was removed *in vacuo* and the residue was passed through a short pad of silica gel (DCM) to give diyne (-)-(*R*)-**164** (4.76 g, 99%) as an amorphous white solid.

The spectra were in an agreement with literature.¹⁶⁸

(-)-2-[(7-Chloro-2-{[(1*R*)-1-methyl-3-(4-methylphenyl)prop-2-yn-1-yl]oxy}naphthalen-1-yl)ethynyl]phenol 165



A Schlenk flask **A** was charged with 2-iodophenol (1.32 g, 6.00 mmol, 3.0 equiv.), Pd(PPh₃)₄ (231 mg, 0.20 mmol, 10 mol%), CuI (76 mg, 0.40 mmol, 20 mol%), flushed with argon, degassed DIPA (223 mg, 310 μL, 2.20 mmol, 1.1 equiv.) was added in degassed toluene (5 mL). A Schlenk flask **B** was charged with the protected diyne (-)-(*R*)-**163** (1.00 g, 2.00 mmol) dissolved in degassed toluene (20 mL) and the degassed solution TBAF·3H₂O (1M in THF, 2.4 mL, 2.4 mmol, 1.2 equiv.) was dropwise added. The resulting solution was stirred for 30 min and then added dropwise into the Schlenk flask **A** at 45 °C within 3 h. The reaction mixture was stirred at 45 °C overnight (16 h). The solvents were evaporated under reduced pressure and the residue was purified by flash chromatography on silica gel (cyclohexane:DCM, 70:30) to afford alcohol (-)-(*R*)-**165** (581 mg, 67%) as white needles.

M.p.: 168.0 - 170.4 °C (cyclohexane-DCM).

Optical rotation: [α]_D²⁰ -217° (c 0.314, THF).

¹H NMR (400 MHz, CD₂Cl₂): 1.91 (d, *J* = 6.5, 3H), 2.31 (s, 3H), 5.41 (q, *J* = 6.5, 1H), 6.73 (s, 1H), 6.97 (ddd, *J* = 7.5, 1.1, 1.1, 1H), 7.03 (dd, *J* = 8.3, 1.1, 1H), 7.07 – 7.12 (m, 2H), 7.25 – 7.29 (m, 2H), 7.32 (ddd, *J* = 8.7, 7.4, 1.7, 1H), 7.38 (dd, *J* = 8.7, 2.1, 1H),

7.55 – 7.57 (m, 1H), 7.59 (d, $J = 9.4$, 1H), 7.79 (d, $J = 8.7$, 1H), 7.85 – 7.92 (m, 1H), 8.27 – 8.33 (m, 1H).

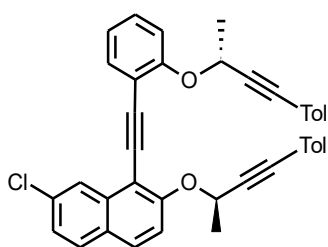
^{13}C NMR (101 MHz, CD_2Cl_2): 21.71, 22.84, 66.72, 87.25, 87.35, 91.68, 94.39, 106.74, 110.45, 115.04, 115.58, 119.36, 120.76, 124.59, 124.62, 126.11, 127.59, 129.61, 130.40, 130.46, 130.84, 131.12, 132.09, 134.23, 134.63, 139.77, 157.82, 158.22.

IR (CHCl_3): 3458 w, 3086 vw, 3058 w, 3015 m, 2990 w, 2939 vw, 2924 w, 2894 vw, 2869 vw, 2282 w, 2250 vw, 2203 vw, 1617 m, 1586 w, 1574 m, 1510 m, 1502 s, 1486 m, 1464 m, 1447 m, 1433 w, 1427 w, 1405 vw, 1379 w, 1368 m, 1349 m, 1330 m, 1311 m, 1294 m, 1288 m, 1251 s, 1247 s, 1227 s, 1195 m, 1178 w, 1164 w, 1153 m, 1120 m, 1105 m, 1083 s, 1061 m, 1038 m, 1028 m, 1020 w, 1002 vw, 956 vw, 938 vw, 917 m, 885 m, 877 m, 864 m, 830 s, 819 m, 719 m, 693 vw, 664 m, 646 vw, 638 vw, 629 vw, 584 vw, 565 w, 559 w, 550 m, 542 w, 523 w, 511 w, 501 w, 482 w, 473 w, 435 m, 411 w cm^{-1} .

APCI MS: 459 ($[\text{M}+\text{Na}]^+$).

HR APCI MS: calculated for $\text{C}_{29}\text{H}_{21}\text{O}_2^{35}\text{ClNa}$ 459.1122 found 459.1115.

(-)-7-Chloro-2-{\[(1R)-1-methyl-3-(4-methylphenyl)prop-2-yn-1-yl]oxy}-1-{\[2-{\[(1R)-1-methyl-3-(4-methylphenyl)prop-2-yn-1-yl]oxy}phenyl]ethynyl]naphthalene 166



To a solution of alcohol **165** (500 mg, 1.14 mmol), (-)-(*S*)-**152**¹⁷⁴ (202 mg, 1.26 mmol, 1.1 equiv.), PPh_3 (360 mg, 1.37 mmol, 1.2 equiv.) in benzene (15 mL), DIAD (250 μL , 1.26 mmol, 1.1 equiv.) was added dropwise under argon while cooling in an ice bath. The reaction mixture was let to heat up to rt and stirred for 3 h. The reaction mixture was quenched with methanol (3 mL) and the solvents were evaporated *in vacuo*, and the residue was purified by flash chromatography on silica gel (cyclohexane:DCM, 70:30) to afford the triyne (-)-(*R,R*)-**166** (534 mg, 81%) as a white solid.

M.p.: 104.7-106.3 $^\circ\text{C}$ (cyclohexane-DCM).

Optical rotation: $[\alpha]_{\text{D}}^{20} = -427^\circ$ (c 0.235, THF).

^1H NMR (400 MHz, CD_2Cl_2): 1.88 (d, $J = 6.5$, 3H), 1.95 (d, $J = 6.5$, 3H), 2.31 (d, $J = 1.9$, 6H), 5.28 (q, $J = 6.5$, 1H), 5.42 (q, $J = 6.5$, 1H), 7.04 (ddd, $J = 7.6, 1.2, 1.2$ 1H),

7.10 (d, $J = 7.9$, 4H), 7.25 - 7.32 (m, 5H), 7.35 - 7.42 (m, 2H), 7.53 (d, $J = 9.0$, 1H), 7.63 (dd, $J = 7.6, 1.7$, 1H), 7.78 (d, $J = 8.7$, 1H), 7.80 - 7.85 (m, 1H), 8.50 - 8.54 (m, 1H).

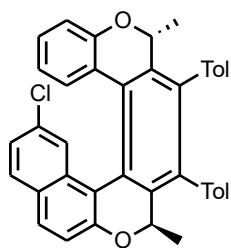
^{13}C NMR (101 MHz, CD_2Cl_2): 21.72, 22.95, 23.13, 66.00, 67.39, 86.63, 86.85, 87.95, 87.97, 88.01, 96.70, 109.10, 114.39, 118.00, 119.66, 119.77, 121.80, 125.09, 126.07, 128.07, 129.56, 129.59, 129.91, 130.19, 130.27, 132.05, 132.08, 133.96, 135.84, 139.45, 139.53, 158.34, 158.66.

IR (CHCl_3): 3077 w, 3056 m, 3032 m, 3011 s, 2993 s, 2938 m, 2924 m, 2906 w, 2889 m, 2232 m, 1866 m, 1780 vw, 1765 vw, 1652 vw, 1615 s, 1596 m, 1587 m, 1574 m, 1510 vs, 1499 vs, 1491 vs, 1451 s, 1444 vs, 1420 m, 1408 w, 1369 s, 1329 vs, 1308 s, 1294 m, 1274 s, 1253 vs, 1227 vs, 1196 m, 1180 m, 1163 s, 1145 m, 1121 vs, 1111 vs, 1102 s, 1085 vs, 1062 m, 1036 vs, 1020 s, 1001 w, 997 w, 946 s, 917 s, 888 m, 877 s, 865 s, 839 s, 829 s, 819 vs, 719 w, 709 vw, 666 m, 648 vw, 637 vw, 628 w, 613 w, 586 vw, 574 vw, 554 m, 544 m, 535 m, 524 m, 508 w, 480 w, 436 m, 408 w cm^{-1} .

ESI MS: 601 ($[\text{M}+\text{Na}]^+$).

HR ESI MS: calculated for $\text{C}_{40}\text{H}_{31}\text{O}_2^{35}\text{ClNa}$ 601.1905, found 601.1896.

(-)-(2*R*,5*R*)-11-Chloro-2,5-dimethyl-3,4-bis(4-methylphenyl)-2,5-dihydrobenzo[*f*]benzo[1,2-*c*:4,3-*c'*]dichromene 167



Microwave vial was charged with a solution of the triyne (-)-(*R,R*)-**166** (100 mg, 0.17 mmol) in chlorobenzene (5 mL) $\text{CpCo}(\text{CO})_2$ (23 μL , 31 mg, 0.17 mmol, 1.0 equiv.) was added in one portion under argon. The reaction mixture was heated to 180 $^\circ\text{C}$ for 20 min in the microwave reactor. The resulting reaction mixture was concentrated *in vacuo*. The purification by a flash chromatography on silica gel (cyclohexane:DCM, 70:30) gave (-)-(*M,R,R*)-**167** (59 mg, 59%) as a yellowish solid.

M.p.: 213.0 - 215.2 $^\circ\text{C}$ (DCM-cyclohexane).

Optical rotation: $[\alpha]_D^{20} = -555^\circ$ (c 0.277, THF).

^1H NMR (400 MHz, CD_2Cl_2): 0.97 (d, $J = 6.7$, 3H), 1.00 (d, $J = 6.6$, 3H), 2.29 (s, 6H), 5.27 (q, $J = 6.5$, 1H), 5.29 (q, $J = 6.5$, 1H), 6.15 - 6.21 (m, 1H), 6.41 (d, $J = 7.8$, 1H), 6.83 (ddd, $J = 11.3, 7.8, 1.9$, 2H), 6.93 - 6.98 (m, 4H), 7.08 (dd, $J = 8.7, 2.1$, 1H), 7.13 - 7.22 (m, 4H), 7.28 (d, $J = 8.7$, 1H), 7.43 (d, $J = 2.1$, 1H), 7.64 (d, $J = 8.7$, 1H), 7.74 (d, $J = 8.7$, 1H).

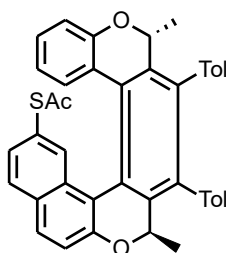
¹³C NMR (101 MHz, CD₂Cl₂): 18.12, 18.98, 21.46, 73.44, 74.22, 118.26, 119.15, 120.57, 121.08, 123.81, 124.49, 124.52, 125.61, 126.55, 127.72, 128.82, 128.95, 129.01, 129.08, 129.11, 129.28, 129.69, 129.79, 129.84, 130.33, 130.70, 131.25, 131.49, 132.18, 135.55, 135.58, 136.90, 136.96, 137.54, 137.62, 139.51, 140.45, 153.62, 154.30.

IR (CHCl₃): 3086 vw, 3049 w, 3024 s, 3007 m, 2985 m, 2868 w, 1908 vw, 1614 s, 1585 m, 1568 vw, 1517 s, 1502 s, 1485 m, 1460 m, 1434 s, 1422 m, 1369 s, 1357 m, 1336 w, 1318 w, 1306 w, 1287 vw, 1272 w, 1246 m, 1194 w, 1183 w, 1151m, 1143 m, 1140 m, 1119 w, 1115 m, 1101 m, 1086 s, 1073 s, 1059 m, 1052 m, 1043 m, 1022 m, 1013 m, 997 m, 973 w, 954 vw, 943 vw, 934 vw, 906 vw, 886 w, 864 m, 836 vs, 819 m, 811 m, 719 s, 691 w, 664 s, 650 vw, 642 vw, 638 vw, 626 w, 607 w, 573 vw, 562 vw, 551 w, 532 w, 522 w, 504 m, 495 m, 470 w, 464 w, 439 w cm⁻¹.

ESI MS: 601 ([M+Na]⁺).

HR ESI MS: calculated for C₄₀H₃₁O₂³⁵ClNa 601.1905, found 601.1897.

(-)-S-[(2R,5R)-2,5-Dimethyl-3,4-bis(4-methylphenyl)-2,5-dihydrobenzo[f]benzo[1,2-c:4,3-c']dichromen-11-yl] ethanethioate 168



A Schlenk flask was charged with sodium methanethiolate freshly prepared from sodium (108 mg, 4.67 mmol, 20.0 equiv.) and dimethyl disulfide (272 mg, 0.260 mL, 2.89 mmol, 12.5 equiv.) in freshly distilled NMP (2.3 mL), and flushed with argon. A degassed solution of (-)-(M,R,R)-**167** (135 mg, 0.23 mmol) in freshly distilled NMP (3.5 mL) was added and the reaction mixture was stirred at 200 °C for 4 h. The reaction mixture was cooled down to rt and acetyl chloride (550 mg, 0.50 mL, 7.0 mmol, 30.0 equiv.) was added. The reaction mixture was stirred at rt for 2 h, poured into ice, and extracted with DCM (3 × 25 mL). The organic layers were washed with brine (3 × 30 mL), the solvents were evaporated under reduced pressure, and the residue was purified by flash chromatography (cyclohexane:DCM, 40:60 → 0:100) to afford (-)-(M,R,R)-**168** (122 mg, 85%) as a white solid.

M.p.: 280.0 - 282.0 °C (DCM- cyclohexane).

Optical rotation: $[\alpha]_D^{20} = -725^\circ$ (c 0.548, THF).

UV/Vis (THF): λ_{\max} (log ϵ) = 262 (4.89), 270 (4.81), 313 (4.36), 363 (4.43) nm.

¹H NMR (400 MHz, CD₂Cl₂): 0.99 (d, *J* = 6.7, 3H), 1.00 (d, *J* = 6.7, 3H), 2.29 (s, 6H), 2.31 (s, 3H), 5.26 (q, *J* = 6.5, 1H), 5.30 (q, *J* = 6.7, 1H), 6.14 (ddd, *J* = 7.5, 1.6, 1.6,

1H), 6.38 (dd, $J = 7.8, 1.6$, 1H), 6.84 (ddd, $J = 8.0, 6.7, 1.6$, 2H), 6.90 (ddd, $J = 8.0, 7.6, 1.6$, 1H), 6.93 – 7.00 (m, 3H), 7.10 – 7.24 (m, 5H), 7.35 (d, $J = 8.8$, 1H), 7.53 (d, $J = 1.6$, 1H), 7.74 (d, $J = 8.5$, 1H), 7.79 (d, $J = 8.8$, 1H).

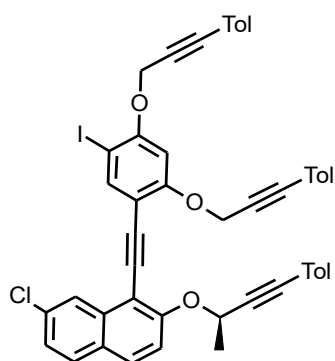
^{13}C NMR (101 MHz, CD_2Cl_2): 17.62, 18.41, 20.91, 29.92, 72.90, 73.64, 118.23, 118.44, 120.56, 121.06, 123.25, 123.91, 125.46, 126.11, 127.42, 128.40, 128.45, 128.53, 128.54, 128.65, 128.75, 129.11, 129.21, 129.33, 129.83, 129.91, 130.70, 130.92, 132.03, 134.98, 136.34, 136.39, 137.00, 137.09, 138.92, 139.97, 152.98, 153.44, 194.30.

IR (CHCl_3): 3130 vw, 3081 vw, 3047 vw, 3028 m, 2985 m, 2928 s, 2867 w, 2853 m, 1697 vs, 1612 m, 1605 m, sh, 1585 m, 1517 m, 1500 m, 1485 m, 1461 m, 1443 m, 1434 m, 1420 m, 1405 w, 1393 w, 1369 vs, 1355 s, 1336 w, 1318 vw, 1310 w, 1306 w, 1288 vw, 1272 m, 1246 m, 1231 s, 1194 w, 1183 w, 1151 m, 1147 m, 1141 m, 1127 m, 1118 m, 1111s, 1102 m, 1090 m, 1073 s, 1060 m, 1051 m, 1033 m, 1022 m, 1013 m, 997 m, 976 w, 952 m, 935 w, 903 w, 887 vw, 864 m, 838 vs, 818 w, 812 w, 691 vw, 686 vw, 656 vw, 641 w, 631 m, 617 m, 606 m, 580 w, 562 vw, 532 w, 523 w, 522 vw, 494 w, 470 w, 464 w, 440 w, 433 w, 426 vw cm^{-1} .

ESI MS: 641 ($[\text{M}+\text{Na}]^+$).

HR ESI MS: calculated for $\text{C}_{42}\text{H}_{34}\text{O}_3\text{NaS}$ 641.2121 found 641.2115.

(-)-7-Chloro-1-[(5-iodo-2,4-bis{[3-(4-methylphenyl)prop-2-yn-1-yl]oxy}phenyl)ethynyl]-2-{[(1R)-1-methyl-3-(4-methylphenyl)prop-2-yn-1-yl]oxy}naphthalene 169



A Schlenk flask was charged with diiodide **102** (1151 mg, 1.86 mmol, 3.0 equiv.), $\text{Pd}(\text{PPh}_3)_4$ (108 mg, 0.093 mmol, 15 mol%), CuI (36 mg, 0.19 mmol, 30 mol%), flushed with argon before degassed DIPA (10 mL) was added. Diyne (-)-(*R*)-**164** (214 mg, 0.62 mmol) was dissolved in degassed toluene (16 mL) under argon and added dropwise to a reaction mixture at rt within 3 h. The reaction mixture was stirred at the same temperature overnight (16 h). The solvents were evaporated under reduced pressure and the residue was purified by flash chromatography on silica gel (hexane:ethyl acetate:toluene, 80:15:5) to afford iodide (-)-(*R*)-**169** (434 mg, 84%) as a yellowish amorphous solid.

Optical rotation: $[\alpha]_D^{20} -133^\circ$ (c 0.123, THF).

¹H NMR (400 MHz, CDCl₃): 1.89 (d, *J* = 6.5, 3H), 2.32 (s, 6H), 2.33 (s, 3H), 5.04 (s, 2H), 5.20 (s, 2H), 5.38 (q, *J* = 6.5, 1H), 7.03 – 7.05 (m, 2H), 7.06 – 7.08 (m, 4H), 7.15 (s, 1H), 7.24 – 7.31 (m, 4H), 7.32 (d, *J* = 8.1, 2H), 7.35 (dd, *J* = 8.7, 2.1, 1H), 7.49 (d, *J* = 8.9, 1H), 7.72 (d, *J* = 8.7, 1H), 7.75 (d, *J* = 8.9, 1H), 7.99 (s, 1H), 8.55 (d, *J* = 2.1, 1H).

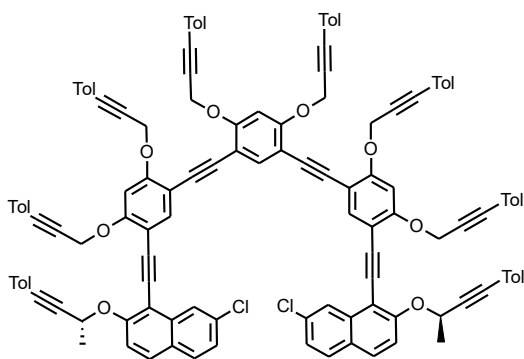
¹³C NMR (101 MHz, CDCl₃): 21.60, 21.62, 21.65, 22.73, 58.15, 58.54, 67.30, 76.00, 82.39, 82.80, 86.83, 87.69, 88.02, 88.58, 88.65, 94.60, 100.33, 109.01, 109.39, 117.94, 118.96, 119.08, 119.37, 125.14, 125.63, 127.64, 129.12 (2C), 129.16 (2C), 129.21 (2C), 129.32, 129.63, 131.74 (2C), 131.85 (2C), 131.88 (2C), 133.43, 135.45, 138.77, 139.04, 139.18, 142.33, 157.70, 157.83, 160.16.

IR (CHCl₃): 3125 vw, 3083 w, 3054 w, 3033 m, 3010 m, 2987 m, 2959 w, 2923 m, 2872 w, 2799 vw, 2735 vw, 2244 w, 2229 m, 1907 w, 1795 vw, 1653 vw, 1615 m, 1591 m, 1568 w, 1554 m, 1510 s, 1495 s, 1453 m, 1423 w, 1400 m, 1373 m, 1360 m, 1349 m, 1337 m, 1322 m, 1310 s, 1292 s, 1264 s, 1253 s, 1227 s, 1195 w, 1178 m, 1155 m, 1141 m, 1119 w, 1106 w, 1086 s, 1040 m, 1022 s, 1016 s, 973 w, 962 w, 918 m, 890 w, 878 w, 865 m, 829 m, 818 s, 709 vw, 688 vw, 664 w, 646 vw, 637 vw, 593 vw, 555 m, 545 w, 527 m, 509 w, 482 vw, 441 w, 414 w cm⁻¹.

APCI MS: 835 ([M+H]⁺).

HR APCI MS: calculated for C₄₉H₃₇IO₃³⁵Cl 835.1480 found 835.1475.

(-)-1,1'-{(4,6-Bis{[3-(4-methylphenyl)prop-2-yn-1-yl]oxy}benzene-1,3-diyl)bis[ethyne-2,1-diyl(4,6-bis{[3-(4-methylphenyl)prop-2-yn-1-yl]oxy}benzene-3,1-diyl)ethyne-2,1-diyl]}bis(7-chloro-2-{(1*R*)-1-methyl-3-(4-methylphenyl)prop-2-yn-1-yl]oxy}naphthalene) **170**



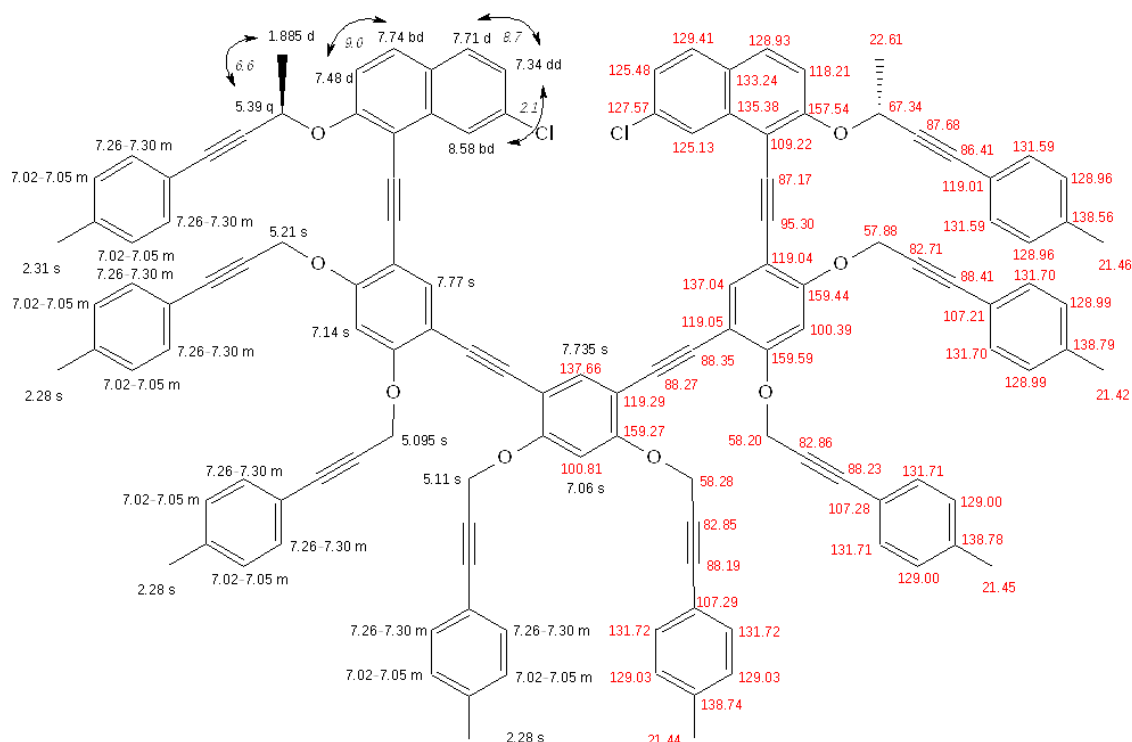
A Schlenk flask was charged with iodide (-)-(*R*)-**169** (177 mg, 0.21 mmol), Pd(PPh₃)₄ (22 mg, 0.02 mmol, 9 mol%), CuI (7 mg, 0.04 mmol, 19 mol%), flushed with argon, and a degassed mixture of DIPA (3 mL) and toluene (1.5 mL) was added. Then a solution of tetrayne **104** (40 mg, 0.097 mmol, 0.45 equiv.) in toluene (2.5 mL) was slowly added at rt within 1.5 h. The reaction mixture was stirred at the same temperature overnight (16h). The solvents were evaporated under

reduced pressure and the residue was purified by flash chromatography on silica gel (hexane:ethyl acetate:toluene 80:15:5) to afford dodecayne (-)-(R,R)-**170** (122 mg, 69%) as a yellowish amorphous solid.

Optical rotation: $[\alpha]^{20}_D -127^\circ$ (c 0.348, THF).

^1H NMR (500 MHz, CDCl_3): 1.85 (d, $J = 6.6$, 6H), 2.28 (s, 6H), 2.283 (s, 6H), 2.283 (s, 6H), 2.31 (s, 6H), 5.095 (s, 4H), 5.11 (s, 4H), 5.21 (s, 4H), 5.39 (q, $J = 6.6$, 2H), 7.02 – 7.05 (m, 16H), 7.06 (s, 1H), 7.14 (s, 2H), 7.26 – 7.30 (m, 16H), 7.34 (dd, $J = 8.7$, 2.1, 2H), 7.735 (s, 1H), 7.48 (d, $J = 9.0$, 2H), 7.71 (d, $J = 8.7$, 2H), 7.74 (bd, $J = 9.0$, 2H), 7.77 (s, 2H), 8.58 (bd, $J = 2.1$, 2H).

^{13}C NMR (126 MHz, CDCl_3): 21.42, 21.44, 21.45, 21.46, 22.61, 57.88, 58.20, 58.28, 67.34, 82.71, 82.85, 82.86, 86.41, 87.17, 87.68, 88.19, 88.23, 88.27, 88.35, 88.41, 95.30, 100.39, 100.81, 107.21, 107.28, 107.29, 109.32, 118.21, 119.01, 119.04, 119.05, 125.13, 125.48, 127.57, 128.93, 128.96 (2C), 128.99 (2C), 129.00 (2C), 129.03 (2C), 129.41, 131.59 (2C), 131.70 (2C), 131.71 (2C), 131.72 (2C), 133.24, 135.38, 137.04, 137.66, 138.56, 138.74, 138.78, 138.79, 157.57, 159.27, 159.44, 159.59.

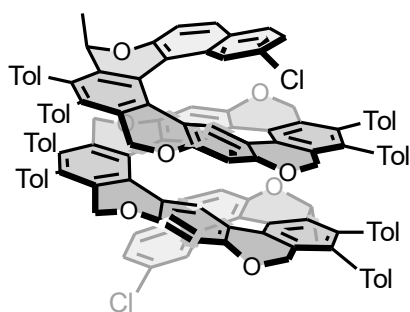


IR (CHCl₃): 3125 vw, 3083 vw, 3055 w, 3032 w, 3023 m, 2993 w, 2953 w, 2934 w, 2875 vw, 2859 vw, 2236 w, 2211 w, 1907 vw, 1653 vw, 1608 m, 1585 w, 1563 w, 1510 s, 1501 s, 1453 m, 1438 w, 1407 w, 1372 w 1364 w, 1320 m, 1287 w, 1264 m 1254 m, 1195 vw, 1181 w, 1171 w, 1149 w 1135 w, 1120 w, 1108 w, 1084 m, 1022 m, 1016 m, 962 w, 917 w, 900 vw, 879 vw, 864 vw, 838 w, 818 s, 719 w, 708 vw, 694 w, 664 w, 648 vw, 636 vw, 617 vw, 556 w, 543 w, 527 m, 520 w, 510 w, 436 vw, 416 vw, 403 vw cm⁻¹.

ESI MS: 1850 ([M+Na]⁺).

HR ESI MS: calculated for C₁₂₈H₉₂O₈³⁵Cl₂Na 1849.6062, found 1849.6065.

(-)-(M,R,R)-2,38-Dichlorooxa[19]helicene **171**



Dichlorooxa[19]helicene **171** was prepared according to the **General procedure for reaction in a flow reactor** from dodecayne (-)-(R,R)-**170** (300 mg, 0.16 mmol) and CpCo(CO)₂ (59 mg, 0.32 mmol, 2.0 equiv.) in distilled THF (14 mL, 5 mg/mL) at a flow rate of 1.0 mL/min (residence time of 8 min).

The resulting reaction mixture was concentrated *in vacuo*. The purification by a flash chromatography on silica gel (hexane:ethyl acetate: toluene, 75:20:5) gave (-)-(M,R,R)-**171** (85 mg, 28%) as a pale yellow solid.

M.p.: >350 °C (acetone).

Optical rotation: [α]_D²⁰ -962° (c 0.170, THF).

¹H NMR (500 MHz, CD₂Cl₂): 1.01 (d, *J* = 6.7, 6H), 2.305 (s, 6H), 2.32 (s, 6H), 2.33 (s, 6H), 2.38 (s, 6H), 3.96 (d, *J* = 13.0, 2H), 4.45 (d, *J* = 14.2, 2H), 4.50 (d, *J* = 14.2, 2H), 4.58 (d, *J* = 13.7, 2H), 4.69 (d, *J* = 13.0, 2H), 4.70 (d, *J* = 13.7, 2H), 5.01 (q, *J* = 6.7, 2H), 5.82 (s, 2H), 6.35 (s, 1H), 6.42 (s, 2H), 6.70 (m, 2H), 6.74 (m, 2H), 6.78 (m, 2H), 6.78 (dd, *J* = 8.5, 2.1, 2H), 6.80 (m, 2H), 6.82 (s, 1H), 6.92 (m, 2H), 6.94 (m, 2H), 6.97 (m, 2H), 6.98 (m, 2H), 7.00 (m, 2H), 7.01 (m, 2H), 7.03 (m, 4H), 7.04 (bd, *J* = 2.1, 2H), 7.05 (s, 2H), 7.065 (m, 2H), 7.07 (d, *J* = 8.7, 2H), 7.12 (m, 2H), 7.14 (m, 2H), 7.17 (d, *J* = 8.5, 2H), 7.53 (d, *J* = 8.7, 2H).

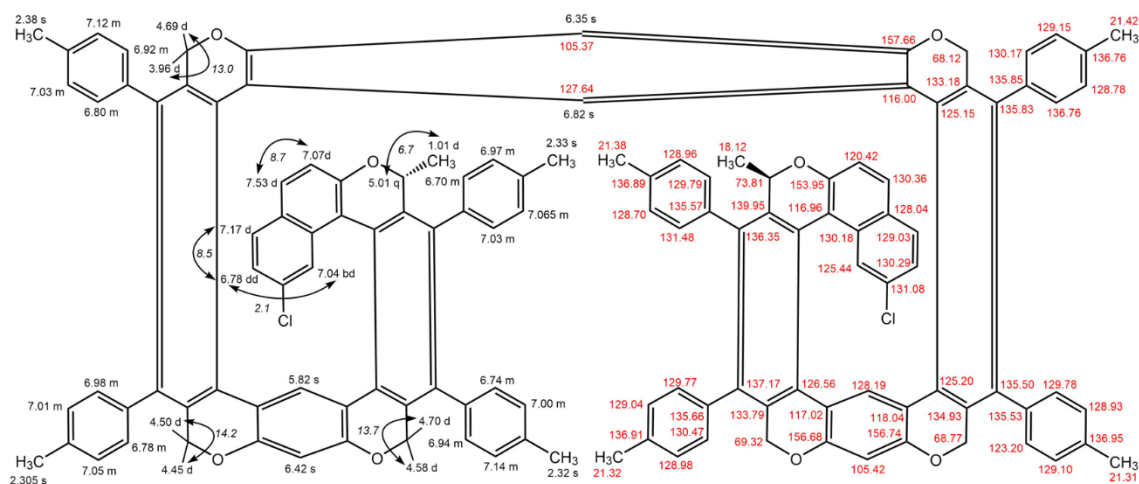
¹³C NMR (151 MHz, CD₂Cl₂): 18.12, 21.31, 21.32, 21.38, 21.42, 68.12, 68.77, 69.32, 73.81, 105.37, 105.42, 116.00, 116.96, 117.02, 118.04, 120.42, 123.20, 125.15, 125.20, 125.44, 126.56, 127.64, 128.04, 128.19, 128.70, 128.78, 128.93, 128.96, 128.98,

129.03, 129.04, 129.10, 129.15, 129.77, 129.78, 129.79, 130.17 (2C), 130.29, 130.36, 130.47, 131.08, 131.48, 133.18, 133.79, 134.93, 135.50, 135.53, 135.57, 135.66, 135.82, 135.85, 136.35, 136.76 (2C), 136.89, 136.91, 136.95, 153.95, 156.68, 156.74, 157.66.

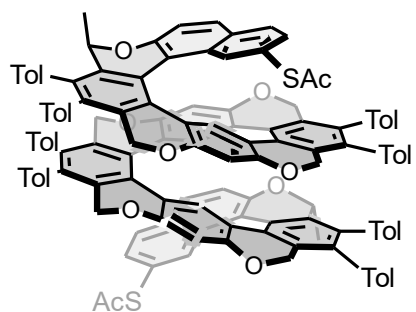
IR (CHCl₃): 3088 vw, 3049 w, 3024 m, 2982 w, 2951 vw, 2924 w, 2874 vw, 2852 w, 1661 w, 1615 s, 1588 w, 1573 w, 1538 vw, 1518 m, 1501 m, 1492 m, 1447 m, 1422 m, 1401 w, 1379 m, 1365 m, 1357 w, 1322 w, 1302 w, 1265 w, 1244 w, 1227 m, 1184 w, 1155 s, 1135 w, 1110 w, 1084 m, 1067 w, 1059 w, 1046 w, 1022 m, 1016 w, 984 w, 973 w, 939 w, 928 w, 896 vw, 885 vw, 878 vw, 870 vw, 852 vw, 832 m, 819 m, 719 m, 695 vw, 664 m, 638 vw, 619 w, 603 w, 587 w, 538 vw, 562 vw, 542 w, 529 w, 509 w, 486 w, 451 vw, 433 vw, 418 vw, 414 vw, 404 vw cm⁻¹.

MALDI MS: 1827 (M⁺).

HR MALDI MS: calculated for C₁₂₈H₉₂O₈³⁵Cl₂ 1826.6164, found 1826.6202.



(-)-(M,R,R)-2,38-Bis(thioacetyl)-oxa[19]helicene **88**



A Schlenk flask was charged with sodium methanethiolate freshly prepared from sodium (115 mg, 5.0 mmol, 50.0 equiv.) and dimethyl disulfide (293 mg, 280 μ L, 3.1 mmol, 31.0 equiv.) in freshly distilled NMP (3 mL), and flushed with argon. A degassed solution of (-)-(M,R,R)-**171** (120 mg, 0.1 mmol) in NMP (3 mL) was added and the reaction mixture was stirred at 200 $^{\circ}$ C for 4 h. The reaction mixture was cooled down to rt and acetyl chloride (590 mg, 0.54 mL, 7.5 mmol, 75.0 equiv.) was added. The reaction mixture was stirred at rt for 2 h, poured into ice, and extracted with DCM (3 \times 50 mL). The organic layers were washed with brine

(3 × 30 mL), the solvents were evaporated under reduced pressure, and the residue was purified by flash chromatography (hexane:ethyl acetate:toluene, 75:20:5) to afford (-)-(M,R,R)-**88** (52 mg, 42%) as a yellowish solid.

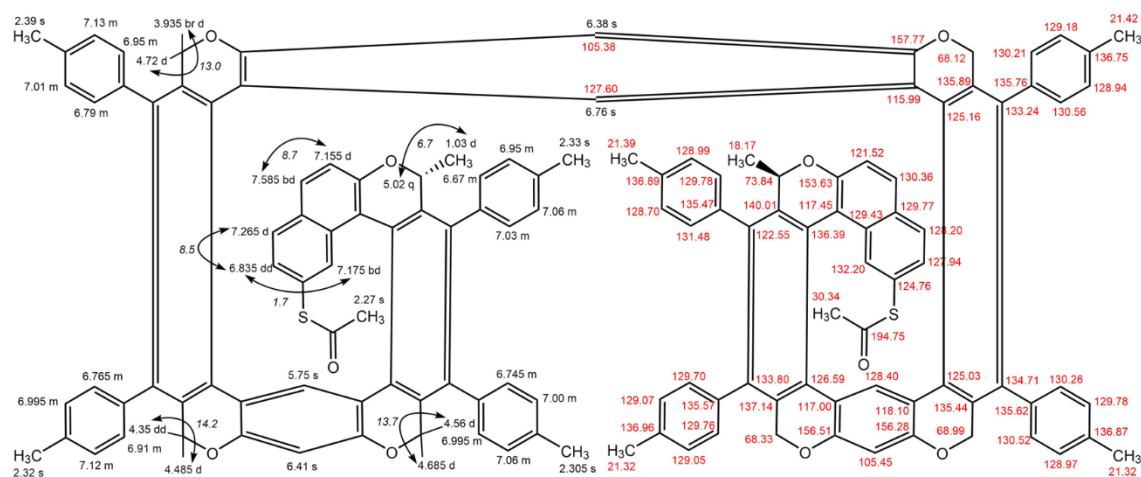
M.p.: > 350 °C (acetone).

Optical rotation: $[\alpha]_D^{20}$ -1283° (c 0.037, THF).

UV/Vis (THF): λ_{\max} (log ϵ) = 265 (5.42) nm.

¹H NMR (500 MHz, CD₂Cl₂): 1.03 (d, *J* = 6.7, 6H), 2.27 (s, 6H), 2.305 (s, 6H), 2.32 (s, 6H), 2.33 (s, 6H), 2.39 (s, 6H), 3.935 (d, *J* = 13.0, 2H), 4.35 (d, *J* = 14.2, 2H), 4.485 (d, *J* = 14.2, 2H), 4.56 (d, *J* = 13.7, 2H), 4.685 (d, *J* = 13.7, 2H), 4.72 (d, *J* = 13.0, 2H), 5.02 (q, *J* = 6.7, 2H), 5.75 (s, 2H), 6.38 (s, 1H), 6.41 (s, 2H), 6.67 (m, 2H), 6.745 (m, 2H), 6.76 (s, 1H), 6.765 (m, 2H), 6.79 (m, 2H), 6.835 (dd, *J* = 8.5, 1.7, 2H), 6.91 (m, 2H), 6.95 (m, 4H), 6.995 (m, 4H), 7.00 (m, 2H), 7.01 (m, 2H), 7.03 (m, 2H), 7.06 (m, 4H), 7.12 (m, 2H), 7.13 (m, 2H), 7.155 (d, *J* = 8.7, 2H), 7.175 (bd, *J* = 1.7, 2H), 7.265 (d, *J* = 8.5, 2H), 7.585 (bd, *J* = 8.7, 2H).

¹³C NMR (151 MHz, CD₂Cl₂): 18.17, 21.32 (2C), 21.39, 21.42, 30.34, 68.12, 68.33, 68.99, 73.84, 105.38, 105.45, 115.99, 117.00, 117.45, 118.10, 121.52, 122.55, 124.76, 125.03, 125.16, 126.59, 127.60, 127.94., 128.20, 128.40, 128.70, 128.94, 128.97, 128.99, 129.05, 129.07, 129.18, 129.43 129.70, 129.76, 129.77, 129.78 (2C), 130.21, 130.26, 130.36, 130.52, 130.56, 131.48, 132.20, 133.24, 133.80, 134.71, 135.44, 135.47, 135.57, 135.62, 135.76, 135.89, 136.39, 136.75, 136.87, 136.89, 136.96, 140.01, 153.63, 156.28, 156.51, 157.77, 194.75.

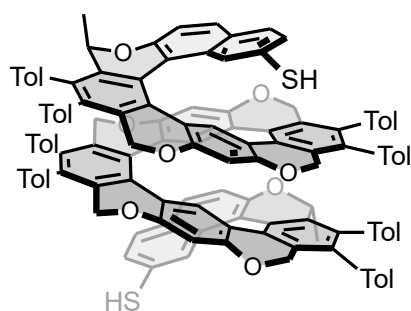


IR (CHCl₃): 3131 vw, 3085 vw, 3049 w, 1697 m, 1614 s, 1588 w, 1518 m, 1499 m, 1491 m, 1426 m, 1375 m, 1369 m, 1358 m, 1325 w, 1303 m, 1296 w, 1244 w, 1200 w, 1184 w, 1154 vs, 1129 m, 1111 m, 1086 m, 1067 w, 1059 w, 1022 m, 1015 w, 974 w, 952 w, 929 vw, 897 w, 882 vw, 870 vw, 856 vw, 834 m, 685 vw, 641 vw, 630 vw, 623 w, 612 w, 603 w, 597 vw, 587 vw, 574 vw, 551 vw, 540 vw, 529 w, 510 vw, 482 vw, 451 vw cm⁻¹.

MALDI MS: 1907 (M⁺).

HR MALDI MS: calculated for C₁₃₂H₉₈O₁₀S₂ 1906.6599, found 1906.6630.

(-)-(M,R,R)-Oxa[19]helicene-2,38-dithiol **172**



A Schlenk flask was charged with (-)-(M,R,R)-**88** (24 mg, 0.013 mmol), flushed with argon, and degassed THF (250 μ L) was added. Then a solution of sodium hydroxide (21 mg, 0.53 mmol, 40.0 equiv.) in degassed methanol (0.5 mL) was added dropwise at rt. The reaction mixture was stirred for 3 h. Then the reaction mixture was slowly acidified with a solution of citric acid (0.5 M in water, 1.3 mL, 50.0 equiv.) and stirred for 10 min. The precipitate was filtered off and washed with water (3 \times 10 mL). The precipitate was dried under vacuum to afford (-)-(M,R,R)-**172** (18 mg, 78%) as a grey powder.

M.p.: ~350 $^{\circ}$ C (water).

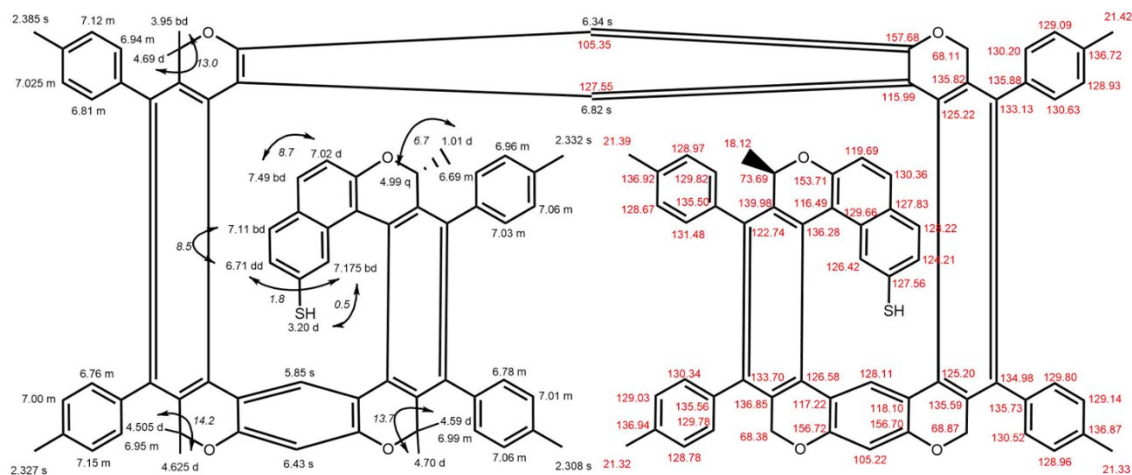
Optical rotation: $[\alpha]_D^{20}$ -1675 $^{\circ}$ (c 0.133, THF).

UV/Vis (THF): λ_{max} (log ϵ) = 269 (5.37) nm.

¹H NMR (500 MHz, CD₂Cl₂): 1.01 (d, J = 6.7, 6H), 2.27 (s, 6H), 2.308 (s, 6H), 2.32 (s, 6H), 2.332 (s, 6H), 2.385 (s, 6H), 3.20 (d, J = 0.5, 2H), 3.95 (d, J = 13.0, 2H), 4.505 (d, J = 14.2, 2H), 4.59 (d, J = 13.7, 2H), 4.625 (d, J = 14.2, 2H), 4.69 (d, J = 13.0, 2H), 4.70 (d, J = 13.7, 2H), 4.99 (q, J = 6.7, 2H), 5.85 (s, 2H), 6.34 (s, 1H), 6.43 (s, 2H), 6.69 (m, 2H), 6.71 (dd, J = 8.5, 1.7, 2H), 6.76 (m, 2H), 6.78 (m, 4H), 6.81 (m, 2H), 6.82 (s, 1H), 6.94 (m, 2H), 6.95 (m, 1H), 6.96 (m, 2H), 6.99 (m, 2H), 7.00 (m, 2H), 7.01 (m, 2H), 7.02 (d, J = 8.7, 2H), 7.025 (m, 2H), 7.03 (m, 2H), 7.06 (m, 4H), 7.11 (d, J = 8.5, 2H), 7.12 (m, 2H), 7.15 (m, 2H), 7.175 (bd, J = 1.7, 2H), 7.49 (d, J = 8.7, 2H).

¹³C NMR (151 MHz, CD₂Cl₂): 18.12, 21.32, 21.33, 21.39, 21.42, 68.11, 68.38, 68.87, 73.68, 105.22, 105.35, 115.99, 116.43, 117.22, 118.10, 119.69, 122.74, 124.21,

125.20, 125.22, 126.42, 126.58, 127.55, 127.56, 127.83, 128.11, 128.22, 128.67, 128.93, 128.96, 128.97, 129.03, 129.09, 129.14, 129.66, 129.78 (2C), 129.80, 129.82, 130.20, 130.34, 130.36, 130.52, 130.63, 131.48, 133.13, 133.70, 134.98, 135.50, 135.56, 135.59, 135.73, 135.82, 135.88, 136.28, 136.72, 136.85, 136.87, 136.92, 136.94, 139.98, 153.71, 156.70, 156.72, 157.68.



IR (KBr): 3130 w, 3047 m, 3020 m, 2985 m, 2923 m, 2853 m, 2564 w, 1903 w, 1615 s, 1587 m, 1518 m, 1500 m, 1490 m, 1422 m, 1376 m, 1301 m, 1244 m, 1224 m, 1212 w, 1183 w, 1161 s, 1110 m, 1088 m, 1059 m, 1047 m, 1022 s, 988 w, 943 w, 928 w, 896 w, 881 w, 870 w, 827 s, 790 w, 751 m, 732 w, 686 w, 642 w, 637 w, 618 w, 606 w, 588 w, 567 w, 549 w, 526 w, 508 w, 484 w, 450 w cm^{-1} .

MALDI MS: 1823 (M^+).

HR MALDI MS: calculated for $\text{C}_{128}\text{H}_{94}\text{O}_8\text{S}_2$ 1822.6390, found 1822.6354.

Table 5. X-ray crystallographic data

Compound	107	136	139	143	146	148	168	171
CCDC		1814579		1539259	1965622		1965623	1814580
Formula	C ₅₈ H ₄₂ O ₂	C ₂₆ H ₁₈ O ₂ S ₂	C ₂₆ H ₁₈ O ₂ S ₂	C ₃₄ H ₂₂ O ₂ S ₂	C ₃₂ H ₂₂ S ₂	C ₃₄ H ₂₂ O ₂ S ₂	C ₄₂ H ₃₄ O ₃ S	C ₁₂₈ H ₉₂ Cl ₂ O ₈ , 5 (C ₃ H ₆ O ₁)
Molecular weight	770.91	426.52	426.52	526.63	470.61	526.63	618.75	2118.29
Crystal system	triclinic	monoclinic	monoclinic	monoclinic	monoclinic	triclinic	orthorhombic	monoclinic
Space group	<i>P</i> -1	<i>P</i> 1 2 ₁ /c 1	<i>C</i> 1 2/c 1	<i>C</i> 1 2/c 1	<i>P</i> 1 2 ₁ /n 1	<i>P</i> -1	<i>P</i> 2 ₁ 2 ₁ 2 ₁	<i>P</i> 2 ₁
<i>a</i> [Å]	11.6807(4)	21.4937(8)	12.3095(6)	14.3809(7)	11.3992(8)	8.6448(4)	9.6920 (3)	13.5694(6)
<i>b</i> [Å]	18.2345(7)	9.3227(4)	10.4572(5)	9.9419(4)	11.2627(8)	12.4706(5)	19.0442(10)	20.2490(9)
<i>c</i> [Å]	21.0650(8)	21.3572(9)	15.0756(7)	18.1561(7)	17.6543(12)	13.5602(6)	19.0442(10)	20.8526(9)
α [°]	105.5470 (10)	90	90	90	90	116.1240 (10)	90	90
β [°]	104.3840(10)	104.637(2)	98.028(2)	99.657(2)	94.256(2)	93.235(2)	90	90.575(2)
γ [°]	102.8440(10)	90	90	90	90	99.9460(10)	90	90
Cell Volume [<i>Å</i> ³]	3981.35	4140.7(3)	1921.56(16)	2559.06(19)	2260.3(3)	1278.21	6488.5(5)	5729.3(4)
<i>Z</i>	4	8	4	8	4	2	8	2
θ_{max} [°]	72.1436	27.49	27.55	27.52	27.55	27.50	72.1678	74.58
Crystal shape	prism	bar	prism	plate	prism	prism	prism	prism
Crystal color	colorless	colorless- yellow	colorless- yellow	yellow	yellow	yellow	light yellow	yellow
Dx [g cm ⁻³]	1.286	1.368	1.474	1.367	1.383	1.368	1.267	1.228
<i>R</i> -Factor [%]	4.83	3.8	3.75	3.3	3.59	4.58	4.52	4.05
No. of parameters	1085	545	137	173	309	345	877	1440

5.3 Break Junction

Break Junction Experiments

Single molecule electrical conductance of all studied compounds: [5]helicene **131**, [7]helicene **143**, pyridooxa[9]helicene **87**, and [19]helicene **88** as well as standards DMBDT **173**,¹⁷⁹ and BIPY **73**,^{98,180,181} and oligo(phenyl acetylene) **174**¹⁸² were measured experimentally by a mechanically controllable break junction (MCBJ)¹⁹¹ or scanning tunneling microscopy-based break junction (STM-BJ)⁹⁸. The device recently constructed in our group at the Institute of Organic Chemistry and Biochemistry of the CAS was used for this purpose (Chapter 3.3). As the contact is broken at 5 Hz frequency and data are recorded at 50 kSa rate, tens of gigabytes of data are accumulated during each overnight measurement. The data were recorded at 100.0 mV. Statistical analysis of the massive data and filtration of incomplete traces is accomplished by an in-house computer program (Chapter 3.3.4).

MCBJ Substrate Preparation

In the MCBJ measurement, the key elements were 25×10×0.3 mm blue-tempered spring steel plates spin-coated with several μm of polyimide (Kapton) or a ceramic plates. A gold wire (25 μm diameter, 99.99% purity, Goodfellow GmbH) was glued on top of the plates and a short gold bridge was modelled with Alteco (30') epoxy. The same resin was used for the sample well that was created around the bridge to hold liquid samples. The gold bridge was notched in the middle to define the junction and make it easier to break in the center. Subsequently, the substrate was baked for *ca* 48 h at 80 °C in low vacuum to cure the epoxy. Copper leads with pins were then connected to the gold wire ends using conductive glue. Finally, the whole plate (except for the sample well with the notched gold bridge) was coated with a thin epoxy layer to improve mechanical stability of the device. For experiments in solution, a custom made measurement cell was placed around the sample well. BJ-chips were fabricated by Dr. J. Vacek-Chocholoušová.



Figure 60: MCBJ-Chip

STM-BJ Substrate Preparation

200 nm of high-purity gold (99.99%) was deposited on the surface of a custom-made glass cell by the thermal evaporation in high vacuum (10^{-6} mBar). A 10 nm layer of chromium was used as the adhesion interlayer. A high-purity gold wire (125 μm diameter, 99.99% purity, Goodfellow GmbH) was electrochemically etched and polished at potential of 6 V to create a sharp gold STM probe. An etching solution based on KI was used.¹⁹² The resulting tip is shown in **Figure 61** All metals were purchased from Goodfellow GmbH.

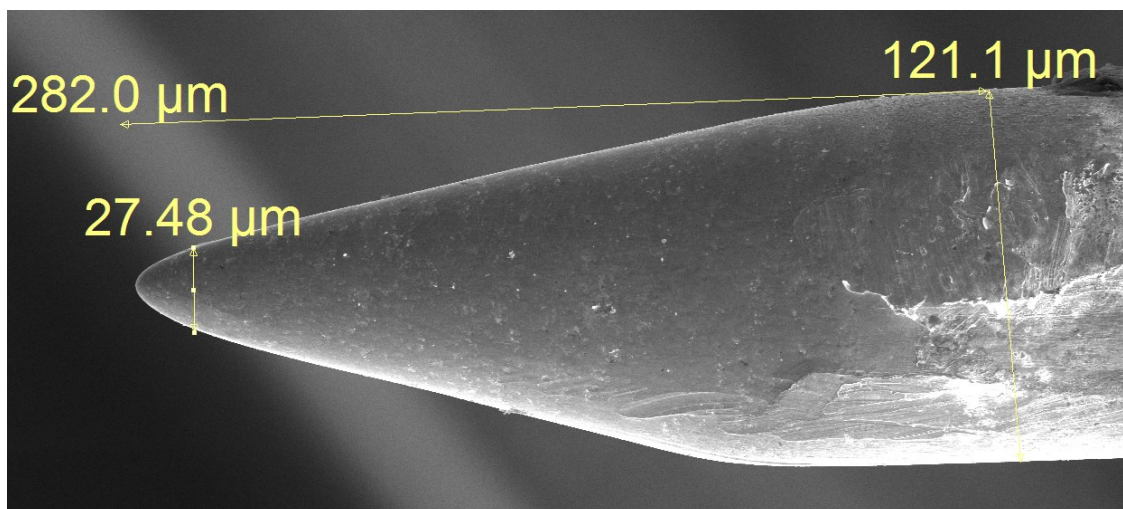


Figure 61: SEM image of the gold STM tip used for conductance measurements

Sample Preparation

All experiments were performed at 0.1 mM concentration of studied compound in freshly distilled mesitylene.

Measurement Conditions

Conditions of the measurement can influence the measurement in many ways. Therefore humidity and temperature were investigated to exclude possible influence on the experiment. The relative humidity (RH) and temperature probe MiniKin (EMS Brno) was used.

It was found that the temperature is almost constant so the thermal noise would not interfere, but the RH was above the acceptable value (**Figure 62**). To decrease the level of humidity, a drying agent (Blaugel) was used to maintain this parameter within the acceptable range inside the shielded area (below 50% RH). The graph shows the effectivity of the process.

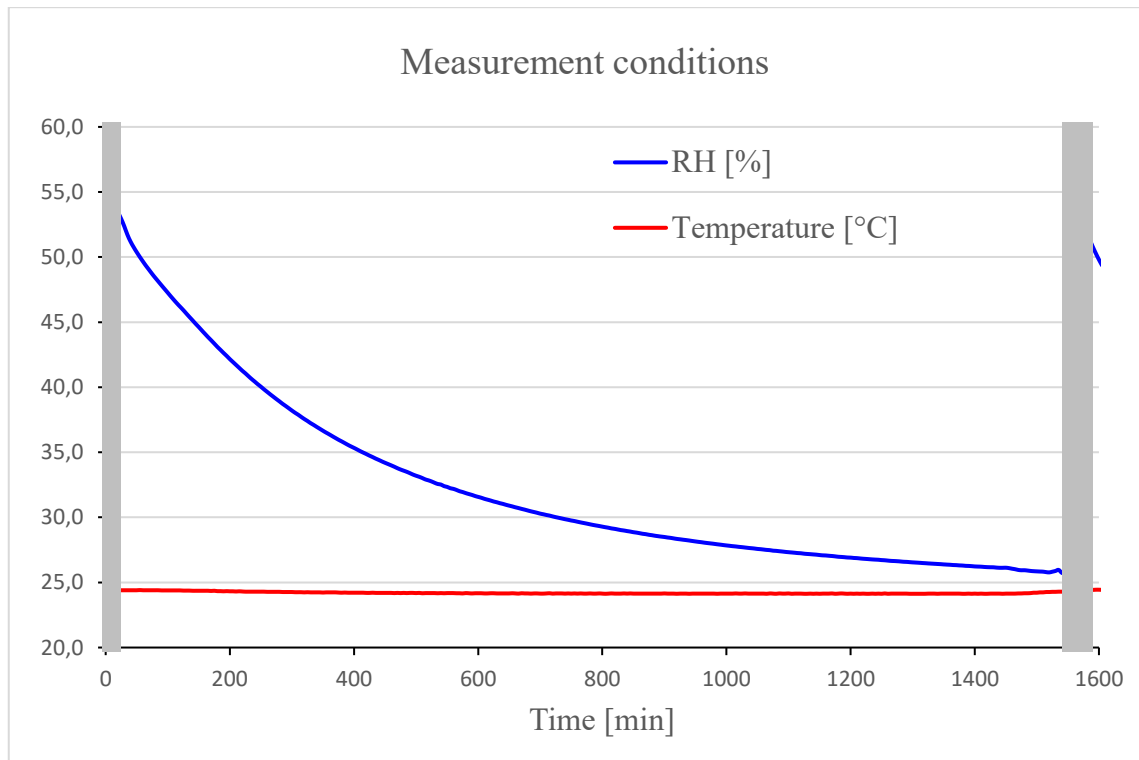


Figure 62: Relative humidity (blue) and temperature (red) graph; operator's access into the shielded area (grey)

Another issue of break junction experiments are vibrations, which might completely devaluate the whole measurement. This issue covers not only mechanical vibration caused by many devices such as vacuum pump or refrigerators or even air-conditioning, but also sound. The device was covered with a sound absorbing material and seated on a vibration-dampening material to eliminate these influences. The vibrations influence

mainly the STM-BJ experiments. The MCBJ setup is more resistant towards them due to mechanical preloading of the system.

Theoretical results

To *in-silico* model the BJ experiment, Non Equilibrium Green's Function (NEGF) approach^{88,89} and Periodic Density Functional GGA/PBE/DZP method or Slater–Koster tight-binding method as implemented in QuantumWise's Atomistix Toolkit¹⁸⁴ were used. First, molecules were optimized at quantum chemical B3LYP/cc-pVDZ/GD3 level with Gaussian09¹⁹³ ([5]helicene **131**, pyridooxa[9]helicene **87**, and [19]helicene **88**). Molecular coordinates obtained from X-ray analysis were used in the case of [7]helicene **143**. The resulting structures were then placed between two gold (1,1,1) electrodes using the VNL graphical interface of QuantumWise^{194,195} and the entire molecular junction device configuration was optimized at PBE/DZP, or semi-empirical DFTB level of theory. Zero bias transmission spectrum of a molecule was then calculated by means of NEGF. It corresponds to ideal conformation with favorable contacts on both sides of the molecule. *In-silico* conductance calculations were performed by Dr. Jaroslav Vacek (IOCB, Prague).

6 Abbreviations

Ac	acetyl
AcCl	acetyl chloride
AFM	atomic force microscopy
APCI	atmospheric pressure chemical ionization
ATK	Atomistix ToolKit
BDT	1,4-benzene dithiol
BMSB	1,4-bis(methylsulfanyl)benzene
BIPY	4,4'-bipyridine
BJ	break junction
Bu	butyl
BuLi	butyllithium
CD	circular dichroism
CDHC	photochemical cyclodehydrochlorination
CISS	chiral-induced spin selectivity
<i>cod</i>	cyclooctadienyl
CSP-HPLC	high performance liquid chromatography with chiral stationary phase
Cy	cyclohexyl
d	doublet
D-A	donor-acceptor
<i>dba</i>	dibenzylideneacetone
DCM	dichloromethane
dd	doublet of doublets
ddd	doublet of doublet of doublets
DFT	density-functional theory
DIPA	<i>N,N</i> -di(isopropyl)amine
DIAD	diisopropyl azodicarboxylate
DMBDT	1,4-bis(methylsulfanyl)benzene
DMDS	dimethyl disulfide
DMF	<i>N,N</i> -Dimethylmethanamide
dt	doublet of triplets
Et	ethyl
<i>fum</i>	dimethylfumarate

EI	electron impact ionization
ESI	electrospray ionization
HMPA	hexamethylphosphoramide
HOPG	highly oriented pyrolytic graphite
HOMO	highest occupied molecule orbital
HPFC	high-performance flash chromatography
HPFL	high-performance liquid chromatography
IR	infrared spectroscopy
IVC	current to voltage converter
kSa	kiloSamples per second
LDA	lithium diisopropylamide
LUMO	lowest unoccupied molecular orbital
M.p.	melting point
MALDI	matrix-assisted laser desorption/ionization
MCBJ	mechanically controllable break junction
Me	methyl
MeOH	methanol
<i>men</i>	menthyl
MesH	mesitylene
MS	mass spectrometry
MTBE	methyl- <i>t</i> -butyl ether
NEGF	nonequilibrium Green's functions
NHC	N-heterocyclic carbenes
NMP	N-methyl-2-pyrrolidone
PCDH	photocyclodehydrogenation
Ph	phenyl
Pr	propyl
Py	pyridine
Pyr	pyrazol
RCM	ring closing metathesis
RH	relative humidity
rt	room temperature
s	singlet (NMR), strong (IR)
SEM	scanning electron microscope

STM	scanning tunneling microscopy
STM-BJ	scanning tunneling microscopy-based break junction
t	triplet
TBAF	tetrabutylammonium fluoride
TBDMS	<i>t</i> -butyldimethylsilyl
THF	tetrahydrofuran
TIPS	tri(isopropyl)silyl protecting group
TIPSA	tri(isopropyl)silylacetylene
TLC	thin layer chromatography
TMS	trimethylsilyl
TMSA	trimethylsilylacetylene
TOF	time-of-flight mass analyzer
Tol	tolyl
TTF	tetrathiafulvalene
UHV	ultra-high vacuum (pressures lower than 10^{-7} Pa)
vs	very strong (IR)
w	weak
xyl	3,5-xylyl

7 Literature

- (1) Moss, G. P.; Smith, P. A. S.; Tavernier, D. Glossary of Class Names of Organic Compounds and Reactivity Intermediates Based on Structure (IUPAC Recommendations 1995). *Pure Appl. Chem.* **1995**, *67* (8–9), 1307–1375. <https://doi.org/10.1351/pac199567081307>.
- (2) Vacek, J.; Vacek-Chocholeušová, J.; Stará, I. G.; Starý, I.; Dubi, Y. Mechanical Tuning of Conductance and Thermopower in Helicene Molecular Junctions. *Nanoscale* **2015**, *7* (19), 8793–8802. <https://doi.org/10.1039/C5NR01297J>.
- (3) Šesták, P.; Wu, J.; He, J.; Pokluda, J.; Zhang, Z. Extraordinary Deformation Capacity of Smallest Carbohelicene Springs. *Phys. Chem. Chem. Phys.* **2015**, *17* (28), 18684–18690. <https://doi.org/10.1039/C5CP02043C>.
- (4) Tanaka, K.; Osuga, H.; Kitahara, Y. Clathrate Formation by and Self-Assembled Supramolecular Structures of a “Molecular Spring.” *J. Chem. Soc. Perkin Trans. 2* **2000**, No. 12, 2492–2497. <https://doi.org/10.1039/b005070i>.
- (5) Yang, Y.; Rice, B.; Shi, X.; Brandt, J. R.; Correa da Costa, R.; Hedley, G. J.; Smilgies, D.-M.; Frost, J. M.; Samuel, I. D. W.; Otero-de-la-Roza, A.; Johnson, E. R.; Jelfs, K. E.; Nelson, J.; Campbell, A. J.; Fuchter, M. J. Emergent Properties of an Organic Semiconductor Driven by Its Molecular Chirality. *ACS Nano* **2017**, *11* (8), 8329–8338. <https://doi.org/10.1021/acsnano.7b03540>.
- (6) Kiran, V.; Mathew, S. P.; Cohen, S. R.; Hernández Delgado, I.; Lacour, J.; Naaman, R. Helicenes-A New Class of Organic Spin Filter. *Adv. Mater.* **2016**, *28* (10), 1957–1962. <https://doi.org/10.1002/adma.201504725>.
- (7) Šámal, M.; Míšek, J.; Stará, I. G.; Starý, I. Organocatalysis with Azahelicenes: The First Use of Helically Chiral Pyridine-Based Catalysts in the Asymmetric Acyl Transfer Reaction. *Collect. Czechoslov. Chem. Commun.* **2009**, *74* (7–8), 1151–1159. <https://doi.org/10.1135/cccc2009067>.
- (8) Ben Hassine, B.; Gorsane, M.; Pecher, J.; Martin, R. H. Synthèses Asymétriques Potentielles Impliquant La Réaction “Ene.” *Bull. Sociétés Chim. Belg.* **2010**, *96* (10), 801–808. <https://doi.org/10.1002/bscb.19870961013>.
- (9) Reetz, M. T.; Sostmann, S. Kinetic Resolution in Pd-Catalyzed Allylic Substitution Using the Helical PHelix Ligand. *J. Organomet. Chem.* **2000**, *603* (1), 105–109. [https://doi.org/10.1016/S0022-328X\(00\)00173-X](https://doi.org/10.1016/S0022-328X(00)00173-X).
- (10) Yamamoto, K.; Shimizu, T.; Igawa, K.; Tomooka, K.; Hirai, G.; Suemune, H.; Usui, K. Rational Design and Synthesis of [5]Helicene-Derived Phosphine Ligands and Their Application in Pd-Catalyzed Asymmetric Reactions. *Sci. Rep.* **2016**, *6*, 36211.
- (11) Reetz, M. T.; Beuttenmüller, E. W.; Goddard, R. First Enantioselective Catalysis Using a Helical Diphosphane. *Tetrahedron Lett.* **1997**, *38* (18), 3211–3214. [https://doi.org/10.1016/S0040-4039\(97\)00562-5](https://doi.org/10.1016/S0040-4039(97)00562-5).
- (12) Nakano, D.; Yamaguchi, M. Enantioselective Hydrogenation of Itaconate Using Rhodium Bihelicene Phosphite Complex. Matched/Mismatched Phenomena between Helical and Axial Chirality. *Tetrahedron Lett.* **2003**, *44* (27), 4969–4971. [https://doi.org/10.1016/S0040-4039\(03\)01183-3](https://doi.org/10.1016/S0040-4039(03)01183-3).
- (13) Reetz, M. T.; Sostmann, S. 2,15-Dihydroxy-Hexahelicene (HELIXOL): Synthesis and Use as an Enantioselective Fluorescent Sensor. *Tetrahedron* **2001**, *57* (13), 2515–2520. [https://doi.org/10.1016/S0040-4020\(01\)00077-1](https://doi.org/10.1016/S0040-4020(01)00077-1).
- (14) Weix, D. J.; Dreher, S. D.; Katz, T. J. [5]HELOL Phosphite: A Helically Grooved Sensor of Remote Chirality. *J. Am. Chem. Soc.* **2000**, *122* (41), 10027–10032. <https://doi.org/10.1021/ja001904n>.

- (15) Hasan, M.; Khose, V. N.; Mori, T.; Borovkov, V.; Karnik, A. V. Sui Generis Helicene-Based Supramolecular Chirogenic System: Enantioselective Sensing, Solvent Control, and Application in Chiral Group Transfer Reaction. *ACS Omega* **2017**, *2* (2), 592–598. <https://doi.org/10.1021/acsomega.6b00522>.
- (16) Dova, D.; Cauteruccio, S.; Manfredi, N.; Prager, S.; Dreuw, A.; Arnaboldi, S.; Mussini, P. R.; Licandro, E.; Abboto, A. An Unconventional Helical Push-Pull System for Solar Cells. *Dyes Pigments* **2019**, *161*, 382–388. <https://doi.org/10.1016/j.dyepig.2018.09.050>.
- (17) Bender, Timothy P.; MacKinnon, Sean M.; Wang, Zhi Yuan. Poly(Aryl Ether)s Containing o-Terphenyl Subunits. III. Random Copoly(Ether Imide)s. *J. Polym. Sci. Part Polym. Chem.* **2000**, *2000* (38), 758–763. [https://doi.org/10.1002/\(SICI\)1099-0518\(20000215\)38:4<758::AID-POLA11>3.0.CO;2-M](https://doi.org/10.1002/(SICI)1099-0518(20000215)38:4<758::AID-POLA11>3.0.CO;2-M).
- (18) Brunsveld, L.; Folmer, B. J. B.; Meijer, E. W.; Sijbesma, R. P. Supramolecular Polymers. *Chem. Rev.* **2001**, *101* (12), 4071–4098. <https://doi.org/10.1021/cr990125q>.
- (19) Nuckolls, C.; Shao, R.; Jang, W.-G.; Clark, N. A.; Walba, D. M.; Katz, T. J. Electro-Optic Switching by Helicene Liquid Crystals. *Chem. Mater.* **2002**, *14* (2), 773–776. <https://doi.org/10.1021/cm010628o>.
- (20) Weitzenböck, R.; Klingler, A. Synthese der isomeren Kohlenwasserstoffe 1, 2-5, 6-Dibenzanthracen und 3, 4-5, 6-Dibenzphenanthren. *Monatshefte Für Chem.* **1918**, *39* (5), 315–323. <https://doi.org/10.1007/BF01524529>.
- (21) Newman, M. S.; Lutz, W. B.; Lednicer, D. A New Reagent for Resolution by Complex Formation; the Resolution of Phenanthro-[3,4-*c*]Phenanthrene. *J. Am. Chem. Soc.* **1955**, *77* (12), 3420–3421. <https://doi.org/10.1021/ja01617a097>.
- (22) Newman, M. S.; Lednicer, D. The Synthesis and Resolution of Hexahelicene. *J. Am. Chem. Soc.* **1956**, *78* (18), 4765–4770. <https://doi.org/10.1021/ja01599a060>.
- (23) Flammang-Barbieux, M.; Nasielski, J.; Martin, R. H. Synthesis of Heptahelicene Benzo [c]Phenanthro [4,3-*g*]Phenanthrene. *Tetrahedron Lett.* **1967**, *8* (8), 743–744. [https://doi.org/10.1016/S0040-4039\(00\)90586-0](https://doi.org/10.1016/S0040-4039(00)90586-0).
- (24) Wismonski-Knittel, T.; Fischer, G.; Fischer, E. Temperature Dependence of Photoisomerization. Part VIII. Excited-State Behaviour of 1-Naphthyl-2-Phenyl- and 1,2-Dinaphthyl-Ethylenes and Their Photocyclisation Products, and Properties of the Latter. *J. Chem. Soc. Perkin Trans. 2* **1974**, 1930. <https://doi.org/10.1039/p29740001930>.
- (25) Martin, R. H.; Flammang-Barbieux, M.; Cosyn, J. P.; Gelbcke, M. 1-Synthesis of Octa- and Nonahelicenes. 2-New Syntheses of Hexa- and Heptahelicenes. 3-Optical Rotation and O.R.D. of Heptahelicene. *Tetrahedron Lett.* **1968**, *9* (31), 3507–3510. [https://doi.org/10.1016/S0040-4039\(01\)99095-1](https://doi.org/10.1016/S0040-4039(01)99095-1).
- (26) Martin, R. H.; Baes, M. Helicenes. *Tetrahedron* **1975**, *31* (17), 2135–2137. [https://doi.org/10.1016/0040-4020\(75\)80208-0](https://doi.org/10.1016/0040-4020(75)80208-0).
- (27) Mori, K.; Murase, T.; Fujita, M. One-Step Synthesis of [16]Helicene. *Angew. Chem. Int. Ed.* **2015**, *54* (23), 6847–6851. <https://doi.org/10.1002/anie.201502436>.
- (28) Dietz, F.; Scholz, M. Chemie angeregter zustände—IV. *Tetrahedron* **1968**, *24* (24), 6845–6849. [https://doi.org/10.1016/S0040-4020\(01\)96798-5](https://doi.org/10.1016/S0040-4020(01)96798-5).
- (29) Hernandez-Perez, A. C.; Vlassova, A.; Collins, S. K. Toward a Visible Light Mediated Photocyclization: Cu-Based Sensitizers for the Synthesis of [5]Helicene. *Org. Lett.* **2012**, *14* (12), 2988–2991. <https://doi.org/10.1021/ol300983b>.

- (30) Richardson, R. D.; Baud, M. G. J.; Weston, C. E.; Rzepa, H. S.; Kuimova, M. K.; Fuchter, M. J. Dual Wavelength Asymmetric Photochemical Synthesis with Circularly Polarized Light. *Chem. Sci.* **2015**, *6* (7), 3853–3862. <https://doi.org/10.1039/C4SC03897E>.
- (31) Daigle, M.; Picard-Lafond, A.; Soligo, E.; Morin, J.-F. Regioselective Synthesis of Nanographenes by Photochemical Cyclodehydrochlorination. *Angew. Chem. Int. Ed.* **2016**, *55* (6), 2042–2047. <https://doi.org/10.1002/anie.201509130>.
- (32) Daigle, M.; Miao, D.; Lucotti, A.; Tommasini, M.; Morin, J.-F. Helically Coiled Graphene Nanoribbons. *Angew. Chem. Int. Ed.* **2017**, *56* (22), 6213–6217. <https://doi.org/10.1002/anie.201611834>.
- (33) Reppe, W.; Schlichting, O.; Klager, K.; Toepel, T. Cyclisierende Polymerisation von Acetylen I Über Cyclooctatetraen. *Justus Liebig's Ann. Chem.* **1948**, *560* (1), 1–92. <https://doi.org/10.1002/jlac.19485600102>.
- (34) Diercks, R.; Vollhardt, K. P. C. Novel Synthesis of the Angular [3]Phenylene (Terphenylene) by Cobalt-Catalyzed Cyclization of Bis(2-Ethynylphenyl)Ethyne: A Molecule with an Internal Cyclohexatriene Ring. *Angew. Chem. Int. Ed. Engl.* **1986**, *25* (3), 266–268. <https://doi.org/10.1002/anie.198602661>.
- (35) Han, S.; Anderson, D. R.; Bond, A. D.; Chu, H.; Disch, R. L.; Holmes, D.; Schulman, J. M.; Teat, S. J.; Vollhardt, K. P. C.; Whitener, G. D. Total Syntheses of Angular [7]-, [8]-, and [9]Phenylene by Triple Cobalt-Catalyzed Cycloisomerization: Remarkably Flexible Heliphenes. *Angew. Chem. Int. Ed.* **2002**, *2002* (41), 3227–3230. [https://doi.org/10.1002/1521-3773\(20020902\)41:17<3227::AID-ANIE3227>3.0.CO;2-T](https://doi.org/10.1002/1521-3773(20020902)41:17<3227::AID-ANIE3227>3.0.CO;2-T).
- (36) Diercks, R.; Eaton, B. E.; Gürtzgen, S.; Jalisatgi, S.; Matzger, A. J.; Radde, R. H.; Vollhardt, K. P. C. The First Metallacyclopentadiene(Alkyne) Complexes and Their Discrete Isomerization to η^4 -Bound Arenes: The Missing Link in the Prevalent Mechanism of Transition Metal Catalyzed Alkyne Cyclotrimerizations, as Exemplified by Cyclopentadienylcobalt. *J. Am. Chem. Soc.* **1998**, *120* (32), 8247–8248. <https://doi.org/10.1021/ja981766q>.
- (37) Hardesty, J. H.; Koerner, J. B.; Albright, T. A.; Lee, G.-Y. Theoretical Study of the Acetylene Trimerization with CpCo. *J. Am. Chem. Soc.* **1999**, *121* (25), 6055–6067. <https://doi.org/10.1021/ja983098e>.
- (38) Stará, I. G.; Starý, I.; Kollárovič, A.; Teplý, F.; Šaman, D.; Tichý, M. A Novel Strategy for the Synthesis of Molecules with Helical Chirality. Intramolecular [2 + 2 + 2] Cycloisomerization of Triynes under Cobalt Catalysis. *J. Org. Chem.* **1998**, *63* (12), 4046–4050. <https://doi.org/10.1021/jo9801263>.
- (39) Teplý, F.; Stará, I. G.; Starý, I.; Kollárovič, A.; Šaman, D.; Rulíšek, L.; Fiedler, P. Synthesis of [5]-, [6]-, and [7]Helicene via Ni(0)- or Co(I)-Catalyzed Isomerization of Aromatic *Cis*, *Cis*-Dienetriynes. *J. Am. Chem. Soc.* **2002**, *124* (31), 9175–9180. <https://doi.org/10.1021/ja0259584>.
- (40) Tanaka, K.; Kimura, Y.; Murayama, K. Enantioselective Helicene Synthesis by Rhodium-Catalyzed [2+2+2] Cycloadditions. *Bull. Chem. Soc. Jpn.* **2015**, *88* (3), 375–385. <https://doi.org/10.1246/bcsj.20140291>.
- (41) Tanaka, K.; Kamisawa, A.; Suda, T.; Noguchi, K.; Hirano, M. Rh-Catalyzed Synthesis of Helically Chiral and Ladder-Type Molecules via [2 + 2 + 2] and Formal [2 + 1 + 2 + 1] Cycloadditions Involving C–C Triple Bond Cleavage. *J. Am. Chem. Soc.* **2007**, *129* (40), 12078–12079. <https://doi.org/10.1021/ja074914y>.

- (42) Liu, L.; Katz, T. J. Simple Preparation of a Helical Quinone. *Tetrahedron Lett.* **1990**, *31* (28), 3983–3986. [https://doi.org/10.1016/S0040-4039\(00\)94478-2](https://doi.org/10.1016/S0040-4039(00)94478-2).
- (43) Willmore, N. D.; Liu, L.; Katz, T. J. A Diels-Alder Route to [5]- and [6]-Helicenes. *Angew. Chem. Int. Ed. Engl.* **1992**, *31* (8), 1093–1095. <https://doi.org/10.1002/anie.199210931>.
- (44) Fox, J. M.; Goldberg, N. R.; Katz, T. J. Efficient Synthesis of Functionalized [7]Helicenes. *J. Org. Chem.* **1998**, *63* (21), 7456–7462. <https://doi.org/10.1021/jo981380y>.
- (45) Dreher, S. D.; Weix, D. J.; Katz, T. J. Easy Synthesis of Functionalized Hetero[7]Helicenes. *J. Org. Chem.* **1999**, *64* (10), 3671–3678. <https://doi.org/10.1021/jo990065o>.
- (46) Collins, S. K.; Grandbois, A.; Vachon, M. P.; Côté, J. Preparation of Helicenes through Olefin Metathesis. *Angew. Chem. Int. Ed.* **2006**, *45* (18), 2923–2926. <https://doi.org/10.1002/anie.200504150>.
- (47) Milde, B.; Leibelng, M.; Pawliczek, M.; Grunenberg, J.; Jones, P. G.; Werz, D. B. π -Helicenes Truncated to a Minimum: Access Through a Domino Approach Involving Multiple Carbopalladations and a Stille Coupling. *Angew. Chem. Int. Ed.* **2015**, *54* (4), 1331–1335. <https://doi.org/10.1002/anie.201408637>.
- (48) Goedicke, Ch.; Stegemeyer, H. Resolution and Racemization of Pentahelicene. *Tetrahedron Lett.* **1970**, *11* (12), 937–940. [https://doi.org/10.1016/S0040-4039\(01\)97871-2](https://doi.org/10.1016/S0040-4039(01)97871-2).
- (49) Martin, R. H.; Marchant, M. J. Thermal Racemisation of Hepta-, Octa-, and Nonahelicene. *Tetrahedron* **1974**, *30* (2), 347–349. [https://doi.org/10.1016/S0040-4020\(01\)91469-3](https://doi.org/10.1016/S0040-4020(01)91469-3).
- (50) Mike, F.; Boshart, G.; Gil-Av, E. Helicenes. Resolution on Chiral Charge-Transfer Complexing Agents Using High Performance Liquid Chromatography. *J. Chem. Soc. Chem. Commun.* **1976**, No. 3, 99. <https://doi.org/10.1039/c39760000099>.
- (51) Grandbois, A.; Collins, S. K. Enantioselective Synthesis of [7]Helicene: Dramatic Effects of Olefin Additives and Aromatic Solvents in Asymmetric Olefin Metathesis. *Chem. - Eur. J.* **2008**, *14* (30), 9323–9329. <https://doi.org/10.1002/chem.200801033>.
- (52) Gay Sánchez, I.; Šámal, M.; Nejedlý, J.; Karras, M.; Klívar, J.; Rybáček, J.; Buděšinský, M.; Bednárová, L.; Seidlerová, B.; Stará, I. G.; Starý, I. Oxahelicene NHC Ligands in the Asymmetric Synthesis of Nonracemic Helicenes. *Chem. Commun.* **2017**, *53* (31), 4370–4373. <https://doi.org/10.1039/C7CC00781G>.
- (53) Jančařík, A.; Rybáček, J.; Cocq, K.; Vacek-Chocholoušová, J.; Vacek, J.; Pohl, R.; Bednárová, L.; Fiedler, P.; Císařová, I.; Stará, I. G.; Starý, I. Rapid Access to Dibenzohelicenes and Their Functionalized Derivatives. *Angew. Chem. Int. Ed.* **2013**, *52* (38), 9970–9975. <https://doi.org/10.1002/anie.201301739>.
- (54) Kimura, Y.; Fukawa, N.; Miyauchi, Y.; Noguchi, K.; Tanaka, K. Enantioselective Synthesis of [9]- and [11]Helicene-like Molecules: Double Intramolecular [2+2+2] Cycloaddition. *Angew. Chem. Int. Ed.* **2014**, *53* (32), 8480–8483. <https://doi.org/10.1002/anie.201404810>.
- (55) Žádný, J.; Jančařík, A.; Andronova, A.; Šámal, M.; Vacek-Chocholoušová, J.; Vacek, J.; Pohl, R.; Šaman, D.; Císařová, I.; Stará, I. G.; Starý, I. A General Approach to Optically Pure [5]-, [6]-, and [7]Heterohelicenes. *Angew. Chem. Int. Ed.* **2012**, *51* (24), 5857–5861. <https://doi.org/10.1002/anie.201108307>.
- (56) Karras, M.; Holec, J.; Bednárová, L.; Pohl, R.; Schmidt, B.; Stará, I. G.; Starý, I. Asymmetric Synthesis of Nonracemic 2-Amino[6]Helicenes and Their Self-

- Assembly into Langmuir Films. *J. Org. Chem.* **2018**, *83* (10), 5523–5538. <https://doi.org/10.1021/acs.joc.8b00538>.
- (57) Stará, I. G.; Alexandrová, Z.; Teplý, F.; Sehnal, P.; Starý, I.; Šaman, D.; Buděšínský, M.; Cvačka, J. Asymmetric Synthesis of [7]Helicene-Like Molecules. *Org. Lett.* **2005**, *7* (13), 2547–2550. <https://doi.org/10.1021/ol047311p>.
- (58) Yavari, K.; Aillard, P.; Zhang, Y.; Nuter, F.; Retailleau, P.; Voituriez, A.; Marinetti, A. Helicenes with Embedded Phosphole Units in Enantioselective Gold Catalysis. *Angew. Chem. Int. Ed.* **2014**, *53* (3), 861–865. <https://doi.org/10.1002/anie.201308377>.
- (59) Nelson, D. J.; Queval, P.; Rouen, M.; Magrez, M.; Toupet, L.; Caijo, F.; Borré, E.; Laurent, I.; Crévisy, C.; Baslé, O.; Mauduit, M.; Percy, J. M. Synergic Effects Between N-Heterocyclic Carbene and Chelating Benzyldiene–Ether Ligands Toward the Initiation Step of Hoveyda–Grubbs Type Ru Complexes. *ACS Catal.* **2013**, *3* (2), 259–264. <https://doi.org/10.1021/cs400013z>.
- (60) Shen, C.; Srebro-Hooper, M.; Jean, M.; Vanthuynne, N.; Toupet, L.; Williams, J. A. G.; Torres, A. R.; Riives, A. J.; Muller, G.; Autschbach, J.; Crassous, J. Synthesis and Chiroptical Properties of Hexa-, Octa-, and Deca-Azaborahelicenes: Influence of Helicene Size and of the Number of Boron Atoms. *Chem. - Eur. J.* **2017**, *23* (2), 407–418. <https://doi.org/10.1002/chem.201604398>.
- (61) Murai, M.; Okada, R.; Nishiyama, A.; Takai, K. Synthesis and Properties of Sila[n]Helicenes via Dehydrogenative Silylation of C–H Bonds under Rhodium Catalysis. *Org. Lett.* **2016**, *18* (17), 4380–4383. <https://doi.org/10.1021/acs.orglett.6b02134>.
- (62) Tok, O. L.; Lang, K.; Růžička, A.; Cvačka, J. Helicenes Built from Silacyclopentadienes via Ring-by-Ring Knitting of the Helical Framework. *Angew. Chem. Int. Ed.* **2019**, *58* (6), 1654–1658. <https://doi.org/10.1002/anie.201811140>.
- (63) Chen, F.; Tanaka, T.; Hong, Y. S.; Mori, T.; Kim, D.; Osuka, A. Closed Pentaaza[9]Helicene and Hexathia[9]/[5]Helicene: Oxidative Fusion Reactions of *Ortho*-Phenylene-Bridged Cyclic Hexapyrroles and Hexathiophenes. *Angew. Chem. Int. Ed.* **2017**, *56* (46), 14688–14693. <https://doi.org/10.1002/anie.201708429>.
- (64) Klívar, J.; Jančařík, A.; Šaman, D.; Pohl, R.; Fiedler, P.; Bednárová, L.; Starý, I.; Stará, I. G. [2+2+2] Cycloisomerisation of Aromatic Cyanodiyne in the Synthesis of Pyridohelicenes and Their Analogues. *Chem. - Eur. J.* **2016**, *22* (40), 14401–14405. <https://doi.org/10.1002/chem.201602747>.
- (65) Yamada, K.; Ogashiwa, S.; Tanaka, H.; Nakagawa, H.; Kawazura, H. [7],[9],[11],[13], and [15]Heterohelicenes Annelated with Alternant Thiophen Ann Benzene Rings. Syntheses and NMR Studies. *Chem. Lett.* **1981**, *10* (3), 343–346. <https://doi.org/10.1246/cl.1981.343>.
- (66) Wynberg, H.; Groen, M. B. Synthesis, Resolution, and Optical Rotatory Dispersion of a Hexa- and a Heptaheterohelicene. *J. Am. Chem. Soc.* **1968**, *90* (19), 5339–5341. <https://doi.org/10.1021/ja01021a088>.
- (67) Tsujihara, T.; Zhou, D.-Y.; Suzuki, T.; Tamura, S.; Kawano, T. Helically Chiral 1-Sulfur-Functionalized [6]Helicene: Synthesis, Optical Resolution, and Functionalization. *Org. Lett.* **2017**, *19* (12), 3311–3314. <https://doi.org/10.1021/acs.orglett.7b01470>.
- (68) Tsujihara, T.; Inada-Nozaki, N.; Takehara, T.; Zhou, D.-Y.; Suzuki, T.; Kawano, T. Nickel-Catalyzed Construction of Chiral 1-[6]Helicenols and Application in

- the Synthesis of [6]Helicene-Based Phosphinite Ligands: Nickel-Catalyzed Construction of Chiral 1-[6]Helicenols and Application in the Synthesis of [6]Helicene-Based Phosphinite Ligands. *Eur. J. Org. Chem.* **2016**, 2016 (29), 4948–4952. <https://doi.org/10.1002/ejoc.201600677>.
- (69) von Hippel, A. Molecular Engineering. *Science* **1956**, 123 (3191), 315–317. <https://doi.org/10.1126/science.123.3191.315>.
- (70) Aviram, A.; Ratner, M. A. Molecular Rectifiers. *Chem. Phys. Lett.* **1974**, 29 (2), 277–283. [https://doi.org/10.1016/0009-2614\(74\)85031-1](https://doi.org/10.1016/0009-2614(74)85031-1).
- (71) Hittinger, W. C. Metal-Oxide-Semiconductor Technology. *Sci. Am.* **1973**, 229 (2), 48–59. <https://doi.org/10.1038/scientificamerican0873-48>.
- (72) Vernon-Parry, K. D. Scanning Electron Microscopy: An Introduction. *III-Vs Rev.* **2000**, 13 (4), 40–44. [https://doi.org/10.1016/S0961-1290\(00\)80006-X](https://doi.org/10.1016/S0961-1290(00)80006-X).
- (73) Giessibl, F. J. Advances in Atomic Force Microscopy. *Rev. Mod. Phys.* **2003**, 75 (3), 949–983. <https://doi.org/10.1103/RevModPhys.75.949>.
- (74) Binnig, G.; Rohrer, H. Scanning Tunneling Microscopy—from Birth to Adolescence. *Rev. Mod. Phys.* **1987**, 59 (3), 615–625. <https://doi.org/10.1103/RevModPhys.59.615>.
- (75) Moreland, J.; Ekin, J. W. Electron Tunneling Experiments Using Nb-Sn “Break” Junctions. *J. Appl. Phys.* **1985**, 58 (10), 3888–3895. <https://doi.org/10.1063/1.335608>.
- (76) Reed, M. A. Conductance of a Molecular Junction. *Science* **1997**, 278 (5336), 252–254. <https://doi.org/10.1126/science.278.5336.252>.
- (77) Metzger, R. M. Unimolecular Electronics. *Chem. Rev.* **2015**, 115 (11), 5056–5115. <https://doi.org/10.1021/cr500459d>.
- (78) Park, J.; Pasupathy, A. N.; Goldsmith, J. I.; Chang, C.; Yaish, Y.; Petta, J. R.; Rinkoski, M.; Sethna, J. P.; Abruña, H. D.; McEuen, P. L.; Ralph, D. C. Coulomb Blockade and the Kondo Effect in Single-Atom Transistors. *Nature* **2002**, 417 (6890), 722–725. <https://doi.org/10.1038/nature00791>.
- (79) He, H. X.; Li, C. Z.; Tao, N. J. Conductance of Polymer Nanowires Fabricated by a Combined Electrodeposition and Mechanical Break Junction Method. *Appl. Phys. Lett.* **2001**, 78 (6), 811–813. <https://doi.org/10.1063/1.1335551>.
- (80) Poot, M.; Osorio, E.; O’Neill, K.; Thijssen, J. M.; Vanmaekelbergh, D.; van Walree, C. A.; Jenneskens, L. W.; van der Zant, H. S. J. Temperature Dependence of Three-Terminal Molecular Junctions with Sulfur End-Functionalized Tercyclohexylidenes. *Nano Lett.* **2006**, 6 (5), 1031–1035. <https://doi.org/10.1021/nl0604513>.
- (81) Tao, N. J. Probing Potential-Tuned Resonant Tunneling through Redox Molecules with Scanning Tunneling Microscopy. *Phys. Rev. Lett.* **1996**, 76 (21), 4066–4069. <https://doi.org/10.1103/PhysRevLett.76.4066>.
- (82) Ohm, G. S. *Die galvanische Kette, mathematisch bearbeitet*; T. H. Riemann, 1827.
- (83) M. de Muynck, W. *Foundations of Quantum Mechanics, an Empiricist Approach*; Kluwer Academic Publishers: Dordrecht, 2004.
- (84) Landauer, R. Spatial Variation of Currents and Fields Due to Localized Scatterers in Metallic Conduction. *IBM J. Res. Dev.* **1957**, 1 (3), 223–231. <https://doi.org/10.1147/rd.13.0223>.
- (85) Sirvent, C.; Rodrigo, J. G.; Agrait, N.; Vieira, S. STM Study of the Atomic Contact between Metallic Electrodes. *Phys. B Condens. Matter* **1996**, 218 (1–4), 238–241. [https://doi.org/10.1016/0921-4526\(95\)00603-6](https://doi.org/10.1016/0921-4526(95)00603-6).

- (86) Sze, S. M. *Physics of Semiconductor Devices*, 2nd Edition.; John Wiley and Sons Ltd.: New York, NY, 1981.
- (87) Tkachov, G.; Hankiewicz, E. M. Spin-Helical Transport in Normal and Superconducting Topological Insulators. *Phys. Status Solidi B* **2013**, *250* (2), 215–232. <https://doi.org/10.1002/pssb.201248385>.
- (88) Stokbro, K.; Taylor, J.; Brandbyge, M.; Guo, H. Ab-Initio Non-Equilibrium Green's Function Formalism for Calculating Electron Transport in Molecular Devices. In *Introducing Molecular Electronics*; Cuniberti, G., Richter, K., Fagas, G., Eds.; Springer Berlin Heidelberg, **2006**; 680, 117–151. https://doi.org/10.1007/3-540-31514-4_5.
- (89) Koentopp, M.; Chang, C.; Burke, K.; Car, R. Density Functional Calculations of Nanoscale Conductance. *J. Phys. Condens. Matter* **2008**, *20* (8), 083203. <https://doi.org/10.1088/0953-8984/20/8/083203>.
- (90) Ulrich, J.; Esrail, D.; Pontius, W.; Venkataraman, L.; Millar, D.; Doerrer, L. H. Variability of Conductance in Molecular Junctions. *J. Phys. Chem. B* **2006**, *110* (6), 2462–2466. <https://doi.org/10.1021/jp056455y>.
- (91) Gotsmann, B.; Riel, H.; Lörtscher, E. Direct Electrode-Electrode Tunneling in Break-Junction Measurements of Molecular Conductance. *Phys. Rev. B* **2011**, *84* (20), 205408. <https://doi.org/10.1103/PhysRevB.84.205408>.
- (92) Quan, R.; Pitler, C. S.; Ratner, M. A.; Reuter, M. G. Quantitative Interpretations of Break Junction Conductance Histograms in Molecular Electron Transport. *ACS Nano* **2015**, *9* (7), 7704–7713. <https://doi.org/10.1021/acs.nano.5b03183>.
- (93) Quek, S. Y.; Kamenetska, M.; Steigerwald, M. L.; Choi, H. J.; Louie, S. G.; Hybertsen, M. S.; Neaton, J. B.; Venkataraman, L. Mechanically Controlled Binary Conductance Switching of a Single-Molecule Junction. *Nat. Nanotechnol.* **2009**, *4* (4), 230–234. <https://doi.org/10.1038/nnano.2009.10>.
- (94) Emberly, E. G.; Kirczenow, G. Theoretical Study of Electrical Conduction through a Molecule Connected to Metallic Nanocontacts. *Phys. Rev. B* **1998**, *58* (16), 10911–10920. <https://doi.org/10.1103/PhysRevB.58.10911>.
- (95) Muller, C. J.; van Ruitenbeek, J. M.; de Jongh, L. J. Experimental Observation of the Transition from Weak Link to Tunnel Junction. *Phys. C Supercond.* **1992**, *191* (3–4), 485–504. [https://doi.org/10.1016/0921-4534\(92\)90947-B](https://doi.org/10.1016/0921-4534(92)90947-B).
- (96) Young, W. C.; Budynas, R. G. *Roark's Formulas for Stress and Strain*, 7th Edition.; McGraw-Hill, 2001.
- (97) Xu, B.; He, H.; Tao, N. J. Controlling the Conductance of Atomically Thin Metal Wires with Electrochemical Potential. *J. Am. Chem. Soc.* **2002**, *124* (45), 13568–13575. <https://doi.org/10.1021/ja027810q>.
- (98) Xu, B.; Tao, N. J. Measurement of Single-Molecule Resistance by Repeated Formation of Molecular Junctions. *Science* **2003**, *301* (5637), 1221–1223. <https://doi.org/10.1126/science.1087481>.
- (99) Binnig, G.; Rohrer, H. Scanning Tunneling Microscopy. *Phys. BC* **1984**, *127* (1), 37–45. [https://doi.org/10.1016/S0378-4363\(84\)80008-X](https://doi.org/10.1016/S0378-4363(84)80008-X).
- (100) Rudnev, A. V.; Kaliginedi, V.; Droghetti, A.; Ozawa, H.; Kuzume, A.; Haga, M.; Broekmann, P.; Rungger, I. Stable Anchoring Chemistry for Room Temperature Charge Transport through Graphite-Molecule Contacts. *Sci. Adv.* **2017**, *3* (6), e1602297. <https://doi.org/10.1126/sciadv.1602297>.
- (101) Mol, J. A.; Lau, C. S.; Lewis, W. J. M.; Sadeghi, H.; Roche, C.; Cnossen, A.; Warner, J. H.; Lambert, C. J.; Anderson, H. L.; Briggs, G. A. D. Graphene-Porphyrin Single-Molecule Transistors. *Nanoscale* **2015**, *7* (31), 13181–13185. <https://doi.org/10.1039/C5NR03294F>.

- (102) Vezzoli, A.; Brooke, R. J.; Ferri, N.; Higgins, S. J.; Schwarzacher, W.; Nichols, R. J. Single-Molecule Transport at a Rectifying GaAs Contact. *Nano Lett.* **2017**, *17* (2), 1109–1115. <https://doi.org/10.1021/acs.nanolett.6b04663>.
- (103) Hsu, J. W. P.; Lang, D. V.; West, K. W.; Loo, Y.-L.; Halls, M. D.; Raghavachari, K. Probing Occupied States of the Molecular Layer in Au–Alkanedithiol–GaAs Diodes. *J. Phys. Chem. B* **2005**, *109* (12), 5719–5723. <https://doi.org/10.1021/jp044246s>.
- (104) Yanson, A. I.; Bollinger, G. R.; van den Brom, H. E.; Agraït, N.; van Ruitenbeek, J. M. Formation and Manipulation of a Metallic Wire of Single Gold Atoms. *Nature* **1998**, *395* (6704), 783–785. <https://doi.org/10.1038/27405>.
- (105) Gordienko, A. B.; Zhuravlev, Yu. N.; Fedorov, D. G. Band Structure and Chemical Bonding in Cu₂O and Ag₂O Oxides. *Phys. Solid State* **2007**, *49* (2), 223–228. <https://doi.org/10.1134/S1063783407020072>.
- (106) Ludoph, B.; Ruitenbeek, J. M. van. Conductance Fluctuations as a Tool for Investigating the Quantum Modes in Atomic-Size Metallic Contacts. *Phys. Rev. B* **2000**, *61* (3), 2273–2285. <https://doi.org/10.1103/PhysRevB.61.2273>.
- (107) Bakker, D. J.; Noat, Y.; Yanson, A. I.; van Ruitenbeek, J. M. Effect of Disorder on the Conductance of a Cu Atomic Point Contact. *Phys. Rev. B* **2002**, *65* (23), 235416. <https://doi.org/10.1103/PhysRevB.65.235416>.
- (108) Smit, R. H. M.; Noat, Y.; Untiedt, C.; Lang, N. D.; van Hemert, M. C.; van Ruitenbeek, J. M. Measurement of the Conductance of a Hydrogen Molecule. *Nature* **2002**, *419* (6910), 906–909. <https://doi.org/10.1038/nature01103>.
- (109) Kaliginedi, V.; V. Rudnev, A.; Moreno-García, P.; Baghernejad, M.; Huang, C.; Hong, W.; Wandlowski, T. Promising Anchoring Groups for Single-Molecule Conductance Measurements. *Phys Chem Chem Phys* **2014**, *16* (43), 23529–23539. <https://doi.org/10.1039/C4CP03605K>.
- (110) Park, Y. S.; Whalley, A. C.; Kamenetska, M.; Steigerwald, M. L.; Hybertsen, M. S.; Nuckolls, C.; Venkataraman, L. Contact Chemistry and Single-Molecule Conductance: A Comparison of Phosphines, Methyl Sulfides, and Amines. *J. Am. Chem. Soc.* **2007**, *129* (51), 15768–15769. <https://doi.org/10.1021/ja0773857>.
- (111) Su, T. A.; Neupane, M.; Steigerwald, M. L.; Venkataraman, L.; Nuckolls, C. Chemical Principles of Single-Molecule Electronics. *Nat. Rev. Mater.* **2016**, *1* (3), 16002. <https://doi.org/10.1038/natrevmats.2016.2>.
- (112) Salomon, A.; Cahen, D.; Lindsay, S.; Tomfohr, J.; Engelkes, V. B.; Frisbie, C. D. Comparison of Electronic Transport Measurements on Organic Molecules. *Adv. Mater.* **2003**, *15* (22), 1881–1890. <https://doi.org/10.1002/adma.200306091>.
- (113) Whetten, R. L.; Price, R. C. Chemistry: Nano-Golden Order. *Science* **2007**, *318* (5849), 407–408. <https://doi.org/10.1126/science.1150176>.
- (114) Leary, E.; La Rosa, A.; González, M. T.; Rubio-Bollinger, G.; Agraït, N.; Martín, N. Incorporating Single Molecules into Electrical Circuits. The Role of the Chemical Anchoring Group. *Chem. Soc. Rev.* **2015**, *44* (4), 920–942. <https://doi.org/10.1039/C4CS00264D>.
- (115) Luo, Y.-R. *Comprehensive Handbook of Chemical Bond Energies*, 1st Edition.; CRC Press: New York, NY, 2007.
- (116) Komoto, Y.; Fujii, S.; Nakamura, H.; Tada, T.; Nishino, T.; Kiguchi, M. Resolving Metal-Molecule Interfaces at Single-Molecule Junctions. *Sci. Rep.* **2016**, *6* (1), 26606. <https://doi.org/10.1038/srep26606>.

- (117) Strange, M.; Lopez-Acevedo, O.; Häkkinen, H. Oligomeric Gold–Thiolate Units Define the Properties of the Molecular Junction between Gold and Benzene Dithiols. *J. Phys. Chem. Lett.* **2010**, *1* (10), 1528–1532. <https://doi.org/10.1021/jz1002988>.
- (118) Zeng, W.; Wang, E.; Qiu, R.; Sohail, M.; Wu, S.; Chen, F.-X. Oxygen-Atom Insertion of NHC–Copper Complex: The Source of Oxygen from N,N-Dimethylformamide. *J. Organomet. Chem.* **2013**, *743*, 44–48. <https://doi.org/10.1016/j.jorganchem.2013.06.017>.
- (119) Denk, M. K.; Thadani, A.; Hatano, K.; Lough, A. J. Steric Stabilization of Nucleophilic Carbenes. *Angew. Chem. Int. Ed.* **1997**, *36* (23), 2607–2609. <https://doi.org/10.1002/anie.199726071>.
- (120) Herrer, I. L.; Ismael, A. K.; Milán, D. C.; Vezzoli, A.; Martín, S.; González-Orive, A.; Grace, I.; Lambert, C.; Serrano, J. L.; Nichols, R. J.; Cea, P. Unconventional Single-Molecule Conductance Behavior for a New Heterocyclic Anchoring Group: Pyrazolyl. *J. Phys. Chem. Lett.* **2018**, *9* (18), 5364–5372. <https://doi.org/10.1021/acs.jpcclett.8b02051>.
- (121) Kamenetska, M.; Quek, S. Y.; Whalley, A. C.; Steigerwald, M. L.; Choi, H. J.; Louie, S. G.; Nuckolls, C.; Hybertsen, M. S.; Neaton, J. B.; Venkataraman, L. Conductance and Geometry of Pyridine-Linked Single-Molecule Junctions. *J. Am. Chem. Soc.* **2010**, *132* (19), 6817–6821. <https://doi.org/10.1021/ja1015348>.
- (122) Doud, E. A.; Inkpen, M. S.; Lovat, G.; Montes, E.; Paley, D. W.; Steigerwald, M. L.; Vázquez, H.; Venkataraman, L.; Roy, X. In Situ Formation of N-Heterocyclic Carbene-Bound Single-Molecule Junctions. *J. Am. Chem. Soc.* **2018**, *140* (28), 8944–8949. <https://doi.org/10.1021/jacs.8b05184>.
- (123) Poater, A.; Ragone, F.; Giudice, S.; Costabile, C.; Dorta, R.; Nolan, S. P.; Cavallo, L. Thermodynamics of N-Heterocyclic Carbene Dimerization: The Balance of Sterics and Electronics. *Organometallics* **2008**, *27* (12), 2679–2681. <https://doi.org/10.1021/om8001119>.
- (124) Kim, N. T.; Li, H.; Venkataraman, L.; Leighton, J. L. High-Conductance Pathways in Ring-Strained Disilanes by Way of Direct σ -Si–Si to Au Coordination. *J. Am. Chem. Soc.* **2016**, *138* (36), 11505–11508. <https://doi.org/10.1021/jacs.6b07825>.
- (125) Ahn, S.; Aradhya, S. V.; Klausen, R. S.; Capozzi, B.; Roy, X.; Steigerwald, M. L.; Nuckolls, C.; Venkataraman, L. Electronic Transport and Mechanical Stability of Carboxyl Linked Single-Molecule Junctions. *Phys. Chem. Chem. Phys.* **2012**, *14* (40), 13841–13845. <https://doi.org/10.1039/c2cp41578j>.
- (126) Sun, Y.-Y.; Peng, Z.-L.; Hou, R.; Liang, J.-H.; Zheng, J.-F.; Zhou, X.-Y.; Zhou, X.-S.; Jin, S.; Niu, Z.-J.; Mao, B.-W. Enhancing Electron Transport in Molecular Wires by Insertion of a Ferrocene Center. *Phys. Chem. Chem. Phys.* **2014**, *16* (6), 2260–2267. <https://doi.org/10.1039/c3cp53269k>.
- (127) Frei, M.; Aradhya, S. V.; Hybertsen, M. S.; Venkataraman, L. Linker Dependent Bond Rupture Force Measurements in Single-Molecule Junctions. *J. Am. Chem. Soc.* **2012**, *134* (9), 4003–4006. <https://doi.org/10.1021/ja211590d>.
- (128) Kamenetska, M.; Koentopp, M.; Whalley, A. C.; Park, Y. S.; Steigerwald, M. L.; Nuckolls, C.; Hybertsen, M. S.; Venkataraman, L. Formation and Evolution of Single-Molecule Junctions. *Phys. Rev. Lett.* **2009**, *102* (12), 126803(4). <https://doi.org/10.1103/PhysRevLett.102.126803>.
- (129) Yoshizawa, K. An Orbital Rule for Electron Transport in Molecules. *Acc. Chem. Res.* **2012**, *45* (9), 1612–1621. <https://doi.org/10.1021/ar300075f>.

- (130) Fu, T.; Smith, S.; Camarasa-Gómez, M.; Yu, X.; Xue, J.; Nuckolls, C.; Evers, F.; Venkataraman, L.; Wei, S. Enhanced Coupling through π -Stacking in Imidazole-Based Molecular Junctions. *Chem. Sci.* **2019**, 9998–10002. <https://doi.org/10.1039/C9SC03760H>.
- (131) Li, H.; Garner, M. H.; Su, T. A.; Jensen, A.; Inkpen, M. S.; Steigerwald, M. L.; Venkataraman, L.; Solomon, G. C.; Nuckolls, C. Extreme Conductance Suppression in Molecular Siloxanes. *J. Am. Chem. Soc.* **2017**, *139* (30), 10212–10215. <https://doi.org/10.1021/jacs.7b05599>.
- (132) Taniguchi, M.; Tsutsui, M.; Shoji, K.; Fujiwara, H.; Kawai, T. Single-Molecule Junctions with Strong Molecule–Electrode Coupling. *J. Am. Chem. Soc.* **2009**, *131* (40), 14146–14147. <https://doi.org/10.1021/ja905248e>.
- (133) Giacalone, F.; Herranz, M.; Grüter, L.; González, M. T.; Calame, M.; Schönenberger, C.; Arroyo, C. R.; Rubio-Bollinger, G.; Vélez, M.; Agraït, N.; Martín, N. Tetrathiafulvalene-Based Molecular Nanowires. *Chem. Commun.* **2007**, 4854–4856. <https://doi.org/10.1039/b710739k>.
- (134) Nitzan, A. Electron Transport in Molecular Wire Junctions. *Science* **2003**, *300* (5624), 1384–1389. <https://doi.org/10.1126/science.1081572>.
- (135) Lörtscher, E.; Gotsmann, B.; Lee, Y.; Yu, L.; Rettner, C.; Riel, H. Transport Properties of a Single-Molecule Diode. *ACS Nano* **2012**, *6* (6), 4931–4939. <https://doi.org/10.1021/nn300438h>.
- (136) Perrin, M. L.; Galán, E.; Eelkema, R.; Thijssen, J. M.; Grozema, F.; van der Zant, H. S. J. A Gate-Tunable Single-Molecule Diode. *Nanoscale* **2016**, *8* (16), 8919–8923. <https://doi.org/10.1039/C6NR00735J>.
- (137) Tada, T.; Yoshizawa, K. Molecular Design of Electron Transport with Orbital Rule: Toward Conductance-Decay Free Molecular Junctions. *Phys. Chem. Chem. Phys.* **2015**, *17* (48), 32099–32110. <https://doi.org/10.1039/C5CP05423K>.
- (138) Xiao; Xu; Tao, N. J. Measurement of Single Molecule Conductance: Benzenedithiol and Benzenedimethanethiol. *Nano Lett.* **2004**, *4* (2), 267–271. <https://doi.org/10.1021/nl035000m>.
- (139) Meisner, J. S.; Ahn, S.; Aradhya, S. V.; Krikorian, M.; Parameswaran, R.; Steigerwald, M.; Venkataraman, L.; Nuckolls, C. Importance of Direct Metal– π Coupling in Electronic Transport Through Conjugated Single-Molecule Junctions. *J. Am. Chem. Soc.* **2012**, *134* (50), 20440–20445. <https://doi.org/10.1021/ja308626m>.
- (140) Arroyo, C. R.; Frisenda, R.; Moth-Poulsen, K.; Seldenthuis, J. S.; Bjørnholm, T.; van der Zant, H. S. Quantum Interference Effects at Room Temperature in OPV-Based Single-Molecule Junctions. *Nanoscale Res. Lett.* **2013**, *8* (1), 234. <https://doi.org/10.1186/1556-276X-8-234>.
- (141) Arroyo, C. R.; Tarkuc, S.; Frisenda, R.; Seldenthuis, J. S.; Woerde, C. H. M.; Eelkema, R.; Grozema, F. C.; van der Zant, H. S. J. Signatures of Quantum Interference Effects on Charge Transport Through a Single Benzene Ring. *Angew. Chem. Int. Ed.* **2013**, *52* (11), 3152–3155. <https://doi.org/10.1002/anie.201207667>.
- (142) Guo, Y.-D.; Yan, X.-H.; Xiao, Y.; Liu, C.-S. U-Shaped Relationship between Current and Pitch in Helicene Molecules. *Sci. Rep.* **2015**, *5* (1), 16731. <https://doi.org/10.1038/srep16731>.
- (143) Treboux, G.; Lapstun, P.; Wu, Z.; Silverbrook, K. Electronic Conductance of Helicenes. *Chem. Phys. Lett.* **1999**, *301* (5–6), 493–497. [https://doi.org/10.1016/S0009-2614\(99\)00085-8](https://doi.org/10.1016/S0009-2614(99)00085-8).

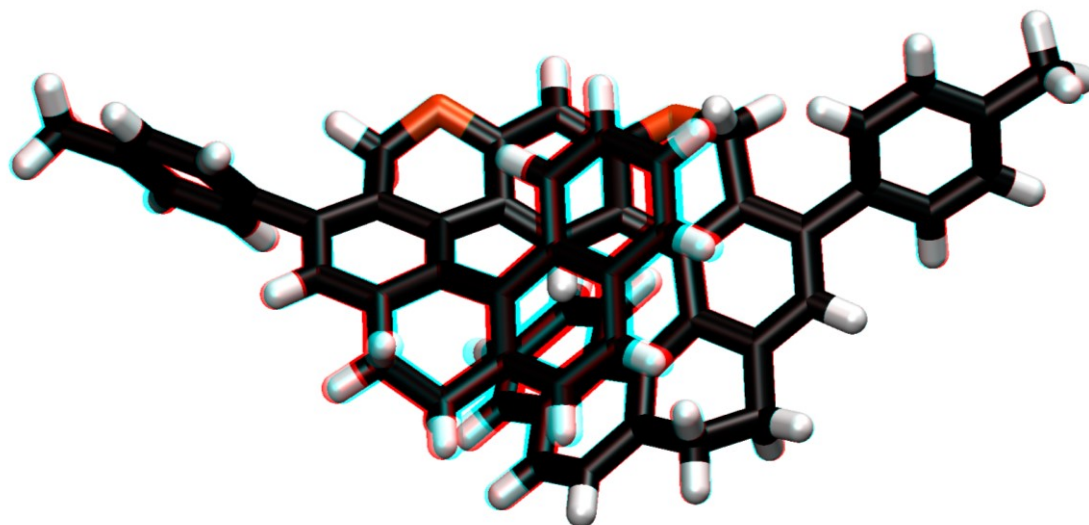
- (144) Pan, T.-R.; Guo, A.-M.; Sun, Q.-F. Spin-Polarized Electron Transport through Helicene Molecular Junctions. *Phys. Rev. B* **2016**, *94* (23), 235448. <https://doi.org/10.1103/PhysRevB.94.235448>.
- (145) Naaman, R.; Waldeck, D. H. Chiral-Induced Spin Selectivity Effect. *J. Phys. Chem. Lett.* **2012**, *3* (16), 2178–2187. <https://doi.org/10.1021/jz300793y>.
- (146) Král, P.; Seideman, T. Current-Induced Rotation of Helical Molecular Wires. *J. Chem. Phys.* **2005**, *123* (18), 184702. <https://doi.org/10.1063/1.2107527>.
- (147) Kettner, M.; Maslyuk, V. V.; Nürenberg, D.; Seibel, J.; Gutierrez, R.; Cuniberti, G.; Ernst, K.-H.; Zacharias, H. Chirality-Dependent Electron Spin Filtering by Molecular Monolayers of Helicenes. *J. Phys. Chem. Lett.* **2018**, *9* (8), 2025–2030. <https://doi.org/10.1021/acs.jpcclett.8b00208>.
- (148) Nejedlý, J.; Šámal, M.; Rybáček, J.; Tobrmanová, M.; Szydło, F.; Coudret, C.; Neumeier, M.; Vacek, J.; Vacek-Chocholoušová, J.; Buděšínský, M.; Šaman, D.; Bednářová, L.; Sieger, L.; Stará, I. G.; Starý, I. Synthesis of Long Oxahelicenes by Polycyclization in a Flow Reactor. *Angew. Chem. Int. Ed.* **2017**, *56* (21), 5839–5843. <https://doi.org/10.1002/anie.201700341>.
- (149) Teplý, F.; Stará, I. G.; Starý, I.; Kollárovič, A.; Šaman, D.; Vyskočil, Š.; Fiedler, P. Synthesis of 3-Hexahelicenol and Its Transformation to 3-Hexahelicenylamines, Diphenylphosphine, Methyl Carboxylate, and Dimethylthiocarbamate. *J. Org. Chem.* **2003**, *68* (13), 5193–5197. <https://doi.org/10.1021/jo034369t>.
- (150) Thomsen, I.; Torssell, K. B. G.; Lund, H.; O'Reilly, K. P. J.; Ertan, A.; Kleinpeter, E. Iodination of Resorcinol, 5-Methoxyresorcinol, Phloroglucinol and Resorcylic Acid. *Acta Chem. Scand.* **1991**, *45*, 539–542. <https://doi.org/10.3891/acta.chem.scand.45-0539>.
- (151) Kleinbeck, F.; Toste, F. D. Gold(I)-Catalyzed Enantioselective Ring Expansion of Allenylcyclopropanols. *J. Am. Chem. Soc.* **2009**, *131* (26), 9178–9179. <https://doi.org/10.1021/ja904055z>.
- (152) Chercheja, S.; Klívar, J.; Jančářík, A.; Rybáček, J.; Salzl, S.; Tarábek, J.; Pospíšil, L.; Vacek-Chocholoušová, J.; Vacek, J.; Pohl, R.; Císařová, I.; Starý, I.; Stará, I. G. The Use of Cobalt-Mediated Cycloisomerisation of Ynedinitriles in the Synthesis of Pyridazinohelicenes. *Chem. - Eur. J.* **2014**, *20* (27), 8477–8482. <https://doi.org/10.1002/chem.201402312>.
- (153) Lipshutz, B. H.; Petersen, T. B.; Abela, A. R. Room-Temperature Suzuki–Miyaura Couplings in Water Facilitated by Nonionic Amphiphiles. *Org. Lett.* **2008**, *10* (7), 1333–1336. <https://doi.org/10.1021/ol702714y>.
- (154) Price, D. W.; Dirk, S. M.; Maya, F.; Tour, J. M. Improved and New Syntheses of Potential Molecular Electronics Devices. *Tetrahedron* **2003**, *59* (14), 2497–2518. [https://doi.org/10.1016/S0040-4020\(03\)00246-1](https://doi.org/10.1016/S0040-4020(03)00246-1).
- (155) Schmidt, L. C.; Rey, V.; Peñeñory, A. B. Photoinduced Nucleophilic Substitution of Aryl Halides with Potassium Thioacetate – A One-Pot Approach to Aryl Methyl and Diaryl Sulfides. *Eur. J. Org. Chem.* **2006**, *2006* (9), 2210–2214. <https://doi.org/10.1002/ejoc.200500955>.
- (156) Soria-Castro, S. M.; Peñeñory, A. B. Efficient Cu-Catalyzed Base-Free C–S Coupling under Conventional and Microwave Heating. A Simple Access to S-Heterocycles and Sulfides. *Beilstein J. Org. Chem.* **2013**, *9*, 467–475. <https://doi.org/10.3762/bjoc.9.50>.
- (157) Rossi, R. A.; De Rossi, R. H.; Lopez, A. F. Reaction of 1-Halonaphthalenes with Nucleophiles by the SRN1 Mechanism of Aromatic Substitution. *J. Am. Chem. Soc.* **1976**, *98* (5), 1252–1257. <https://doi.org/10.1021/ja00421a033>.

- (158) Mulder, P.; Arends, I. W. C. E.; Santoro, D.; Korth, H.-G. The Surprisingly Facile Thermal Dehalogenation of Chlorinated Aromatics by a Hydroaromatic Donor Solvent. Tautomerization of Chlorinated Phenols and Anilines. *J. Org. Chem.* **2003**, *68* (11), 4247–4257. <https://doi.org/10.1021/jo0265885>.
- (159) Songis, O.; Míšek, J.; Schmid, M. B.; Kollárovič, A.; Stará, I. G.; Šaman, D.; Císařová, I.; Starý, I. A Versatile Synthesis of Functionalized Pentahelicenes. *J. Org. Chem.* **2010**, *75* (20), 6889–6899. <https://doi.org/10.1021/jo1013977>.
- (160) Gay Sánchez, I.; Šámal, M.; Nejedlý, J.; Karras, M.; Klívar, J.; Rybáček, J.; Buděšínský, M.; Bednářová, L.; Seidlerová, B.; Stará, I. G.; Starý, I. Oxahelicene NHC Ligands in the Asymmetric Synthesis of Nonracemic Helicenes. *Chem. Commun.* **2017**, *53* (31), 4370–4373. <https://doi.org/10.1039/C7CC00781G>.
- (161) Biet, T.; Fihey, A.; Cauchy, T.; Vanthuynne, N.; Roussel, C.; Crassous, J.; Avarvari, N. Ethylenedithio-Tetrathiafulvalene-Helicenes: Electroactive Helical Precursors with Switchable Chiroptical Properties. *Chem. - Eur. J.* **2013**, *19* (39), 13160–13167. <https://doi.org/10.1002/chem.201301095>.
- (162) Goretta, S.; Tasciotti, C.; Mathieu, S.; Smet, M.; Maes, W.; Chabre, Y. M.; Dehaen, W.; Giasson, R.; Raimundo, J.-M.; Henry, C. R.; Barth, C.; Gingras, M. Expeditive Syntheses of Functionalized Pentahelicenes and NC-AFM on Ag(001). *Org. Lett.* **2009**, *11* (17), 3846–3849. <https://doi.org/10.1021/ol9014255>.
- (163) Shaw, J. E. Preparation of Thiophenols from Unactivated Aryl Chlorides and Sodium Alkanethiolates in N-Methyl-2-Pyrrolidone. *J. Org. Chem.* **1991**, *56* (11), 3728–3729. <https://doi.org/10.1021/jo00011a057>.
- (164) Chakraborty, P. Sodium Methanethiolate. In *Encyclopedia of Reagents for Organic Synthesis*; John Wiley & Sons, Ltd: Chichester, UK, **2014**; pp 1–5. <https://doi.org/10.1002/047084289X.rm01716>.
- (165) Vahlkamp, T.; Meijer, A. J.; Wilms, J.; Chamuleau, R. A. F. M. Inhibition of Mitochondrial Electron Transfer in Rats by Ethanethiol and Methanethiol. *Clin. Sci.* **1979**, *56* (2), 147–156. <https://doi.org/10.1042/cs0560147>.
- (166) Shaporenko, A.; Elbing, M.; Błaszczak, A.; von Hänisch, C.; Mayor, M.; Zharnikov, M. Self-Assembled Monolayers from Biphenyldithiol Derivatives: Optimization of the Deprotection Procedure and Effect of the Molecular Conformation. *J. Phys. Chem. B* **2006**, *110* (9), 4307–4317. <https://doi.org/10.1021/jp056833z>.
- (167) Vonlanthen, D.; Mishchenko, A.; Elbing, M.; Neuburger, M.; Wandlowski, T.; Mayor, M. Chemically Controlled Conductivity: Torsion-Angle Dependence in a Single-Molecule Biphenyldithiol Junction. *Angew. Chem. Int. Ed.* **2009**, *48* (47), 8886–8890. <https://doi.org/10.1002/anie.200903946>.
- (168) Nejedlý, J.; Šámal, M.; Rybáček, J.; Gay Sánchez, I.; Houska, V.; Warzecha, T.; Vacek, J.; Sieger, L.; Buděšínský, M.; Bednářová, L.; Fiedler, P.; Císařová, I.; Starý, I.; Stará, I. G. Synthesis of Racemic, Diastereopure, and Enantiopure Carba- or Oxa[5]-, [6]-, [7]-, and -[19]Helicene (Di)Thiol Derivatives. *J. Org. Chem.* **2020**, *85* (1), 248–276. <https://doi.org/10.1021/acs.joc.9b02965>.
- (169) Terfort, A.; Görls, H.; Brunner, H. The First Helical-Chiral Phosphane Ligands: Rac-[5]- and Rac-[6]-Heliphos. *Synthesis* **1997**, *1997* (01), 79–86. <https://doi.org/10.1055/s-1997-1498>.
- (170) Šámal, M. Unpublished Results.

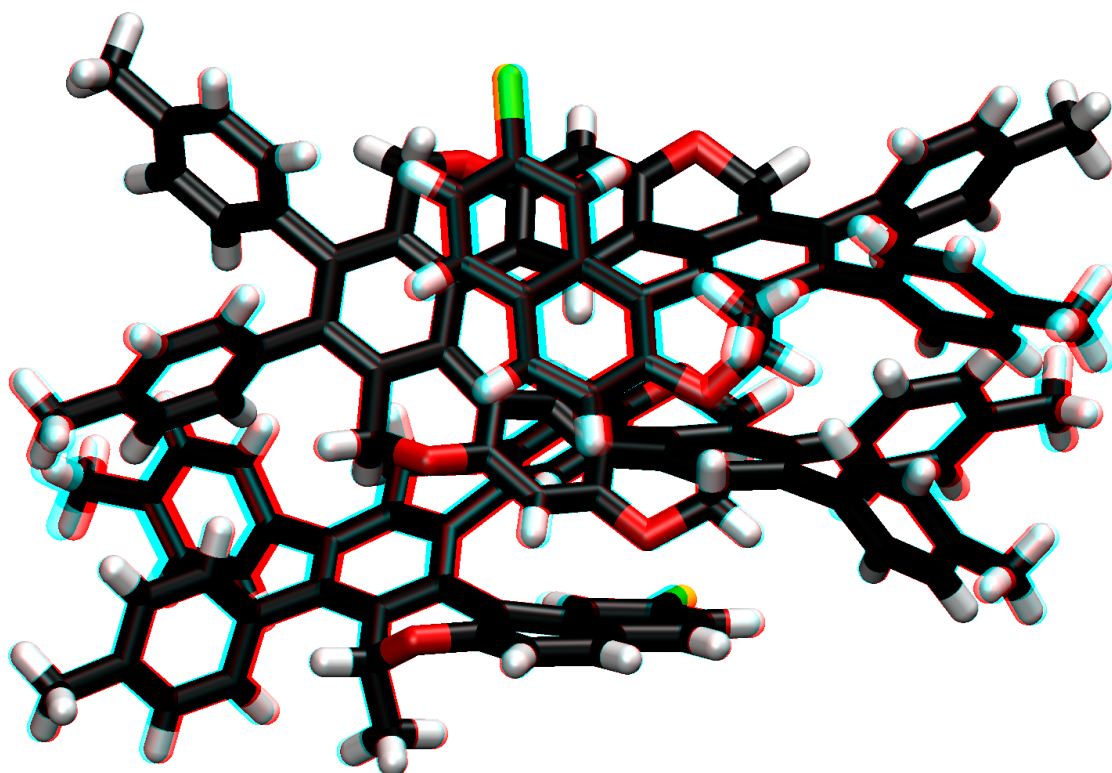
- (171) Stetsovych, O.; Mutombo, P.; Švec, M.; Šámal, M.; Nejedlý, J.; Císařová, I.; Vázquez, H.; Moro-Lagares, M.; Berger, J.; Vacek, J.; Stará, I. G.; Starý, I.; Jelínek, P. Large Converse Piezoelectric Effect Measured on a Single Molecule on a Metallic Surface. *J. Am. Chem. Soc.* **2018**, *140* (3), 940–946. <https://doi.org/10.1021/jacs.7b08729>.
- (172) Greenwood, N. N.; Earnshaw, A. *Chemistry of the Elements - 2nd Edition*, 2nd Edition; Butterworth-Heinemann, 1997.
- (173) Schmidt, B.; Riemer, M.; Karras, M. 2,2'-Biphenols via Protecting Group-Free Thermal or Microwave-Accelerated Suzuki–Miyaura Coupling in Water. *J. Org. Chem.* **2013**, *78* (17), 8680–8688. <https://doi.org/10.1021/jo401398n>.
- (174) Alexandrová, Z.; Stará, I. G.; Sehnal, P.; Teplý, F.; Starý, I.; Šaman, D.; Fiedler, P. Synthetic Studies Toward Chiral Aromatic Triynes as Key Substrates for the Asymmetric Synthesis of Helicene-Like Molecules. *Collect. Czechoslov. Chem. Commun.* **2004**, *69* (12), 2193–2211. <https://doi.org/10.1135/cccc20042193>.
- (175) Tsuji, J. *Perspectives in Organopalladium Chemistry for the 21st Century*; Elsevier science & Technology: Oxford, United Kingdom, 1999.
- (176) Teplý, F.; Stará, I. G.; Starý, I.; Kollárovič, A.; Šaman, D.; Fiedler, P. Transition Metal Control in the Reaction of Alkyne-Substituted Phenyl Iodides with Terminal Alkynes: Sonogashira Coupling vs Cyclic Carbopalladation. *Tetrahedron* **2002**, *58* (44), 9007–9018. [https://doi.org/10.1016/S0040-4020\(02\)01154-7](https://doi.org/10.1016/S0040-4020(02)01154-7).
- (177) LabView - National Instruments <https://www.ni.com/en-us/shop/labview.html> (accessed Nov 7, 2019).
- (178) *Fortran Programming Language*; 2015.
- (179) Park, Y. S.; Widawsky, J. R.; Kamenetska, M.; Steigerwald, M. L.; Hybertsen, M. S.; Nuckolls, C.; Venkataraman, L. Frustrated Rotations in Single-Molecule Junctions. *J. Am. Chem. Soc.* **2009**, *131* (31), 10820–10821. <https://doi.org/10.1021/ja903731m>.
- (180) Kim, T.; Darancet, P.; Widawsky, J. R.; Kotiuga, M.; Quek, S. Y.; Neaton, J. B.; Venkataraman, L. Determination of Energy Level Alignment and Coupling Strength in 4,4'-Bipyridine Single-Molecule Junctions. *Nano Lett.* **2014**, *14* (2), 794–798. <https://doi.org/10.1021/nl404143v>.
- (181) Borges, A.; Fung, E.-D.; Ng, F.; Venkataraman, L.; Solomon, G. C. Probing the Conductance of the σ -System of Bipyridine Using Destructive Interference. *J. Phys. Chem. Lett.* **2016**, *7* (23), 4825–4829. <https://doi.org/10.1021/acs.jpcclett.6b02494>.
- (182) Frisenda, R.; Perrin, M. L.; Valkenier, H.; Hummelen, J. C.; van der Zant, H. S. J. Statistical Analysis of Single-Molecule Breaking Traces: Statistical Analysis of Single-Molecule Breaking Traces. *Phys. Status Solidi B* **2013**, *250* (11), 2431–2436. <https://doi.org/10.1002/pssb.201349236>.
- (183) Brandbyge, M.; Mozos, J.-L.; Ordejón, P.; Taylor, J.; Stokbro, K. Density-Functional Method for Nonequilibrium Electron Transport. *Phys. Rev. B* **2002**, *65* (16), 165401. <https://doi.org/10.1103/PhysRevB.65.165401>.
- (184) Soler, J. M.; Artacho, E.; Gale, J. D.; García, A.; Junquera, J.; Ordejón, P.; Sánchez-Portal, D. The SIESTA Method for *Ab Initio* Order- *N* Materials Simulation. *J. Phys. Condens. Matter* **2002**, *14* (11), 2745–2779. <https://doi.org/10.1088/0953-8984/14/11/302>.

- (185) Kokkin, D. L.; Zhang, R.; Steimle, T. C.; Wyse, I. A.; Pearlman, B. W.; Varberg, T. D. Au–S Bonding Revealed from the Characterization of Diatomic Gold Sulfide, AuS. *J. Phys. Chem. A* **2015**, *119* (48), 11659–11667. <https://doi.org/10.1021/acs.jpca.5b08781>.
- (186) Mairena, A.; Mendieta, J. I.; Stetsovych, O.; Terfort, A.; Stará, I. G.; Starý, I.; Jelínek, P.; Ernst, K.-H. Heterochiral Recognition among Functionalized Heptahelicenes on Noble Metal Surfaces. *Chem. Commun.* **2019**, *55* (71), 10595–10598. <https://doi.org/10.1039/C9CC05317D>.
- (187) Kolivoška, V.; Šebera, J.; Severa, L.; Mészáros, G.; Sokolová, R.; Gasior, J.; Kocábová, J.; Hamill, J. M.; Pospíšil, L.; Hromadová, M. Single Molecule Conductance of Electroactive Helquats: Solvent Effect. *ChemElectroChem* **2019**, *6* (23), 5856–5863. <https://doi.org/10.1002/celec.201901801>.
- (188) Sheldrick, G. M. *SHELXT* – Integrated Space-Group and Crystal-Structure Determination. *Acta Crystallogr. Sect. Found. Adv.* **2015**, *71* (1), 3–8. <https://doi.org/10.1107/S2053273314026370>.
- (189) Sheldrick, G. M. Crystal Structure Refinement with *SHELXL*. *Acta Crystallogr. Sect. C Struct. Chem.* **2015**, *71* (1), 3–8. <https://doi.org/10.1107/S2053229614024218>.
- (190) Stará, I. G.; Kollárovič, A.; Teplý, F.; Starý, I.; Šaman, D.; Fiedler, P. Synthesis of Aromatic Triynes as Precursors to Helicene Derivatives. *Collect. Czechoslov. Chem. Commun.* **2000**, *65* (4), 577–609. <https://doi.org/10.1135/cccc20000577>.
- (191) Xiang, D.; Jeong, H.; Lee, T.; Mayer, D. Mechanically Controllable Break Junctions for Molecular Electronics. *Adv. Mater.* **2013**, *25* (35), 4845–4867. <https://doi.org/10.1002/adma.201301589>.
- (192) Hu, Z.; Ritzdorf, T. Cyanide- and Thiourea-Free Electrochemical Etching of Gold for Microelectronics Applications. *J. Electrochem. Soc.* **2007**, *154* (10), D543. <https://doi.org/10.1149/1.2768901>.
- (193) Frisch, M. J.; Trucks, G. W.; Schlegel, H. B.; Scuseria, G. E.; Robb, M. A.; Cheeseman, J. R.; Scalmani, G.; Barone, V.; Mennucci, B.; Petersson, G. A.; Nakatsuji, H.; Caricato, M.; Li, X.; Hratchian, H. P.; Izmaylov, A. F.; Bloino, J.; Zheng, G.; Sonnenberg, J. L.; Hada, M.; Ehara, M.; Toyota, K.; Fukuda, R.; Hasegawa, J.; Ishida, M.; Nakajima, T.; Honda, Y.; Kitao, O.; Nakai, H.; Vreven, T.; Montgomery, Jr., J. A.; Peralta, J. E.; Ogliaro, F.; Bearpark, M.; Heyd, J. J.; Brothers, E.; Kudin, K. N.; Staroverov, V. N.; Kobayashi, R.; Normand, J.; Raghavachari, K.; Rendell, A.; Burant, J. C.; Iyengar, S. S.; Tomasi, J.; Cossi, M.; Rega, N.; Millam, J. M.; Klene, M.; Knox, J. E.; Cross, J. B.; Bakken, V.; Adamo, C.; Jaramillo, J.; Gomperts, R.; Stratmann, R. E.; Yazyev, O.; Austin, A. J.; Cammi, R.; Pomelli, C.; Ochterski, J. W.; Marin, R. L.; Morokuma, K.; Zakrzewski, V. G.; Voth, G. A.; Salvador, P.; Dannenberg, J. J.; Dapprich, S.; Daniels, A. D.; Farkas, Ö.; Foresman, J. B.; Ortiz, J. V.; Cioslowski, J.; Fox, D. J. *Gaussian G09*, Revision E.01; Gaussian, Inc.: Wallingford CT, 2009.
- (194) *Virtual NanoLab 2016.0*; QuantumWise A/S: Copenhagen, Denmark, 2016.
- (195) *QuantumATK 2019.3*; Synopsys Corporate: Mountain View, CA, 2019.

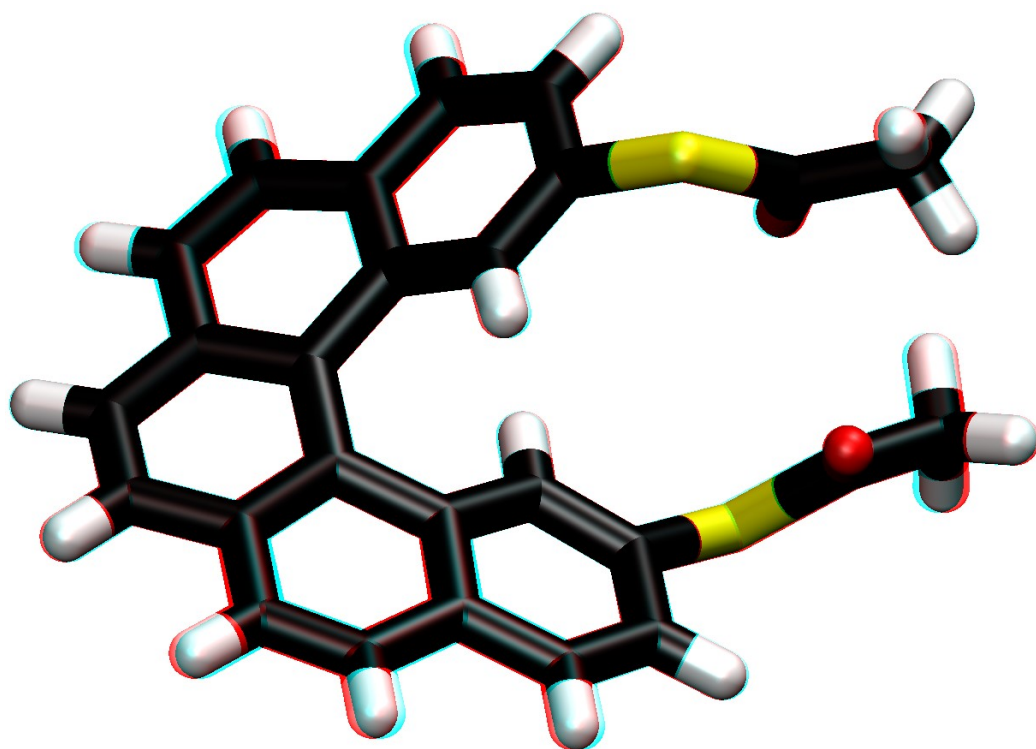
8 Appendix A: 3D structures of helicenes



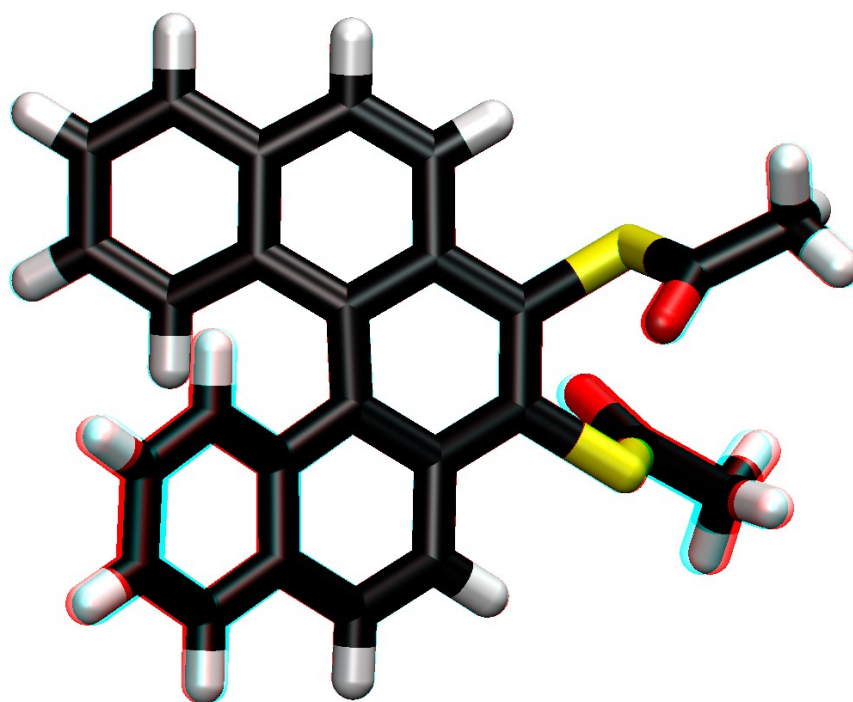
(P)-107 – X-ray analysis



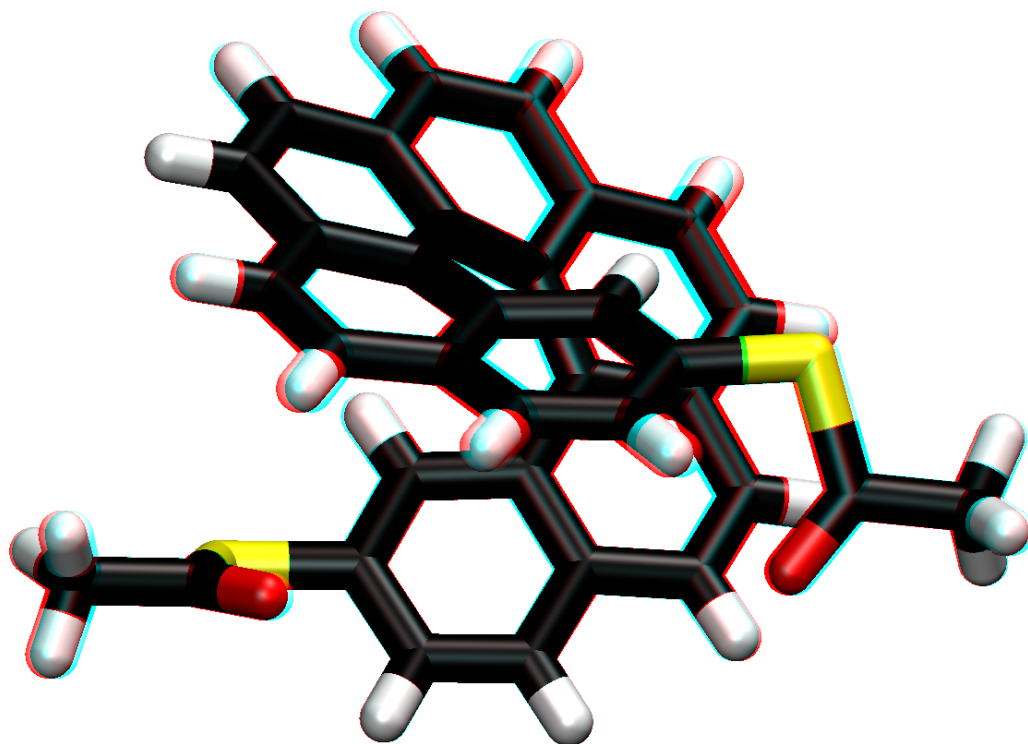
(M,R,R)-171 – X-ray structure



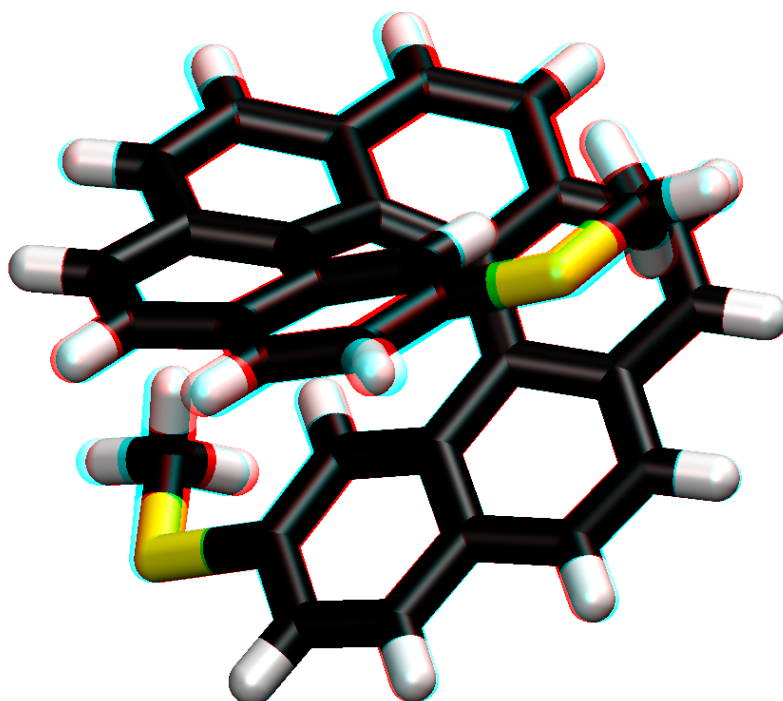
(M)-136-X-ray structure



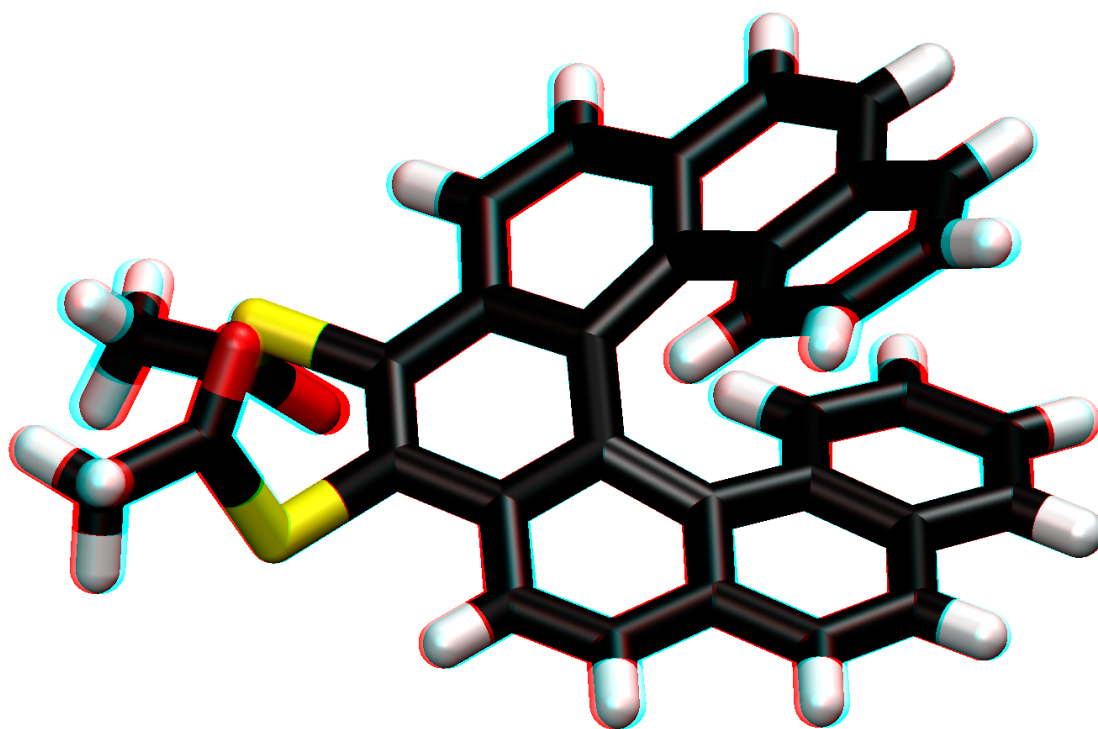
(M)-139 – X-ray structure



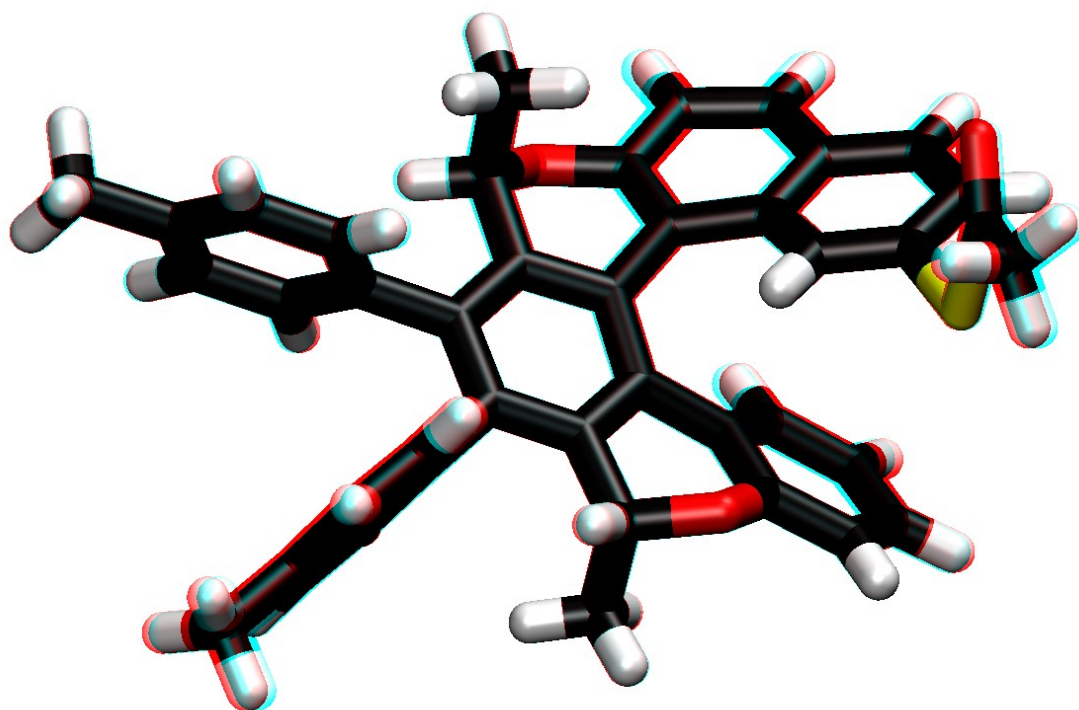
(P)-143 – X-ray structure



(P)-146 – X-ray structure



(M)-148 – X-ray structure



(M,R,R)-169 – X-ray structure